Functional miRNA-based Phenotypic Screening as a tool to delineate HIV-host interactions and facilitate Novel Drug Discovery

by
Jerolen Naidoo
(NDXJER010)

Thesis submitted to The University of Cape Town in fulfilment of
the requirements for the degree Doctor of Philosophy
Faculty of Health Sciences
UNIVERSITY OF CAPE TOWN
MARCH 2016

Supervisors:

Prof. FRANK BROMBACHER

Division of Immunology, Institute of Infectious Diseases and Molecular Medicine & Centre for Genetic Engineering and Biotechnology (ICGEB),
University of Cape Town Medical School. 7925

Prof. MUSA M. MHLANGA
Council for Scientific and Industrial Research/ University of Cape Town
Integrative Biomedical Science,
Division of Chemical, Systems & Synthetic Biology,
University of Cape Town Medical School. 7925

Dr. SAMANTHA BARICHIEVY
Innovative Medicine Division,
AstraZeneca,
Gothenburg , Sweden

Declaration

I, Jerolen Naidoo hereby declare that the work on which this thesis is based on is my original work (except where acknowledgements indicate otherwise) and that neither the whole work nor any part of it has been, is being, or is to be submitted for another degree in this or any other university.

I empower the university to reproduce for the purpose of research either the whole or any portion of the contents in any manner whatsoever.

Signed by candidate

Signature: Date: 13 MAY 2016

Dedication

I dedicate this thesis to my beautiful wife Jessika, you have been my shoulder to lean on, my muse, my guiding star and the ‘Lily’ to my ‘Marshall’ throughout this epic journey that has been my PhD. I would not have been able to reach this goal without your support and encouragement, your scientific input and your beautiful smile which have kept me going every step of the way. Thank you for putting up with my crazy work hours and moody ways, for sacrificing countless weekends and holidays so that I could culture cells and run experiments and finally for always believing in me. I love you. I also dedicate this thesis to my late grandfather Mr. R.B Naidoo, the lessons you taught me and your memory will stay with me always as I aspire to greater heights.

Acknowledgements

This thesis would not have been possible without the guidance, support and assistance of several individuals who have in various ways contributed to my development and ultimately to the completion of this thesis.

The completion of a PhD, much like mastery of the 'The Force' requires the guidance, tutelage and support of a skilled mentor. I have been fortunate enough to blessed with two of greatest mentors that a young padawan could ask for. To Musa (Yoda) and Sam (Obi-Wan), this journey would truly not have been possible without you both. Thank you for giving me the opportunity to start this PhD, the freedom to let me find my passion and for your gentle guidance which has allowed me to grow as a graduate student and as a researcher. Sam, your passion, strong conviction and unparalleled work ethic have set very high bar which I will always aspire to reach. Thank you also for the countless hours and experiments you sacrificed to help me get this thesis ready for submission. Musa, you have have taught me to never underestimate the force, to always aim for the stars and that no task is impossible for an Mhlanga lab 'F1'. Thanks to you the philosophy of 'Kaizen' will forever be ingrained in everything that do and in all aspects of my life. Musa and Sam, you have both served as mentor and friend to me over these years and wherever life may take us you will both always have a special place in my heart.

I would also like to thank Prof Frank Brombacher for welcoming me into his group, your input and sage advice over the years has been much appreciated. I would also like to thank Dr. Paula Sommer, your patience, encouragement and tutelage many years ago provided me with the confidence and the tools to pursue this PhD.

To my family, my Mum, my Dad, my Sister, Aunty Judy, Adrian and Lisa. Thank you for your understanding and patience over these past years for all the family gatherings and events that I have had to miss for work and for your unwavering support throughout this PhD. To my labmates, my colleagues, my friends, you have all made this journey unforgettable and fun. You have kept me motivated, inspired and given me so many great memories that I will forever cherish. This PhD would never have been the same without you all so thank you.

Finally, I would also like to thank the Council for Scientific and Industrial Research (CSIR) for funding my PhD and providing me with a great environment to hone my skills and excel as a researcher.

Abstract

Human Immunodeficiency Virus (HIV) is the causative agent of AIDS, a disease which affects over 24 million people globally and for which there is neither curative treatment nor vaccine available. As an intracellular pathogen that encodes only 15 proteins HIV-1 is highly dependent upon its host's cellular machinery in order to complete its life cycle. Host-directed therapy thus represents a potentially lucrative strategy for the development of novel anti-HIV therapies. microRNAs (miRNAs) are short noncoding RNA molecules that function as part of the endogenous RNA interference system which governs post transcriptional gene regulation. Current knowledge has placed miRNAs at the crux of HIV-host interactions, yet the functional relevance of the majority of the human miRNAome with regards to HIV replication has remained unknown. A microscopy-based high content screening (HCS) approach was thus developed to systematically evaluate the significance of augmenting or inhibiting the function of individual host miRNAs on the replication dynamics of HIV. A bespoke image analysis and data mining pipeline recovered 56 host miRNAs associated with suppressed HIV replication and 28 host miRNAs associated with enhanced HIV replication. Notably, the HIV-modulating potential of 80 of these miRNAs was previously unknown. Furthermore, HCS also uncovered a novel role for the miR-200 family in the modulation of HIV replication. *In silico* miRNA target identification and pathway enrichment analysis identified 24 pathways associated exclusively with suppressed HIV replication, 10 pathways associated exclusively with enhanced HIV replication and 38 functional pathways enriched for both enhanced and suppressed viral replication. These included a number of pathways previously implicated in HIV replication such as the PI3K, MAPK, TNF and WNT signalling pathways but also revealed novel functional associations including that of the Hippo signalling pathway. Intriguingly pathway analysis revealed an enrichment for host factors associated with viral carcinogenesis and a convergence on host processes and functional targets classically associated with chemotherapy including host DNA damage repair, cell cycle and tyrosine kinase receptor-mediated signalling. Experimental validation confirmed that HIV replication induced an aberrant cell survival phenotype in response to chemically induced DNA damage but this effect was reversed when DNA damage was induced prior to HIV exposure. A series of compound-based validation screens were thus undertaken in order to verify the functional associations recovered by miRNA screening. A targeted collection of 293 small molecule inhibitors, including a number of FDA-approved chemotherapeutics, were screened for HIV modulating activity. Novel anti-HIV activity was recovered for over 40 compounds including a number of FDA-approved therapies. Compound-target enrichment analysis revealed a strong concordance with functional associations initially described by miRNA-based HCS including EGFR-mediated signalling and DNA damage repair. Concordant HIV-suppressive activity was also recovered for miRNAs and compounds with common functional targets. The outcomes of this study thus represent a significant and novel contribution to current knowledge on HIV-host interactions. Furthermore, these findings have characterised novel miRNA and small molecule candidates for the treatment of HIV and have successfully demonstrated the utility of miRNA-based HCS for novel-drug discovery and drug repositioning.

List of Abbreviations

AIDS	Acquired immunodeficiency syndrome
ARV	Antiretroviral
BER	Base excision repair
CDK	Cyclin dependent kinase
CNS	Central nervous system
CRF	Circulating recombinant forms
CSIR	Council for Scientific and Industrial Research
EC	Elite controllers
ESCRT	Endosomal sorting complexes required for transport
FOV	Field of View
HAART	Highly active antiretroviral therapy
HCV	Hepatitis C virus
HDF	Host dependency factor
HLA	Human leukocyte antigen
HSP	Heat shock protein
HT	High throughput
ICC	Imunnocytochemistry
IRES	Internal ribosome entry site
LEDGF	Lens epithelium-derived growth factor
LTNP	Long term non progressors
LTR	Long terminal repeat
MDDC	Monocyte-derived dendritic cells
MDM	Monocyte-derived macrophages
MHC	Major histocompatibility complex
NNRTI	Non-nucleoside reverse transcriptase inhibitors
NPC	Nuclear pore complex
NRTI	Nucleoside reverse transcriptase inhibitors
ORF	Open reading frames
PAZ	Piwi-Argonaute-Zwille
PBMC	Peripheral blood mononuclear cells
PIC	Preintegration complex
RISC	RNA induced silencing complex
RLC	RISC loading complex
RNAPII	RNA polymerase II
ROI	Region of interest
RP	Rapid progressor
RSS	RNAi silencing suppressor
RT	Reverse transcriptase
RTC	Reverse Transcription Complex
RTI	Reverse transcription inhibitors

RTK	Receptor Tyrosine Kinase
SFM	Serum-free media
SIV	Simian Immunodeficiency Virus
SNP	Single nucleotide polymorphisms
TAR	Transactivating responsive
TBP	TATA box binding protein
TSS	Transcriptional start site
VprBP	Vpr binding protein
VRF	Viral restriction factors

List of Figures and Tables

Research outputs

Patents:

I. Jerolen NAIDOO, Samantha BARICHIEVY, Rethabile KHUTLANG, Musa M MHLANGA (2015) 'A method for identification of anti-hiv human mirna mimics and mirna inhibitors and anti-hiv pharmaceutical compounds', Publication number: WO 2015092707 A3.

II. Janine SCHOLEFIELD, Jerolen NAIDOO, Musa M MHLANGA, Samantha BARICHIEVY (2016) 'Pathogenic control of apoptosis' Publication number: WO 2016024257 A1.

Peer review publications:

I. Barichievy S, Naidoo J, Boule M, Sigal A, Scholefield J and Mhlanga MM (2016). HIV-1 targets MAP2K1/ERK2 to evade lincp21 mediated apoptosis. *Submitted, under review process.*

II. Barichievy S, Naidoo J and Mhlanga MM (2015) Non-coding RNAs and HIV: viral manipulation of host dark matter to shape the cellular environment. Front. Genet. 6:108. doi: 10.3389/fgene.2015.00108.

III. Naidoo J, Brackin R, Savulescu AF, Khutlang R and Mhlanga MM. Chapter 5: Systems Biology Tools to Understand the Role of Host MicroRNAs in Infection: a Closer Look at HIV in Applied RNAi: From Fundamental Research to Therapeutic Applications (2014) Caister Academic Press. ed. Patrick Arbuthnot and Marc S. Weinberg.

IV. Chapters 4 and 5 of this thesis are being prepared for submission as a research article

Selected Conferences:

I. RNAi Global Meeting 2015, CO, USA

II. RNAi Global Meeting 2014, Heidelberg, GER

III. High Content Analysis 2013, CA, USA

IV. 3rd Regional Synthetic Biology Forum 2013, GP, RSA

V. 6th SA AIDS Conference 2012, KZN, RSA

Table of Contents

Chapter 1: Introduction

1.1 HIV/AIDS : A brief history and current epidemiology

Acquired immunodeficiency syndrome (AIDS) is a disease characterised by the depletion of a specific subset of immune cells which express the cell surface cluster differentiation 4 (CD4) receptor. The consequence of $CD4^+$ cell depletion is a diminished immune system, which renders afflicted individuals highly susceptible to opportunistic infections and various forms of cancer (Gottlieb, 1981; Engels, 2006). The first documented case of AIDS was reported in 1981 when a number of homosexual men in the United States of America (USA) presented with cases of Kaposi's Sarcoma and pneumonia, which had previously only been seen in individuals with severely impaired immune systems (CDC, 1981; Gottlieb, 1981). In 1982 AIDS was recognised as an infectious disease which is transmitted by bodily fluids including blood, and by 1983 the first cases of hetereosexual transmission of AIDS were recorded by the CDC (CDC, 1982 and 1983). A French research group at Institut Pasteur, led by Luc Montagnier, was the first to isolate a novel retrovirus from an at-risk AIDS patient, while a separate group led by Robert Gallo became the first to demonstrate that this retrovirus was in fact the causative agent of AIDS (Barre-Sinoussi, 1983; Gallo, 1984). Three years after it was first identified, this virus became known as the Human Immunodeficiency Virus (HIV; Coffin, 1986).

Since its discovery HIV/AIDS has become one of the most significant infectious pandemics in human history, inflicting a devastating effect on global health (UNAIDS, 2014). The Joint United Nations programme on HIV and AIDS (UNAIDS) was piloted in 1996 in response to the global pandemic, and its findings reported an estimated 22.6 million infections worldwide and 6.4 million estimated AIDS related mortalities since the onset of the pandemic (UNAIDS, 1996). By 2006 the number of HIV/AIDS related mortalities had risen to ~25 million with an estimated 40 million infected individuals globally (UNAIDS, 2006). The latest global UNAIDS report revealed that as of December 2013, there were an estimated 35 million infected individuals worldwide, 24.7 million of which were accounted for by the Sub-Saharan Africa region (UNAIDS, 2014). There were also 2.1 million new infections in 2013, 70% of which were recorded in Sub-Saharan Africa (UNAIDS, 2014; WHO, 2014). HIV/AIDS is now estimated to have resulted in 39 million deaths since 1981, with 1.5 million deaths recorded in 2013 alone (WHO, 2014). Strikingly only 38% of the infected adults and only 24% of infected children worldwide had access to life saving antiretrovirals (ARVs) in 2013 (UNAIDS, 2014). More than 30 years since it was first discovered, HIV remains a globally relevant health issue, especially in Sub-Saharan Africa. Despite the success of ARV therapies in prolonging the lifespan of afflicted individuals, HIV infection remains a disease for which

there is still no cure and only limited availability of treatment, especially in countries that carry the majority of the global HIV/AIDS burden.

1.2 HIV origins and diversity

HIV has evolved from multiple zoonotic transfer events of Simian Immunodeficiency Virus (SIV) from non-human African primates to humans (Santiago, 2005; Keele, 2006; D'arc, 2015). These distinct transmission events, along with the high mutation rate associated with HIV replication, have given rise to the vast genetic heterogeneity that belies the name "HIV" (Figure 1.1.). Firstly, there are two different strains of HIV: HIV-1 and HIV-2. Despite possessing a similar genetic structure, these strains have been demonstrated to exhibit up to 45% variability in their nucleotide sequences, and up to 65% variability in their amino acid sequences (Motomura, 2007). HIV-2 originated from the cross-species transfer of SIV from Sooty Mangabeys (*Cercocebus atys*) to humans, and was first described in West African individuals afflicted with AIDS in the mid 1980s (Clavel, 1986; Santiago, 2005). HIV-2 infections are principally confined within West Africa and are associated with inferior rates of virulence and transmission compared to HIV-1 (Pepin, 1991; Kanki, 1994; Marlink, 1994; Marchant, 2006). The origin of HIV-1 has been traced to distinct zoonotic transmission events between chimpanzees (*Pan troglodytes*) or gorillas (*Gorilla gorilla*) and humans, thus resulting in broad heterogeneity within the HIV-1 classification (Keele, 2006; D'arc, 2015). HIV-1 can be divided into 4 phylogenetically distinct groups M, N, O, and P. While groups N, P and O infections are generally rare or endemic, group M viruses are recognised as the main protagonists of the global AIDS pandemic (Leys, 1990; Mauclère, 1997; Simon, 1998; Plantier, 2008; Vallari, 2011; Sharp, 2011). HIV-1 group M viruses can be further differentiated into subtypes A-K and circulating recombinant forms (CRFs) based on variations in the nucleotide sequences encoding the viral envelope protein (*env*) and(or) other regions of the viral genome (Hemelaar, 2004). In addition to geographically distinct distribution patterns, these HIV-1 group M subtypes have also been linked to variable rates of disease progression and varied responses to antiretroviral therapy, suggesting that the genetic variability within HIV-1 viruses may contribute to variations in the molecular pathology of HIV infection (Kanki, 1999). For the purpose of this thesis all future references to HIV/HIV-1 will refer to HIV-1 Group M viruses, unless otherwise stated.

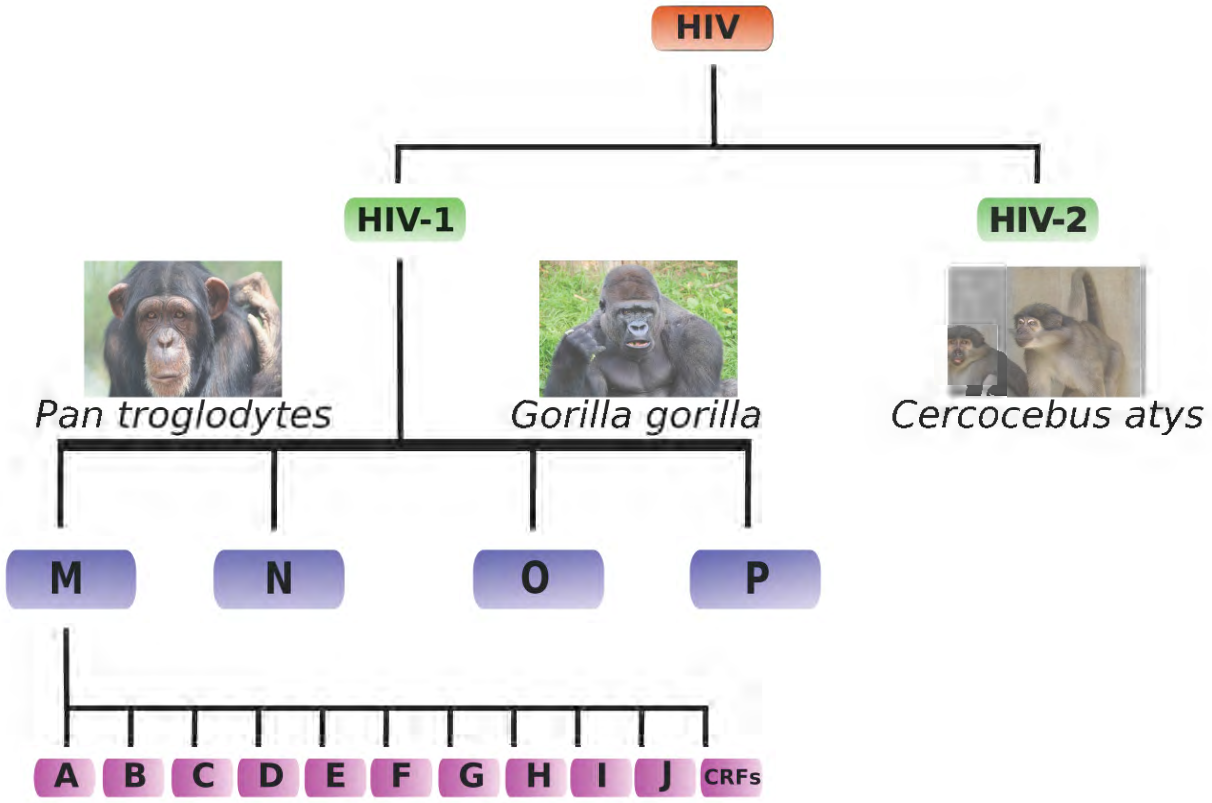

Figure 1.1. Phylogenetic diversity of HIV.

HIV is comprised of two genetically distinct strains: HIV-1 and HIV-2. These strains originated from distinct zoonotic transfer events traced to Chimpanzees (*Pan troglodytes*) and Gorillas (*Gorilla gorilla*) for HIV-1 and Sootey mangabeys (*Cercocebus atys*) for HIV-2. HIV-1 is the most widespread strain and can be divided into 4 phylogenetically distinct groups (M, N, O, P). Group M viruses are responsible for the global HIV pandemic and these can be further divided into genetically distinct subtypes (A-J) and circulating recombinant forms (CRFs).

1.3 Natural history of infection

A single HIV-infected $CD4^+$ T cell is estimated to be capable of producing 5 x 10^4 virions per day with a half life of ~1.6 days (Perelson, 1996; De Boer, 2010). A single infection event is thus sufficient to catalyse a graduated de-regulation of the host immune response, which is characteristic of HIV pathogenesis (Coffin, 2013). The eclipse phase occurs within the first 2 weeks of infection, and is characterised by asymptomatic replication and dissemination of the virus within specific lymphoid tissues, thus establishing stable reservoirs of infection (Coffin, 2013). The next phase, the acute phase, generally occurs 2-4 weeks following initial infection and is characterised by a peak in viral replication and a corresponding depletion of the circulating $CD4^+$ T cell population (Little, 1999). Additionally, patients may exhibit flu-like symptoms, consistent

with the production of antibodies against HIV proteins (seroconversion), and mobilisation of $CD4^+$ T cell populations that facilitate further spread of the virus (Gurunathan, 2009). Viral infection next progresses into a chronic phase of variable length (~10 years) and is preceded by a sharp decline in viral load and partial recovery of the $CD4^+$ T cell population (Coffin, 1995; Coffin, 2013). During this phase, a set point of viral load is established along with a balance between restricted viral replication and gradual $CD4^+$ T cell decline, which is maintained by a functional host immune system (Pantaleo, 1993; Coffin, 2013).

Rapid depletion of $CD4^+$ T cells to levels below ~200 cells per cubic millimeter (mm^3) of blood, and subsequent failure of the host immune system characterise this final stage and progression to an AIDS phenotype. Intriguingly, while the HIV replication cycle itself ultimately results in the death of productively infected cells, massive depletion of the global $CD4^+$ T cell population is largely attributed to non-productive infection events within bystander cells (Finkel, 1995; Doitsh, 2014; Monroe, 2014). In response to the rapid $CD4^+$ T cell decline, steady production of new virus is predominantly supported by productively infected macrophage populations, which are comparatively long lived (Coffin, 2013). During this stage, unrestricted viral replication and $CD4^+$ T cell decline lead to immunodeficiency rendering the afflicted individual highly susceptible to opportunistic infections that result in mortality in the absence of ARV intervention (Coffin, 2013).

1.4 HIV genome and structure

The complete sequence of the HIV-1 genome was first described in 1985 and contains a long terminal repeat region preceding 9 open reading frames (ORFs) that encode 15 viral proteins (Ratner, 1985; Wain-Hobson, 1985). The viral genes *env, pol* and *gag* encode proteins that undergo a post-translational cleavage process to produce shorter functional products, while the remaining genes encode the accessory proteins Nef, Rev, Tat, Vif, Vpr and Vpu (Figure 1.2.). Cleavage of the *env*-derived polyprotein (gp160) gives rise to gp41 and gp120 proteins (McKeating, 1989). The protein product of *pol* produces the viral enzymatic proteins integrase (IN), reverse transcriptase (RT) and protease (PR), which are three of the major targets of current ARVs (Jacks, 1988). *Gag*-derived polyprotein cleavage results in the production of capsid-associated structural proteins p24 (CA), p17 (MA), p7 (NC) and p6 (Göttlinger, 1989). Two copies of the single-stranded, positive sense RNA genome, along with selected viral proteins, are encapsulated within a conical inner core (CA), which lies within a protein matrix (MA) surrounded by an outer coat consisting of host cell-derived plasma membrane and viral proteins gp120 and gp41 (Figure 1.3.). The inner viral core is estimated to be roughly 119 x 60 nm in size while the complete mature virion is reported to have an average diameter of 145 nm with projections extending ~7.5 nm from the surface of the outer membrane (Briggs, 2003). These outer projections consist of trimeric gp120 molecules

anchored by transmembrane gp41 heterodimers and constitute the effector molecule of the receptor-mediated entry step in the replication cycle of HIV-1 (McKeating, 1989; Kwong, 1998).

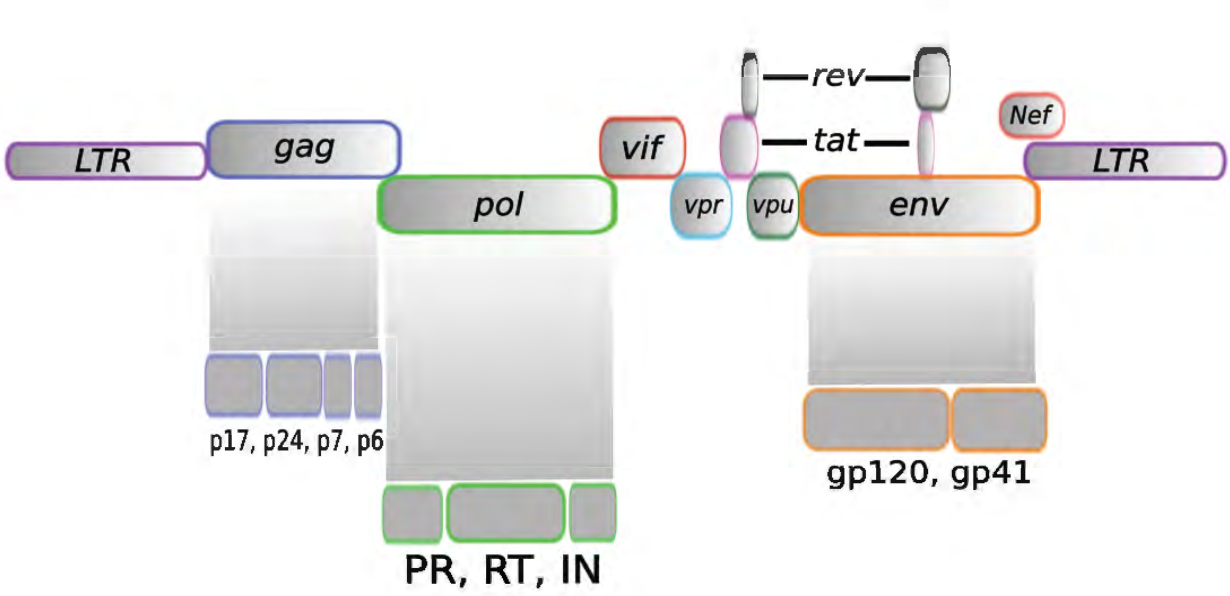

Figure 1.2. Structure of the HIV genome.

The HIV genome is roughly 9.7 Kb in length and contains 9 genes encoding 15 proteins, flanked on either end by a long terminal repeat sequence (LTR). The *gag*, *pol* and *env* genes encode polyproteins that undergo enzymatic cleavage to produce the structural elements p17 (MA), p24 (CA), p7 (NC), p6; the viral enzymes Protease (PR), Reverse transcriptase (RT) and Integrase as well the envelope proteins gp120 and gp41. The HIV genome also encodes 2 regulatory proteins, Tat and Rev as well as the accessory proteins Nef, Vif, Vpr and Vpu.

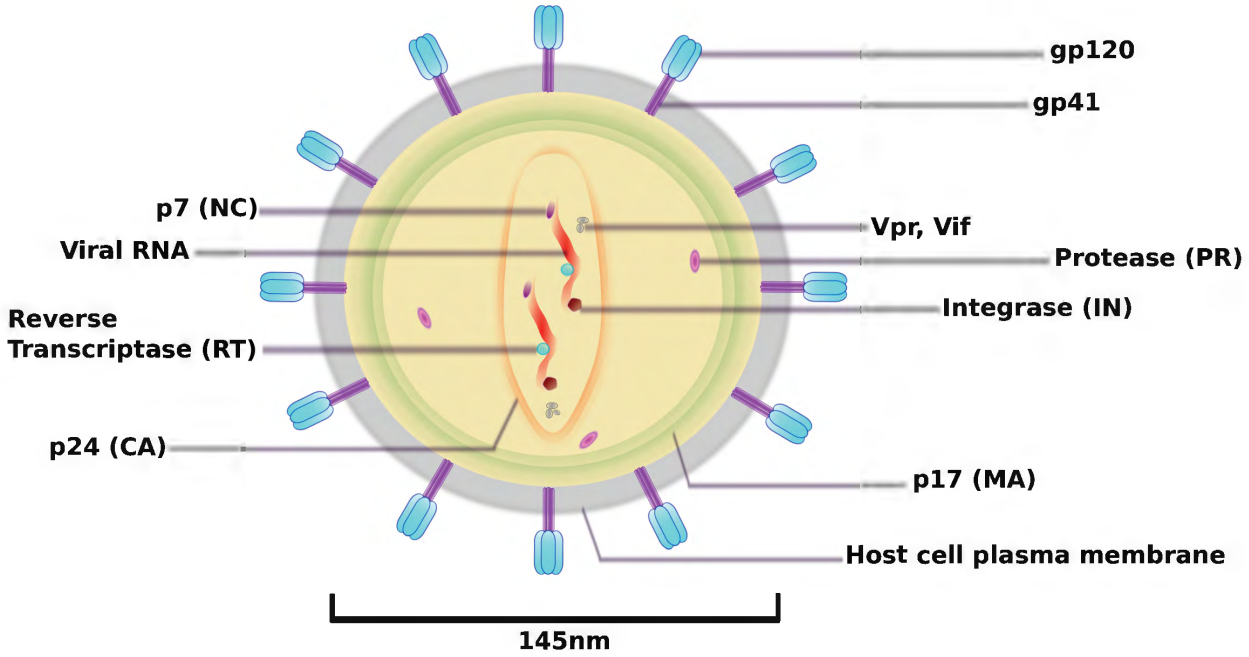

Figure 1.3. Structure of a mature HIV virion.

The HIV virion is ~145 nm in diameter and consists of 3 layers, the first is a host-derived outer membrane that contains the viral envelope proteins gp120 and gp41. The second structural layer is comprised of the viral matrix protein (p17) that protects and stabilizes the 3rd structural element, the viral core. The viral core is a conical structure made up by the viral capsid protein (p24), and houses the two positive RNA strands that constitute the viral genome bound to p7 (NC) along with specific viral factors (RT, IN, Vif, Vpr).

1.5 HIV replication cycle

Successful completion of the HIV replication cycle relies on a series of spatially and temporally coordinated interactions between host and pathogen, culminating in the production of infectious virions (Figure 1.4.). The last 30 years of HIV research have dramatically enhanced our understanding of the dynamic nature of the viral life cycle and have driven development of the current arsenal of ARVs (Arts, 2012).

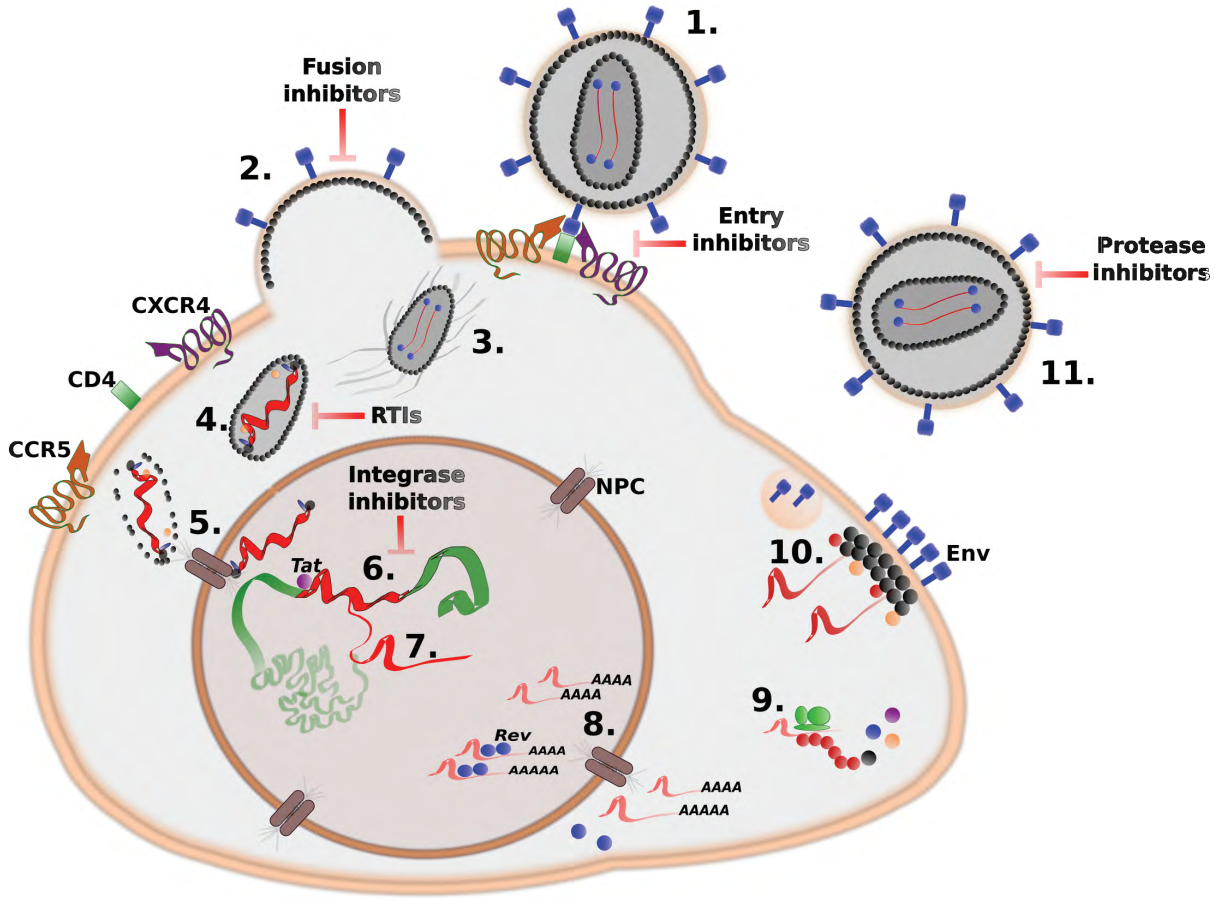

Figure 1.4. The HIV replication cycle.

1) Host cell receptor engagement.:The gp120 trimers on the surface of a mature virion bind the host cell surface receptor CD4 promoting a conformational change in gp120 and the binding of a co-receptor (either CXCR4 or CCR5). **2) Membrane Fusion:** Coreceptor binding triggers the gp41 mediated fusion of the viral and host membranes thus introducing the viral capsid into the cytosol **3) Intracellular trafficking:** The viral capsid proteins engage the host microtubule network in order to promote the trafficking of the viral core toward the nuclear membrane **4) Reverse transcription:** HIV RT begins to convert the viral RNA genome into a DNA intermediate via reverse transcription **5) Uncoating and Nuclear entry:** The docking of the capsid at the NPC results in the disassembly of the viral core and capsid mediated interactions with NPC proteins then facilitates the nuclear import of fully reverse transcribed viral preintegration complex (PIC) **6) Integration:** The PIC-NPC-LEDGF association facilitates proviral integration into transcriptionally active regions of host chromatin via the activity of HIV integrase **7) Transcriptional activation:** Tat mediated transactivation of the HIV LTR promoter results in the stabilized transcription of viral genes **8) Transcript processing and nuclear export:** Transcripts undergo 5' capping and 3' polyadenylation steps, Rev mediated nuclear export is utilised by unspliced transcripts and the canonical host mRNA export pathway utilised by spliced transcripts **9) Translation of viral proteins:** Translation of viral products is completed by the host ribosomal machinery **10) Virion**

assembly and budding: The newly synthesized viral proteins, predominantly polyprotein precursors, are localised to the host cell membrane by the Gag precursor which also recruits full length RNA transcripts that serve as the viral genome, Env is expressed at the cell surface via the endogenous secretory pathway and the budding of new virions is initiated by Gag-mediated subversion of the host ESCRT machinery **11) Maturation:** The cleavage events induced by HIV protease results the liberation of functional protein units from the polyprotein complexes and the subsequent rearrangement of these units to form a 3 layered structure (Figure 1.3) results in the maturation of the now infectious virion. Currently available **ARVs** are able to target specific stages of the viral life cycle, namely, receptor engagement (1), the fusion step (2), the reverse transcription process (4), integration of the PIC (6) and protease mediated maturation (11).

1.5.1 Entry

The gp120 subunits of HIV Env have a high affinity for the CD4 receptor, which is expressed by a number of cell types specifically associated with cell-mediated immunity including macrophages, antigen-presenting dendritic cells and T lymphocytes. The binding of gp120 to its primary receptor CD4 results in a conformational change in the variable loop regions of gp120, thereby exposing a secondary binding domain for a chemokine coreceptor (Kwong, 1998). Depending on the tropism of the virus this can either be a CXCR4 or CCR5 receptor, while dual tropic viruses are able to utilize either receptor (Connor, 1997; Keele, 2008).

The fusion of viral and host membranes is catalysed by gp41, which undergoes a conformational change in response to gp120 coreceptor engagement (Herold, 2014). This conformational change results in exposure of the gp41 fusion domain and its subsequent insertion into the target host membrane, thus creating a membrane fusion pore (Chan, 1998). Formation of the membrane fusion pore facilitates the injection of the viral core into the cytosol, thus completing the entry process (Figure 1.4; Chan, 1998). There are currently a number of ARVs within the drug development pipeline that function as either inhibitors of viral fusion or antagonists of receptor binding (Arts, 2012). Maraviroc, an antagonist of the CCR5 coreceptor, was the first host-directed anti-HIV therapy approved for use by the FDA in 2007, while Enfuvirtide, a gp41-binding peptide, was the first fusion inhibitor approved for use in 2003 (Arts, 2012).

1.5.2 Reverse transcription and uncoating

The processes of reverse transcription and nuclear import are tightly coupled to viral capsid degradation (uncoating). Studies utilizing various p24 (CA) stabilisation mutants have demonstrated that either delayed or premature uncoating can negatively impact the reverse transcription process (Arhel, 2010a; Hulme, 2011; Ambrose, 2014). This relationship is further validated by the antiviral activity of the non-human primate cellular restriction factor tripartite motif 5-alpha (Trim5-α). Trim5-α, was initially identified as a

key determinant of HIV-1 resistance in monkey cells as a result of its ability to promote rapid and premature degradation of the HIV-1 capsid both *ex vivo* and *in vivo* (Anderson, 2008; Stremlau, 2004; Stremlau, 2006).

Following entry into the cytoplasm, viral capsid proteins are able to engage the microtubule network in order to promote cytoplasmic shuttling of the capsid structure towards the nuclear membrane (Gaudin, 2013). During the transit phase to the nuclear membrane, the viral capsid may remain fully intact or become partially degraded, but eventually plays a role in the downstream nuclear import process (McDonald, 2002; Arhel, 2007; Yamashita, 2009; Matreyek, 2013). The reverse transcription process is completed prior to complete dissociation of the capsid, and molecular rearrangements within the capsid resulting from reverse transcription may contribute to the uncoating processing (Arhel, 2007; Hulme, 2011). HIV RT possesses both DNA polymerase and RNase-H functionality, which it utilises to convert the single stranded viral RNA genome into a double-stranded DNA intermediate (Furfine, 1991; Sarafianos, 2008; Hu, 2012). This process occurs within the nucleoprotein structure known as the Reverse Transcription Complex (RTC) and is dependent on a host transfer RNA (tRNA) primer (Lys3) along with the recruitment of deoxynucleoside triphosphate molecules (dNTPs) to the viral RNA template (Furfine, 1991; Kleiman, 2002; Sarafianos, 2008).

Reverse transcription is estimated to occur over a 10 hour period following viral entry and culminates in conversion of the RTC into the preintegration complex (PIC) (Arts, 2012; Hu, 2012). It is during this time frame that the virus is susceptible to therapeutic intervention using reverse transcription inhibitors (RTIs) and ~50% of all currently approved anti-HIV therapies are comprised of RTIs (Pincus, 1990; Klarmann, 2000; Arts, 2012). RTIs (Figure 1.4) can be divided into two classes of molecules, nucleoside reverse transcriptase inhibitors (NRTIs) and non-nucleoside reverse transcriptase inhibitors (NNRTIs). In the absence of RTI intervention, the newly formed PIC, comprised of a full-length viral DNA genome bound to MA, Vpr and integrase, is primed for nuclear entry (Vandegraaff, 2006; Al-Mawsawi, 2007).

1.5.3 Nuclear import

The nuclear pore complex (NPC) is a highly structured multiprotein assembly that functions as a selective barrier to bidirectional nuclear transport (Allen, 2000). The size of the PIC naturally precludes it from passively traversing through the nuclear membrane but HIV has acquired the ability to actively transport the PIC through nuclear pores (Pante, 2002; Matreyek, 2013). The ability to traverse an intact nuclear membrane permits HIV to efficiently infect terminally differentiated and non-dividing cells types like macrophages and dendritic cells, in addition to T lymphocytes (Yamashita, 2009; Lahaye, 2013; Rasaiyaah, 2013). The nuclear trafficking process is largely mediated by the viral capsid protein and is initiated by the interaction of the HIV capsid with the cytoplasmic extensions of the NPC protein Nup358 (Yamashita, 2009; Di Nunzio, 2012;

Matreyek, 2013). The CA-Nup358 interaction permits docking and subsequent disassembly of the viral capsid at the nuclear pore and likely facilitates a series of downstream interactions with various NPC-associated components localized along the nuclear pore channel. Nup98 which is present in both the cytoplasmic and nuclear domains of the channel likely functions as an intermediary binding partner between the cytoplasmic nucleoporins and the intranuclear and chromatin-associated proteins like Nup153 and Nup155 (Lee, 2010; Ambrose, 2014). These PIC-nucleoporin interactions result in translocation of the PIC through the mesh-like filaments that constitute the central domain of a nuclear pore (Walther, 2002; Di Nunzio, 2012; Matreyek, 2013). Specific interactions between CA and host proteins have also been identified as key determinants of NPC cofactor selection. The interaction of CA and Cyclophilin A (CypA) in addition to stabilising the cytosolic capsid, has been identified as a mediator of downstream interactions with Nup358, Nup153 and TNPO3 (Schaller, 2011; Rasaiyaah, 2013; Ambrose, 2014). Likewise, a functional cleavage and polyadenylation specificity factor 6 (CPSF6) binding domain on CA has also been identified as a determinant of nucleoporin usage (Nup358, TNPO3) as well a requirement for the infection of non-dividing cell types (Lee, 2010; De Iaco, 2013; Shah, 2013).

1.5.4 Integration

Following nuclear entry, the HIV PIC must integrate into the host cell's DNA in order to complete the next stage of the viral replication cycle. A number of studies have demonstrated that the site of HIV integration is not entirely random and that HIV preferentially integrates into transcriptionally active regions of host chromatin (Schroder, 2002; Wang, 2007; Sherrill-Mix, 2013; Marini, 2015). CA-NPC interactions along with the lens epithelium-derived growth factor (LEDGF/p75) function as a critical determinants of HIV integration site selection (Ciuffi, 2005; Shun, 2007; De Rijck, 2010; Lee, 2010; Schaller, 2011; De Iaco, 2013; Matreyek, 2013). Following nuclear entry the sustained interaction between the PIC and NPC brings the PIC into close proximity with structurally relaxed and transcriptionally active chromatin regions (Marini, 2015). HIV integrase is then directed to specific transcriptionally active recognition sites by its interaction with LEDGF, which functions both as a molecular tether and guide during the integration process (Maertens, 2003). Integration is initiated by a 3' processing event where 2 nucleotides are removed from each 3' end of the viral DNA genome (Craigie, 2001). The 3' processing event exposes a pair of 3'-hydroxyl groups on the viral DNA which are required for a subsequent strand transfer step. During the DNA strand transfer step, the exposed hydroxyl groups on the viral DNA attack a pair of phosphodiester bonds in the proximal host DNA resulting in a covalently bound viral/host DNA intermediate (Craigie, 2001). The 3' resectioning and strand transfer events are mediated by HIV integrase but the subsequent events of strand repair and ligation are completed by the host DNA repair machinery (Craigie, 2001; Espeseth, 2011). Integrase inhibitors interact with both the viral DNA and integrase thereby disrupting the integrase active site via magnesium ion sequestration (Figure 1.4; Grobler, 2002).

1.5.5 Transcriptional activation

The integrated HIV genome (referred to as the provirus) serves as a template for transcription of viral genes. The 5' HIV LTR functions as the main viral promoter while the 3' LTR plays a role in termination of transcription and subsequent polyadenylation events (Pereira, 2000; Gilmartin, 1995). The 5' and 3' LTR sequences are identical and comprised of 3 domains, a unique 3' end (U3), a repeat domain (R) and a unique 5' end (U5) (Figure 1.5; Pereira, 2000). The U3 domain contains an extensive number of host transcription factor binding sites and can be further differentiated into a modulatory region, an enhancer region and a core promoter region (Rittner, 1995; Pereira, 2000; Krebs, 2001). Notably the enhancer region contains two NFKβ binding sites, while the modulatory region encodes binding sites for constitutive and inducible transcription factors including SP1 and NFAT respectively (Krebs, 2001). A TATA box is located 25 base pairs (bp) upstream of the transcriptional start site (TSS) within the core promoter region of U3 (Garcia, 1989). The TSS is present at the junction between the U3 and R domains, and the first 60bp of the R domain following the TSS contains the transactivating responsive (TAR) element (Pereira, 2000). The TAR element encodes a nuclease-resistant stem looped RNA transcript (TAR RNA) which is present at the 5' end of all viral transcripts and functions as a molecular scaffold and regulatory signal (Berkhout, 1989; Selby, 1989). Of particular importance to the viral transcription process, TAR RNA serves as a recruitment signal for the HIV transactivating protein (Tat), which facilitates stabilized proviral transcript elongation (Sodroski, 1985; Feinberg, 1991).

LTR-mediated transcription is initiated by assembly of the transcriptional pre-initiation complex at the core promoter region. Briefly, TFIID, which contains the TATA box binding protein (TBP), is first recruited to the promoter followed by TFIIA and TFIIB, which function to stabilize the interaction between TFIID and the promoter DNA (He, 2013). RNA polymerase II (RNAPII) is then recruited to the growing complex along with TFIIF (He, 2013). Subsequent recruitment of TFIIE and TFIIH completes assembly of the pre-initiation complex, which then facilitates targeting of RNAPII to the TSS, transcriptional initiation and promoter clearance (Matsui, 1980; Goodrich, 1996; Roeder, 1996). In the absence of Tat, restricted RNAPII activity (in part due to inhibition by the negative regulator of elongation NELF) results in a high number of abortive or truncated transcripts (Zhou, 2000; Williams, 2006; Zhang, 2007). This low level of transcriptional activity is however sufficient to produce the viral proteins Tat and Rev. Following its translation and nuclear localisation, recruitment of Tat to TAR RNA loop structures results in an interaction between Tat, the positive transcription elongation factor complex (pTEF-b) and the TAR RNA scaffold (Dingwall, 1990; Wei, 1998). The pTEF-b complex is composed of a catalytic cyclin dependent kinase (CDK) 9 subunit and a regulatory cyclin T1 subunit (Marshall, 1996; Wei, 1998).

Tat is able to directly bind cyclin T1 and the T loop of CDK9 thus recruiting pTEF-b to the TAR RNA structures on nascent viral transcripts (Tahirov, 2010). Tat binding results in a conformational change and constitutive activation of CDK9 (Zhou, 2000; Tahirov, 2010). The Tat-activated pTEF-b complex then executes a series of phosphorylation events, including phosphorylation of the RNAPII subunit Rbp1, at serines 2 and 5 of the carboxy terminal domain, as well phosphorylation and inactivation of NELF (Fujinaga, 1998; Kim, 2002; Zhou, 2000). Stabilisation of RNAPII activity and interaction of the TAR complex with additional host coactivators like ELL2 then dramatically enhances proviral transcription (Kim, 2002; He, 2010). High levels of proviral transcription create a positive feedback loop of Tat-mediated transactivation, which can result in a nearly 100 fold increase in transcript elongation capacity (Feinberg, 1991). Tat-mediated transcription is still however highly dependent on host transcriptional initiation processes, and conditions that may perturb global transcription (such as cellular quiescence) have a knock-on effect of diminishing Tat availability. Reduction of Tat levels below a critical threshold can result in halted proviral transcription and a transition into a dormant state referred to as latency (Karn, 2011). Latency represents the primary obstacle to curative treatment of HIV and a conserved survival strategy employed by HIV where stochastic gene expression from the HIV LTR during the early stages of infection functions as determinant of latency (reviewed by Weinberger, 2015).

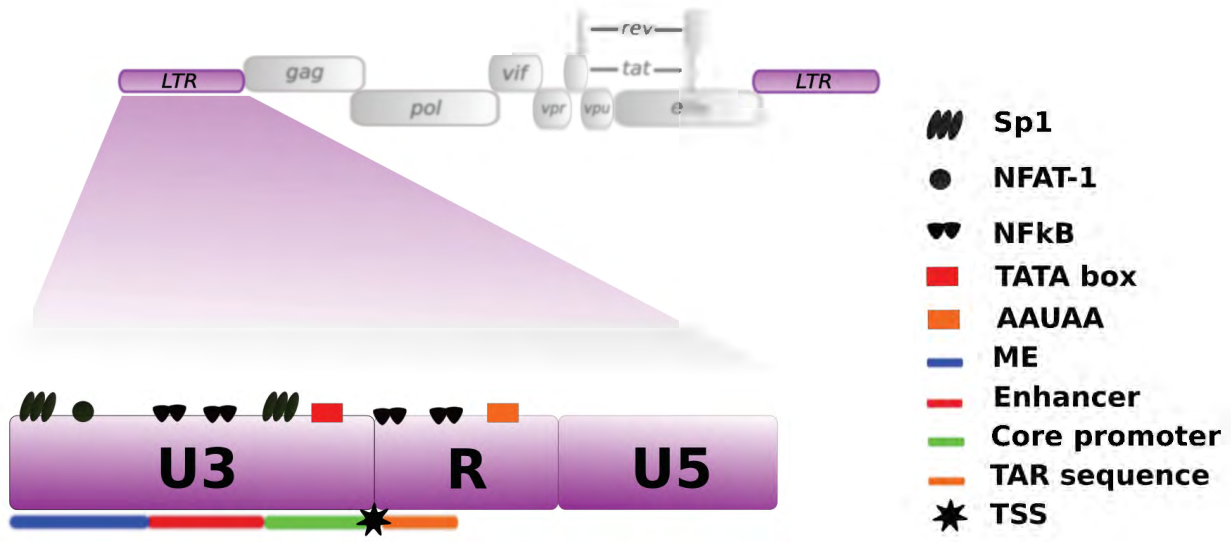

Figure 1.5. Structure of the HIV LTR.

The HIV LTR is ~640 bp in length and can be divided into 3 distinct domains: the unique 3 (U3) region, the repeat domain (R) and the unique 5 domain (U5). The U3 domain can be further segmented into the Modulatory Element region (ME), the enhancer region and a core promoter region. Key landmarks within the LTR include Sp1 transcription factor binding sites in the ME and core promoter regions, an NFAT binding site in the ME, pairs of NFKβ binding sites in the enhancer region and R domain respectively, a TATA box in the core promoter region, a transcriptional start site (TSS) located at the junction of the U3 and R domains, a TAR sequence within the first 60 bp of the R domain, and an AAUAAA polyadenylation signal in the R domain.

1.5.6 RNA processing and nuclear export of viral transcripts

Much like their host counterparts, HIV transcripts also undergo post-transcriptional processing in order to enhance stability and facilitate their nuclear export and downstream functions (Gilmartin, 1995; Gontarek, 1996; Yedavalli, 2010). Post-transcriptional processing may involve 3 main modifications: i) 5' capping (Gu, 2005; Ghosh, 2011; Picard-Jean, 2013), ii) 3' polyadenylation and iii) splicing (Colgan, 1997). The 5' cap is acquired during transcription and subsequently functions to regulate nuclear export, confer immunity to ribonuclease cleavage and eventually serves as a recognition element for protein translation and mRNA turnover (Gu, 2005; Ling, 2011; Topisirovic, 2011).. The polyadenylation process is initiated by recruitment of host polyadenylation machinery to the polyadenylation signal (AAUAAA) encoded within the R domain of the HIV 3' LTR (Gilmartin, 1995; Millevoi, 2010). Identical signals are present in both 5' and 3' LTR sequences, and HIV has thus evolved a number of regulatory mechanisms to ensure preferential use of the 3' LTR signal and silencing of its 5' counterpart (Ashe, 1995; Gilmartin, 1995; Das, 1999; Valente, 2009). The poly(A) modification plays an important role in transcript stabilization and translation, and is critical to nuclear export of fully spliced HIV transcripts which utilise the endogenous mRNA nuclear export pathway (Bilodeau, 2001; Millevoi, 2010; Stewart, 2010; Katahira, 2012).

HIV exploits the host's endogenous spliceosome machinery in order to produce a diverse selection of RNA variants from a limited viral genome (Schwartz, 1990a; Purcell, 1993; Stoltzfus, 2006; Ocwieja, 2012). These RNA species can be differentiated into 3 categories i) unspliced, ii) partially spliced and iii) completely spliced. The transcripts that encode the Gag-Pol polyprotein also serve as full-length genomic RNA for new virions and remain unspliced at ~9 kb (Schwartz, 1990a; Purcell, 1993). The transcripts that encode Env, Vif, Vpr and Vpu are partially spliced to produce ~4 kb products, and Tat, Rev and Nef are translated from ~1.8 kb fully spliced RNA transcripts (Schwartz, 1990b; Purcell, 1993). Rev binds and then oligomerises at the RRE present in unspliced and partially spliced HIV transcripts (Zapp, 1991; Daugherty, 2008). This precludes viral transcripts from interacting with the spliceosome and also facilitates their nuclear export (Hadzopoulou-Cladaras, 1989; Felber, 1990; Gontarek, 1996). Rev oligomer-bound transcripts are able to interact with the karyopherin exportin-1 (XPO1), also known as chromosomal maintenance 1 (CRM1), thus facilitating nuclear export of these transcripts via the NPC (Wolff, 1997; Daugherty, 2010). The Rev-RRE complex dissociates upon cytoplasmic entry and released Rev monomers are then transported back into the nucleus (Henderson, 1997). The intranuclear Rev concentration thus functions as a molecular switch that regulates the balance between spliced and unspliced transcripts.

1.5.7 Translation

Eukaryotic translation is initiated by recognition of the 5' cap structure by the eukaryotic initiation factor 4E complex (eIF4E) and subsequent interactions with eIF4G, eIF4A, eIF4B and poly(A) binding protein (PABP) (reviewed by Jackson, 2010 and Hinnebusch, 2014). Despite the fact that HIV has acquired mechanisms such as 5' capping and 3' polyadenylation, which allow it to effectively utilise the host translational machinery, there are still a number of unique requirements for successful translation of viral transcripts (Schwartz, 1990b; Purcell, 1993). Structures produced by the TAR sequence, poly(A) loop, tRNA primer binding site and the RNA packaging signal (ψ) naturally preclude the translation initiation process. However, HIV has evolved a number of strategies to circumvent this (Schwartz, 1990a; Purcell, 1993; Lu, 2011). The use of an internal ribosome entry site (IRES) allows HIV to bypass the canonical cap-dependent initiation process and 5' UTR scanning, while the TAR loop secondary structure present in all HIV transcripts functions as a docking site for the pre-initiation machinery (Brasey, 2003; Plank, 2014). Additionally HIV is able to regulate the production levels of specific proteins like Env and Gag by selectively utilising ribosomal shunting (Schwartz, 1990b; Krummheuer, 2007) and ribosomal frameshifting respectively (Parkin, 1992; Dulude, 2006; Namy, 2006).

1.5.8 Assembly, budding and maturation

The Env precursor (gp160) is heavily glycosylated and processed into gp120 and gp41 subunits by the host protease Furin as it traverses the golgi complex (Decroly, 1994; Moulard, 1999). Env is ultimately integrated into lipid raft domains within the host cell membrane by the endogenous secretory pathway (Campbell, 2001). Gag precursors (p55) undergo a myristoylation step which directly targets them to the cell membrane along specific viral and host factors bound by Gag (Frankel, 1998; Freed, 2001; Ono, 2004; Saad, 2006). The ψ packaging signal is present upstream of *gag* in unspliced full length viral transcripts and is recognised by the RNA binding domain of Gag thus facilitating the inclusion of full length viral RNA into budding virions (Lu, 2011; Chen, 2014a). Gag monomers and dimers are trafficked through the cytoplasm to the cell membrane but extensive Gag multimerization only occurs at the cell membrane with Gag-bound RNA serving as points of nucleation (Jouvenet, 2009). Viral mediated subversion of endosomal sorting complexes required for transport (ESCRT) machinery facilitates membrane remodelling and fission processes that are required for virion release (Usami, 2009; Carlson, 2010; Hurley, 2010; Peel, 2011). Budding occurs with the release of an enveloped virion containing a spherical array of Gag molecules bound to two RNA genomes, host and viral proteins and Gag-Pol precursors (Bell, 2013). Virion maturation occurs post-release and is dependent on an initial autocatalytic cleavage event which liberates the HIV PR to then produce MA, CA, NC, p6, IN and RT (Hill, 2005; Bell, 2013). Pharmacological inhibition of HIV Protease cleavage inhibits virion

maturation and protease inhibitors are designed to competitively bind and sequester the active sites of HIV PR molecules (Figure 1.4; Brik, 2003).

1.6 Viral accessory proteins

The accessory proteins expressed by HIV are able to exert a broad range of effects which ultimately synergise to create a favourable intracellular environment for viral replication via inhibition of specific host restriction factors and subversion of essential host processes (Strebel, 2013; Laguette, 2015). These effects are summarized below:

Vif

The human apolipoprotein B mRNA-editing enzyme-catalytic polypeptide-like 3 (APOBEC3) family is comprised of 7 cytidine deaminases which function as innate cellular restriction factors of retroviral infection (Munk, 2012). The APOBEC3G protein in particular has a well characterised ability to suppress HIV replication (Malim, 2009). APOBEC3G molecules are able to localise within HIV virions by binding viral and host RNA transcripts that are readily bound by HIV Gag (Cen, 2004). The cytidine deaminase activity of APOBEC3G promotes hypermutation of the HIV DNA genome within virions, resulting in a replication-deficient virus (Malim, 2009). However, this restriction mechanism is effectively countered by the activity of HIV viral infectivity factor (Vif) during the natural course of infection (Sheehy, 2002). Vif is able to significantly deplete intracellular levels of APOBEC3G thus dramatically reducing the chance that APOBEC3G molecules might be packaged within budding virions (Mangeat, 2003; Zhang, 2003). Cellular depletion of APOBEC3G is achieved both by suppressing translation of APOBEC3G mRNAs, and by directly targeting cellular reservoirs of APOBEC3G for ubiquitin-mediated degradation (Stopak, 2003; Yu, 2003). Additionally Vif has recently been demonstrated to suppress the cytidine deaminase activity of APOBEC3G in a degradation-independent manner within nascent virions (Wang, 2014). In combination with the observation that Vif-deficient viral strains exhibit a severely impaired ability to produce infectious virions (Strebel, 1987; Sheehy, 2002), Vif is clearly an indispensable tool within the HIV replication process.

Vpu

HIV viral protein U (Vpu) functions as the viral countermeasure to the host restriction factor bone marrow stromal antigen 2 (BST-2) also known as tetherin (Neil, 2008). Tetherin is a transmembrane lipid raft-associated protein, which prevents release of mature virions from virus-producing cells resulting in their attachment to the cell surface (Neil, 2008). Therefore, while tetherin may suppress the cell-free spread of HIV, it has been demonstrated to have little effect on cell-to-cell transmission of HIV and thus may not significantly impact viral replication kinetics (Terwilliger, 1989). The exact mechanism

by which Vpu is able to antagonise tetherin remains unclear but one school of thought suggests that Vpu may facilitate deregulation of tetherin recycling, thus reducing its availability at the cell membrane (Dube, 2011). Additionally a direct interaction between Vpu and CD4 within the ER results in the rapid degradation of nascent CD4 protein, thereby suppressing its expression at the cell surface and enhancing viral release and dissemination (Willey, 1992; Bour, 1995).

Vpr

Viral protein R (Vpr) has been identified as the effector of a diverse set of molecular processes that are required during the early stages of HIV infection (Guenzel, 2014). This is further supported by the fact that Vpr is actively recruited into budding virions via its interaction with Gag (Bachand, 1999). Vpr activity has been described to be particularly relevant for efficient replication of HIV within macrophages via its roles in nuclear import, stabilisation of reverse transcription and enhancement of integrase-independent integration (Connor, 1995; Eckstein, 2001; Chen, 2004; Koyama, 2013). Additional functions of Vpr have been reviewed extensively and include induction of DNA damage, subversion of host DNA repair machinery, regulation of HIV-mediated apoptosis, and transcriptional regulation (Guenzel, 2014). Furthermore, Vpr activity has long been implicated in HIV-associated G2 cell cycle arrest in proliferating cell types, and recent findings have demonstrated that Vpr-mediated activation of the endonuclease regulatory complex (SLX4) promotes cell cycle arrest in addition to its primary purpose of masking non-integrated viral DNA from innate immune sensors within infected cells (Guenzel, 2014; Laguette, 2014).

Nef

The HIV negative effector factor (Nef) has been implicated as a master coordinator of cell surface receptor localization and stability, as well as downstream receptor-mediated signaling processes (Landi, 2011). Nef is thus able to mediate a wide array of molecular effects within different cell lines. Notably, interaction of Nef with adapter proteins 1 and 2 (AP-1 and AP-2) facilitates clathrin-mediated endocytosis of CD4, CD8 and major histocompatibility complex (MHC) receptors (Roeth, 2004; Jin, 2005). Enhanced endocytosis of CD4 serves to complement Vpu-mediated degradation of nascent CD4 proteins, restrict superinfection, promote virion release and also suppress T cell activation signals in response to infection (Zhou, 2003; Michel, 2005). Likewise, down-modulation of MHC and CD8 proteins at the cell surface retards the antigen-presenting capability of infected cells and masks them from cytotoxic immune cells, thus subverting the host immune response to infection (Landi, 2011). In addition to its ability to sequester target proteins from the cell surface, Nef also promotes enhanced stability of gp41 and gp120 at the cell membrane of infected cells, thus enhancing HIV replication (Lundquist, 2004).

1.7 Current treatment strategies

Current classes of ARV drugs are able to target different stages of the viral replication cycle (Figure 1.4). Diversification of therapeutic targets is essential for the success of current anti-HIV treatment regimes, which consist of a combinatorial ARV (cARV) approach that was first pioneered in 1997 as 'highly active antiretroviral therapy' (HAART; Autran,1997; Delaney, 2006). In the absence of therapeutic intervention, diagnosis with AIDS is typically followed by mortality within 2 years (Osmond, 1994; Crum, 2006). A canonical HAART regimen consists of 2 NRTIs in combination with either a protease or integrase inhibitor, and is usually initiated following the decline of $CD4^+$ T cell levels to ~350 cells per mm^3 of blood (Lederman, 1998; Arts, 2012). The successful implementation of HAART results in a significant suppression of viral replication and subsequent reconstitution of the host immune system (Autran,1997; Komanduri, 1998; Lederman, 1998). The advent of HAART and improved diagnostics have thus dramatically reduced global AIDS-related mortality and improved the life expectancy of afflicted individuals (Palella, 1998; Nakagawa, 2013). However, despite the many benefits of HAART there are still a number of caveats that exist within the current treatment strategy.

The HIV genome evolves at a rapid rate with an estimated 1-10 mutations introduced during each replication cycle (O'Neil, 2002; Abram, 2010). This high rate of viral evolution results in tremendous levels of viral heterogeneity within infected individuals, and has major implications for drug resistance (Coffin, 1995). Indeed early HIV treatments that utilised a monotherapy-based approach, including the first anti-HIV drug AZT, resulted in rapid treatment failure due to the emergence of drug-resistant viral variants (Larder, 1989; St Clair, 1991). The high rate of viral evolution has thus necessitated use of a 3 pronged cARV approach in order to increase the barrier to viral escape by mutagenesis (Autran,1997; Arts, 2012). Alarmingly, a number of HIV variants resistant to frontline components of cARV treatments continue to emerge and remain transmitted in response to ongoing treatment (Wittkop, 2011). These drug-resistant variants have the greatest prevalence in regions such North America and Europe where cARV treatments were first introduced, suggesting that continued use of the current cARV strategy will ultimately drive diversification and dissemination of drug-resistant viral variants across the globe (Frentz, 2012). Additionally, the prolonged use of cARV treatments have also been linked to a number of adverse side effects, including an increased risk of heart disease, diabetes and osteoporosis to name a few (Visnegarwala, 1997; Brinkman, 1998; Henry, 1998; Tebas, 2000). The lifelong use of ARVs, which is required to suppress HIV replication, may therefore also negatively impact of the quality of life for people receiving cARV therapy. Furthermore, the complete eradication of HIV remains beyond the reach of current ARV therapies and is antagonised by low levels of

viral replication and cellular reservoirs of infection that persist even during active cARV treatment (Sharkey, 2001; Palmer, 2003; Alexaki, 2008).

The most well characterized reservoir of infection is comprised of a small populations of latently infected resting $CD4^+$ T cells which are established during the early stages of infection prior to the initiation of cARV treatment (Chun, 1998; Dahabieh, 2013). Latency can be established via a number of molecular mechanisms, such as activation or differentiation state of the cell, transcription factor dynamics, specific host restriction mechanisms, as well repressive chromatin states (reviewed extensively in Alexaki, 2008; Siliciano, 2011). Latently infected cells harbour integrated proviral DNA which is transiently silenced and thus effectively 'hidden' from viral protein targeting drug regimens (Alexaki, 2008; Siliciano, 2011). The extended longevity of these latent reservoirs in combination with their sporadic activation in response to environmental cues perpetuates the lifetime persistence of HIV even in individuals receiving functional cARV treatment (Siliciano, 2003; Strain, 2003). The problem of latency may be further compounded by the prevalence of HIV infectable cell types within anatomical compartments that are poorly accessible to ARVs, such as the central nervous system (CNS) and lymphoid tissues (Vyas, 2006; Schnell, 2009; Alexaki, 2008; Fletcher, 2014). These compartments harbour cell types such as tissue-resident macrophages and CNS-fated immunogenic cells which may also facilitate low levels of viral replication thereby sustaining latent reservoirs even during active cARV treatment (Schnell, 2009; Fletcher, 2014). The cellular reservoirs established by HIV thus necessitate a lifelong treatment programme with a rebound in viral replication reported to occur within a matter of weeks after the cessation of cARV treatment (Davey, 1999). The lack of a viable cure in combination with unsuccessful vaccine efforts and inadequate availability of treatment in many countries portend the continued persistence of the global HIV pandemic (Pitisuttithum, 2006; Burton, 2012; UNAIDS, 2014). As the current state of HIV treatment remains imperfect, it warrants the development of more robust therapeutics in order to surpass the limitations of the traditional virocentric approach to ARV drug discovery.

1.8 HIV-host interactions

As an obligate intracellular pathogen with a seemingly limited arsenal of effector proteins, HIV is highly dependent on the function of certain host factors in order to complete its life cycle (reviewed by Arhel, 2010b and Friedrich, 2011). On the other hand the virus also requires the deregulation of a number of host processes that may prove restrictive to viral replication (Strebel, 2013). Host factors thus serve as critical determinants of the fate of HIV replication as either HIV dependency factors (HDFs) or suppressive viral restriction factors (VRFs). The comprehensive identification and characterization of all host factors that fall into either of these functional classes is therefore of great significance to our fundamental understanding of HIV, as well as the effective exploitation of these host factors for therapeutic gain. VRFs may be exploited

by mimicking or enhancing their restrictive properties as in the case of chimeric Trim5-α variants, while the functional silencing of HDFs via pharmacological or molecular means may likewise be utilised as in the case of the CCR5 antagonist, Maraviroc (Dorr, 2005; Stremlau, 2006; Anderson, 2008).

Indeed host factors present very attractive targets for ARV development as their inherently low mutation rates compared to viral proteins precludes the rapid emergence of drug resistance that has been characteristic of viral targeted therapies (Schwegmann, 2008; Abram, 2010). Furthermore, therapies directed towards HDFs that cannot be circumvented by HIV's flexible use of host factors, may also serve as impermeable barriers to viral escape via simple mutagenesis (Schwegmann, 2008; Arts, 2012). The challenge with host-directed therapy however is twofold. Firstly it requires the identification of specific host factors that can be utilised or modulated to suppress HIV replication. This requirement alone is no simple task when considering the vast number of functional products encoded by the ~3.2 billion bp human genome compared to its ~9 700 bp viral counterpart. Secondly the effective utilisation of host-directed therapy requires the exclusion of host factors that are essential for normal cellular function and whose inhibition or modulation may result in undesired effects (Schwegmann, 2008).

The identification and characterization of HDFs and VRFs have traditionally emanated from the interrogation of HIV-host interactions by focusing on host factors that directly associate with viral proteins and those that are differentially expressed or modulated during infection (Greene, 2007). It has been estimated that the 18 protein products encoded by HIV are able to directly interact with 435 different host proteins, and there are currently also thousands of host factors that are differentially regulated in response to infection (Bosinger; 2004; Jager, 2012; Ako-Adjei, 2015). While still informative, these data do not directly provide functional roles for those host factors during the HIV replicative process. As functional relevance is critical to the identification of therapeutically useful HDFs and VRFs (Friedrich, 2011), this represents a key area of ongoing HIV research.

1.9 Natural restriction of HIV

Scrutinisation of host factors in order to guide ARV development is further justified by the prevalence of unique disease progression phenotypes within ARV-naive subsets of the human population (Okulicz, 2009; Gurdasani, 2014). Rapid progressors (RPs) are generally characterised as individuals who exhibit a $CD4^+$ cell count below 100 cells per μL within the first year of seroconversion and who go on to rapidly develop AIDS within 3-5 years post infection without cARV intervention (Oslon, 2014; Gurdasani, 2014). Long term non progressors (LTNPs) on the other hand are individuals who, in the absence of ARVs, are still capable of maintaining CD4 counts above 500 cells per μL of blood for at least 10 years following HIV infection thus delaying the natural progression to AIDS

(Mikhail, 2003; Westrop, 2009; Gurdasani, 2014). Elite controllers (ECs) constitute a very rare subset (< 1%) of the HIV infected population who are characterised by their ability to spontaneously restrict viral replication (<50 copies per mL) for at least 1-10 years following infection in the absence of cARV treatment (Okulicz, 2009; Walker, 2013). While all of these phenotypes represent intriguing models for the evaluation of host resilience and susceptibility to HIV, delineation of the mechanisms of viremic control in such stratified patients hold great promise for the development of more robust therapies (Baker, 2009; Walker, 2013; Gurdasani, 2014).

A number of host and virological factors have been canonically associated with the natural control of HIV (Blankson, 2010; Poropatich, 2011; Walker, 2013). The exact role of virological factors in viremic control however remains tenuous (Bailey, 2008). While a number of early data points had suggested that LTNPs and ECs may be infected with attenuated viral strains with reduced fitness, recent findings have demonstrated that it is more likely the host response which drives restriction of viral replication as well as emergence of attenuated viral variants (Bailey, 2008; Poropatich, 2011).

Enhanced cell-mediated immunity is essential for sustained elite control of HIV (Blankson, 2010). EC-derived $CD8^+$ cytotoxic T cells effectively suppress HIV replication in $CD4^+$ T cells via the recognition of HIV Gag and EC-characteristic polyfunctional activity that includes improved cytotoxicity, proliferation and autocrine secretion (Walker, 2013). Specifically, the host transcription factor TBX21 has been associated with an increased production of cytotoxic enzymes like perforin and granulysin in EC-derived $CD8^+$ T cells, which also exhibit augmented secretion of interleukin-2 (IL-2; Blankson, 2010; Walker, 2013). The exact role of $CD4^+$ T cells in ECs remains less clear although it has been suggested that they support antiviral activities of HIV-specific $CD8^+$ T cells via secretion of cytokines such as IL-2 and IL-21 (Blankson, 2010; Walker, 2013). Furthermore, macrophages derived from ECs are recalcitrant to productive infection by HIV, but the molecular mechanism behind this phenotype is not yet understood (Saez-Cirion, 2011).

The results from a number of genome-wide association studies to identify known single nucleotide polymorphisms (SNPs) in viremic controllers and RPs have also revealed that SNPs within the human leukocyte antigen (HLA) class I locus are preferentially associated with extreme progression phenotypes (Walker, 2013). Furthermore, the expression of specific HLA alleles, including HLA□B*57, HLA□B*27 and HLA□B*13, have been demonstrated to be relevant to viremic control in some EC populations but not others thus further highlighting the heterogeneity of possible viremic control mechanisms (Poropatich, 2011; Walker, 2013). Additionally, the CDK inhibitor p21, has also been described to contribute to viremic control as a putative viral restriction factor (VRF). An innate and significant upregulation of p21 was observed in $CD4^+$ T cell populations derived from two distinct groups of ECs (Yu, 2011). Elevated p21 expression was demonstrated to inhibit CDK9-dependent viral transcription within one EC group, and subsequent suppression of p21 expression by small interfering RNAs (siRNAs)

rendered EC-derived $CD4^+$ T cells susceptible to viral replication (Yu, 2011). However, direct association of p21 upregulation to viremic control in only one of the two EC groups suggests that p21 activity alone may not be enough to elicit the observed control phenotype, and that additional restriction mechanisms may be at work (Saez-Cirion, 2011). The physiological manifestation of viremic control therefore likely results from the prevalence of specific combinations of favourable host determinants which are able to restrict viral replication on both a molecular level and at the level of the immune response against HIV. While the exact mechanisms remain poorly characterized, the ability to recapitulate these natural restriction phenotypes within HIV infected or HIV naive individuals still represents the "holy grail" of HIV-directed therapy.

Polymorphisms in a number of chemokine coreceptors and their ligands (CCR5, CCR2, CX3CR1 CXCR4) have also been associated with protective HIV phenotypes (Poropatich, 2011). The most well characterised of these is a 32 base deletion in the gene encoding the chemokine coreceptor CCR5 (*CCR5 Δ32*; Liu, 1996). Briefly, the *CCR5 Δ32* mutation is most common in individuals of eastern european descent and results in a nonfunctional protein product (Liu, 1996; Zimmerman, 1997). *CCR5 Δ32* homozygosity confers a high degree of immunity against R5 tropic viral variants that dominate transmission events (Liu, 1996; Zimmerman, 1997). This protective homozygous phenotype was further shown to be transferable via stem cell-mediated transplantation resulting in the long term control of HIV within a previously infected and naturally progressing individual (Hutter, 2009). *CCR5 Δ32* heterozygosity was also initially reported to result in a delayed onset of AIDS, but this phenotype has more recently been called into question (Zimmerman, 1997; Liu, 2012). Likewise the prevalence of a mutation in the promoter region of CCR5 (*CCR5P1/P1*) which results in increased surface expression of CCR5 was shown to account for 10-17% of all rapid progressor (RP) phenotypes, thus further validating the potential of chemokine coreceptors as therapeutically relevant HDFs (Martin, 1998).

1.10 RNAi as a tool to understanding HIV-host interactions

Sequencing of the human genome and subsequent advances in RNA interference (RNAi) and its application within mammalian models facilitated the advent of a new era in functional genomics (Elbashir, 2001; Hannon, 2004). The ability to readily and systematically achieve functional silencing of specific mRNA species by siRNAs or short hairpin RNAs (shRNAs) has provided researchers with a means to evaluate the functional relevance of individual human genes against a backdrop of complex cellular processes using cell-based readouts (Hannon, 2004). In the case of HIV, RNAi was readily adopted to suppress viral replication in cellular models by targeting specific viral-specific RNAs, and known HDFs such as CD4, CXCR4 and CCR5 (Novina, 2002; Anderson, 2003). The combination of RNAi with high throughput (HT) experimental

design lead to the ability to timeously perform functional screening at a genomic scale. A related seminal study utilized a library of siRNAs targeted to 510 human kinase genes, in order to identify specific modulators of TNF-related apoptosis-inducing ligand (TRAIL)-mediated apoptosis in HeLa cells (Aza-Blanc, 2003). This pilot study established the utility of large-scale RNAi screening in mammalian cell models and since then a multitude of functional genome-wide RNAi screens have led to delineation of countless endogenous processes, identification of novel host determinants of pathogenesis and improved drug discovery (Cherry, 2009; Mohr, 2014).

Specific to HIV, the first genome-wide RNAi screens were undertaken in 2008 by 3 independent research groups (Brass, 2008; Konig, 2008; Zhou, 2008). All 3 of these pioneering screens utilised commercially available synthetic siRNA libraries in combination with cell-based measures of viral replication and cellular toxicity in order to identify host factors that could significantly affect HIV replication without negatively impacting cell viability (Pache, 2011). Studies by the Brass and Zhou groups assessed host factors that may contribute to all stages of the viral life cycle, from entry to production of infectious virions, in Hela-derived cell lines (Brass, 2008; Zhou, 2008). Konig and colleagues on the other hand only evaluated the impact of host factor depletion on viral replication from a post-entry stage until the point of stable proviral transcription, using the HEK293T human embryonic kidney cell line. (Konig, 2008). These screens each interrogated ~20 000 human genes and collectively were able to identify over 800 host factors relevant to HIV replication (referred to as 'hits'), the majority of which were novel potential HDFs (Bushman, 2009). There were however only 3 genes identified as hits by all three screens and only 31 other genes identified as hits in at least 2 screens (Table 1.1). The poor concordance between hits was determined to be largely attributable to major differences in both the experimental and analytical parameters utilised by each research group including differences in cell types, viral variants, assay readouts and hit selection criteria, to name a few (Pache, 2011).

Despite the diverse experimental conditions across the three studies, there was still a strong enrichment of host factors previously implicated in HIV replication (Table 1). This finding further strengthened confidence in the newly identified HDFs and implied that the replicative requirement for these specific host factors was likely inflexible and highly conserved by viral evolution, thus making these hits prime candidates for drug development (Bushman, 2009). Notably, members of the Mediator complex protein family were for the first time implicated as potential HDFs that regulated proviral transcription, while TNPO3 was identified as a regulator of PIC nuclear import, and the cytosolic trafficking of HIV was associated with MAP4, MID1IP1 and CAV2 (Bushman, 2009). Additionally a number of semi-concordant hits with poorly described endogenous functions (DMXL and IDH1) were also uncovered, although they mediate unknown aspects of HIV replication (Bushman, 2009). Meta analysis of the screen hits in combination with databases of known HIV-host and host-host protein interactions was able to further reveal a prevalence of distinct protein interaction clusters that correlated with proviral transcription, molecular chaperoning, splicing and the cellular immune

response (Bushman, 2009). Therefore, in spite of the issues surrounding concordance, these 3 pioneering screens were able to successfully demonstrate the tremendous potential of genome-wide RNAi approaches to rapidly characterizing HDFs (Bushman, 2009).

Table 1.1 The 34 hits identified by at least of 2 of 3 genome-wide siRNA screens

Gene symbol	Konig, 2008	Brass, 2008	Zhou, 2008	Previously associated with HIV
MED6	✓	✓	✓	
MED7	✓	✓	✓	
RELA	✓	✓	✓	✓
ADRBK1		✓	✓	
AKT1		✓	✓	✓
ANAPC2	✓		✓	
ANKRD30A		✓	✓	
CAV2		✓	✓	
CCNT1		✓	✓	✓
CD4		✓	✓	✓
CHST1	✓		✓	✓
CTDP1	✓	✓		✓
CXCR4		✓	✓	✓
DMXL1	✓	✓		
DDX3X		✓	✓	✓
HMCN2	✓		✓	
IDH1	✓	✓		
JAK1		✓	✓	✓
MAP4	✓	✓		

MED4		✓	✓	
MED14	✓	✓		
MED19	✓		✓	
MED28		✓	✓	
MID1IP1	✓	✓		
MRE11A	✓		✓	
NUP153	✓	✓		✓
RAB28		✓	✓	
NUP358	✓	✓		
RNF26		✓	✓	
RGPD8		✓	✓	
TCEB3		✓	✓	✓
TNPO3	✓	✓		
TRIM55	✓	✓		
WNK1		✓	✓	

Subsequent to the initial three siRNA-based screens, Yeung and colleagues undertook a genome-wide screen targeting ~54 000 human transcripts in clonal T cell lines that were stably transduced with shRNA-expressing lentiviral vectors (Yeung, 2009). This shRNA-based screen identified and validated 5 host factors NRF1, STXBP2, NCOA3, PRDM2, and EXOSC5 as potential HDFs from a primary hit list of 252 candidates (Yeung, 2009). A different shRNA-based screen targeted to >800 human kinases and phosphatases was further able to identify 14 novel HDFs that were dispensable for normal host cell function but essential for viral replication (Rato, 2010). The activities of the majority of these host factors was demonstrated to restrict viral replication at stages prior to proviral integration, and were mapped to the ERK, JNK and MAPK signalling cascades as well as host DNA repair and vesicular transport processes (Rato, 2010). Using a combination of ultra high throughput screening via printed siRNA arrays and multidimensional image based profiling, Genevesio and colleagues identified 56 HDFs that exhibited a visual infection phenotype similar to CD4 depletion in a HeLa-derived GFP reporter cell line (Genovesio, 2011). Eleven of these host factors were previously associated with HIV

replication while the remaining 45 factors represented novel HDFs (Genovesio, 2011). The Non-homologous end-joing (NHEJ) -associated DNA repair factor Ku70, along with RNAseH2A and PAK1 were selected for further validation and their depletion was shown to significantly inhibit HIV replication in a Jurkat T cell line (Genovesio, 2011). A more focused siRNA-based screen was also published in the same year where a library of 232 siRNA pools was utilised to uncover novel HDFs specifically associated with the DNA repair process (Espeseth, 2011). The base excision repair (BER) pathway was found to be the mostly highly enriched within the 35 total hits identified by the screen, while Homologous repair (HR) -mediated repair proteins were almost as highly represented. Depletion of the BER-associated hits MUTYH, NTHL1, NEIL3, XRCC1, LIG3, and POLB resulted in a >40% inhibition of viral replication, which could be rescued by re-expression of these factors.

Taken together, the advent of large scale RNAi based screening has had a great impact on delineation of the global HIV-host interaction landscape (Bushman, 2009; Yeung, 2009; Rato, 2010; Espeseth, 2011; Genovesio, 2011). This statement is even more relevant when we consider that RNAi-based experiments have led to the characterisation of over 1200 potential HDFs thus far, which accounts more than a quarter of all host genes currently implicated in HIV infection (Ako-Adjei, 2015). While much of the early focus on host pathogen interactions rested on the coding region of the host genome, the last decade has ushered in a dramatic shift in this paradigm with the noncoding component of the human genome becoming more relevant across all disciplines of biology, including HIV-host interactions (Barichievy, 2015). Notably, the long noncoding RNAs (lncRNAs) lincRNA-p21 and NEAT-1 are co-opted by HIV to facilitate deregulation of the host apoptotic response and the nuclear export of viral transcripts respectively (Barichievy, 2015; Zhang, 2013). While the current number of lncRNA-HIV interactions appears modest, the emerging role of lncRNAs as critical mediators of gene expression in response to pathogenic stress suggests that many more HIV-specific interactions may be uncovered in the years to come. Furthermore small non-coding RNAs have emerged as major regulators of post-transcriptional gene expression. Within this class, host microRNAs (miRNAs) that constitute the backbone of the endogenous RNAi system, are most interesting as they represent a potentially significant resource for the delineation of HIV-host interactions and the development of novel host-directed therapies.

1.11 microRNAs

miRNAs are short non-coding RNA molecules ~ 22 nucleotides in length that were first described in *C.elegans* when two small RNA transcripts derived from the gene *lin-4,* a known negative regulator of lin-14, were revealed to exhibit homology to a repeated sequence encoded within the 3’ UTR of mRNAs encoding lin-14 (Lee, 1993). The subsequent discovery of the endogenous RNAi pathway and the role of dsRNA in post-

transcriptional gene regulation heralded a new era in RNA biology, and two decades of research have placed miRNAs at the centre of this exciting field of research (Fire, 1998; Elbashir, 2001; Salmena, 2011). miRNAs have now been identified in a multitude of organisms from worms to humans, where they function as molecular guides that direct the endogenous RNAi machinery to specific targets (Bartel, 2009). Additionally a number of miRNAs and their target transcripts are highly conserved across different species, suggesting a strong selection pressure for miRNA-mediated gene regulation throughout evolution (Friedman, 2009). Recent advancements in deep sequencing technologies have bolstered miRNA discovery and there are currently over 2500 miRNAs species identified in humans alone, which is more than double the number of human miRNAs annotated only two years ago (Kozomara, 2014). While miRNAs may exhibit similar functional properties to other small non-coding RNA families like PIWI- interacting RNAs (piRNAs) and siRNAs, they are also readily distinguished by their unique biogenesis (Figure 1.6.) and constitute the dominant class of small non-coding RNAs in most human cell types (Bartel, 2009).

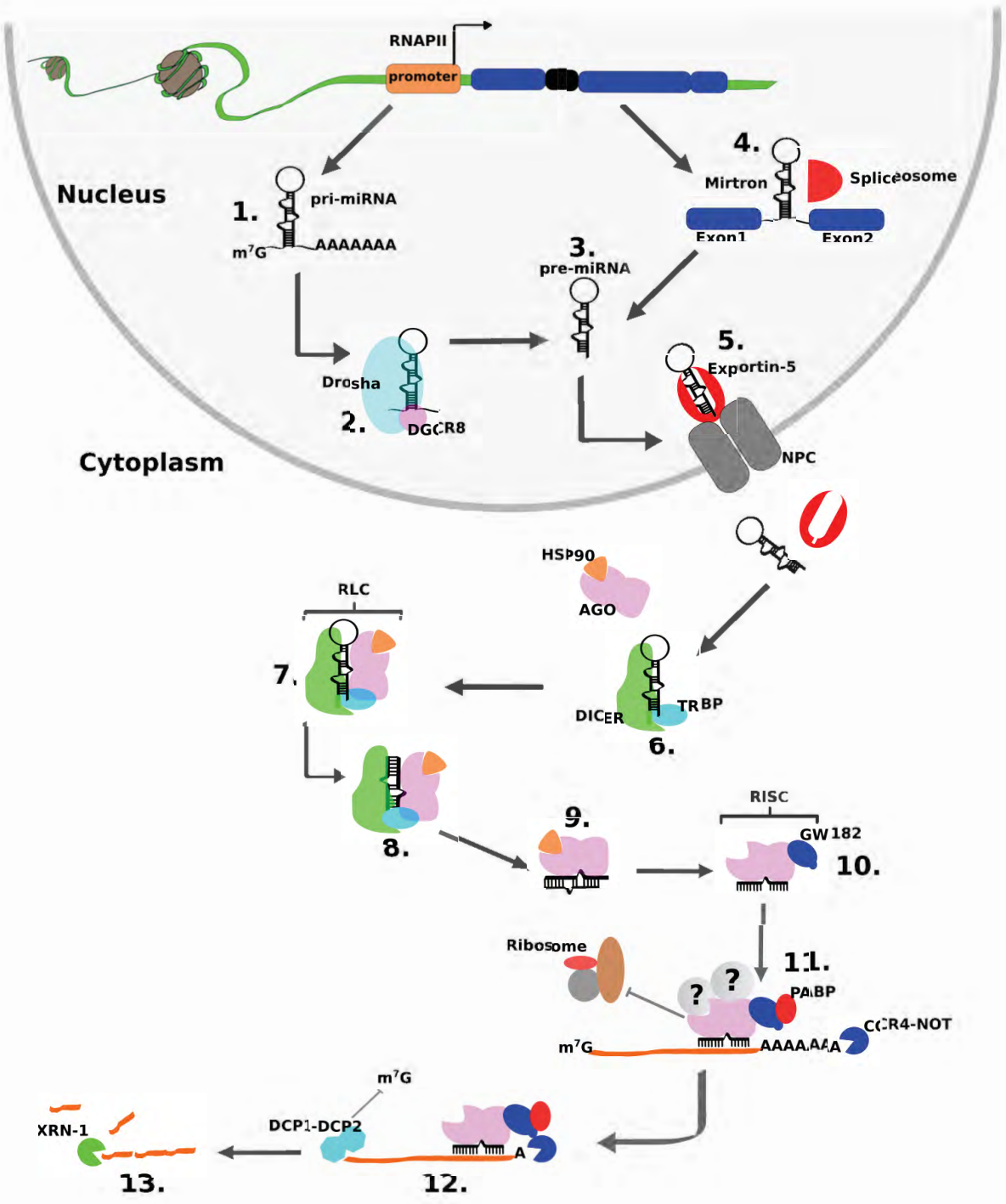

Figure 1.6. Canonical miRNA biogenesis and function.

1) miRNAs are actively transcribed by RNAPII to produce pri-miRNA molecules. **2)** Pri-miRNAs are cleaved by the Drosha-DiGeorge microprocessor complex to produce pre-miRNAs **3)** which are ~70 nt long stem loop structures that contain a 2 nt 3' overhang. **4)** An alternative route of miRNA biogenesis results in pre-miRNA structures known as mirtrons that are produced directly as a result of splicing events **5)** Both pre-miRNAs and mirtrons are actively transported into the

cytoplasm by Exportin-5. **6)** Cytosolic pre-miRNAs are bound by a DICER-TRBP complex. **7)** The pre-miRNA-DICER complex is bound by AGO-HSP90 thus forming a RISC loading complex (RLC) **8)** The RLC cleaves the pre-miRNA to produce a ~22 nt RNA duplex. **9)** The mature miRNA duplex is loaded onto AGO and detaches from the RLC **10)** The mature single stranded guide RNA bound to AGO and GW182 form the core RISC complex (miRISC). **11)** miRISC target recognition is determined by sequence homology and miRISC binding predominantly results in translational repression of a target mRNA which may be followed by the degradation of the target transcript. **12)** mRNA degradation is initiated by deadenylation of the target mRNA by CCR4-NOT and is followed by removal of the 5' cap by decapping enzymes DCP1 and DCP2. **13)** The unprotected mRNA transcript is degraded by the exonuclease XRN1.

1.11.1 microRNA biogenesis

The genetic sequences encoding miRNAs can occur within intergenic, intronic or exonic regions, where the majority of non-intergenic human miRNAs are located within the introns of coding and noncoding transcripts (Rodriguez, 2004). miRNAs can either be expressed directly by RNAPII-mediated transcription, or indirectly via transcription of another host gene (Cai, 2004). miRNA expression is therefore subject to many of the same regulatory mechanisms that govern canonical gene expression, and is tightly regulated by epigenetic factors such as histone modifications and DNA methylation signatures, as well the activity of specific transcription factors including p53, ZEB1 and MYC (reviewed by Krol, 2010 and Ha, 2014). These factors contribute to cell and tissue-specific miRNA expression profiles, and are further augmented by autoregulatory miRNA feedback circuits that govern the expression of specific miRNAs (Kim, 2007; Tsang, 2007). Canonical miRNA biogenesis results in the RNAPII-dependent expression of primary miRNAs (pri-miRNAs) which undergo both 5' capping and 3` polyadenylation, are generally over 1 kb in length and are comprised of ~33-35 bp stem-loop structures flanked by single stranded RNA (ssRNA; Ha, 2014). These stem-loop structures are liberated from the pri-miRNA structure by a microprocessor complex in order to produce precursor miRNA (pre-miRNA) molecules (Krol, 2010).

The microprocessor complex is comprised of the RNAseIII endonuclease Drosha and the double stranded RNA (dsRNA) binding complex, DiGeorge syndrome critical region 8 (DCGR8) (Ha, 2014). DCGR8 directly interacts with both Drosha and the pri-miRNA structure to stabilize Drosha-mediated cleavage (Ha, 2014). The two RNAseIII domains of Drosha function as a processing centre and are directed to a cleavage site ~11 bp upstream of the juncture between the ssRNA and dsRNA loop structure (Ha, 2014). Drosha first cleaves the 3' strand of the pri-miRNA stem loop and then the 5' strand, to release a hairpin structure with a 2 nucleotide overhang at the 3' end (Ha, 2014). This hairpin molecule is ~70 bp in length and is referred to as a pre-miRNA (Krol, 2010). An alternative route of miRNA biogenesis results in production of pre-miRNA molecules via intronic splicing, and these are known as mirtrons (Lee, 2004; Sibley, 2011).

Nuclear export of pre-miRNA molecules is facilitated by a nuclear transport complex comprised of exportin 5 (XPO5) and RanGTP (Yi, 2003). RanGTP-bound XPO5 is able to specifically recognise and bind both the dsRNA stem and 2 nucleotide 3' overhang of pre-miRNA molecules (Ha, 2014). The pre-miRNA-XPO5 interaction facilitates cytoplasmic trafficking of pre-miRNAs and mirtrons through the NPC and also shields these molecules from nuclear degradation (Yi, 2003). DICER is an RNA endonuclease that contains two RNAseIII domains, a helicase domain and a Piwi-Argonaute-Zwille (PAZ) domain (MacRae, 2006). The helicase and PAZ domains facilitate pre-miRNA recognition, while the dimerised RNAse domains function as a catalytic centre (Ha, 2014). The helicase domain interacts with the terminal loop of the pre-miRNA hairpin, while the PAZ domain specifically binds the 2 nucleotide 3' overhang (Ha, 2014). The distance between the RNAseIII domains and the PAZ domain functions as a "molecular ruler", which directs cleavage at a fixed distance from the 3' end to produce a ~22 nucleotide long mature miRNA duplex with a 2 nucleotide 3' overhang and 5' phosphate group (MacRae, 2006).

The RNA induced silencing complex (RISC) is the ribonucleoprotein effector of both miRNA (miRISC) and siRNA-mediated gene silencing (Ha, 2014). The core components of a functional mammalian miRISC complex include a single stranded RNA guide sequence, one of four argonaute proteins (AGO1-4) and a GW182 protein (Krol, 2010). Canonical miRISC assembly is therefore dependent on the loading of a DICER-processed mature miRNA duplex onto an AGO protein. The formation of the Risc-loading complex (RLC) comprised of DICER, AGO, TRBP and a heat shock protein (HSP) has been posited as a major route of miRISC assembly (Liu, 2012). In this model, pre-miRNAs are first bound by a DICER-TRBP complex which then recruits an AGO-HSP complex (Liu, 2012). DICER-mediated cleavage occurs within the RLC and transfer of the mature miRNA duplex to AGO occurs following a conformational change in AGO, mediated by HSP90 (Iwasaki, 2010). DICER-mediated cleavage and AGO-miRNA loading then promote release of the miRNA-AGO complex from the RLC (Liu, 2012). The next stage in miRISC assembly requires conversion of the miRNA duplex into a ssRNA guide sequence, and is mediated by AGO following its release from the RLC (Liu, 2012; Ha, 2014). The guide strand of the miRNA duplex is preferentially incorporated into AGO during loading, while the passenger strand is later removed either by unwinding of a mismatched RNA duplex or in rare instances by AGO2-mediated cleavage of perfectly paired duplexes (Ha, 2014). Strand selection is largely determined by thermodynamic stability of the RNA duplex, with guide strand selection favouring 5' instability (Khvorova, 2003).

1.11.2 Target recognition and mRNA silencing

miRNA target recognition is determined predominantly by a seed region located between nucleotides 2-8 at the 5' end of a guide RNA (Lewis, 2003; Bartel, 2009). This seed sequence adopts an A-form helix structure within miRISC in order to facilitate mRNA scanning for specific miRNA binding sites (Ha, 2014). The majority of functionally relevant human miRNA binding sites are located within the 3' UTRs of mRNA transcripts and can be identified by the seed region (reviewed by Grimson, 2007 and Bartel, 2009). mRNAs may encode multiple binding sites specific to a single miRNA or many different miRNAs thereby creating a non-orthogonal relationship between miRNAs and their targets (Bartel, 2009). This relationship also has important functional consequences, as the relative concentration of specific miRNAs and the availability of their target binding sites can influence both miRISC target selection and the degree of suppression (Mukherji, 2011; Pasquinelli, 2012). miRISC target recognition and miRNA-mRNA binding occur via classical Watson-Crick base pairing and can result in either mRNA cleavage, translational repression or mRNA decay (reviewed by Fabian, 2012). While all RISC-loaded human AGO proteins are capable of repressing mRNA translation and facilitating mRNA degradation, AGO2 is the only protein that possesses the ability to actively cleave perfectly matched mRNA targets (Liu, 2004). The majority of miRNA-mRNA interactions are however only partially complementary and translational repression therefore represents the predominant form of miRISC-mediated mRNA silencing (Lewis, 2003; Fabian, 2012).

The exact molecular mechanisms and temporal events that govern miRNA mediated translational repression are not well understood and are likely constituted by multifaceted inhibitory processes (reviewed by Fabian, 2012). miRISC-mediated translational repression can result in either the transient silencing mRNAs, or their subsequent deadenylation, decapping and decay (reviewed by Pillai, 2005). Sequestration of PABP by GW182 and the recruitment of factors such as RCK/p54 can specifically repress 5' cap recognition and recruitment of ribosomal machinery to target mRNAs (Cy, 2006; Mathonnet, 2007). Additionally, the GW182-PABP interaction may also function to further inhibit the initiation process by stifling eIF4G-mediated mRNA circularization (Fabian, 2012). miRISC can block translation following initiation by prompting premature dissociation of ribosomes from target mRNAs during the elongation process (Nottrott, 2006; Petersen, 2006). These translationally blocked mRNAs preferentially localise with cellular P-bodies and it is within these structures that their subsequent fates are determined (Pillai, 2005). mRNA destabilization is initiated by the CCR4-NOT and PAN2-PAN3 complexes, which facilitate deadenylation of the 3' poly(A) tails of target mRNAs (Fabian, 2012). Following deadenylation, miRISC promotes removal of the 5' cap from target mRNAs via recruitment of decapping factors like DCP1 and DCP2 to target mRNAs (Nishihara, 2013). Unprotected mRNAs are then rapidly degraded by the 5'-3' exonuclease, Xrn1 (Fabian, 2012). Alternatively, transiently repressed mRNAs may also be released from P-bodies in response to specific environmental cues (Bhattacharyya, 2006).

1.11.3 Functional relevance of host miRNAs

A single mRNA transcript may be regulated by multiple miRNAs and a single miRNA may in turn regulate the expression levels of hundreds of transcripts to varying extents (Bartel, 2009). Intriguingly, mRNAs that are regulated by a common miRNA, or family of miRNAs, often belong to a single functional pathway or one that is closely related (Gennarino, 2012). The non-orthogonal nature of miRNA-mRNA interactions and the relaxed binding requirements for miRNA-mediated silencing thus enable the concurrent regulation of specific subsets of genes that are involved in functionally related processes. This is particularly significant when we consider that over 60% of all human coding transcripts are subject to miRNA-mediated regulation, and that the number of documented regulatory interactions between miRNAs and lncRNAs is also on the rise (Friedman, 2009; Jalali, 2013; Wang, 2013). It is not surprising then that miRNAs have been implicated in a number of complex physiological processes that require high-level coordination of multiple functional pathways and temporal control over the expression patterns of specific cohorts of genes (reviewed by Ivey 2015).

In developmental biology miRNAs have been implicated in various aspects of embryogenesis and organ development (reviewed by Ivey 2015). Manipulation of miRNA expression levels can result in the reprogramming of human cells to pluripotent states, and likewise a number of miRNAs have also been implicated as critical determinants of cellular differentiation and lineage selection within pluripotent cell populations (reviewed by Gangaraju, 2009; Ivey, 2010; Anokye-Danso, 2011; Miki, 2015). Additionally miRNAs have emerged as critical regulators of cell cycle, proliferation and apoptosis thus placing them as critical factors in tumorigenesis (reviewed by Hwang, 2006). Briefly, deregulated miRNA expression may result in loss of transcriptional control over pro-oncogenic factors or the emergence of miRNA themselves as oncogenic molecules known as “oncomirs” (reviewed by Esquela-Kerscher, 2006). A number of studies have also documented a pivotal role for miRNAs in immunity and inflammation along with their associated pathologies (reviewed by Contreras, 2012 and O'Connell, 2012). Of particular interest, miRNAs have been implicated as crucial mediators of a diverse set of host responses to pathogenic challenge (reviewed by He, 2014 and Seddiki, 2014).

The role of miRNA-mediated gene silencing in restriction of various forms of pathogenic bacteria have recently been well characterised (reviewed by Eulalio, 2012). The origin of host RNAi however can be linked to the intrinsic restriction of foreign dsRNAs that are characteristic of viral infection (reviewed by Obbard, 2009). Furthermore, a number of viruses have evolved sophisticated RNAi silencing suppressor (RSS) molecules, which suggests a prominent role for the host RNAi pathway in viral evolution (Obbard, 2009). Notably, ebola, hepatitis C virus (HCV) and influenza have all evolved protein-based RSS effectors, while adenoviruses employ an RNA-based strategy aimed at saturating the endogenous miRNA biogenesis pathway (reviewed by Bivalkar-Mehla, 2011). A number miRNAs have been identified as putative VRFs for a wide array of viruses (Lecellier, 2005; Lagos, 2010; Santhakumar, 2010). Alternatively, miRNAs may also

function as host dependency factors, such as in the case of miR-122 and HCV (Jopling, 2005). These findings position miRNA biology at the crux of the viral-host interface and HIV-host interactions have proven to be no exception.

1.12 Host miRNAs and HIV

HIV infection has been reported to perturb global miRNA expression profiles to variable degrees in different studies (reviewed by Klase, 2012). Like many other viruses, HIV has evolved a number of strategies to both evade host miRNA-mediated repression, and selectively subvert the host miRNA network in order to promote a cellular environment conducive to viral replication (reviewed by Swaminathan, 2014). Furthermore, a number of specific host miRNAs have been identified as potential VRFs that act either by directly targeting viral transcripts, or indirectly by repressing endogenous targets that function as HDFs (Klase, 2012). Conversely, a small number of miRNAs, which themselves may function as putative HDFs, have also been recently uncovered (Swaminathan, 2014). The relationship between HIV and the host miRNA network is thus characterised by a number of complex interactions between virus and host (Figure 1.7.).

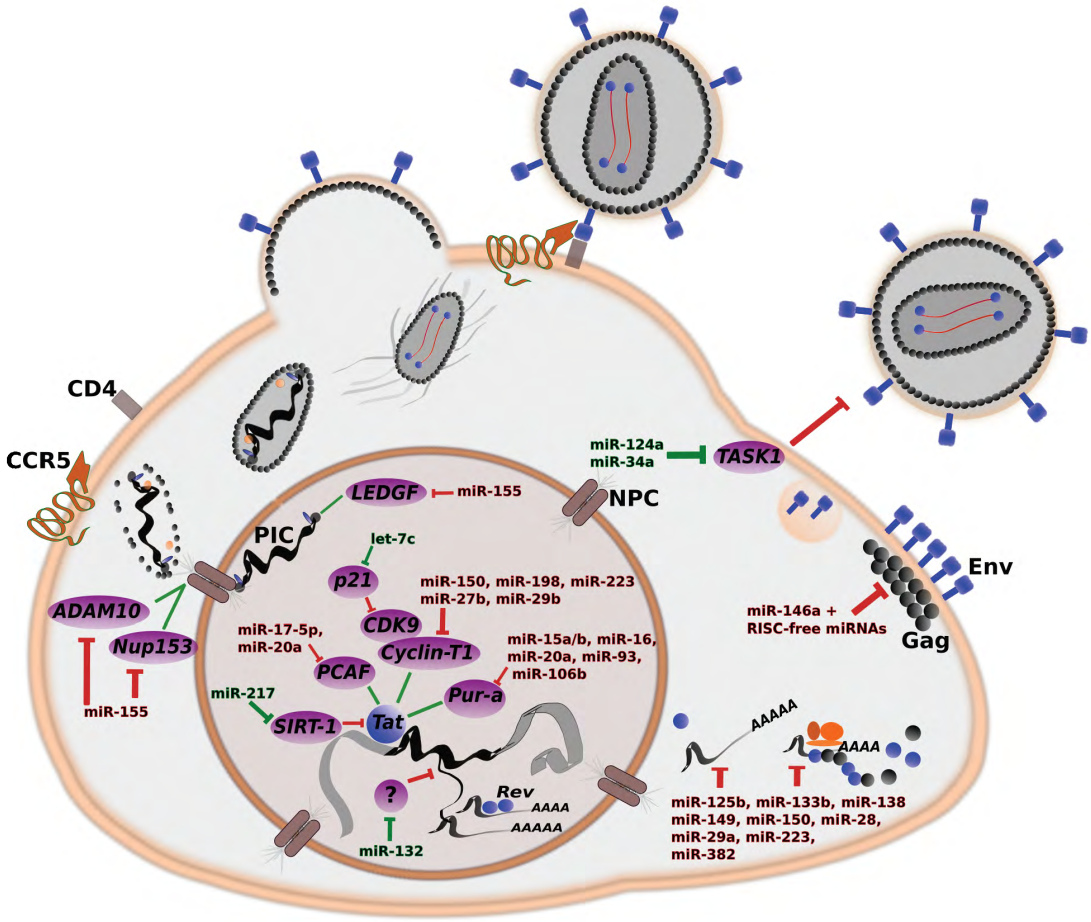

Figure 1.7. Host miRNAs that modulate HIV replication.

Specific host miRNAs can either positively or negatively regulate HIV replication. miRNAs that negatively regulate HIV (red) do so either by directly targeting viral products, or via translational inhibition of specific HDFs required for viral replication. Likewise, miRNAs that positively regulate HIV replication (green) do so by suppressing potential VRFs.

1.12.1 Perturbed miRNA expression in response to infection by HIV

Perturbation of the host miRNA expression profile in response to HIV was noted by a seminal study that utilized a microarray-based approach to evaluate the relative expression of 312 host miRNAs in HeLa cells transfected with an infectious clone of HIV, pNL4-3 (Yeung, 2005). Not a single host miRNA was found to be significantly upregulated in response to HIV infection, while 43% of the interrogated miRNAs were downregulated (Yeung, 2005). This observation led to the hypothesis that HIV infection may exert a unilaterally suppressive effect on the expression of host miRNAs. This notion was however called into question by a subsequent study which utilized the same microarray platform to evaluate the effect of HIV infection in Jurkat cells and patient-derived peripheral blood mononuclear cells (PBMCs; Triboulet, 2007). This latter study demonstrated upregulation of 11 host miRNAs and specific downregulation of the miR-17-92 family in response to infection. Additionally miR-122, miR-370, miR-373* and miR-297 were found to be exclusively expressed in HIV-infected cells but not in uninfected controls (Triboulet, 2007). These early findings thus alluded to a potential cell type-specific miRNA response to HIV, and the prevalence of a multifaceted effect on host miRNA expression following HIV infection (Yeung, 2005; Triboulet, 2007).

Indeed, subsequent studies have suggested that the effect of HIV infection on miRNA expression may be highly selective and 'purposely orchestrated'. A microarray-based evaluation of miRNA expression levels across 3 different cell types revealed miR-21, miR-26a, miR-155, miR-29a, miR-29b and miR-29c to be significantly downregulated following infection in PBMCs, while miR-223 was found to be significantly upregulated (Sun, 2011). Changes in miRNA expression levels were more modest in CEM and Jurkat cell lines with only miR-29 and miR-155 found to downregulated following infection, while miR-223 was again shown to be upregulated (Sun, 2011). The differential expression of 21 host miRNAs in HIV-infected PBMCs was correlated with the differential expression of 444 host genes that mediate specific aspects of the apoptotic, MAPK, T cell receptor and Wnt signalling cascades (Gupta, 2011). All of these pathways have been previously associated with HIV replication thus implying that HIV may modulate the expression levels of specific miRNAs in order to subvert specific functional processes (Gupta, 2011). In addition, selective modulation of miRNA expression by HIV may also be temporally coordinated within infected cells (Chang, 2013). Fifteen host miRNAs were observed to be differentially expressed at 5, 12 and 24

hours post infection (hpi) in SupT1 cells using small RNA sequencing (Chang, 2013). Furthermore, miRNAs that were differentially expressed at early infection time points were shown to revert back to their basal expression levels after 24 hours (Chang, 2013). These observations further support the the idea that HIV may selectively modulate specific host processes by regulating the expression levels of distinct subsets of host miRNAs.

Two of the miRNAs (miR-143-3p and miR-10a-5p) previously identified to be differentially expressed at 24 hpi (Chang, 2013) were also observed to exhibit a similar trend 72 hpi in another study (Whisnant, 2013). A comparison the of miRNA expression profiles between 3 cell types (TZM-bl, C8166 T cells and PBMCs) infected with R5-tropic (BAL) and X4-tropic (pNL4-3) viral variants revealed that HIV infection only perturbed the expression levels of a few host miRNAs 72 hpi (Whisnant, 2013). Notably, a single miRNA miR-30b-5p, was found to be upregulated in PBMCs infected with BAL but not those infected by pNL4-3, while the miR-17-92 miRNA family was not differentially expressed (Whisnant, 2013). These findings contradict previous reports that described a more diverse perturbation of host miRNA expression in response to HIV infection, and further contribute to the poor concordance that has plagued expression-based evaluations of the host miRNA response to HIV (Klase, 2012).

Despite the many contradictions within expression-based datasets, some robust yet subtle HIV-host interactions are clear. Notably, perturbation of miRNA expression following HIV infection is suggested to be highly selective and temporally coordinated. This level of control over the host miRNA network can facilitate viral modulation of discrete functional pathways at distinct stages of viral replication. The very nature of miRNA-based repression however, as determined by variable functional thresholds, makes extrapolation of functional significance from miRNA expression data alone very challenging (Mukherji, 2011). Additionally, discrimination between host and viral-driven changes in miRNA expression levels in infected cells requires further investigation in order to accurately interpret the significance of observed deviations. Thus while delineation of specific miRNA expression signatures relevant to HIV may serve to advise biomarker development and provide valuable correlative information on potential HIV-host interactions, the identification of therapeutically relevant viral restriction factors (VRFs) and host dependency factors (HDFs) requires a more functional approach.

1.12.2 The role of miRNAs in host and cell susceptibility to HIV

The role of host miRNAs in natural viremic control phenotypes has been a subject of great interest but unfortunately one that has also not yielded much clinically relevant data. Comparison of miRNA expression profiles between patient samples from elite controllers and infected and uninfected normal progressors revealed miR-31 and miR-31* to be suppressed in elite controller samples along with miR-125b and miR-150 (Witwer, 2012). These latter miRNAs were also suppressed in infected normal

progressor samples thus implying that a common host or viral response related to miR-125b and miR-150 expression still persists even under viremic control (Witwer, 2012). Plasma miRNA expression levels from samples of elite controllers, chronically infected patients and healthy uninfected donors revealed that 16 miRNAs were differentially expressed in chronically infected individuals, and miR-29b-3p, miR-33a-5p and miR-146a-5p were significantly upregulated in elite controllers (Reynoso, 2014). Notably, elite controller and healthy donor groups showed no significant differences in plasma miRNA expression patterns, suggesting that HIV susceptibility may be closely linked to the expression levels of specific host microRNAs in response to infection.

Susceptibility is also connected to the differentiation or activation state of HIV-infectable cell types. Activated T cells are more permissive to HIV replication compared to resting $CD4^+$ T cell populations were HIV replication can be arrested in a latent state (Tyagi, 2010). Additionally, while macrophages are susceptible to HIV infection, their monocytic progenitors are highly recalcitrant to permissive HIV replication (Bergamaschi, 2010). A number of host miRNAs that regulate the differentiation or activation states of target cells have been implicated as putative mediators of HIV replication (Swaminathan, 2014). These miRNAs modulate cell susceptibility either by directly targeting viral transcripts or via their regulation of specific HDFs, and examples of each are presented in the following section.

1.13 miRNAs as viral restriction factors

A number of host miRNAs have been described to suppress HIV replication by directly targeting viral transcripts via miRISC-mediated translational repression (Hariharan, 2005; Huang, 2007; Ahluwalia, 2008). A seminal study demonstrated the utility of an *in silico* prediction tool to identify putative host miRNA binding sites within HIV transcripts (Hariharan, 2005). Binding sites for miR-29a and miR-29b were found to be conserved within HIV Nef transcripts across multiple clades of HIV, while conserved binding sites for miR-149, miR-378 and miR-324-5p were identified in transcripts encoding Vpr, Env and Vif respectively (Hariharan, 2005). In a follow up study, exogenous expression of miR-29a but not miR-29b downregulated Nef protein levels in Jurkat cells (Ahluwalia, 2008). These findings were however later contradicted by the observation that miR-29b was one of 5 host miRNAs that could negatively regulate HIV transcripts in 42CD4 cells (Houzet, 2008). Likewise, overexpression of miR-29b-3p and miR-33a-5p, but not miR-29a, could suppress HIV replication in both the MT2 cell line and primary $CD4^+$ T cells (Reynoso, 2014). Photoactivatable ribonucleoside-enhanced cross-linking and immunoprecipitation (PAR-CLIP) analysis revealed 4 potential miRNA binding sites within the HIV genome that corresponded to miR-423, miR-301a, miR-29a and miR-155 (Whisnant, 2013). While miR-423, miR-301a and miR-155 were observed to directly associate with and negatively regulate viral transcripts, miR-29a overexpression did not have a significant effect on viral protein levels (Whisnant, 2013). In accordance with

initial predictions (Hariharan, 2005) and in partial disagreement with prior findings (Reynoso, 2014; Whisnant, 2013) overexpression of both miR-29a and miR-29b significantly suppressed HIV replication and HIV Nef transcripts in a HeLa-derived cell line (Sun, 2012). Additionally miR-15a, miR-15b, miR-16, miR-24 and miR-150 were also predicted to target Nef transcripts, although these have not been functionally validated (Sun, 2011).

In addition to miRNAs that target HIV transcripts involved in active replication, miRNAs that mediate HIV-resistance and latency have also been identified. miRNAs that were upregulated in resting $CD4^+$ T cells were compared to conserved miRNA binding sites in HIV transcripts to identify those which potentially regulated viral latency (Huang, 2007). In functional assays, these miRNAs were shown to be within a cluster comprised of miR-28, miR-125b, miR-150, miR-223 and miR-382, and were demonstrated to actively suppress viral transcripts in $CD4^+$ T cells, thus implicating them in the maintenance of viral latency (Huang, 2007). The role of this miRNA cluster in monocyte and macrophage susceptibility to HIV replication has also been evaluated (Wang, 2009). Interestingly, repression of miR-28, miR-150, miR-223 and miR-382 by synthetic inhibitors enhanced HIV replication in patient-derived samples, presumably via relief of HIV-directed translational repression (Wang, 2009). In addition, these miRNAs were significantly down-regulated during monocyte to macrophage differentiation, and furthermore transfection with of synthetic mimics of these miRNAs recapitulated monocyte-like resistance to HIV in cultured monocyte-derived macrophages (MDMs; Wang, 2009). Together, these data suggest miRNAs targeted to viral transcripts regulate HIV activity and ‘inactivity’ in the case of latency.

A novel mechanism of viral restriction was recently described whereby overexpressed RISC-free miR-146a and miR-888, bound directly to HIV Gag and antagonised its multimerization at the cell membrane (Chen, 2014a). The nonspecific association between HIV Gag and both host and viral mRNAs promotes Gag multimerization and virion assembly (Jouvenet, 2009). Thus, saturation of Gag RNA binding domains with by unbound small RNAs species like miRNAs, perturbed Gag stabilisation and internalization at the cell membrane (Chen, 2014a). In addition, depletion of AGO2 recapitulated this restrictive phenotype, probably due to a consequential accumulation of RISC free miRNAs (Chen, 2014a). However, as AGO2 has been implicated in virion packaging and is known to associate with Nef (Aquil, 2013), the significance of these relationships in context of an AGO2-depletion phenotype, remains unclear. Furthermore, characterisation of host miRNAs that are able to reproducibly target viral transcripts across different viral variants and experimental conditions has proven challenging (Klase, 2012). While pursuit of these potential VRFs has uncovered valuable knowledge regarding miRNA-specific escape strategies and cell susceptibility to HIV, any miRNA-based therapy that directly targets viral transcripts is inherently susceptible to the same inadequacies as treatments. miRNAs that function as VRFs via suppression of host HDFs thus represent much more attractive prospects for VRF-based therapies.

Less than 20 putative miRNA-HDF regulatory associations have been characterised to date. This number appears far too modest when we consider the hundreds of potential HDFs already characterised by RNAi screening, and the critical role of the human miRNA network in the regulation of virtually every aspect of cellular biology. The HDF, p300-Creb binding protein associated factor (PCAF), is negatively regulated by miR-17-92-associated miRNAs in Jurkats and PBMCs (Triboulet, 2007). PCAF-mediated acetylation of Tat promotes Tat-mediated viral transcription and overexpression of both miR-17-5p and miR-20a specifically suppress PCAF translation in Jurkat cells (Triboulet, 2007). The purine-rich element binding protein alpha (Pur-α) has been identified as a miRNA-regulated HDF, which serves as a transcriptional co-activator of HIV Tat (Shen, 2012). Host miRNAs miR-15a, miR-15b, miR-16, miR-93 and miR-106b antagonise Pur-α translation in HIV-restrictive monocytes, but this regulation is lost following differentiation into HIV-permissive monocyte-derived dendritic cells (MDDCs; Shen, 2012). Ectopic application of synthetic mimics of these miRNAs was able to suppress HIV replication in MDDCs, while the same synthetic inhibitors relieved the restriction on HIV replication in monocytes (Shen, 2012).

Cyclin-T1 is another well characterised Tat-associated HDF, which may be subject to active miRNA-mediated repression under certain conditions. In HIV-restrictive monocytic cell lines, Cyclin-T1 proteins are repressed by miR-198-mediated silencing and this phenotype is lost following monocyte to macrophage differentiation (Sung, 2009). Ectopic expression of miR-198 via synthetic mimics suppressed upregulation of cyclin-T1 in differentiating monocytes, and inhibited HIV transcription in monocytes transfected with an HIV proviral plasmid (Sung, 2009). In addition, miR-27b, miR-29b, miR-150 and miR-223 restricted HIV replication in resting $CD4^+$ T cells via the suppression of Cyclin-T1 (Chiang, 2012). While miR-27b and miR-29b are able to suppress Cyclin-T1 transcripts directly, miR-150 and miR-223 suppress Cyclin-T1 indirectly by an unknown mechanism (Chiang, 2012).

Activation of Toll-like receptor 3 (TLR3) can impede HIV replication in MDMs (Swaminathan, 2012). This restriction has further, in part, been attributed to RISC-associated activity of miR-155, which is upregulated in response to TLR activation (Swaminathan, 2012; Seddiki, 2014). The mechanism of miR-155-mediated restriction occurs via suppression of the known HDFs ADAM10, TNPO3, Nup153 and LEDGF/p75, which have all been implicated in HIV nuclear import (Friedrich, 2011; Swaminathan, 2012). Furthermore, a recent study also implicated miR-155 as a pro-latency factor that suppresses the HIV activator protein, TRIM32 (Ruelas, 2015). The human Vpr binding protein (VprBP) mediates interaction of Vpr with specific host cell cycle-associated factors (Belzile, 2007). The host miRNA miR-1236 negatively regulates VprBP expression in HIV-restrictive monocytes but not MDDCs (Ma, 2014). In addition, both ectopic expression of miR-1236, and siRNA-mediated suppression of VprBP, similarly inhibited HIV replication in MDDCs only in the presence of Vpr-expressing viral variants (Ma, 2014).

Current knowledge on miRNA-HDF interactions, while limited, has highlighted some interesting prospects that warrant further attention. Notably, four miRNAs that reportedly suppress HIV replication by directly targeting viral transcripts, also reportedly do so indirectly via repression of HDFs (miR-150, miR-155, miR-223 and miR-29b). This observation would suggest that specific subsets of host miRNAs may potentially exert multiple modes of repression against HIV, and warrants a comprehensive characterisation of these potentially therapeutically relevant miRNAs. In addition, a number of host miRNAs have been identified as significant determinants of host cell susceptibility and latency, suggesting that continued investigation of HIV-miRNA interactions may also yield valuable insights into novel mechanisms that govern both innate viral restriction and HIV latency.

1.14 RNAi evasion strategies utilised by HIV

RNA silencing suppressor activity

HIV reportedly utilises a diverse set of RSS effectors including Tat, Vif, Vpr, Nef and viral TAR RNAs. The prevalence of these diverse RSS strategies thus suggests an important role for the host miRNA pathway in the evolution of HIV (Bennasser, 2006; Coley, 2010; Hayes, 2011). Similar to the RSS activity of adenoviral-encoded VA1 RNAs, TAR RNA structures encoded by HIV have been proposed to exert a broad disruptive effect on miRNA biogenesis by binding TRBP (Bennasser, 2006). Specifically, association of TRBP with TAR RNAs preclude its association with DICER, thereby affecting stabilisation of DICER protein levels (Bennasser, 2006). The RSS potential of Tat was first brought to light when a group of researchers stumbled upon the observation that exogenous Tat was able to suppress shRNA-mediated knockdown in cultured cells (Bennasser, 2005). A series of systematic validation experiments eventually mapped this phenotype to Tat-mediated suppression of DICER activity (Bennasser, 2005). The RSS function of Tat was further demonstrated to be independent of its transcriptional activity, but sensitive to a specific lysine to alanine point mutation in the RNA binding domain of Tat (TatK51A;Bennasser, 2005). The RSS-deficient TatK51A viral variant was subsequently demonstrated to have only a modest effect on naturally progressing HIV replication, while significantly sensitising viral replication to shRNA-mediated silencing of viral transcripts (Bennasser, 2005). The role of Tat as an RSS was further supported in a subsequent study (Qian, 2009), although in contrast to the earlier findings, the TatK51A mutation significantly retarded HIV replication, and Tat-mediated RSS activity was shown to occur downstream of DICER processing (Qian, 2009). Significantly, Tat-RSS activity was also proposed to selectively regulate specific host miRNAs as opposed to having a global effect on miRNA biogenesis (Qian, 2009).

Infection assays utilising Nef and Vpr-deficient viral variants resulted in attenuated antagonisation of DICER activity, thus implying that both Vif and Vpr may possess RSS activity (Coley, 2010). This hypothesis was further strengthened by observations that ectopic Vpr expression downregulated DICER protein levels, and that Nef could suppress RISC-mediated cleavage via its association with AGO2 (Coley, 2010; Aqil, 2013). Comparison of miRNA expression levels between T cell lines infected with either a wildtype HIV variant or an RSS-deficient Tat variant, revealed that only a discrete subset of 19 host miRNAs were differentially expressed in response to attenuated Tat RSS activity (Hayes, 2011). Likewise only 5 host miRNAs were found to be differentially expressed in T cells infected with a Vif/Vpr deficient virus compared to those infected with wildtype virus (Hayes, 2011). Each of these discrete subsets represented only a small fraction of the 170 host miRNAs that were observed to be differentially expressed in infected T cells compared to uninfected control cells (Hayes, 2011). These findings thus strongly support the idea that each of the individual RSS effectors encoded by HIV are able to selectively antagonize distinct subsets of host miRNAs. Furthermore these findings imply that large scale dysregulation of host miRNA expression reported by some studies may represent a cumulative effect of multiple RSS effectors and host-driven responses.

Secondary structure of viral-encoded RNAs

The notion that complex secondary structures within HIV RNAs can render them refractory to RNAi-mediated suppression was first documented many years ago (Westerhout, 2005). Stable expression of a siRNAs targeted to viral transcripts was initially found to effectively suppress HIV replication, although suppression was subsequently lost following emergence of viral escape variants that had either acquired nucleotide substitutions within siRNA binding sites, or occluded siRNA binding sites within altered secondary RNA structures (Westerhout, 2005). This evasive strategy has also been noted in models of miRNA-mediated viral suppression where increased RNA secondary structure complexity negatively correlated with miRNA-mediated suppression (Sun, 2011). Briefly, ectopic expression of synthetic mimics of miR-29a and miR-29b both only modestly suppressed a full-length Nef-luciferase reporter transcript (Sun, 2011). Interestingly suppression was significantly improved (up to 80%) when a shorter reporter transcript, unable to form loop structures, was used (Sun, 2011). Addition of 17 extra base pairs to the short reporter transcript permitted formation of stem-loop RNA structures and resulted in attenuation of miR-29-mediated suppression (Sun, 2011). PAR-CLIP data also revealed that while HIV transcripts constitute a major fraction of the RNA population within infected cells (up to 50%), these viral transcripts are also a 100 times more refractory to miRISC binding than their host counterparts (Whisnant, 2013). Cumulative knowledge thus suggests that prevalence of complex secondary structures within HIV transcripts represents a highly effective strategy to mitigate miRNA-mediated regulation of these transcripts. However, the question of whether these structures have evolved specifically for this purpose or some other function remains to be determined. Additionally these findings may also have important implications for the use of reporter

constructs in miRNA target validation, as constructs that do not take the secondary structure of endogenous RNAs into consideration may generate phenotypes that are not physiologically accurate.

1.15 miRNAs as potential host dependency factors

Recently, exploitation of miR-122 as an indispensable HDF during Hepatitis C Virus (HCV) replication, has led to clinical success and fueled a great interest in characterising a similar relationship for HIV (Jopling, 2005; Janssen, 2013). miR-217 has been put forth as a potential HDF due to its translational repression of SIRT-1, which was previously described to disrupt Tat-mediated transcription (Zhang, 2012). Exogenously added Tat upregulated miR-217 expression in a HeLa-derived reporter cell line (MAGI), while modestly suppressing SIRT-1 protein levels (Zhang, 2012). in addition, suppression of miR-217 by a synthetic inhibitor only resulted in a 34% reduction in LTR transcriptional activity (Zhang, 2012). miR-132 was found to be highly upregulated in activated $CD4^+$ T cell populations, and augmentation of miR-132 expression with a synthetic mimic enhanced viral replication in Jurkats by potently reactivating latent proviral transcription (Chiang, 2013). These findings place miR-132 as an intriguing positive regulator of HIV replication. Perplexingly however, the effect of inhibiting miR-132 activity on HIV replication was omitted from this study, thus excluding an important control and leaving the potential of miR-132 as a therapeutically relevant HDF unknown (Chiang, 2013). A more recent study identified let-7c, miR-34a and miR-124a as potential HDFs that are also upregulated following infection in T lymphocytes and a HeLa-derived cell line (Farberov, 2015). let-7c suppressed translation of the putative VRF, p21, following infection, while miR-124a and miR-34a were shown to target TASK (also known as KCNK3), which has been previously implicated as a target of Vpu-mediated degradation and in virion release (Farberov, 2015). Subsequent suppression of these miRNAs was found to inhibit viral replication as well as *in vitro* dissemination of HIV (Farberov, 2015)

There are currently only 5 host miRNAs that have been proposed as potential HDFs and unfortunately none of these relationships appear to be as robust as the one described for HCV and miR-122. Nevertheless, considering that functional relevance with regards to HIV interactions, for the majority of the host miRNome is unknown, there is still hope for identification and characterisation of a more ‘miR-122/HCV-like’ phenotype. Furthermore, positive regulation of HIV replication by specific host miRNAs succinctly demonstrates how HIV can ‘hijack’ the host miRNA network to subvert specific host restriction factors in order to favour viral replication.

1.16 Aims of this study

A decade of research has placed host miRNAs and its associated miRNA pathway as critical determinants in the etiology of HIV-host interactions (reviewed by Klase, 2012 and Barichievy, 2015). This dynamic relationship is now understood to be characterised by both host and viral-driven changes in cellular miRNA expression, subversion of specific subsets of host miRNAs in order to promote viral replication, and a diverse set of viral strategies to counter a select contingent of host miRNAs that may suppress viral replication. It must also be noted that much of the miRNA/siRNA-HIV research field is also littered with examples of poor concordance and inconsistencies between various bodies of work. Although these shortcomings are present in virtually all areas of HIV-related research, they are perpetuated by varying experimental parameters, and are confounded by the highly complex and tissue-specific nature of miRNA functionality. In contrast to a wealth of information available on functional relevance of the entire human coding genome with regards to HIV, current knowledge regarding functional significance of all host miRNAs covers only a small fraction of the human miRNome. Intriguingly, even this limited knowledge has proven more than sufficient to posit that the human miRNome is a valuable tool in delineating HIV-host biology. Clearly, the absence of large-scale functional miRNA data, similar to the seminal siRNA-HIV screens (reviewed by Pache, 2011) represents a major shortfall in current HIV research.

Primary Aim

The host miRNome has been identified as a critical mediator of host-pathogen interactions in the context of HIV replication. There is however a large gap in current knowledge regarding the functional relevance of each host miRNA within this relationship. The primary aim of this thesis was thus to address this shortcoming by first establishing and then utilising a high-content screening approach to characterise the functional relevance of host miRNAs during HIV replication.

Objectives

1) Establishment of a robust high-content screening workflow

The miRNA screens reported in this study represent the first large-scale, high-throughput RNAi screens conducted within the Gene Expression and Biophysics Group, and thus a considerable amount of time was dedicated to the optimisation of specific cellular assays, and evaluation of technical requirements essential to the establishment of a robust high-content image-based screening platform. These optimisations and technical requirements were divided to into the following sub-categories:

i) The rational design of a preliminary HCS experimental workflow

-Establishment of best practices for effective management and utilisation of reagent libraries, experimental plate design

ii) Validation of a suitable HCS assay for the quantification of HIV replication by image based screening

iii) *Optimisation of experimental conditions for screening of miRNAs in microwell plates*

-Optimisation of cell seeding densities, transfection conditions, infection conditions, validation of experimental controls

iv) Establishment and validation of an effective image acquisition, image analysis and data management pipeline

-Optimisation of imaging parameters for HCS, optimisation of image analysis parameters, development and implementation of appropriate quality control measures, optimisation of data processing and hit selection criteria

2) To utilize the screening workflow established in objective 1 in order to screen a commercial library of 1239 synthetic miRNA mimics and 1245 miRNA inhibitors in duplicate to identify host miRNAs, whose functional modulation, results in either enhanced or suppressed HIV replication phenotypes

3) To utilise a bioinformatics-based approach to identify putative functional targets of the miRNAs identified by objective 2 as well as specific regulatory pathways enriched for these targets

4) To utilise the HCS approach established by objective 1 to screen a library of small molecules in order to validate the functional relevance of the pathways/functional targets recovered by objective 3

Chapter 2: General materials and methods

All optimisation and experimental procedures were undertaken at the Council for Scientific and Industrial Research (CSIR) site in Pretoria within the laboratories of the Gene Expression and Biophysics Group led by Dr. Musa M. Mhlanga (UCT/CSIR).

2.1 Mammalian cell lines and culture conditions

All tissue culture and cell culture based experimental steps were conducted within class II, type A2 biological safety cabinets (Labconco, USA) using standard aseptic techniques, and cell cultures were maintained within water-jacketed Forma™ Direct Heat CO_2 incubators (Thermo Fisher Scientific, USA). Additionally these experiments were conducted within a dedicated biosafety level II (BSL II) tissue culture facility. Standard CO_2 incubator conditions of 37 °C and 5% CO_2 were maintained for routine culture and experimental conditions. Adherent cell lines were passaged using 1x TrypLE™ Express dissociation reagent (Thermo Fisher Scientific, USA). GHOST(3) X4/R5 cells, referred to as GHOST(3) cells, were obtained from the National Institute of Health (NIH) AIDS reagent programme (catalogue # 3942). GHOST(3) cell lines were cultured in phenol red-free Dulbecco's Modified Eagle's Medium (DMEM; Thermo Fisher Scientific, USA) supplemented with 10% heat-inactivated fetal bovine serum (FBS; Merck Millipore, USA), 2 mM Gibco® GlutaMAX™ (Thermo Fisher Scientific, USA) and an antibiotic selection cocktail comprised of 10 µg/mL Hygromycin B (Thermo Fisher Scientific, USA), 1 µg/mL Puromycin (Thermo Fisher Scientific, USA) and 300 µg/mL Geneticin (G418) (Thermo Fisher Scientific, USA). HEK293T cell lines were cultured in phenol red-free DMEM (Thermo Fisher Scientific, USA) supplemented with 10% heat-inactivated FBS (Merck Millipore, USA) and 2mM Gibco® GlutaMAX™ (Thermo Fisher Scientific, USA). TZM-bl cell lines were obtained from the NIH AIDS reagent database (catalogue # 8129) and maintained in the same media as HEK293T cells.

2.2 Plasmids and plasmid purification

An expression plasmid containing an Env-deficient PSG3-derived clone of HIV along with an ampicillin resistance (Amp^R) cassette ($PSG3^{\Delta Env}$) and another plasmid containing an R5-tropic HIV BAL-derived Env protein (pBAL-Env-Amp^R) were kindly provided by the Aptamer Research Group at CSIR Biosciences. A full length molecular clone of X4 tropic, pNL4-3-derived HIV (HIV Gag-iGFP) was also obtained from the NIH AIDS reagent programme (catalogue # 12457). Plasmids received from the NIH AIDS reagent programme were recovered from filter paper in Tris-EDTA (TE) buffer at pH 8.0 and the recovered DNA was quantified using a NanoDrop® ND-1000 UV-Vis spectrophotometer

(Thermo Fisher Scientific, USA). Plasmid stocks were amplified by propagation within stable DH5-α bacterial cultures under the relevant antibiotic selection. Briefly, an aliquot of competent DH5-α bacterial cells (50 µL in a microcentrifuge tube) was removed from the -80 ˚C freezer and thawed on ice. The cells were mixed gently in a circular motion using a pipette tip without aspirating any of the cell mixture and by using aseptic techniques. A total of between 10-50 ng of plasmid DNA was pipetted onto the thawed cell mixture and gently mixed using a pipette tip. The DNA-cell mixture was left submerged in ice for 30 minutes and then incubated at 42 ˚C for exactly 30 seconds in an AccuBlock™ digital dry bath (Labnet International Inc., USA) before being submerged in ice for 2 minutes. A 250 µL volume of antibiotic-free luria-broth (LB) media, pre-warmed to 37 ˚C, was added to the bacterial cells and the bacterial cell mixture was then placed in a shaking incubator for 1 hour. A volume of 100-200 µL of the bacterial culture was spread over LB-agar plates containing the relevant antibiotic. The plates were allowed to dry at room temperature for ~ 20 minutes, then inverted and incubated at 37 ˚C overnight. Bacteria were harvested from a single colony on agar plates for propagation and plasmid purification using the Nucleobond® Xtra Maxi plasmid purification kit (Macherey-Nagel GmbH & Co.KG, Germany) as per the manufacturer's guidelines. Bacterial plates were sealed with parafilm and stored at 4 ˚C for up to 3 weeks. Glycerol-stocks of all bacterial cultures were prepared during the early stages of the plasmid purification process and stored at -80 ˚C.

2.3 Virus production

HEK293T cells were co-transfected with $PSG3^{\Delta Env}$ and pBAL-Env plasmids using Fugene 6 lipid-based transfection reagent (Promega, USA) in order to produce single-cycle infectious BAL-pseudotyped PSG3 virions ($PSG3^{BAL}$). Briefly HEK293T cells were seeded in 23 mL of standard cell culture media within T-150 vented tissue culture flasks (TPP, Switzerland) at ~5000 cells/ flask 24 hr prior to transfection. On the day of transfection, 120 µL of Fugene 6 reagent was added directly to 3080 µL of serum-free basal DMEM media (SFM) within a sterile tube. The solution was gently mixed and incubated at room temperature for 5 minutes. 13,3 µg of pBAL-Env and 26,7 µg of $PSG3^{\Delta Env}$ plasmid were added to the diluted Fugene 6 solution, mixed gently and incubated at room temperature for ~ 25 minutes. The transfection mixture was added to the horizontally oriented flask in a dropwise manner and the flask was gently rocked to evenly distribute the transfection mixture. The transfected flask was then placed into a CO_2 incubator for 6-8 hr. Approximately 6-8 hr post transfection the media was replaced with 30 mL of standard cell culture media and the flask was returned to a CO_2 incubator for 48 hrs. The supernatant from the transfected flask was then harvested, supplemented with an extra 10% of FBS, filtered through a 0.45 micron (um) filter and subsequently aliquoted and stored at - 80 °C. HIV Gag-iGFP virions were produced in a similar manner except that HEK293Ts were transfected with 30 µg of a single HIV Gag-iGFP plasmid during the transfection step.

Viral titre

The approximate number of infectious HIV virions per mL of viral stock (viral titre) was determined using an end point dilution assay based on the calculation of the 50% tissue culture infectious dose ($TCID_{50}$) in TZM-bl cells (Kappes, 2005; reviewed by Richards, 2006). TZM-bls are a HeLa-derived cell line that stably express CD4, CXCR4 and CCR5 receptors as well as a Tat-sensitive reporter construct that drives co-expression of firefly luciferase and β-galactosidase (Kappes, 2005). Briefly, 150 µL of standard cell culture medium was added to all wells of a flat bottom 96-well tissue culture plate. Two viral stocks from separate harvests were incubated at 37 °C until fully thawed and 50 µL of thawed viral solution from each aliquot was added to each of the first 4 wells, or last 4 wells of column 1 respectively of the 96-well plate. A 4-fold serial dilution was prepared by repeated mixing of the contents within each well of column, and 50 µL of virus containing media was then transferred from the wells in column 1 to those in column 2 and sequentially on from column 2 to column 11, with 50 µL discarded from each well in column 11. The wells in column 12 of the plate were used as uninfected control samples. TZM-bls were seeded into all 96 wells at a density of 10 000 cells/per well, in 100 µL of standard cell culture media containing 7.5 mg/mL DEAE dextran. Following 48 hours of incubation at at 37^{o}C and 5% CO_2, 100 µL of supernatant was removed from each well, replaced with 100 µL of Bright-Glo™ luciferase assay substrate (Promega, USA) and incubated at room temperature for 2 minutes to allow cell lysis. The contents of each well were mixed by repeated pipetting and 150 uL was then removed from each well and transferred to a corresponding well on a black Corning costar® 96-well luminometer plate (Corning, USA). Luciferase activity within each well was recorded as a relative light unit (RLU) value using a FLx800™ multi-detection microplate reader and the accompanying Gen5 software package (BioTek®, USA). The RLU values were then used to determine the 50% endpoint dilution ($TCID_{50}$ /mL) of each viral stock using the Reed-Muench method of $TCID_{50}$ calculation (http://www.hiv.lanl.gov/content/nab-reference-strains/html/TCID501.xls). These titres were generally used as a point of reference and the infectivity of viral stocks were always evaluated in the relevant cell line (e.g GHOST(3) cells) before use.

2.4 RNAi transfection

All miRNA mimic, miRNA inhibitor and siRNA transfections were carried out using Lipofectamine® RNAiMAX (Thermo Fisher Scientific, USA) as per the manufacturer's guidelines. Approximately 5000 cells were seeded in 80 µL of cell culture media per well of a 96 well plate 24 hours prior to transfection. On the day of transfection 0.15 µL of RNAiMax transfection reagent was added to 9,85 µL of SFM in a sterile microcentrifuge tube, and 2,5 µL of a 1 µM siRNA/miRNA mimic/miRNA inhibitor stock solution was

added to 7,5 µL of SFM in a separate tube. Each microcentrifuge tube was mixed gently, and then combined. The transfection mixture was incubated at room temperature for ~ 20 minutes and all 20 µL of the transfection mixture was then added to the culture media to give a 25 nanomolar (nM) final concentration of siRNA/miRNA mimic/miRNA inhibitor, unless otherwise stated. Cells were cultured for 48 hour post transfection before downstream analysis. Transfection reactions were scaled according to the manufacturer's guidelines for the transfection of cells seeded in larger multiwell plates and flasks. ON-TARGET*plus* (OTP) siRNA pools, a non-targeting dye-labelled siGLO green transfection control, all miRIDIAN miRNA mimic and inhibitor non-targeting controls and a Dy547-labelled non-targeting miRNA mimic transfection control were all purchased from Dharmacon™ (GE Healthcare, USA)

2.5 HIV infection assays

Viral stocks were thawed to 37 °C before use. Thawed virus was diluted in prewarmed (37 ˚C) infection media (IM), comprised of basal DMEM (Thermo Fisher Scientific, USA), 2mM Gibco® GlutaMAX™ and 20 ng/mL of Polybrene® (Sigma-Aldrich®, USA), according to the required multiplicity of infection (MOI). An MOI of 0.5 (1 virion for every 2 cells) was generally used for imaging based analyses and an MOI of 1 was used for all population based assessments including, qPCR and western blot analyses.

2.6 RNA purification

Total RNA was purified from cultured cells using TRIzol® lysis reagent (Thermo Fisher Scientific, USA) as per the manufacturer's instructions. Briefly, for adherent cells grown in a 35 mm tissue culture dish, culture media was removed and replaced with 1 mL of TRIzol® lysis reagent within an active fume hood. The TRIzol® lysis reagent was then repeatedly pipetted several times using a 1 mL pipette tip to ensure cell detachment and lysis. Cell lysates were incubated at room temperature for 5 minutes to facilitate dissociation of nucleoprotein structures, transferred to a sterile microcentrifuge tube and 200 µL of ≥99% anhydrous Chloroform (Sigma-Aldrich®, USA) was added directly. The microcentrifuge tube was vigorously shaken by hand for 15 seconds resulting in a milky pink solution that was then incubated at room temperature for 3 minutes. The solution was then centrifuged at 12 000 x g for 15 minutes at 4 °C in a Microfuge 22R refrigerated benchtop microcentrifuge (Beckman Coulter Incorporated, USA).

Following centrifugation the solution separated into three distinct phases including a lower red phase containing protein, a gelatinous intermediate phase containing DNA and a clear upper phase containing RNA. The upper RNA-containing aqueous phase was carefully transferred to another sterile microcentrifuge tube and 500 µL of 99.5%

anhydrous 2-Propanol (Sigma-Aldrich®, USA) was added, the mixture was incubated at room temperature for 10 minutes, and then centrifuged as before. The supernatant was carefully discarded so as to not disturb the RNA pellet visible at the bottom of the microcentrifuge tube. Absolute ethanol (Sigma-Aldrich®, USA) was diluted to 75% in sterile water and 1 mL was added to the RNA pellet. The microcentrifuge tube was vortexed briefly to dislodge the RNA pellet and then centrifuged at 7 500 x g for 5 minutes at 4 °C. The ethanol was carefully discarded and the RNA pellet was partially dried at room temperature for ~ 5-10 minutes depending on the size of the pellet. The RNA pellet was then resuspended in ~30 µL of sterile RNAse-free water using a 20 µL filtered pipette tip and repeated pipetting. The RNA solution was incubated at 56.5 °C for ~ 12 minutes, cooled on ice and quantified using a NanoDrop® ND-1000 UV-Vis spectrophotometer (Thermo Fisher Scientific, USA). Only RNA samples with a 260 nanometer (nm) to 280 nm absorbance ratio > 1.8 and < 2.2 were retained for downstream cDNA synthesis. RNA quality was further validated by RNA gel electrophoresis and samples were aliquoted and stored at -80 °C to minimize the number of freeze-thaw cycles per aliquot.

RNA gel electrophoresis

The integrity of all RNA samples was validated by gel electrophoresis before their inclusion in downstream applications. RNA samples were prepared by adding the RNA sample to an equal volume of 2X denaturing RNA Loading Dye (Thermo Fisher Scientific, USA), followed by incubation at 70 ˚C for 10 minutes in an AccuBlock™ digital dry bath (Labnet International Inc., USA). Samples were cooled to room temperature and loaded onto a 3% SeaKem® LE Agarose (Lonza Group, Switzerland) 3-(N-morpholino)propanesulfonic acid (MOPS) gel. RNA gels were run in 1x MOPS running buffer containing both formamide and ethidium bromide and gels were visualised under UV light using a Syngene G:Box gel imaging system and associated GeneSys image acquisition software (Synoptics Ltd., United Kingdom). 1 µg of sample RNA was loaded in each well and the presence of intact 18S and 28S ribosomal RNA bands were used to evaluate the quality of RNA samples (Appendix II, Figure A2.1).

2.7 cDNA synthesis

DNAse treatment

RNA samples were thawed on ice and treated using RQ1 RNAse-free DNAse (Promega, USA) prior to reverse transcriptase polymerase chain reaction (RT-PCR). All DNAse treatment reactions and cDNA synthesis reactions were prepared on ice. Briefly, a standard amount of 1 µg of starting RNA was used for all DNAse treatment reactions. 1 µL of RQ1 RNase-Free DNase 10X Reaction Buffer (Promega, USA) and 1 µL of RQ1 RNase-Free DNase (Promega, USA) were added to 1 µg of starting RNA in a sterile

microcentrifuge tube and the reaction was made up to a final volume of 10 µL using sterile RNAse-free water (Promega, USA), followed by incubation at 37 °C for 30 minutes using a T100™ thermal cycler (Bio-Rad, USA). 1 µL of stop solution was added to the reaction, followed by incubation at 65 °C for 10 minutes as before to terminate DNAse activity.

Reverse transcription PCR

RT-PCR was performed using the SuperScript® III First-Strand Synthesis system (Thermo Fisher Scientific, USA) as per the manufacturer's guidelines. Briefly, 1 µL of the supplied 50 µM oligo(dT) primer or 50 ng of random hexamer primer was added to 8 µL of DNAse-treated RNA solution in a sterile microcentrifuge tube followed by 1 µL of the supplied dNTP mix. The reaction was incubated at 65 °C for 5 minutes in a T100™ thermal cycler (Bio-Rad, USA). The microcentrifuge tube was submerged in ice for 2 minutes and a cDNA synthesis mastermix was prepared in a separate sterile microcentrifuge tube by the sequential addition of 2 µL of 10x RT buffer , 4 µL of 25 mM $MgCl_2$, 2 µL 0.1 M Dithiothreitol (DTT), 1 µL of RNaseOUT™ and 1 µL of SuperScript® III reverse transcriptase enzyme. The 10 µL cDNA synthesis mastermix solution was then added to the chilled RNA-primer solution and depending on the primer used, the reactions were then subjected to different incubation steps. For oligo(dT) primer reactions, the microcentrifuge tube was incubated at 50 °C for 50 minutes and then at 85 °C for 5 minutes. For random hexamer primer reactions, the microcentrifuge tube was first incubated at 25 °C for 10 minutes, then at 50 °C for 50 minutes and finally at 85 °C for 5 minutes. Microcentrifuge tubes were chilled on ice for 2 minutes and briefly centrifuged. 1 µL of RNase H was added to the solution and the microcentrifuge tube was then incubated at 37 °C for 20 minutes in order to remove residual RNA. Reverse transcriptase deficient (no-RT) control reactions were prepared for each RT sample in exactly the same manner as described for RT samples (including DNase treatment) except that RT was replaced with nuclease-free water in the preparation of the cDNA master mix solution. 1 µL/reaction of sample cDNA or noRT control was utilized in all downstream PCR applications.

2.8 Primers

All primer sets utilised in this study were purchased from Inqaba Biotechnologies™ (South Africa) and were designed using the NCBI primer blast online primer designing resource (www.ncbi.nlm.nih.gov/tools/primer-blast/). The following general criteria were used for primer design: Human mRNA REFseq accession numbers were used as input templates for the design of primer set targeted to human transcripts. The sequence of relevant regions of HIV-PSG3 viral genome were used as the input templates for the design of primer sets targeted to specific viral transcripts. A PCR product size range of between 100-1000 bp was used. Optimal primer melting temperature (T_m) was set at 60

˚C and the minimum and maximum T_ms were set to 58 ˚C and 62 ˚C respectively. Primer specificity was evaluated by blasting each primer set against the *Homo sapien* Refseq RNA database. Primers were reconstituted to 100 µM stocks in nuclease free water (Invitrogen, USA), aliquoted at stored at -20°C. Working dilutions of 10 µM were prepared for each primer, and stored at -20°C. A summary of the primers utilised in this study are presented in Table 2.1. All individual primers were utilised at a final concentration of 500 nM.

Table 2.1. Primer information

Primer	Sequence (5'-3')	PCR product size (bp)
ß-actin forward	CGAGCACAGAGCCTCGCCTTT	878
ß-actin reverse	CCACAGGACTCCATGCCCAGG	
CD4 forward	CTGTGGTGGCAGGCGGAGAG	143
CD4 reverse	TGGGGCAGGGTGAGGTGGAG	
CDKN1A forward	AGTCAGTTCCTTGTGGAGCC	842
CDKN1A reverse	AGGAGAACACGGGATGAGGA	
EGFR forward	CTGTCCAACGAATGGGCCT	656
EGFR reverse	TGATCTTGACATGCTGCGGT	
HIV Gag forward	GGCCTTCAGCCCAGAAGTAA	593
HIV Gag reverse	CTTTATGGCTGGGTCCTCCC	
HIV Tat forward	GTGGCAATGAGAGTGACGGA	959
HIV Tat reverse	AGTGCTCTGCCTGGTCCTAT	
HPRT forward	GCAGCCCTGGCGTCGTGATTA	499
HPRT reverse	CGTGGGGTCCTTTTCACCAGCA	
Lincp21 forward	CAGGGAACCCCTTCAATCCC	400
Lincp21 reverse	TTTTTGCCCACATGAGCCTG	
TP53 forward	TGACACGCTTCCCTGGATTG	610
TP53 reverse	ACCATCGCTATCTGAGCAGC	

2.9 Conventional PCR and DNA gel electrophoresis

Conventional PCR (PCR) was utilized either to identify the optimal annealing temperature(s) for new primer sets or for the qualitative assessment of gene expression. A final reaction volume of 25 µL was utilised per reaction using the Kappa HiFi DNA polymerase kit (Kapa Biosystems, USA) and the following cycling conditions: initial denaturation at 95 ˚C for 5 min followed by 35 cycles of 98°C for 20 seconds, 60°C for 15 seconds and 72°C for 60 seconds, followed by a final extension step of 72 ˚C for 60 seconds and a 4 ˚C hold step. The 60 ˚C annealing step was replaced with a suitable temperature gradient as required and all conventional PCRs were run in a T100™ thermal cycler (Bio-Rad, USA).

DNA agarose gel electrophoresis

PCR products were subjected to size-dependent separation using agarose gel electrophoresis. Briefly, agarose gels were prepared by diluting 2% (w/v) SeaKem® LE Agarose (Lonza Group, Switzerland) in 1x Tris-Borate-EDTA (TBE) electrophoresis buffer. Ethidium bromide (Sigma-Aldrich, USA) was added to the agarose solution at a final concentration of 0.5 µg/mL before the gel was cast. 6x DNA gel loading dye (Thermo Fisher Scientific, USA) was diluted to 1x for each PCR product and loaded into individual wells of the agarose gel. A DNA molecular weight marker (MWM), GeneRuler™ 100 bp Plus DNA Ladder (Thermo Fisher Scientific, USA) was included on the first and/or last lane of each gel to confirm the size of PCR products.

2.10 Quantitative real-time PCR (qPCR)

qPCR was utilised in order to quantify and compare the expression levels of transcripts of interest between specific experimental conditions. A final reaction volume of 20 µL and the SsoFast™ EvaGreen® Supermix (Bio-Rad, USA) was utilized for all qPCR reactions, and they were run in a CFX96™ real-time PCR detection system (Bio-Rad, USA) using the CFX Manager™ software interface. The following general protocol was utilized for all qPCR runs: 1) an initial denaturation step of 94 °C for 2 minutes, 2) 40 cycles of 94 °C for 15 seconds, 60 °C for 30 seconds, 72 °C for 1 minute, a single plate read in the SYBR green channel, 3) a 72°C extension step for 10 minutes, and 4) a melt curve analysis. The melting curve analysis ranged from 50 °C to 95 °C in 0.5 °C increments with a plate read (SYBR-Green) for every 1 °C increment following a 5 second hold step. The 60 ˚C annealing step was replaced with an alternative temperature as required by specific primer sets. The melting temperature obtained for each qPCR product was confirmed using DNA gel electrophoresis as described above. Three technical replicates of every transcript of interest and references gene(s) were included for each experimental condition in a single qPCR run and three experimental runs were performed for each set of qPCR results presented in this dissertation (n=3).

The quantification cycle (C_q), also known as threshold cycle or C_T, values obtained for each reaction were then normalised using the $2^{-\Delta\Delta C_T}$ method (Livak, 2001) in order to determine the relative expression levels of transcripts of interest (see below). *Hypoxanthine-guanine phosphoribosyltransferase* (*HPRT*), *Beta-actin* (*ß-actin*) and *Ribosomal Protein S12* (*RPS12*) were evaluated/utilised as reference genes in this study.

$2^{-\Delta\Delta C_T}$ analysis

The average C_q value of the technical replicates of each transcript of interest in each experimental condition were normalized against the average C_q of the internal reference gene for that particular experimental condition. Where possible, the geometric mean of the average C_q values of multiple reference genes were utilised. These normalised C_q values were then normalised against the values obtained for the experimental control in order to determine the relative fold-change in transcript expression levels between experimental conditions.The statistical significance of the fold change values derived from 3 separate experimental runs was determined using either a two-tailed Student's T-test or a single factor analysis of variance (ANOVA) depending on the number of transcripts being investigated in an experimental run. Kolmogorov-Smirnov tests were utilised to confirm a normal distribution of the data. All statistical analyses were performed using SPSS v.15.0 (IBM® Corporation, USA). Transcript expression levels are presented as bar graphs and error bars represent the standard error of the mean (SEM).

2.11 Protein extraction

Whole cell lysis

Whole cell lysate was extracted using radio-immunoprecipitation assay (RIPA) lysis buffer (150 mM sodium chloride, 1% NP-40, 0.5% sodium deoxycholate, 0.1% SDS, 50 mM Tris pH 8.0) supplemented with cOmplete™ mini EDTA-free protease inhibitor cocktail (Roche, Switzerland). Cultured cells were were harvested in ice cold RIPA buffer using a cell scraper (TPP, Switzerland) and transferred to a pre-chilled (on ice) sterile microcentrifuge tube. The lysis solution was then incubated at 4 ˚C for ~ 45 minutes on an agitator before being centrifuged at 16 000 x g for 20 minutes at 4 ˚C in a Microfuge 22R refrigerated benchtop microcentrifuge (Beckman Coulter Incorporated, USA). The supernatant (whole cell lysate) was transferred to a pre-chilled (on ice) sterile microcentrifuge tube and the pellet (cell debris) was discarded. Protein concentration was quantified by absorbance using a NanoDrop® ND-1000 UV-Vis spectrophotometer (Thermo Fisher Scientific, USA) and samples were snap frozen in liquid nitrogen and stored at -80 ˚C.

Nuclear and cytoplasmic fractionation

Nuclear and cytoplasmic protein fractions were purified from cultured cells using the NE-PER® nuclear and cytoplasmic extraction kit (Thermo Fisher Scientific, USA) as per the manufacturer's instructions. All centrifugation steps were performed at 4 ˚C in a Microfuge 22R refrigerated benchtop microcentrifuge (Beckman Coulter Incorporated, USA) and all reactions were prepared on ice. The required volumes of CERI and CERII buffers were supplemented with cOmplete™ mini EDTA-free protease inhibitor cocktail (Roche, Switzerland) prior to use. Briefly, cultured cells were harvested in ice cold 1x PBS buffer using a cell scraper (TPP, Switzerland) and transferred to a sterile microcentrifuge tube. Cells were pelleted by centrifugation at 500 x g for 3 minutes and the supernatant was discarded. The pelleted cells were resuspended in CERI buffer by vortexing at maximum speed for 15 seconds and then incubated on ice for 10 minutes. An appropriate volume of CERII buffer, relative to the volume of CERI buffer used, was added to the resuspended cell mixture, samples were then vortexed at maximum speed for 5 seconds and incubated on ice for 1 minute. Samples were then similarly vortexed and centrifuged at 16 000 x g for 5 minutes. The supernatant containing the cytoplasmic protein fraction was carefully removed and transferred to a pre-chilled (on ice) sterile microcentrifuge tube. The remaining nuclear pellet was resuspended in 100 µL of ice-cold NER buffer and vortexed at maximum speed for fifteen seconds. The sample was placed in ice and vortexed at maximum speed for 15 seconds every 10 minutes for a total of 40 minutes. The sample was centrifuged at 16 000 x g for 10 minutes and the supernatant containing the nuclear protein fraction was transferred to a sterile and pre-chilled (on ice) microcentrifuge tube. Nuclear and cytoplasmic fractions were aliquoted and snap frozen in liquid nitrogen before being stored at - 80 ˚C. The protein concentration of specific aliquots was quantified using a NanoDrop® ND-1000 UV-Vis spectrophotometer (Thermo Fisher Scientific, USA) prior to use.

2.12 Western Blot Analysis

Rabbit anti-EGFR (ab2430), mouse anti-p24 (ab9071) and rabbit anti-Histone H3 (ab1791) primary antibodies were purchased from Abcam plc (UK). A goat anti-Actin C-11 (sc-1615) antibody was purchased from Santa Cruz Biotechnology® Inc. (USA). Horseradish peroxidase (HRP)-conjugated secondary antibodies raised against rabbit, mouse and goat were purchased from Rockland Immunochemicals Inc. (USA).

Total cell lysates as well as nuclear and cytoplasmic protein fractions were resolved by sodium dodecyl sulfate polyacrylamide gel electrophoresis (SDS-PAGE) on 10% bis-acrylamide denaturing gels. Protein isolates were diluted in Laemmli sample loading buffer (Bio-Rad, USA), incubated at 95 ˚C for 5 min and cooled to room temperature before loading. A total of 20 µg of whole cell lysate, 40 µg of cytoplasmic protein extract

and 20 µg of nuclear protein extract were loaded per well and at least one lane on every gel was reserved for a Precision Plus Protein™ marker (Bio-Rad, USA). SDS-PAGE gels were run in pre-chilled (4 ˚C) Tris-glycine running buffer (25 mM Tris, 192 mM Glycine, pH 8.3) at 130 volts (V) for ~2 hours. Proteins were transferred to an Immun-Blot® polyvinyl difluoride (PVDF) membrane (Bio-Rad, USA) in pre-chilled (-20 ˚C) transfer buffer (25 mM Tris, 192 mM Glycine, 10% Methanol, 5% SDS) at 55 V for ~ 2.5 hours. Membranes were blocked in 5% (w/v) bovine serum albumin (BSA, Sigma-Aldrich, USA) and 1x PBS buffer for 1 hour at 4 ˚C on a rotating shaker and then rinsed in 0.5 % (v/v) Tween® 20 (Sigma-Aldrich, USA) in 1x PBS buffer (PBS-T). Membranes were incubated at 4 ˚C overnight with primary antibodies diluted in 0.5 % PBS-T as follows:rabbit anti-EGFR at 1:250, mouse anti-p24 at 1:500, rabbit anti-Histone H3 at 1:1000 and goat anti-Actin at 1:500. Membranes were washed 3 times in 0.5% PBS-T for 10 minutes at room temperature on a rotating shaker and incubated with an appropriate HRP-conjugated secondary antibody diluted in 0.5% PBS-T for 1 hour at room temperature on a rotating shaker. Membranes were washed three times in 0.5% PBS-T on a rotating shaker for 10 minutes at room temperature before being incubated with Clarity™ enhanced chemiluminescence substrate (Bio-Rad, USA) for 5 minutes at room temperature on a rotating shaker. HRP activity was visualized as immunoreactive bands using a ChemiDoc™ XRS+ system (Bio-Rad, USA). Blots were acquired as images and were subjected to densitometric analyses for interpretation when required.

Densitometric analysis

Densitometric analyses were performed using FIJI open source image analysis software (Schindelin, 2012) and Microsoft excel 2011 (Microsoft, USA). Briefly, the raw images obtained from the ChemiDoc™ XRS+ system were converted to 8-bit images and analysed in FIJI using the *Analyze>Gels* function. The profile of each lane on a blot was defined in order to include band(s) representing the protein of interest (e.g. EGFR) as well as the band representing the reference protein for that sample (e.g. Actin). The intensities of the bands defined by each lane were then measured and recorded as peaks in signal intensity. All of the recorded measurements for each lane were then exported to Excel for further analysis. The signal intensity value(s) for the protein of interest in each experimental condition was first normalised against the intensity value of the reference protein for that lane in order to normalise the signal intensity measurement against the amount of total protein loaded per lane. The normalised signal intensity for the protein of interest (∆ Intensity) in each experimental condition was then normalised again, this time using the ∆ Intensity value for the control condition in order to determine the relative expression level of the protein of interest in each experimental condition as compared to the experimental control.

2.13 Immunocytochemistry (ICC)

Indirect immunofluorescence was utilized in order to evaluate the expression levels and subcellular locations of specific proteins by fluorescent microscopy. Primary antibodies were purchased from Abcam (UK) and ATTO dye-conjugated secondary antibodies were purchased from Rockland Immunochemicals Inc. (USA). Cultured cells were fixed in 4% Paraformaldehyde (PFA, Sigma-Aldrich®, USA) solution at room temperature for 15 minutes. Fixed cells were washed 3 times in 1x PBS for 5 minutes at room temperature per wash and then permeabilized in a 0.25% (v/v) Triton X-100 (Sigma-Aldrich®, USA) solution made up in 1x PBS for 15 minutes at room temperature. The permeabilization solution was removed and then replaced with a blocking solution comprised of 2% (w/v) BSA in 1x PBS, and cells were incubated at room temperature for 1 hour. The blocking solution was removed and replaced with primary antibody diluted in antibody dilution buffer comprised of 1% (w/v) BSA and 0.15% (v/v) Triton™ X-100 in 1x PBS using the following dilutions: rabbit anti-EGFR (ab2430) at 1:200, mouse anti-p24 (ab9071) at 1:100 and mouse anti-H2AX-γ phospho-serine 139 (ab1174) at 1:500. Cells were incubated in primary antibody solution for either 1 hour at room temperature (EGFR, H2AX-γ) or overnight at 4 ˚C (p24). Following the primary antibody incubation step, cells were subjected to three 5 minute washes in 0.2% PBS-T at room temperature.

Cells were incubated with an appropriate dye-conjugated secondary antibody for 1 hour at room temperature with samples covered in aluminum foil. Secondary antibodies were diluted (1:1000) in antibody dilution buffer prior to use. All steps following the secondary antibody incubation were performed with samples shielded from light using aluminium foil. Following the secondary antibody incubation step, cells were subjected to three 5 minute washes in 0.2% PBS-T and nuclei were counterstained with 2 μM Hoechst 33258 (Sigma-Aldrich, USA) in 1x PBS for 15 minutes at room temperature. Cells were washed with 1x PBS and then either imaged in a suitable volume of 1x PBS (cells seeded in μClear® 96 well imaging plates (Greiner Bio-One International GmbH, Germany) or glass-bottomed tissue culture dishes (MatTek corporation, USA)) or mounted prior to imaging (cells seeded on coverslips were mounted onto glass slides using VECTASHIELD® antifade mounting medium (Vector Laboratories, USA), and the edges of the coverslips were sealed using clear nail polish before imaging). Antibody-specific negative controls were prepared in each ICC experimental set where either the primary or secondary antibody was excluded from the ICC process. These controls were included in order identify primary antibodies that were autofluorescent and secondary antibodies that exhibited non-specific binding.

2.14 Imaging

Two imaging systems were utilised for the microscopy-based experimental work described in this dissertation. The first was a spinning disk confocal microscope system (Andor Technology, UK) comprised of an Axio Observer Z1 inverted light microscope (Zeiss, Germany) equipped with a ProScan™ PZ100 motorized microscope stage (Prior Scientific, UK), a Polychrome V monochromator (TILL Photonics GmbH, Germany) with a 320-680 nm output range, Lambda 10-3 optical filter changers and *SMART*SHUTTER™ control system (Sutter instrument company, USA), a CSU-X1 spinning disk confocal scanner unit (CSU, Yokogawa electric corporation, Japan), a Definite Focus infra-red LED-based automatic focus unit (Zeiss, Germany), an iXON^{EM}+ electron multiplying charge coupled device (EMCCD) camera (Andor Technology, UK) and a Revolution laser combiner 400 series (Andor Technology, UK). The following excitation and emission wavelengths were utilised: Hoechst/ DAPI: 405/, GFP/ ATTO 488: 500/520, CY3/ ATTO 550: 550/570, CY5/ ATTO 647: 649/670. Images were acquired as 14-bit Tagged image file format (TIFF) files. The following Zeiss objectives were utilised: 10x Plan-apochromat (NA 0.45), 20x Plan-apochromat (NA 0.8) and 40x Plan Neofluar® oil (NA 1.3). Image acquisition settings (i.e exposure times, laser power, gain, averaging etc.) were kept constant across all samples within an experimental set for each channel acquired.

The ImageXpress® Ultra (IXU) confocal high content screening system (Molecular Devices LLC, USA) was the the second imaging system utilised in this study. All of the image-based screens were undertaken using this closed-box point-scanning confocal microscope system comprised of 4 solid state lasers (405 nm, 448 nm, 532 nm, 635 nm), 16-bit photomultiplier tube (PMT) detectors, a motorised stage, a dedicated 690 nm laser autofocus system, 5 self-aligning beam splitters and four Nikon objectives (Nikon, Japan). Images were acquired using the MetaXpress® image acquisition and analysis software programme (Molecular Devices LLC, USA) and were saved as individual (per channel/FOV) 16-bit TIFF files containing specific meta-data such as plate and well ID, acquisition channel information and FOV location data. Image acquisition settings (i.e binning, laser power, gain, averaging etc.) were kept constant for each acquisition channel within an experimental set and across all plates within a single screening replicate. Images obtained from miRNA and compound screens were acquired sequentially for each channel per FOV using the 20x Plan-apochromat λ objective (NA 0.75) and 4 FOVs (100 µm apart) were acquired per well. The 10x Plan-apochromat λ (NA 0.45) and 40x Plan-apochromat λ objective (NA 0.95) were utilised in optimisation and downstream validation experiments and imaging parameters were adjusted as required for these experiments.

2.15 Image analysis

Routine image processing for ICC and other low throughput imaging experiments was carried out using the open source image analysis software package, FIJI (Schindelin, 2012). The image analysis approaches utilised for HCS are discussed in detail in Chapter 3. The development of bespoke MATLAB® (Mathworks Inc, USA) scripts and their subsequent optimisation and execution for HCS were performed by Mr. Rethabile Khutlang and Dr. Johnathan Warrell, members of the Gene Expression and Biophysics Group at CSIR.

2.16 Statistical analysis and data mining for HCS

HCStratomineR (HCSR) is a web based statistical analysis and data mining solution that was specially designed for the analysis of HCS data. HCSR was designed by a collaborator, Mr. Wienand Omta, at the University Medical Centre Utrecht in Holland (publication under review) and was utilised for all of the quality control monitoring, data visualization, data transformation, data reduction and hit selection steps in the HCS image analysis pipeline developed for this study.

2.17 miRNA pathway analysis

miRNA target prediction and subsequent pathway analysis was completed using an open source web-based miRNA pathway analysis tool, miRpath (Vlachos, 2015). miRpath integrates the functionality of a miRNA target prediction tool (microT-CDS), a database of experimentally validated miRNA-target interactions (TarBase v7.0) and the Kyoto Encyclopedia of Genes and Genomes (KEGG) pathway resource in order to evaluate the statistical and hierarchical probability of miRNA-pathway interactions. miRNA hit lists were uploaded on the miRpath server and where available, TarBase was utilised as the primary miRNA target identification resource. False discovery rate (FDR) correction and conservative statistical analyses were applied and miRNA target data was merged using the *pathways union* option. A p-value threshold of 0.05 and a microT-CDS threshold of 0.8 were applied.

2.18 Compound-protein interaction analysis

Compound interaction analyses were performed for compounds identified as screen hits using the online chemical-protein interaction resource, STITCH 4.0 (Kuhn, 2008). Compound hit lists from pre- and post- exposure drug screens were uploaded to the

STITCH 4.0 web page using the *batch import* function and protein interactions were predicted using the *Neighbourhood, Gene Fusion, Co-occurrence, co-expression, Experiments, Databases and Textmining* prediction options along with the requirement of a high confidence (> 0.7) interaction score. Gene ontology (GO) term functional and spatial enrichment and analyses were also applied within STITCH 4.0.

2.19 miRIDIAN miRNA library

The miRIDIAN miRNA library based on miRbase v.16 was purchased from Dharmacon™ (GE Healthcare, USA). The library was divided into two components, a miRNA mimic library and a miRNA inhibitor library. The miRNA mimic library comprised 1239 synthetic dsRNA oligonucleotides that have sequences based on endogenous miRNAs, and are chemically modified to ensure correct guide strand selection during RISC programming. miRNA mimics function to augment intracellular levels and functional activities of specific endogenous miRNAs, leading to downregulation of the target mRNA species (Figure 2.1). In contrast, miRNA inhibitors are ssRNA oligonucleotides that are chemically modified to resist RISC-mediated cleavage, and exhibit secondary structures that facilitate binding to a specific host miRNA. miRNA inhibitors therefore function as sponges by sequestering specific miRISC complexes leading to suppression of specific endogenous miRNAs (Figure 2.1). The Dharmacon inhibitor library component was comprised of 1245 miRNA inhibitors.

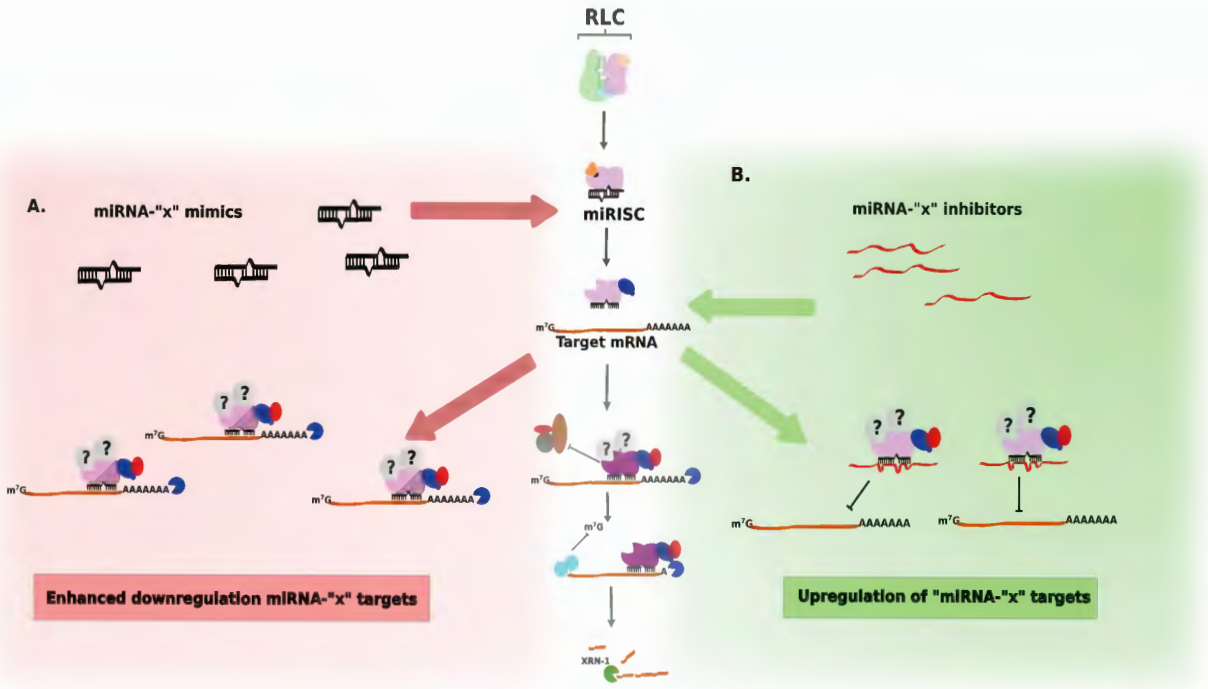

Figure 2.1 miRIDIAN miRNA library.

miRNA mimics function as mature miRNA molecules and feed into the miRNA functional pathway at the point of miRISC programming resulting in an increased intracellular levels of the specific miRNAs, in turn promoting miRISC-target interactions and downregulation of mRNA target species (A). In contrast, miRNA inhibitors are able to preferentially bind and suppress the functional activity of specific miRISC complexes (B). Ectopic expression of a miRNA inhibitor therefore results in enhanced levels of mRNA species that would otherwise be negatively regulated by specific endogenous miRNAs.

2.20 Customised compound libraries

Two customised compound libraries were kindly provided by Roderick Beijersbergen (Netherlands Cancer Institute, Holland). The first library comprised 101 US food and drug administration (FDA)-approved oncology drugs (APPENDIX Table A2.1). The second library comprised 192 kinase inhibitors (APPENDIX, Table A2.2). Both of these libraries were comprised of well annotated compounds with clearly defined endogenous targets and form part of larger compound collections that are routinely utilized in a commercial research environment.

Chapter 3: Establishment and optimisation of high content screening workflows

3.1 Introduction

High throughput screening (HTS) can be achieved through the miniaturization of experimental reactions (e.g using microplates) and improved liquid handling procedures (e.g. robotics, multichannel micropipettes) in order to execute a large number of independent experiments in a relatively short time frame (reviewed by Zanella, 2010 and Zhang, 2012). Cell-based HTS approaches in particular, traditionally rely on quantification of a single reporter readout (e.g. using a plate reader) in order to detect cellular changes in a biological process or molecular target of interest. While this approach is extremely useful in specific applications, such as generating dose response curves, traditional HTS approaches are not able to fully capitalise on all of the potential systems biology readouts that are inherent to cell-based assays (Zanella, 2010; Swinney, 2011). In contrast to biochemical assays, cell-based assays provide a considerably higher level of physiological relevance with regards to recapitulation of endogenous cellular responses, such as variations in cellular morphology and subcellular rearrangements. Traditional HTS approaches that utilise a single readout are therefore not able to comprehensively resolve discrete phenotypes, and are also unable to differentiate between heterogeneous single cell responses within a population of cells (Swinney, 2011).

High content screening (HCS) refers to an HTS approach where not one but multiple measurements are extracted from each experimental reaction (Shariff, 2010; Zhang, 2012). Cellular image-based screens in particular have become synonymous with the term HCS and all references to HCS within this dissertation refer to image-based HCS approaches. Imaging represents a robust tool for the spatio-temporal resolution of complex biological phenomena via the extraction and quantification of specific biologically relevant subcellular measurements (Zanella, 2010; Xia, 2012). Fluorescent proteins and fluorophore-conjugated molecular probes facilitate labelling of almost all cellular structures, from the scale of individual cells and nuclei, up to specific proteins, and even specific sequences of DNA and RNA. Such fluorescent tags allow researchers to label multiple subcellular structures within a population of cells and thus permit visualization and quantification of a number of functional and morphometric phenotypes, at a single cell level, using fluorescence microscopy (Zanella, 2010). Furthermore, the ability to differentiate between individual cells within a given population also allows researchers to readily differentiate between heterogenous cellular responses, and to monitor variations in cell number in response to specific treatments, as well as other functional readouts.

Since its inception, HCS has been widely utilised in a commercial setting in order to profile toxicity, efficacy and potential off-target effects of drug candidates (Zhang, 2012). The combination of HCS with genome-wide RNAi strategies (miRNA, siRNA, shRNA) on the other hand, has allowed both academic and commercial researchers to efficiently interrogate the functional relevance of the human proteome (~ 1 x 10^6 proteins) by screening using a relatively small number of reagents (~2000 miRNAs targeted to 25 000 genes). This RNAi-based screening approach has been successfully utilised to characterise gene function in a number of biological models including stem cell differentiation, tumorigenesis and host pathogen interactions (Whitehurst, 2007; Reviewed by Brodin, 2011 and Xia, 2012).

Despite the fact that recent advancements in automated microscopy, image analysis solutions and molecular labeling technologies have made HCS technologies more readily accessible, academic HCS facilities are not widely prevalent, even globally. This is in part due to the fact that not many research facilities possess the specialized technical expertise, infrastructure and funding required to establish and maintain a functional HCS platform (Buchser, 2004). The existing infrastructure and availability of specialised equipment at in Gene Expression & Biophysics laboratory thus provided an ideal setting to establish an HCS platform in South Africa.

A major aim of this PhD project was therefore to exploit the appropriate resources within the laboratory to establish a functional HCS platform that could be utilized for screening pharmaceutically relevant compounds and RNAi reagents in cellular models relevant to the South African research climate. A major aim of this study was therefore to develop and then execute a HCS-based approach to delineate HIV-host interactions. Specifically, the identification of novel host factors required for successful HIV infection by using pharmaceutical compounds and RNAi reagents. Successful implementation and execution of an HCS approach is highly dependent on the development of a robust HCS experimental pipeline, which in turn is established through a series of rigorous experimental design and optimisation steps (Boutros, 2008; Johnston, 2014). These steps, including the development of guidelines for management of reagent libraries and optimisation of various experimental parameters are presented in this chapter.

3.2 Automated vs. non automated liquid handling considerations

One of the first steps in the design process was to determine whether screens would be executed using an automated liquid handling solution or by hand. The available robotics option was thus rigorously evaluated for its suitability to the proposed HCS workflow using a number of simulated liquid handling procedures. Limitations in the minimum volume of liquid that could be accurately transferred using the available dispensing arms, and the location of the instrument within a ‘clean room’ facility that was not BSL-2 certified influenced the final decision that planned screens would instead be executed by

hand within a BSL-2 tissue culture facility. This decision in turn influenced the choice of using only a 96 well microplate format, as 384 well (and higher throughput) microplates are not readily conducive to non-automated screening approaches. Apart from reconstitution and daughtering of the miRNA libraries, all other liquid handling steps were executed by hand using multi or single channel micropipettes as required. A number of liquid handling procedures and experimental steps were therefore specifically adapted and optimised for use with multichannel micropipettes and screening in a 96 well microplate format (discussed in detail below).

3.3 Library management

Reagent libraries generally represent one of the most valuable commodities in a HCS setup and should therefore be well curated. The configuration and concentration of reagents within reagent library plates can impact many experimental design parameters, and the choice of storage plate type and storage conditions are also important factors that can influence stability of the reagents during long term storage and transport. Establishment of effective library management strategies should therefore be considered during the early stages of the HCS design process. In the context of this thesis 'master plates' refer to the library plates in which miRNA reagents or compounds were originally reconstituted/diluted and 'daughter plates' refer to plates produced by aliquoting the reagents present in a master plate. The process of distributing reagents from a master plate to daughter plates is referred to as 'daughtering'. The concentration and volumes selected for reagents in master and daughter plates, as well as configuration of these reagents within each plate type were important parameters that were considered during the development of the library management guidelines.

miRIDIAN microRNA library

The miRIDIAN miRNA library was shipped from the supplier in a 96 well format with a specific miRNA mimic or inhibitor aliquoted in each well as a 0.15nmol lyophilised pellet. Wells in the first and last column of each library plate were empty. A total of 33 plates, 16 plates containing miRNA mimics and 17 plates containing miRNA inhibitors, were received. miRIDIAN miRNA master plates were reconstituted using aseptic techniques and the JANUS® automated liquid handling workstation (PerkinElmer, USA). Customised operating protocols were developed and optimised for the specific purpose of reconstituting master plates and production of daughter plates. Specifically, dispensing and aspiration heights and pressures were optimised for use with the library-specific brand of 96 well plates, required pipetting volumes and required action (e.g mixing well contents vs. adding or removing liquid). Briefly, 96 well master plates containing lyophilized pellets were centrifuged at 500 x g for 5 minutes and reagents were resuspended in 1x Dharmacon™ siRNA buffer (GE Healthcare, USA) at a final concentration of 1 µM. A pipetting error-buffered volume of each reagent, suitable for 5x

uses, was then aliquoted into 3 daughter plates. Daughter and the master plates were sealed with Rotilabo® AllumaSeal II™ sterile adhesive seals (Carl Roth GmbH + Co. KG, Germany) and placed into storage at - 20 ˚C (A detailed version of the daughtering process is available in the Appendix).

A number of technical parameters were considered to determine the final volume, concentration and configuration of reagents in both master and daughter plates. Higher reagent concentrations favour reagent stability during long-term storage but also necessitate the use of either smaller volumes of reagent or additional liquid handling steps in downstream applications. As the generation of daughter plates relied intimately on the robustness of various multichannel micropipettes, a number of simulated liquid transfer experiments using water were completed, and a lower volume of 2 µL was determined to be the minimum reproducible volume. miRNA reagents in daughter plates were thus maintained at a concentration of 1 µM to facilitate a downstream transfection reaction volume of 2.5 µL (See Transfection). Dharmacon™ recommends a maximum of 5 freeze-thaw cycles for miRIDIAN miRNA library reagents following reconstitution. A volume of 15 µL of each reagent was therefore aliquoted to each daughter plate to allow for 5 x 2.5 µL uses as well as an extra 2.5 µL to compensate for reagent loss due to pipetting error. The well configuration of each master plate was maintained during production of daughter plates (Figure 3.1), and this was also influenced by the intended format of the experimental plates (See *Experimental plate selection and design*).

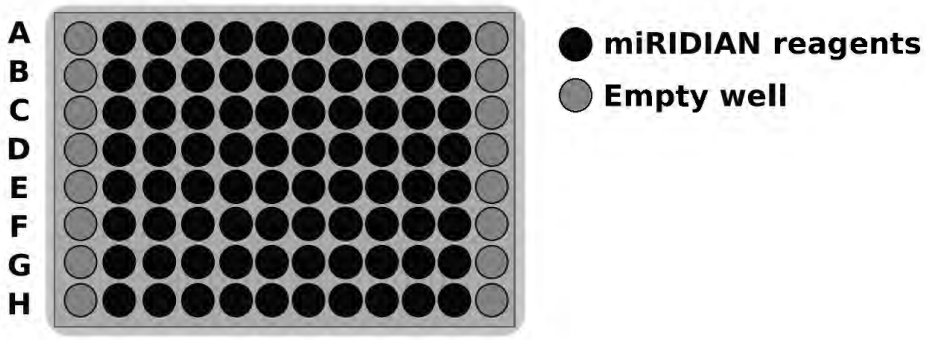

Figure 3.1 Configuration of reagents in miRIDIAN miRNA master and daughter plates.

miRNA mimic/inhibitor molecules (black wells) were located in rows A-H and columns 2-11 only.

Compound libraries

The FDA-approved oncology and kinase inhibitor libraries were each received in a 96 well plate format. 101 oncology compounds were distributed across 2 plates while 192 kinase inhibitors were supplied in three 96 well plates. Compounds were received as frozen 10 mM droplets reconstituted in DMSO, and were diluted to 1 mM stock solutions in 1x PBS, using the miRIDIAN library plate configuration. (Figure 3.2). Two sets of master plates were produced for each compound library and compounds were screened

at 3 concentrations i.e 100 nM, 1 µM and 10 µM. Three iterations of daughter plates were produced for each library from a single set of master plates in order to keep the volume of compound dispensed during the screening protocol constant regardless of the final concentration of compound used. Daughtered plates were produced at 100 µM, 10 µM and 1 µM concentrations with a standard volume of 10 µL of reagent. Compounds were reported to be stable for up to 1 month at -20 ˚C following initial dilution, but screens were completed within two weeks to maximise the functional potency of compounds.

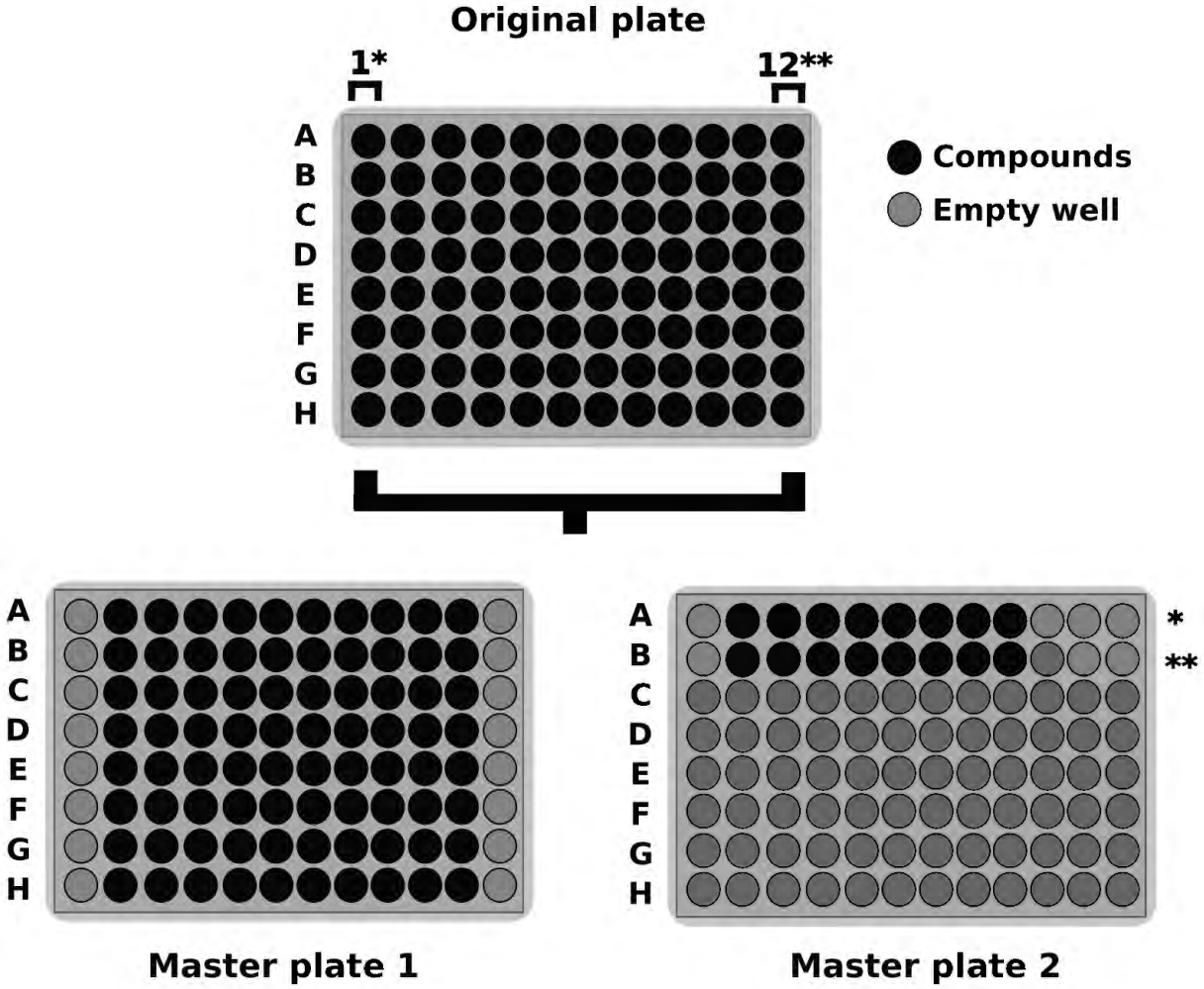

Figure 3.2 Configuration of compound library plates.

Master plates produced from the original compound library plates were re-configured to resemble the format of miRNA library plates. The reagents in columns 1 and 12 of the original library plates were transposed and transferred to a rows 1 and 2 on master plate 2.

3.4 Experimental plate selection and design

Three experimental plates were evaluated for their suitability in the phenotypic screening workflow and 96 well µClear® imaging plates (Greiner Bio-One International GmbH, Germany) were selected. Placement of control wells, the potential impact of edge effects and simplification of downstream liquid handling procedures were all major factors that influenced the design of the experimental plate layouts. Edge effects refers to the phenomenon whereby an increased rate of evaporation occurs within the outer wells of a multiwell plate as compared to the inner wells during long incubation times (Lundholt, 2003). This differential rate of evaporation can result in skewed reagent concentrations and can thus bias the biological phenotypes within specific wells (Lundholt, 2003). Addition of high volumes of aqueous solution to either the outer wells of a multiwell plate, or the use of moat-like structures built into the outer edges of specialised reservoir plates have been described to effectively mitigate edge effects. The outer 30 wells on each experimental plate were thus filled with PBS prior to cell seeding and only the inner 60 wells were utilised for experimental reactions. (Figure 3.3).

The number of control wells allocated per experimental plate as well as their location are important parameters that influence downstream image analysis (Zhang, 2008; Bray, 2012). Wells located in rows B and E on each experimental plate were specifically utilised as control wells. Thus each experimental plate included 20 control wells and 40 experimental test wells (Figure 3.3). Experimental control rows were purposefully selected to be technical replicates of each other. Positioning of identical control wells specifically at rows B and E readily facilitated the identification of inadvertent 180 ° plate rotations, and possible edge effects or pipetting biases (Bray, 2012). Plate rotations occur when an experimental plate is either acquired or treated in the wrong orientation and both instances can occur as a result of human error. A robust experimental plate layout must therefore also provide a contingency that facilitates identification of such events (Zhang, 2008).

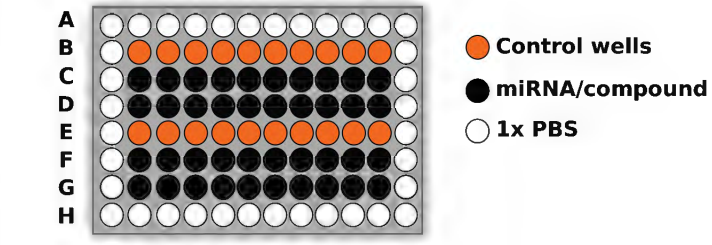

Figure 3.3 Position of control wells on experimental plates.

Control wells (orange) were always located in rows B and E in experimental plates utilised for both miRNA and compound screens. Experimental well locations are shown in black. The outer 36 wells (white) were filled with 1x PBS to minimise edge effects. The asymmetric layout of the control wells facilitated identification of inadvertent plate rotation.

Human error is a major concern for non-automated screening practices and simplification of the required liquid handling steps was thus a major focus of the experimental design process. The layouts selected for all plates were designed with 'ease-of-execution' in mind regarding transfection, compound treatment and infection steps. Furthermore regardless of the type of screen, transfer of reagents from daughter to experimental plates was kept constant so that reagents from row A on daughter plate 1 would always be present in row C on experimental plate 1A and reagents from row E would be always be present in row C in experimental plate 1B and so on (Figure 3.4). This design layout dramatically simplified the required liquid handling steps, and also maintained continuity in pipetting requirements for both miRNA and compounds screens. In addition, the simple layout facilitated downstream reagent identification. Based on this experimental plate design, a total of 63 experimental plates were generated from a single replicate of the miRIDIAN library (both mimics and inhibitors), and 6 experimental plates were generated per replicate, per concentration and per screening format for the compound libraries.

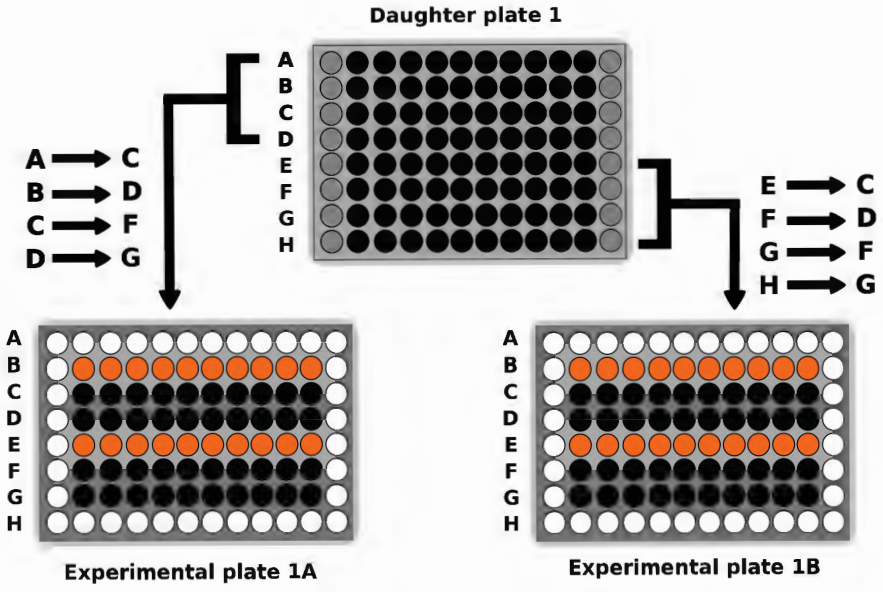

Figure 3.4 Standardised daughter plate to experimental plate reagent transfer process.

A single daughter plate containing 80 reagents (either miRNA or compound) generated 2 experimental plates, using a simple, standardised transfer format. Empty wells (dark grey), miRNA/compounds (black), 1x PBS (white), control wells (orange).

3.5 Development of HCS framework

3.5.1 Characterisation of HCS assay

Since a major aim of this study was to identify host factors that were functionally relevant to HIV replication using a miRIDIAN library in a HCS image-based approach, selecting a robust cell-based assay that facilitated quantification of HIV replication by fluorescent microscopy was essential. A HCS assay must produce a visual phenotype that i) is relevant to the biological process(s) of interest, ii) can be quantified using image analysis, and iii) produces distinct variations that reflect significant changes in the biological process of interest, where these variations can also be differentiated by image analysis (Boutros, 2008; Zanella, 2010; Bray, 2012). With these requirements in mind, the infection of GHOST(3) reporter cells with a lab-adapted BSL-2/3 compliant HIV pseudovirus was selected as the basis of the HCS assay (Cecilia et al. 1998).

The GHOST(3) X4/R5 cell line was derived from a human osteosarcoma line (HOS) stably transduced with a MV7neo-T4 retroviral vector containing an HIV-2 LTR promoter sequence driving expression of humanised GFP (hGFP). Expression of hGFP in GHOST(3) cells is therefore dependent on activity of the stably expressed LTR-promoter. Following exposure to HIV, successfully infected GHOST(3) cells express viral Tat protein which is then able to activate the LTR-reporter construct resulting in stable expression of hGFP (Figure 3.5). The level of GFP expression within an infected population of GHOST(3) cells is thus directly proportional to the number of successfully infected cells within the population, as well the level of Tat production within the infected cells. HIV replication can therefore be both visualized and quantified in GHOST(3) cells using fluorescence microscopy (Figure 3.5). In addition, the GHOST(3) reporter system is sensitive to multiple HIV-1 subtypes, as well as HIV-2, and has previously been validated as a suitable tool for the quantification of HIV-1 replication in cultured cells (Cecilia et al. 1998). Use of similar Tat-sensitive cellular reporter assays have also been documented for other HCS applications (Brass, 2008; Genovesio et al. 2011).

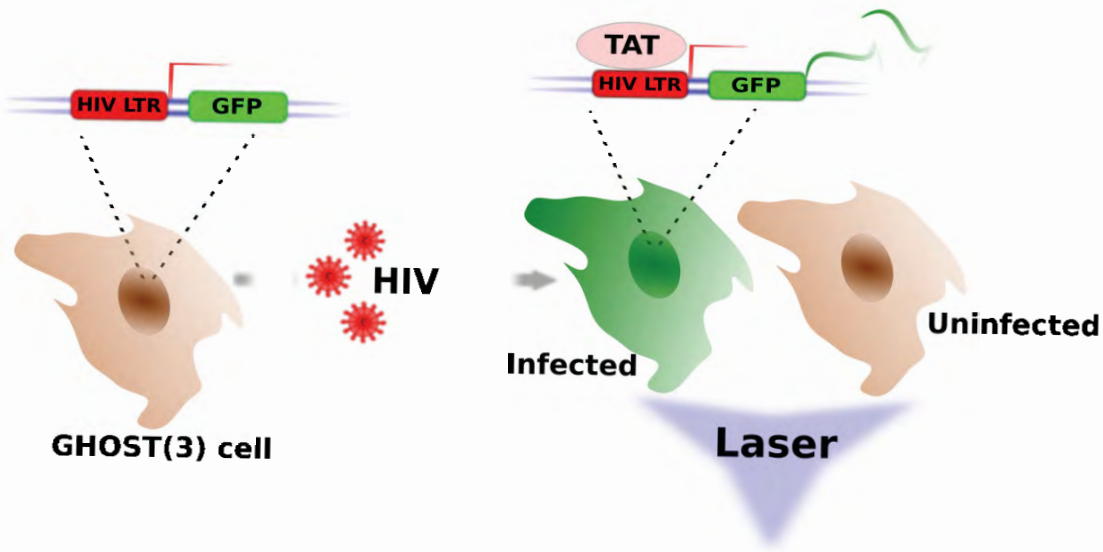

Figure 3.5 GHOST(3) reporter assay.

GHOST(3) cells stably express a Tat-sensitive GFP reporter construct. Following exposure to HIV, successfully infected cells produce viral Tat protein that activates the LTR-hGFP reporter construct resulting in expression of GFP by infected cells. GFP expression is detected by fluorescence microscopy and can be used to quantify HIV replication.

Having chosen GHOST(3) reporter cells for the HCS assay, it was important to determine if they could express GFP specifically in response to infection with HIV. GHOST(3) cells were transduced at different multiplicities of infection (MOIs) with the $PSG3^{BAL}$ gp120-expressing pseudovirus in order to evaluate the relationship between GFP reporter signal output and viral input. Cells were fixed, stained and imaged on the IXU 48 hours following infection and a positive correlation was observed between increased viral input (higher MOI) and increased GFP expression (Figure 3.6 A). These observations suggested that GHOST(3) cells were indeed sensitive to $PSG3^{BAL}$ infection, and also that the GFP reporter could be 'tuned' based on viral input. Next, an important control was included to ensure that $PSG3^{BAL}$ infection, specifically viral entry, was required for GFP reporter expression. GHOST(3) cells were transfected with an siRNA targeting CD4 (25 nM) or a non targeting control (25 nM) and 48 hours post transfection these cells were exposed to $PSG3^{BAL}$ at an MOI of 0.5. siRNA-mediated knockdown of CD4 prior to HIV exposure was shown to result in a significant ($p < 0.05$) decrease in GFP expression, suggesting that infection was indeed dependent on CD4 availability and represented a receptor-mediated mechanism of infection (Figure 3.6 B).

The relationship between $PSG3^{BAL}$ infection and GFP reporter expression was further characterised by measuring p24 expression following infection. Based on ICC data and image analysis, ~90% of GHOST(3) that expressed GFP were also found to express HIV p24 48 hpi (Figure 3.6 C). Specificity of the p24 immunoassay was further verified by western blot (Figure 3.6 D), and PCR analysis confirmed that infected populations of

GHOST(3) cells also expressed *Gag* transcripts at 48 hpi (Figure 3.6 E). Together, these observations confirmed that GFP expression in GHOST(3) cells correlated with CD4 receptor-mediated entry of $PSG3^{BAL}$ pseudovirus, and that GFP reporter expression could be tuned based on viral input.

Viral infection-mediated GFP reporter expression was key for success of the HCS assay, and while it had been established that GFP expression could be altered based on varying the viral input (MOIs), additional ways to augment GFP expression were also explored. Polycationic compounds have been reported to enhance viral infection by increasing the number of virion-cell contact events (Konopka, 1991; Hodgson, 1996). To test if additional virus-cell interactions led to increased GFP expression, GHOST(3) cells were infected with $PSG3^{BAL}$ media containing different concentrations of DEAE-Dextran (Sigma-Aldrich®), USA) or Polybrene® (Sigma-Aldrich®). Cells were fixed stained and imaged on the Andor confocal system 48 hpi. No significant difference was observed between the total GFP output in non-treated control cells and cell populations that received either polycationic additive. Given that GFP expression required Tat-mediated activation and this was in turn dependent on the timing of virus infection, the length of infection was also optimised to ensure maximum GFP expression. GHOST(3) cells were infected for 24hr, 48 hr and 72hr at a constant MOI of 0.5 and were then fixed, counterstained with Hoechst and imaged on the IXU system. GFP expression was quantified using FIJI and and a 48 hour infection was found to be the shortest infection time course that produced a robust GFP readout as compared to uninfected control cells (Figure A3.2, Appendix III).

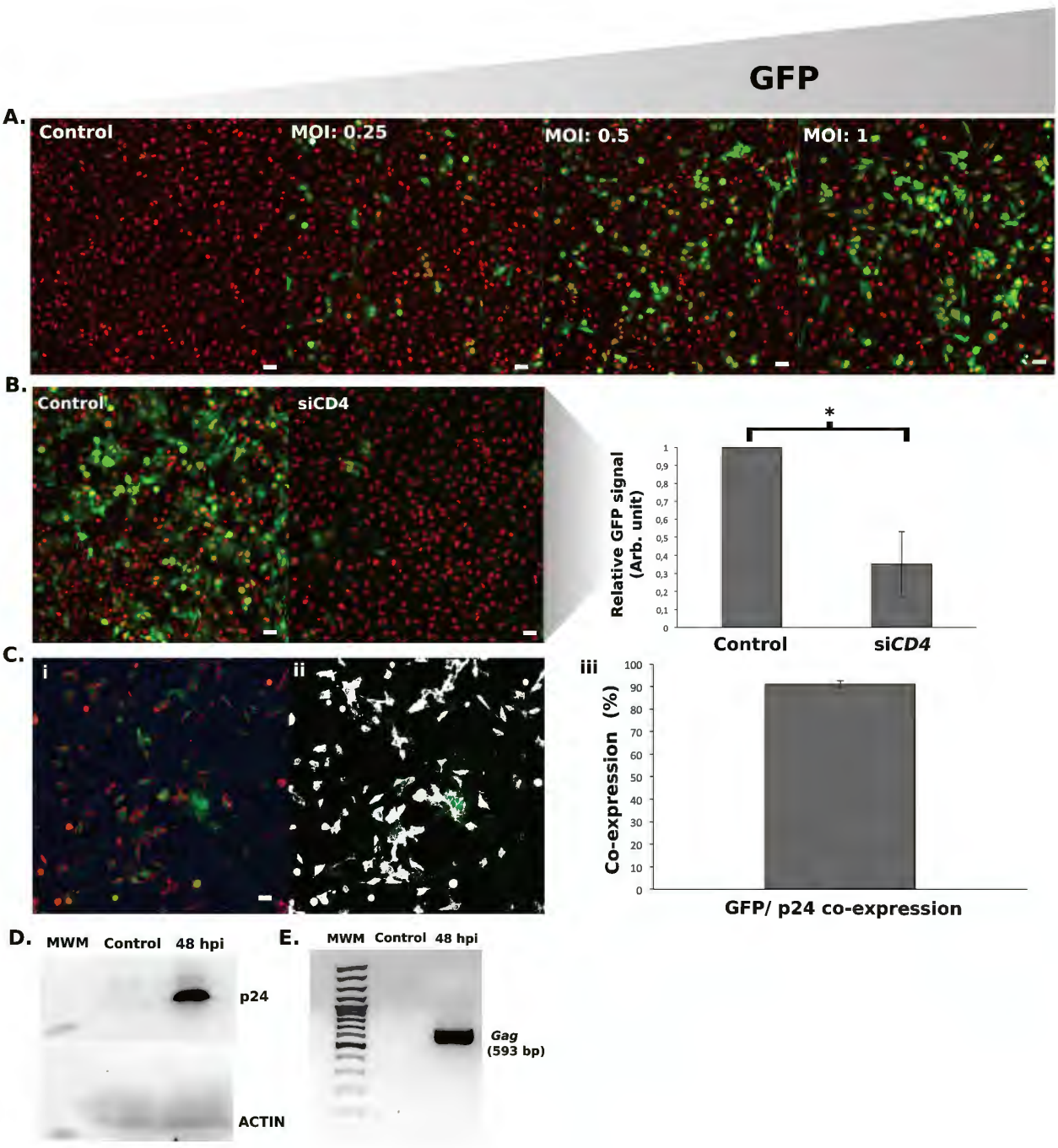

Figure 3.6 Experimental validation of GHOST(3) infection assay.

A) GFP expression positively correlates with an increasing MOI, nuclei are counter stained with Hoechst (red) and GFP expression (green) is indicative of positive infection, cells were fixed and imaged 48 hpi. **B)** Infection of GHOST(3) cells by $PSG3^{BAL}$ is dependent on CD4 receptor-mediated entry. GFP expression 48 hpi is attenuated by 65% ± 0.18 SEM in GHOST(3) cells treated with siCD4 48 hours prior to infection as compared to mock transfected control wells (n=8, *p< 0.05). **C)** GHOST(3) cells expressing GFP at 48 hpi also express HIV p24 as seen in i) an overlay of p24 conjugated Alexa Fluor 550 (red) and GFP (green) signals. ii) Saturated pixels

(white) indicate colocalization of GFP and p24-conjugated Alexa Fluor 550 signals estimated by image analysis to be iii) ~90% ± 1.49 SEM of infected GHOST(3) cells (n=3). **D)** Western Blot analysis of p24 protein expression in uninfected (control) and infected GHOST(3) cell populations 48 hpi showed p24 protein only in the latter samples. E) HIV *Gag* is only expressed in infected GHOST(3) cells at 48 hpi as per gel electrophoresis of PCR amplicons. MWM = molecular weight marker. Scale bars = 20 um.

3.5.2 Development of an HCS experimental framework

Following the characterization of the GHOST(3) reporter system as a suitable HCS assay that would facilitate the quantification of HIV replication by microscopy, the next step in the developmental pipeline was to layout a theoretical framework for each of the planned screens (i.e miRNA vs. compound) and to determine the number of replicates that would be required for each screen. Conducting multiple screening replicates can strengthen phenotypic classifications, reduce FDRs and improve the confidence of screen hits (Bray, 2012). The higher level of complexity associated with HCS assays suggests at least two replicates should be completed, although this also results in a large increase in reagent and consumable costs. This must also be weighed against the cost of secondary confirmation screens, which are performed at smaller scales but include variations in experimental conditions such as dose responses and screening formats. Most primary HTS and HCS studies are therefore performed in duplicate, and subsequent validation screens are performed with higher numbers of replicates (Bray, 2012). The miRNA screens performed in this study were run in duplicate, and the compound screens in triplicate.

The miRNA-based experimental workflow was designed and executed prior to optimisation of the compounds screens. miRNA mimics and inhibitors were only screened in a single experimental format, which was termed ‘pre-HIV exposure’. In this screening format GHOST(3) cells were first treated with miRNA mimics/inhibitors and then exposed to HIV (Figure 3.7). In contrast, the compound screens were performed using three different screen formats, namely ‘pre-HIV exposure’ (Figure 3.8), ‘post-HIV exposure’ (Figure 3.8) and ‘drug only’. As with the miRNA screens, in pre-HIV exposure compound screens GHOST(3) cells were first treated with specific compounds prior to HIV exposure. In post-exposure screens, GHOST(3) cells were first exposed to HIV and then treated with compounds. In drug only screens, GHOST(3) cells were treated with compounds alone for 24hr prior to sample processing and imaging. The data derived from this screening format was used to establish a baseline phenotype for each compound treatment in terms of toxicity and compound-specific effects on the LTR-GFP reporter system. In addition, while miRNA screens were executed at a single concentration of 25 nM for miRNA mimics and miRNA inhibitors, compounds were screened at 3 different concentrations within each experimental format in order to evaluate any potential dose-response phenotypes. Optimisation of individual

experimental processes and parameters are discussed in subsequent sections of this chapter along with a detailed account of the HCS image analysis pipeline.

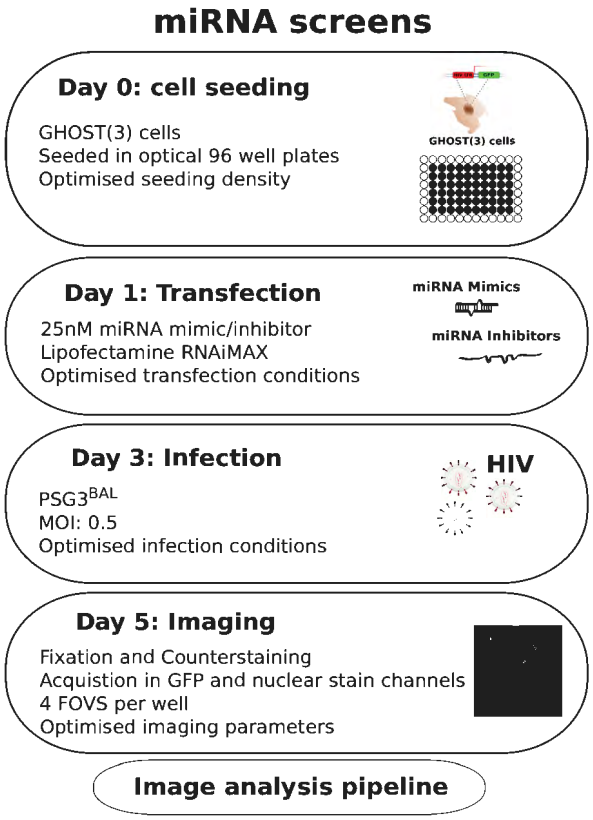

Figure 3.7 Summary of experimental framework for miRNA screens.

GHOST(3) cells were seeded in 96 well µClear® plates. Cells were transfected with miRNA mimics or inhibitors the following day. 48 hours post transfection cells were exposed to HIV. 48 hours post infection cells were fixed and stained and experimental plates were imaged using optimised acquisition settings. The resulting images were processed through an HCS image analysis pipeline.

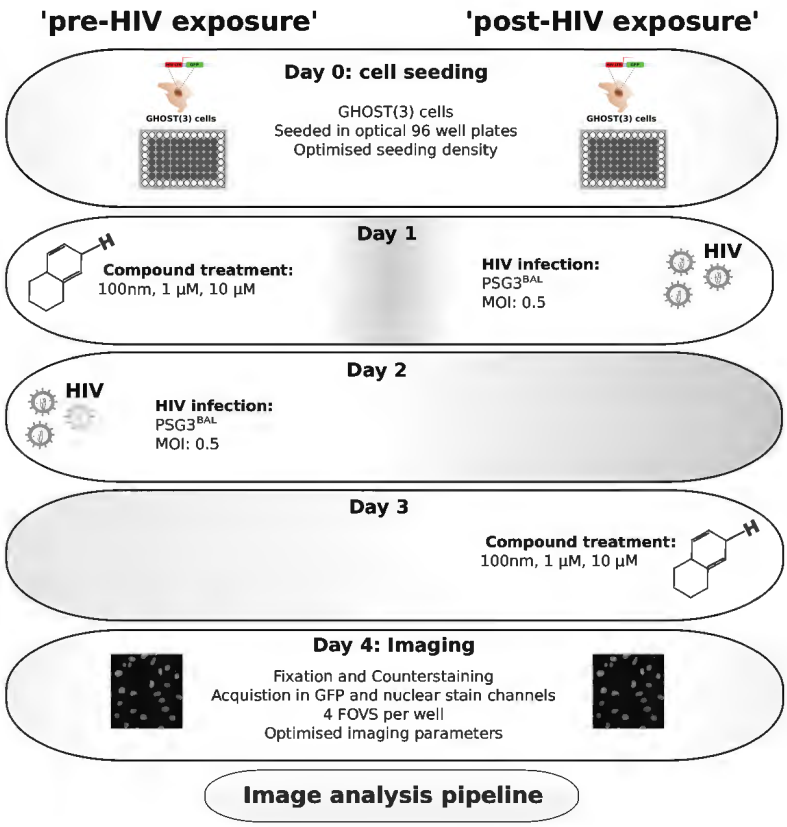

Figure 3.8 Experimental framework of 'pre-HIV exposure' and 'post-HIV exposure' compound screens.

GHOST(3) cells were seeded on Day 0 for both screening formats. Compounds were screened at final concentrations of 100 nM, 1 µM and 10 µM. Infections were executed at an MOI of 0.5. Both methods fed into a common image analysis pipeline.

3.5.3 Cell seeding

Identifying the optimal cell seeding density is an important step in the design of a robust HCS workflow. The optimal seeding density for a specific biological assay may vary depending on the type of cells used, the experimental time course and experimental treatments, and should therefore be optimised for individual screening applications. Cell seeding density influences the number of cells in a given well at each experimental treatment step (e.g transfection or infection), and also impacts the number of cells present at the assay endpoint. The final cell count or density at the experimental end point is an extremely important parameter for phenotypic screening and downstream image analysis. High cellular densities can confound image analysis approaches that rely on identification of discrete objects/cells that are not in contact with each other. Alternatively, low cellular densities limit the amount of biological information acquired per field of view (FOV), and can result in toxicity following certain treatments like transfection. The actual cell count at the point of infection is also an important variable in

determining the MOI of an infection assay. Optimisation of cell seeding densities was thus essential when establishing the screening workflows utilised in both the miRNA and compound screens. The goal of this optimisation step was to identify a suitable cell seeding density range that was compatible with downstream image analyses and experimental treatments and to evaluate the robustness of the selected cell seeding protocol.

To identify the optimal cell seeding density for image analysis, multiple seeding densities within a range of 500-15 000 cells per well were evaluated. Cells were seeded and cultured for 96 hours as this was the experimental end point of the miRNA screening workflow. Cells were then fixed in 4% PFA and nuclei were counterstained with Hoechst before imaging at 20x on the IXU system. Seeding densities ≥10 000 cells/well were observed to negatively impact downstream analyses (Figure 3.9 i and ii), while a seeding density between 5000-7000 cells/well maximised the number of cells per FOV without compromising image analysis (Figure 3.9 iii and iv). The same optimisation process was also applied to the compound screening workflow.

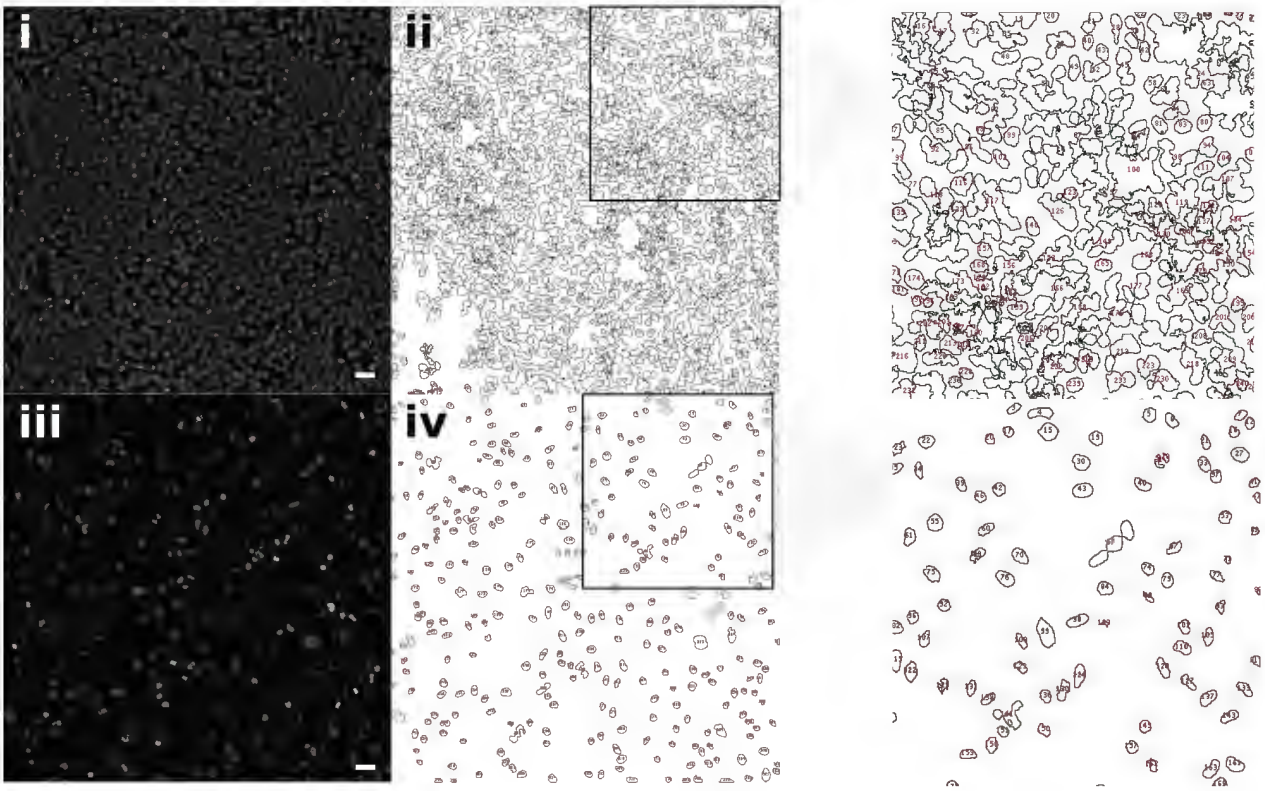

Figure 3.9 The impact cell seeding density on image analysis.

i) A cell seeding density in excess of 10 000 cells per well resulted in a large number of cell to cell contact events in the resultant microscopy images, and **ii)** cell to cell contact events confounded image analysis approaches by distorting the perceived boundaries of individual cells resulting in an inaccurate cell count. **iii)** A cell seeding range of 5000-7000 cells resulted in significantly less cell to cell contact events at the experimental endpoint, and **iv)** was determined

to be suitable to the identification of discrete cells by image analysis. Nuclei (grey) were counterstained with Hoechst. Scale bars= 20 µm.

The proliferation rate of GHOST(3) cells was also evaluated in order to accurately predict the number of cells present at each experimental treatment point given a known seeding density. GHOST(3) cells were seeded at a density of 7 000 cells per well in a µClear® 96 well plate and allowed to attach overnight. The following day cells were transfected with a non-targeting miRNA mimic control and 48 hours later the number of cells present in each well was calculated using a haemocytometer. An average of 57 500 ± 4 950 cells were present in each well (n= 60) thereby suggesting a doubling time of ~24 hour (Figure 3.10). This proliferation rate was utilised to estimate the number of cells present in each well of an experimental plate at the infection assay time point for the miRNA screens.

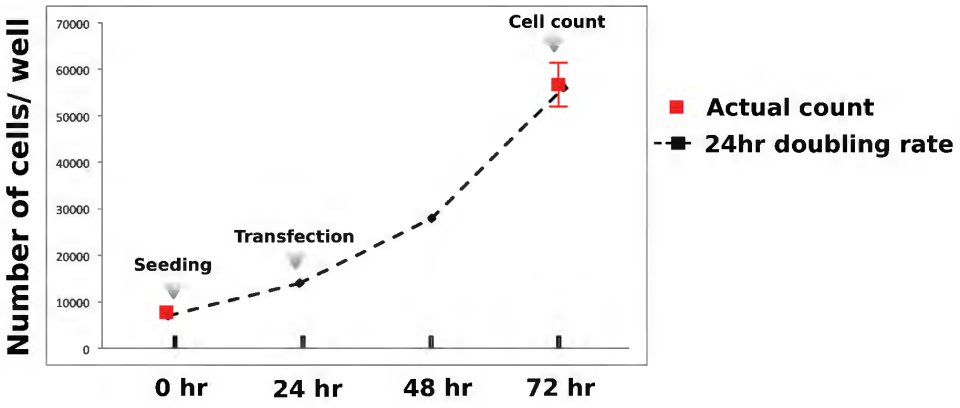

Figure 3.10 Evaluation of GHOST(3) proliferation rate.

GHOST(3) cells were seeded at a density of 7000 cells per well in a 96 well plate, transfected the following day with a fluorescently labelled miRNA, and then detached and counted 48 hours following transfection. Black lines/squares represent the expected cell counts based on a doubling time of 24 hours. Red blocks represent the actual cell counts from the seeding experiment. Cell count data corresponds to an average doubling time of ~24 hours under the reported culture conditions, SEM ± 4.95 x 10^3.

To ensure that no inter-well directional biases were introduced during cell seeding, the fidelity of the seeding process was evaluated by comparing cell counts within the wells present in the first and last rows of 96 well plates. GHOST(3) cells were seeded into the inner 60 wells of µClear® 96 well plates using a multichannel micropipette and allowed to adhere overnight before being detached and counted using a haemocytometer (Figure 3.11). No significant differences were observed between the average number of cells seeded in the first (A) and last (G) rows of three test plates (Figure 3.11). In addition, variability between the number of cells dispersed by individual channels of a multichannel micropipette were observed to be negligible, as represented by the error bars on each column (Figure 3.11). Inter-plate differences in cell seeding densities were

not a major concern as all cell count data was normalised on a per plate basis using cell counts from the negative control wells on each experimental plate (See *HCS quality control* below).

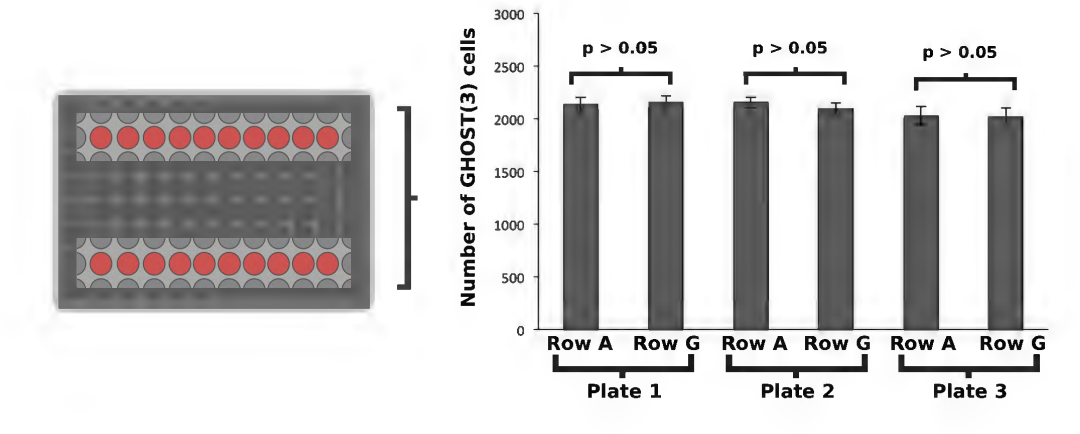

Figure 3.11 Fidelity of cell seeding protocol.

No significant differences in the average cell counts were observed between experimental wells located on distinct rows within the same test plates ($p > 0.05$, n=10 wells).

3.5.4 Transfection

Optimisation of transfection conditions was a key factor in the development of a miRNA screening workflow. A final concentration of 25 nM was previously described to be the maximal concentration of miRNA-based reagent that could be used without nonspecific toxicity in mammalian cells (Schoolmeesters, 2009; Santhakumar, 2010). The principal aim of this optimisation step was thus to evaluate whether the proposed transfection conditions were able to produce suitable transfection phenotypes in GHOST(3) cells using a 25 nM final concentration of miRNA reagent. Given the lack of suitable positive controls to directly quantify the functional activity of miRNA reagents during the optimisation stage, a small interfering RNA (siRNA) targeted to CD4 was used as a proxy for miRNA mimic activity. The siRNA was obtained from the same vendor that supplied the miRNA library (Dharmacon™, USA) and was therefore subjected to the same chemical modifications as miRNA mimics, additionally the basic structure (short dsRNA) and functional activity (miRISC-mediated gene silencing) of miRNA mimics and siRNAs are also quite similar with the exception being that a single miRNA may have many molecular targets while a single siRNA is generally designed to target a single mRNA species. Three important transfection parameters were evaluated including the successful uptake of miRNA reagents by cultured cells term (uptake efficiency), the functional effect of the transfection process on target mRNA (transfection efficacy), and cell viability in response to transfection. A minimum uptake efficiency rate of 70% and a minimum transfection efficacy rate of 50% were set as the lower cut-off limits for

acceptable transfection readouts. GHOST(3) cells were seeded as previously described, and the following day cells were transfected with either siGLO Green or miRNA mimic Dy547 non-targeting transfection control reagents. Twenty-four hours later, the cells were washed thoroughly in 1x PBS to remove any excess transfection reagent and were then fixed in 4% PFA, counterstained with HCS CellMask™ blue stain and imaged on the Andor confocal system (Figure 3.12 A).

HCS Cellmask™ stains both nuclei (strong signal) and the cytoplasm (weaker signal) of cells thereby allowing for visual identification of the total area occupied by individual cells. The acquired images were then analysed in FIJI and visual inspection. Briefly, the raw images acquired in the CellMask™/405 channel were processed by applying an automatic background subtraction and were then converted into a binary format (8-bit). Auto thresholding was then applied using the Li method and the resulting image was used to create mask/overlay in which black objects (individual cells) were defined as regions of interest (ROIs;Figure 3.12 B). The raw images acquired for each corresponding FOV in the Dy547 or siGLO Green channel were then processed (automatic background subtraction and despeckling), and the 405 image mask was overlaid (Figure 3.12 B). The total number of ROIs (cells) present in the image was recorded along with the number of ROIs that also contained a positive signal in the 488/547 channel. The total number of ROIs in each image was then compared to the number of cells that were also positive for the dye-labeled transfection control reagent in order to determine the percentage of cells that had successfully taken up the miRNA/siRNA reagents.

A 78.9% transfection efficiency rate was observed for the miRNA-Dy547 transfection control while a 79.7% transfection rate was observed for the siGLO Green reagent. Accuracy of the FIJI transfection efficiency analysis method was evaluated using visual inspection (Figure 3.12 C), and the difference was negligible (< 2%) for both miRNA-Dy547 and siGLO-488 transfections (n=9). In addition, no significant impact on cell proliferation was noted in response to the transfection process. Based on these data, both the transfection process and the image analysis-based method of evaluating transfection efficiency were determined to be suitable for HCS purposes.

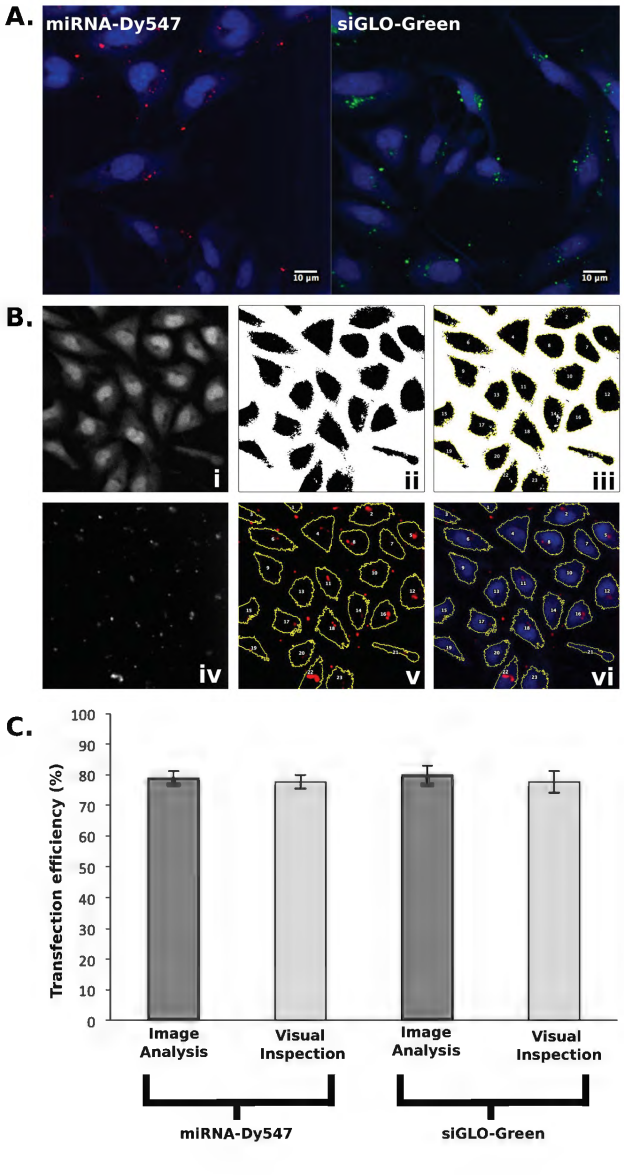

Figure 3.12 Optimisation of transfection efficiency for HCS.

A) Composite images of GHOST(3) cells transfected with either miRNA DY547 (red spots) or siGLO Green (green spots) and counterstained with HCS CellMask™ (blue), scale bars = 10 µm. **B)** Transfection efficiency was determined by image analysis: **i)** raw images acquired in the HCS CellMask™ fluorescence channel were processed and converted to a **ii)** binary version, and **iii)** and a mask defining the ROIs (cells seen as black shapes) was created. **iv)** The same image acquired in the miRNA-Dy547 channel was processed and **v)** overlaid with the mask from iii. **vi)** Finally, a composite image was generated that overlaid the ROIs (yellow), miRNA-Dy547 signal (red) and HCS CellMask™ fluorescent signal (blue) from a single FOV. **C)** Transfection efficiency calculations based on image analysis suggested that both miRNA-Dy547 and siGLO 488 controls had an average transfection efficiency rate of ~79%. Visual inspection revealed an average transfection efficiency rate of ~78% for miRNA-Dy547 and ~79% for siGLO 488 (n=9).

CD4 mRNA transcript levels were interrogated by qPCR analysis 48 hours following transfection of GHOST(3) cells with either siCD4 or a non-targeting siRNA control, both at a final concentration of 25 nM. CD4 expression levels in each treatment were normalised against those of the reference gene *HPRT*. CD4 expression was significantly ($p<0.05$) downregulated by ~70% in the siCD4 treatment as compared the control treatment (Figure 3.13). This finding suggested that the experimental conditions utilized for the transfection process were indeed effective for siRNA-mediated knockdown and would therefore also be effective for the transfection of miRNA mimics. A positive control or proxy for miRNA inhibitor activity under different transfection conditions was unfortunately not available at the time of optimization and this potentially important parameter was thus reluctantly omitted from the optimisation process in lieu of data suggesting that miRNA mimics and inhibitors could be used at similar transfection conditions (Santhakumar, 2010).

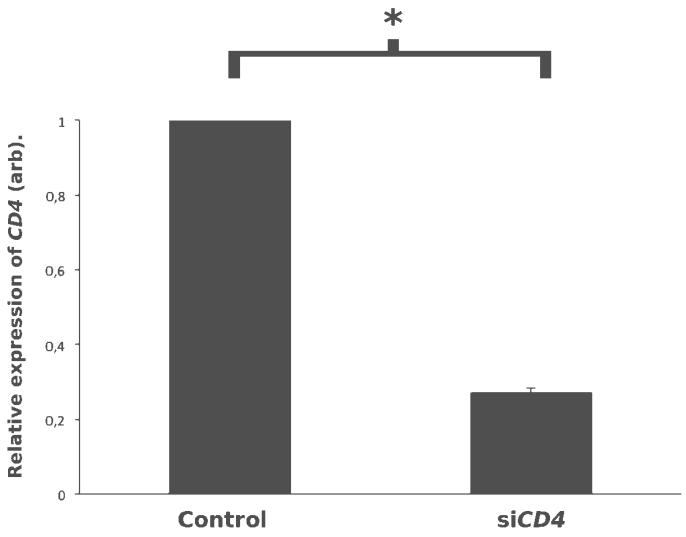

Figure 3.13 Evaluation of transfection efficacy for HCS.

qPCR analysis revealed a ~75% knockdown of CD4 transcripts in GHOST(3) cells 48 hours post-transfection with an siRNA targeting CD4 (n=3). CD4 expression levels in each treatment were normalised against those of *HPRT,* * $p< 0.05$.

HCS transfection protocol

Having established the appropriate concentrations of miRNA and transfection reagents to use, a protocol for doing so in a 96 well format complementary to the experimental plate layout was established. miRNA mimic/inhibitor transfection reactions were prepared in 96 well v-bottom plates (transfection plates) and transferred to experimental plates that had been seeded with cells as previously described (Figure 3.14). Lipofectamine RNAiMax transfection reagent was first diluted in a sterile tube using 1.5

µL of RNAimax per 1 mL of serum free media (SFM) and incubated while the plates were being prepared. For each transfection plate, 7.5 µL of SFM was added to each of the inner sixty wells. For each negative control well ('natural infection'), 2.5 µL of SFM was added. For each non-targeting control well, 2.5 µL of 1µM working solutions of Dharmacon™ miRNA mimic and inhibitor non-targeting controls were added. For each infection control well 2.5 µL of a 1 µM working solution of siCD4 was added. Finally, 2.5 µL of each miRNA reagent from the appropriate daughter plate was transferred to each transfection plate. Following this, 10 µL of the diluted RNAiMax solution was carefully dispensed directly into each transfection plate (Figure 3.14). Transfection plates were incubated at room temperature for ~20 minutes and the contents of each well were then transferred to their corresponding well on the experimental plate. Experimental plates were briefly agitated by hand before being placed in a CO_2 incubator for 48 hours.

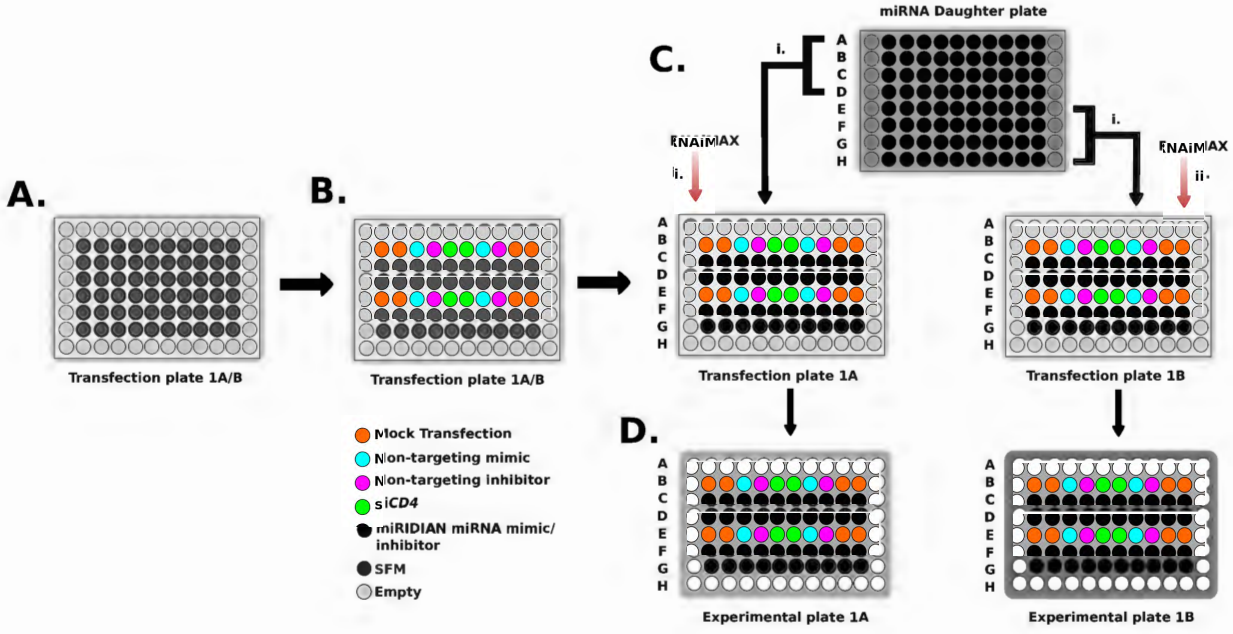

Figure 3.14 HCS transfection protocol.

A) SFM was added to the inner 60 wells of a v-bottom transfection plate. **B)** The appropriate control reagents were added to each control well. **C)** i. Mimics/inhibitors were transferred from a miRNA library daughter plate to the appropriate wells in two transfection plates. ii Diluted RNAiMAX transfection reagent was added to each reagent well and plates were incubated at RT for ~20 minutes. **D)** The contents of each well on a transfection plate were transferred to their corresponding wells on an experimental plate that had been previously seeded with GHOST(3).

3.5.5 Phenotypic controls

As mentioned earlier, a suitable HCS assay must be able to reflect changes in a biological process of interest. These 'changes' can be purposefully engineered to create visually and analytically distinct phenotypes that are required for hit selection through image analysis, as well as to provide specific quality control steps in an HCS workflow (Bray, 2012: Zhang, 2012). Such engineered phenotypes are referred to as 'phenotypic controls' and include both 'negative' and 'positive' controls. Negative controls are utilised to define a 'baseline' phenotype and provide an analytical reference point for experimental reagents that do not elicit a significant phenotypic effect. Thus negative controls also function as important reference points for normalisation and standardisation of HCS data (Bray, 2012). Positive controls are utilised to define the phenotype of interest and thus provide an analytical reference point for experimental reagents that elicit similar phenotype(s) (Shariff, 2010). The distinction between these two contrasting visual control phenotypes (positive and negative) is also an important factor in the development of supervised machine learning based classifications (Shamir, 2010). However, to further stratify phenotypes that may be observed during an HCS assay, additional controls should be included. These additional controls can monitor fidelity of various steps in the experimental procedure, and serve as reference points for the accuracy of downstream classification and analytics (Zhang, 2012).

miRNA screen controls

A summary of the phenotypic controls utilised in the miRNA mimic and inhibitor screens is presented in Table 3.1 below. Briefly, Natural infection controls were prepared by mock transfecting and then infecting GHOST(3) cells with $PSG3^{BAL}$. Infected non-targeting miRNA mimic/inhibitor controls were prepared by transfecting GHOST(3) cells with a non-targeting miRNA mimic or inhibitor at a final concentration of 25 nM prior to infection. The siCD4 phenotypic controls were prepared by transfecting GHOST(3) cells with a 25 nM final concentration of pooled siRNA 48hr prior to infection. Uninfected non-targeting miRNA controls were transfected with a 25 nM final concentration of non-targeting miRNA mimic or inhibitor and cultured in 'HIV-naive' infection media for 48hr. 'Mock transfected, uninfected controls' were mock transfected and then cultured in HIV-naive' infection media for 48hr. All infections were carried out using a 48hr infection time course. Mock transfected and uninfected controls were combined with siCD4 controls in image analysis to create a broader definition of a positive control (POS) phenotype for suppressed HIV replication. Ideally, positive controls for the functional activity of miRNA mimic and inhibitor reagents should also be included among the phenotypic controls used to monitor experimental quality, specifically the fidelity and efficacy of the transfection process. The quantitative assessment of the HIV- suppressive phenotype resulting from the efficient knockdown of CD4 by an siRNA pool (siCD4) was used in lieu of these miRNA reagent controls as the required reagents were not available during the optimisation stage.

Table 3.1 Phenotypic controls for miRNA screens

Phenotypic Control	Significance
Natural Infection	● Negative Control (NEG) ● Baseline phenotype for image analysis
Infected non-targeting miRNA control	● Quality control monitoring ● Should be classified with NEG by image analysis
siCD4	● Positive control (POS) for suppressed HIV replication ● Quality control for the efficacy & consistency of transfection
Uninfected non-targeting miRNA control	● Quality control monitoring ● Should be classified with POS by image analysis
Mock transfected uninfected control	● Positive control (POS) for suppressed HIV replication ● Quality control for baseline GFP-reporter activity without treatment

To optimise the phenotypic controls, GHOST(3) cells were prepared for each control condition, fixed at the relevant endpoints, counterstained with Hoechst and imaged on the IXU system. Images were analysed in FIJI by quantifying the average total GFP output for all images in each condition. Visual inspection revealed that non-targeting infected controls and natural infection controls were indeed similar, and this observation was confirmed by image analysis (Figure 3.15). In addition, siCD4 controls, uninfected non-targeting controls and uninfected controls were also visually distinct from both non-targeting infected controls and natural infection controls (Figure 3.15). Together, these observations confirmed that a combination of siCD4-treated and uninfected controls would represent suitable positive controls for image analysis, and that transfection of miRNA mimics/inhibitors did not have a detectable nonspecific effect on the GHOST(3) reporter system both in the presence and absence of HIV.

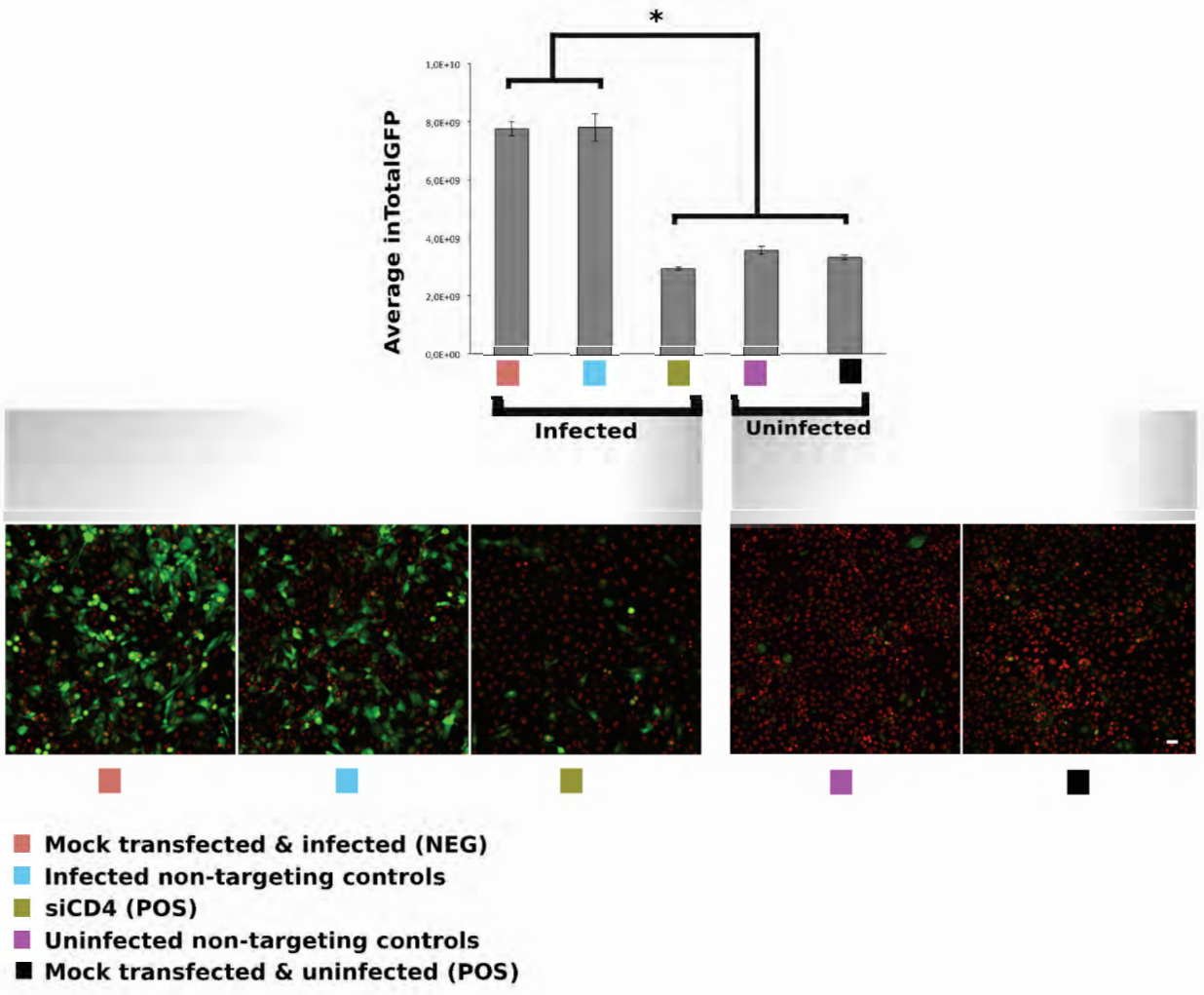

Figure 3.15 Evaluation of phenotypic controls for miRNA-based HCS.

GHOST(3) cells were prepared for each phenotypic control condition, imaged on the IXU and the average total GFP intensity for each condition and significant differences between them were determined by image analysis ($p < 0.05$, $n = 6$). Mock transfected & infected negative controls (NEG, orange) controls and infected non-targeting miRNA reagent controls (blue) resulted in similar visual profiles. These were distinct from those exhibited by siCD4-treated infected controls (yellow) as well as uninfected mock transfected (black), and uninfected non-targeting miRNA reagent controls (purple). The combination of the siCD4 (yellow) and uninfected (black) treatments were used to define the positive control phenotype (POS). Each image represents a single FOV acquired at 20x with 4 FOVs acquired per condition. Scale bar = 20 μM.

Compounds screen controls

Similar processes were followed for optimisation of controls for the compound screens, although these were modified to accommodate the different screening formats used for the compound screens. DMSO was the solvent used to reconstitute compounds and DMSO treatment was thus utilised as a vehicle-control (negative) for compound treatments.

The phenotypic controls for all compound screens are summarised Table 3.2 below. Natural infection controls were prepared by treating GHOST(3) with an appropriate dilution of DMSO either 24hr prior to infection (pre-HIV exposure screens) or 48hr post infection (post-HIV exposure screens). The positive control (POS) phenotype was created by treating GHOST(3) cells with specific ARVs (Maraviroc/ Raltegravir) prior to HIV exposure for both pre- and post- HIV exposure screen formats. Maraviroc inhibits HIV entry while Raltegravir inhibits HIV integration. Both of these ARVs were therefore used to obtain a broader analytical definition for suppressed HIV replication. Infected DMSO-naive treatments were prepared by treating cells with an appropriate volume of 1x PBS either 24hr prior to infection (pre-HIV exposure screens) or 48hr post infection (post-HIV exposure screens). Uninfected controls were treated with an appropriate dilution of DMSO either 24hr prior to (pre-HIV exposure screens) or 48hr post (post-HIV exposure screens), culture with HIV-naive infection media. All compound treatments were applied for 24 hours.

Table 3.2 Phenotypic controls for compound screens

Phenotypic Control	Significance
Natural Infection (DMSO-treated)	● Negative Control (NEG) ● Baseline phenotype for image analysis
Infected, DMSO-naive	● Quality control ● To monitor combined effects of DMSO treatment and infection on reporter activity
Maraviroc (10 μM)	● Positive control (POS) for suppressed HIV replication ● Quality control for the efficacy & consistency of compound treatments
Raltegravir (10 μM)	● Positive control (POS) for suppressed HIV replication ● Quality control for the efficacy & consistency of compound treatments
Uninfected, DMSO-treated	● Positive control (POS) for suppressed HIV replication ● Quality control for baseline GFP-reporter activity without infection

Selection of the ARVs and their respective concentrations as positive controls for suppressed HIV replication was determined by a dose-response experiment. Briefly, GHOST(3) cultures were treated with 3 different concentrations (100 nM, 1 µM and 10 µM) of 3 different ARVs (T20, Maraviroc and Raltegravir) for 24 hours prior to exposure to $PSG3^{BAL}$ for 48 hr. Negative controls relevant to each drug concentration were prepared in parallel by treating GHOST(3) cells with an appropriate dilution of DMSO prior to infection. Cells were then fixed, counterstained with Hoechst and imaged on the IXU. Images were subjected to visual inspection to determine which ARVs/concentrations suppressed HIV replication (GFP) without broad cytotoxicity. The fusion inhibitor, T20, was found to be effective at suppressing HIV replication at all of the concentrations tested without any significant toxicity (Figure 3.16). The CCR5 antagonist, Maraviroc as well as the integrase inhibitor, Raltegravir, were only able to suppress viral replication at 1 µM and 10 µM concentrations (Figure 3.16). However, due to limited availability of T20, Maraviroc and Raltegravir were both utilised at a final concentration of 10 µM for all compound screens.

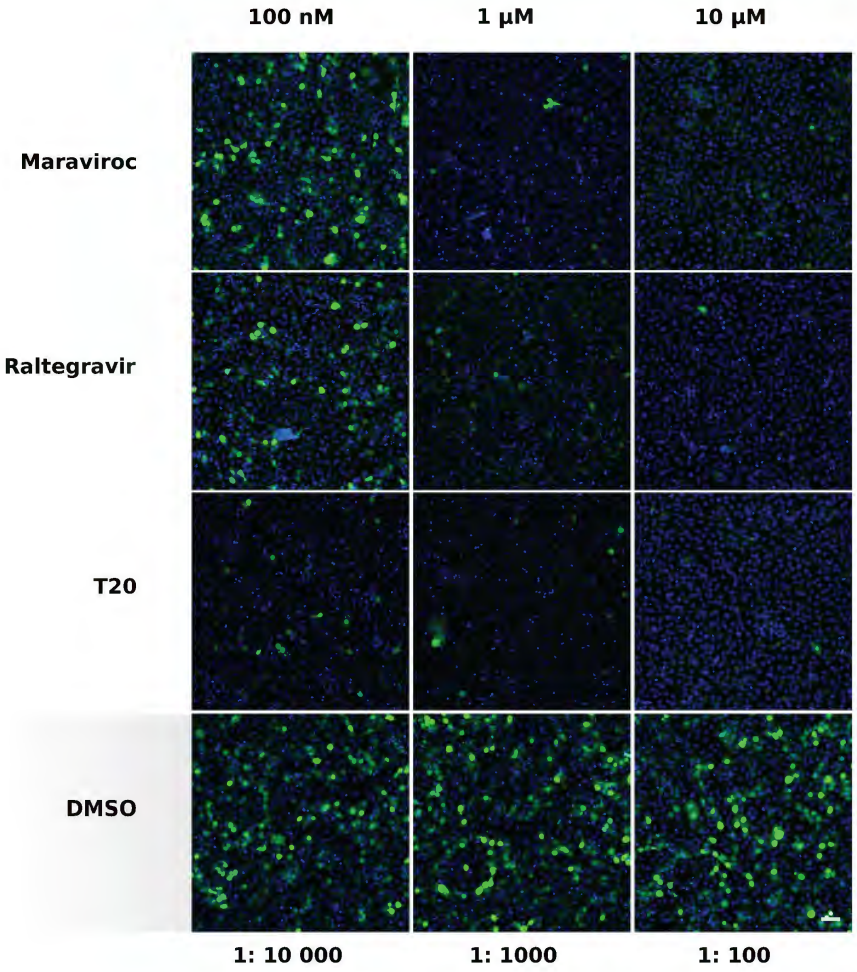

Figure 3.16 ARV dose response phenotypes for GHOST(3) assay.

GHOST(3) cells were treated with Maraviroc, Raltegravir or T20 for 24 hours prior to HIV infection. Cells were fixed 48hr post infection, and nuclei were counterstained with Hoechst (Blue) before imaging. LTR activity (GFP/Green) is indicative of HIV replication. The effect of each drug on HIV replication was evaluated at 100 nM, 1 μM and 10 μM concentrations. DMSO at dilutions equivalent to those for each ARV served as negative controls. Scale bar = 40 μm.

Having established the appropriate ARV conditions, all phenotypic controls were evaluated in both pre- and post-exposure screening formats. In the pre-exposure format, GHOST(3) cells were seeded in 96 well plates and allowed to adhere overnight. The following day, cells were treated with appropriate compounds for 24 hours, before being exposed to $PSG3^{BAL}$ at an MOI of 0.5. Cells were fixed, counterstained with Hoechst and imaged on the IXU at 48 hpi. Visual inspection and image analysis revealed that DMSO-treated and DMSO naive infected samples exhibited higher levels of GFP expression as compared to Maraviroc and Raltegravir-treated infected samples as well as DMSO-treated uninfected samples (Figure 3.17). DMSO treatment prior to infection resulted in a slight but noticeable increase in GFP compared to DMSO-naive infected samples (Figure 3.17). This suggested that treatment with DMSO may either subtly influence the GFP reporter system or increase background signal. Thus DMSO-treated infected samples were used instead of untreated GHOST(3) cells as the negative control for pre-exposure compound screens.

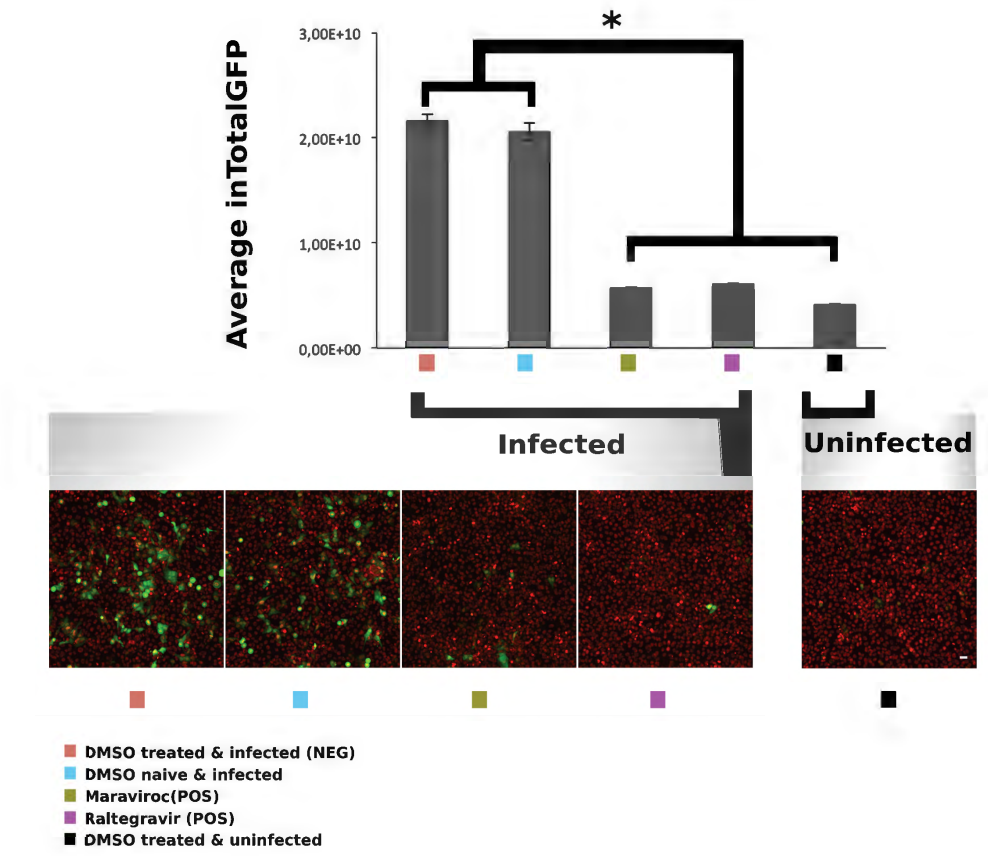

Figure 3.17 Pre-exposure assay format phenotypic controls.

GHOST(3) cells were prepared for each phenotypic control condition, imaged on the IXU and the average total GFP intensity for each condition and significant differences between them were determined by image analysis ($p < 0.05$, $n = 6$). DMSO-treated infected (NEG, orange) and DMSO-naive infected (blue) controls resulted visual profiles (GFP expression) that were distinct to those of the ARV-treated and uninfected & DMSO-treated controls. A slight increase in GFP was however observed for DMSO-treated versus DMSO-naive infected samples. Maraviroc (yellow) and Raltegravir-treated (purple) infected as well as DMSO-treated uninfected (black) controls produced similar visual profiles (suppressed GFP expression). Each image represents a single FOV acquired at 20x with multiple FOVs acquired per condition. Scale bar = 20 µm.

In the post-exposure screens, GHOST(3) cells were seeded in 96 well plates and allowed to adhere overnight. The following day, cells were exposed to $PSG3^{BAL}$ at an MOI of 0.5 and cultured for 48 hours. The infective media was removed and cells were then treated with appropriate compounds for 24 hours before being fixed, stained and imaged on the IXU. Notably, ARV treatments were prepared as described for the pre-exposure format, (i.e. treated then infected) as neither Maraviroc nor Raltegravir are effective following viral integration, and an ARV that could specifically suppress LTR activity within the 24 hour compound treatment time was not available. Visual inspection again revealed that DMSO-treated and DMSO naive infected samples exhibited higher levels of GFP expression as compared to Maraviroc and Raltegravir-treated infected controls as well as DMSO-treated uninfected samples (Figure 3.18). DMSO treatment following infection also resulted in increased GFP compared to the DMSO-naive infected samples (Figure 3.18). Again, this suggested that treatment with DMSO may either influence the GFP reporter system or increase background signal, thus DMSO-treated infected samples were used as negative controls (NEG) indicative of a natural infection.

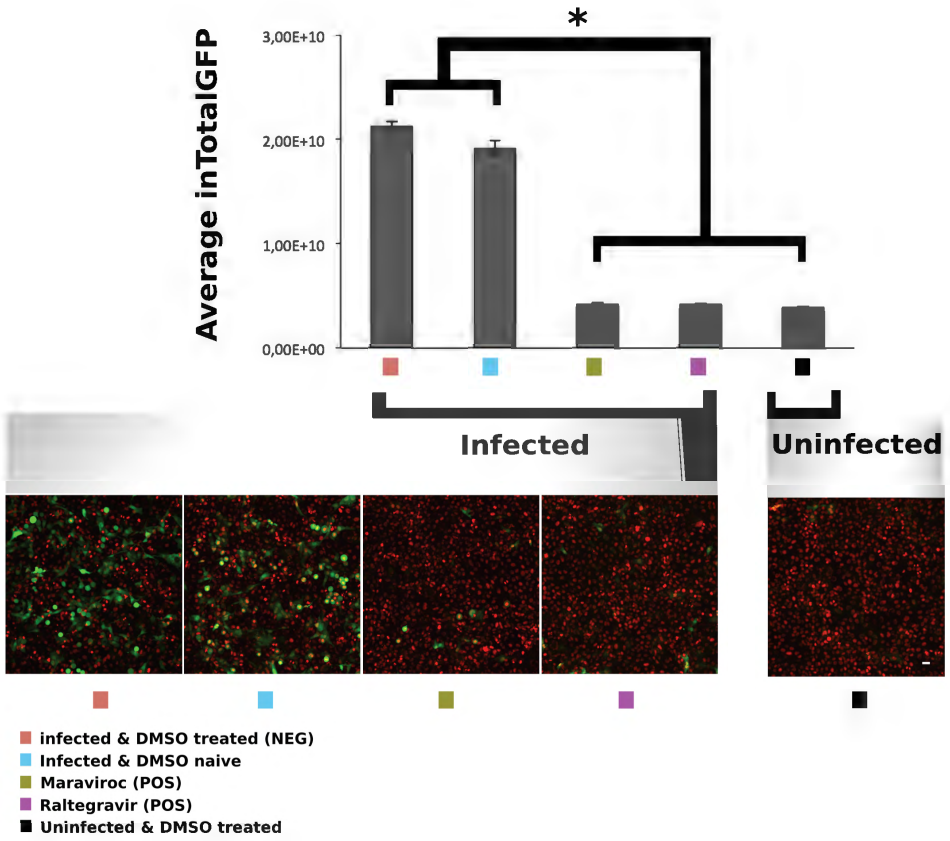

Figure 3.18 Post-exposure assay format phenotypic controls.

GHOST(3) cells were prepared for each phenotypic control condition, imaged on the IXU, and the average total GFP intensity for each condition and significant differences between them were determined by image analysis ($p < 0.05$, $n = 6$). Infected & DMSO-treated (NEG, orange) controls and Infected & DMSO-naive (blue) controls resulted distinct visual profiles (GFP expression) in comparison to the ARV-treated and DMSO-treated uninfected controls. A slight increase in GFP readout was observed in response to DMSO-treatment following infection as compared to Infected & DMSO-naive samples. Maraviroc (yellow) and Raltegravir-treated infected (purple) and DMSO-treated uninfected (black) controls produced similar visual profiles (suppressed GFP expression). Each image represents a single FOV acquired at 20x with 4 FOVs acquired per condition. Scale bar = 20 µm.

3.5.6 Sample processing

Having established the optimal methodology to run each phenotypic assay, it was important to ensure that the processing of samples for imaging was compatible as certain fixatives, stabilising agents and labelling approaches have been described to quench fluorescent signals (Schnell, 2012). In addition, prolonged fixation may also negatively affect downstream experimental procedures like Fluorescent In Situ Hybridization (FISH) and immunochemistry (Yamashita-Kashima, 2014). The choice of fixative, length of fixation and general design of sample processing protocols were thus

important factors taken into consideration in the HCS workflow. As opposed to using live imaging, GHOST(3) cells were fixed in order to standardise the experimental endpoint used across all experimental wells and plates regardless of the order in which they were imaged. A nuclear stain was included to facilitate identification of individual cells and to monitor significant variations in cell viability. A number of different fixatives and nuclear stains, as well different reagent concentrations and treatment times were evaluated to determine which fixation and staining procedures consistently produced a strong nuclear readout with minimal negative impact on GFP fluorescence. A 15 minute room temperature fixation step using 4% methanol-free formaldehyde (pH 7.4) and nuclear staining using a 2 nM final concentration of Hoechst without permeabilization was found to be optimal.

Imaging parameters

The choice of imaging system (Andor or IXU) as well as the imaging parameters utilized for both miRNA and compound screens were important factors in the HCS design process. A side by side comparison of both imaging systems was undertaken with a particular focus on image quality, acquisition time and well coverage (number of cells per FOV) (Table 3.3). Each microscope system was evaluated using a 20x acquisition as higher magnifications on the ANDOR system required oil emersion, which was not suitable for screening purposes. The results are summarised in Table 3.3 below. While the ANDOR system was able to acquire a greater number of FOVs in a shorter time frame, and could image in brightfield (standard light microscopy), the IXU system was selected for screening based on a number of criteria (Figure 3.19) including a superior signal to noise ratio (particularly in the GFP channel), a larger detection area, and the availability of an HCS-tailored software interface. Notably, the IXU system was also able to directly label each acquired raw image with metadata including the imaging site, well location, acquisition channel and the corresponding plate ID. In contrast, metadata had to be assigned to images acquired on the ANDOR system using a bespoke script designed in MATLAB®. The IXU system also exhibited a superior level of consistency in well to well focusing ability across multiple 96 well plates during testing. In addition, the Andor system was not designed for screening multiwell plates and thus a bespoke plate screening protocol was developed to guide the motorised stage to 9 manually programmed acquisition sites within each target well. In comparison, the imaging settings including selection of acquisition sites, number of acquisition sites, specific wells to be acquired, and plate type (96 vs. 384) was easily manipulated using the IXU software. All of these factors, including that the HCS assay did not require brightfield imaging, contributed to selection of the IXU system over the Andor system.

Table 3.3 Comparison of ANDOR and IXU imaging systems

Microscope System	Detector type and size	HCS specific software interface	Automated metadata recording	Oil immersion required for 40x	Brightfield imaging	Acquisition time*	Autofocus at each acquisition site	Average number of cells acquired
Andor	EMCCD: 512p x 512p	No	No	Yes	Yes	~25 min	No	~150-200/9
IXU	PMT: 1000p x 1000p	Yes	Yes	No	No	~30-35min	Yes	~350-400/4

*based on 9 FOVs for the ANDOR system and 4 FOVs for the IXU system

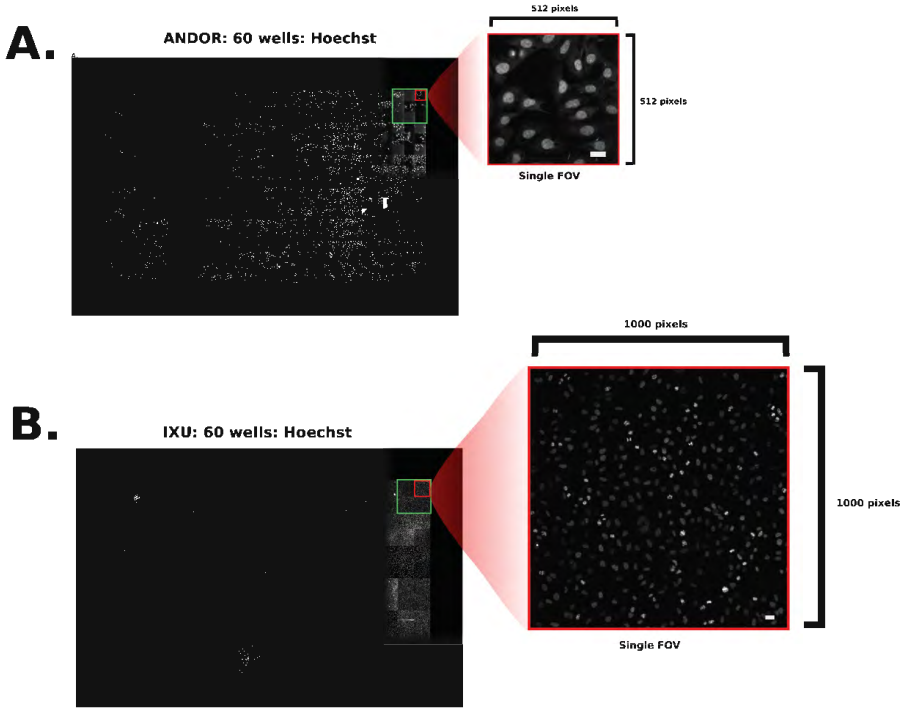

Figure 3.19 Comparison of ANDOR and IXU systems.

A) Plate reconstruction from images acquired on the ANDOR system at 20x in the 405 channel. 9 FOVs were acquired in each well (green square) and each FOV (red square) comprised a single 512 x 512 pixel image. **B)** Plate reconstruction from images acquired on the IXU system at 20x in the 405 channel. 4 FOVs were acquired in each well (green square) and each FOV (red square) comprised a single 1000 x 1000 pixel image. The single FOV images for each system are depicted to scale. Scale bars = 10 µm.

Acquisition settings

Once a microscope system was selected, the next step was to identify optimal acquisition settings for the GHOST(3)-PSG3^{BAL} HCS assay. Image resolution, well area coverage and acquisition time were major factors that determined the appropriate acquisition settings for all screens. The allocated daily imaging time on the IXU system was 8 hours and imaging 4 FOVs, 100 µm apart, in two channels (Hoechst and GFP) positioned at the centre of each well required 30-35 minutes of imaging time per plate. A major concern was that the use of only 4 FOVs located at the centre of each well would result in a biased phenotype that was not representative of the general phenotype within each well. In addition, while 20x acquisition had been tested in the side by side comparison previously, the resolution of the resulting images had not been tested using a downstream image analysis pipeline. To assess these imaging parameters, GHOST(3) cells thus were seeded into two µClear ® 96 well plates and infected with HIV at varying MOIs between 1 and 0.01. One plate was acquired at 10x and 20x and the other at 20x and 40x (Figure 3.20 A).

Nine FOVs were acquired per well during the 10x acquisition and 4 FOVs were acquired per well for both 20x and 40x acquisitions (Figure 3.20 B). A standard 100 µm distance between acquisition sites was utilised to ensure there was no overlap in cells acquired at each site. The average GFP intensity scores were extracted from all images acquired, at each magnification. The log of the average GFP scores obtained for each well were then plotted against the average GFP scores obtained for the same well, but at a different magnification. The 10x acquisition resulted in a large coverage area within each well and was thus used as a benchmark for the general phenotype within each well (Figure 3.20 B). The 20x acquisition adequately recapitulated the phenotype observed at 10x (n = 30; Figure 3.20 C). These findings suggested that acquisition of 4 FOVs at 20x at specified acquisition sites, while representative of only a small area of each well, provided an accurate representation of the general phenotypic trend within the well. A comparison between 20x and 40x acquisitions revealed a similar trend (n = 16; Figure 3.20 D). This observation demonstrated that lower resolutions (20x acquisition) did not misrepresent the phenotypic trend in each well as compared to a higher resolution acquisition. Based on these results, the following imaging parameters were used for all screens: the number of averages per acquisition, laser intensity, pinhole size and exposure times were selected in reference to the control wells on the first plate imaged per replicate; four FOVs, each 100 µm apart, positioned at the centre of each well were acquired in the 488 and 405 channels; and the IXU system was set to refocus at each acquisition site.

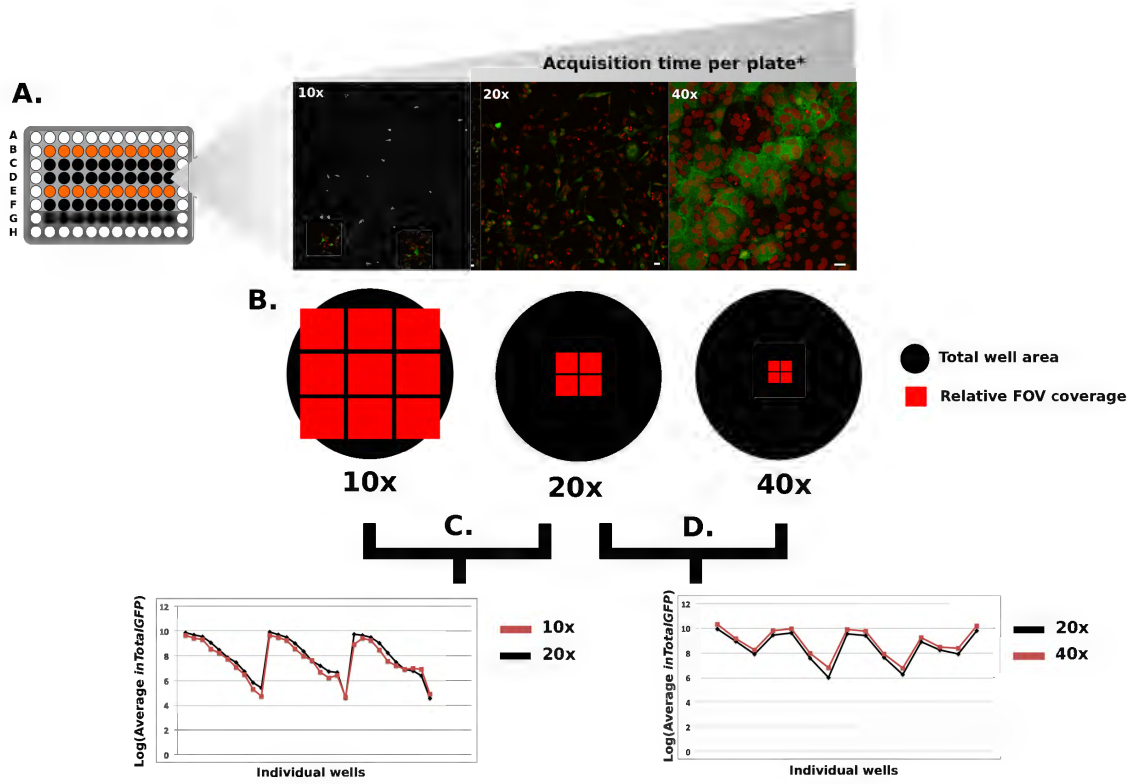

*Assuming that the same number of FOVs and channels are acquired per magnification

Figure 3.20 Comparison of different acquisition parameters on the IXU system.

A) GHOST(3) cells were infected with HIV and then imaged 48 hpi at 10x, 20x and 40x, nuclei (red), LTR-GFP expression (green). **B)** Scaled representation of FOV to well size ratios and coverage at different magnifications. **C)** A comparison of the average total GFP scores extracted from 9 FOVs with a high well area coverage acquired at 10x and 4 FOVs with a smaller well coverage acquired at 20x showed similar phenotype (n = 30). **D)** A similar trend occurred between 4 FOVs acquired at 20x and 40x.

3.6 Image analysis: infrastructure and HCS pipeline

HCS results in the generation of large volumes of images that are too large be efficiently curated manually and analysed (Shariff, 2010). Automated analysis of microscopy images through the integration of computer vision, pattern recognition and specialized data mining strategies has thus become an integral aspect of most current HCS approaches (Jackson, 2010; reviewed by Shamir, 2010). Such image analysis pipelines often require highly specialised expertise, equipment and software. Therefore, establishment of an image management, image analysis and data mining pipeline represented an important step in the development of a functional HCS workflow. A high level summary of the HCS image analysis pipeline is presented in Figure 3.21. Briefly, raw images derived from the various HCS experimental pipelines were indexed within a

bespoke image management database, parallel to this, images were processed to enhance signal to noise ratio, subjected to segmentation analyses and specific subcellular measurements (features) were then extracted from the images. The extracted features were used as numerical representations of the images and these numerical datasets were then sequentially subjected to specific quality control and data transformation methods within a statistical analysis and data mining tool, HCStratomineR (HCSR). The transformed and validated datasets were then subjected to hit selection in order to identify reagents/treatments that produced predefined phenotypes of interest (Figure 3.21).

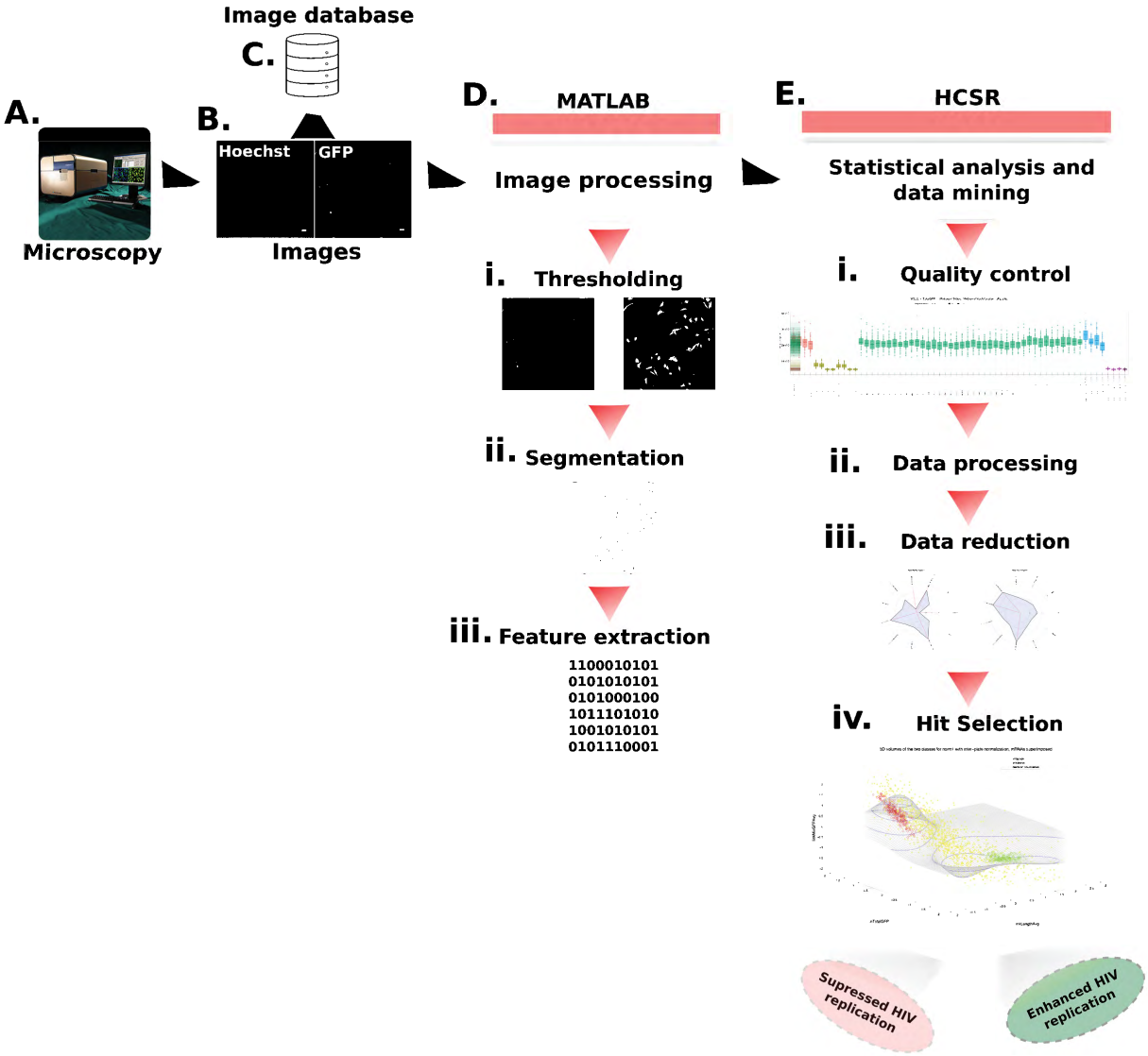

Figure 3.21 HCS image analysis pipeline.

A) Images were acquired on the IXU confocal system. **B)** Images were acquired in the 405 (Hoechst) and 488 (GFP) channels. **C)** Images were curated in a bespoke image management database. **D)** Images were processed through automatic thresholding **(i)** and segmentation **(ii)** and specific numerical features were extracted from images **(iii)**. **E)** Statistical analyses and data mining were performed in HCSR to confirm the quality of the data **(i),** process data for analysis e.g normalization **(ii)**, data reduction was applied when needed **(iii)** and hits were identified using specific selection criteria **(iv)**.

3.6.1 Image management database

The images produced by HCS should be well curated in order to efficiently locate specific images related to experimental plates/treatments of interest. Large scale HCS can result in millions of images and manually locating specific sets of images is cumbersome even for well organised datasets. Many HCS workflows rely on specialised image management solutions (Jackson, 2010; Allen, 2012) that often require specialised software licensed at premium prices. To circumvent this a bespoke HCS image management tool was designed on the open source Ruby on Rails® web framework by a collaborator, Dr. Juergen Helmers, following a number of consultations to determine the HCS needs of the project. Briefly, master and experimental plate annotations for each reagent library were defined within the application. Raw images acquired from each experimental plate were transferred to a local storage device and the location of each folder corresponding to a given experimental plate was then specified. The metadata for each image was collated and attached on a per plate basis. This resulted in an indexed database directly linked to all screening-related images. Furthermore, identification of images from specific plates, replicates and treatments was facilitated by a graphical user interface and search tool. In addition, the application was able to reconstruct images of each well at each FOV by overlaying pseudocoloured versions of each individual fluorescence image. This image managment system was primarily utilised to visually inspect screen hits and to visualize phenotypes related to specific reagents of interest (such as miRNAs/compounds/controls).

3.6.2 Image processing, segmentation and feature extraction

Computer vision is a field of research that focuses on the use of computer-aided methodologies to objectively interpret and classify visual datasets (Shamir, 2010; Shariff, 2010). Within the HCS arena, images are generally preprocessed to differentiate true signal from background noise (Shariff, 2010). This image processing step improves subsequent identification of objects of interest within individual images, and increases the efficiency of downstream segmentation and extraction scripts. Optimisation of specific thresholding strategies for each dataset is therefore important. Segmentation is one such strategy that partitions an image into specific ROIs (cells, organelles etc.)

thereby reducing the total number of pixels, which in turn limits downstream analyses to objects of interest (Al-Amri, 2010; Zuva, 2011).

Once images have been segmented, multiple subcellular measurements known as' 'descriptors or 'features' can be extracted and these 'feature scores' then serve as a numerical representation of the visual phenotypes depicted within each image (Shamir, 2010). The numerical scores are then processed and analysed in order to categorize images into distinct groups, and to visualise specific trends within a dataset/screen. A number of different types of features can be extracted from images including various descriptors of cell morphology, distribution of objects and pixels, textural descriptors and pixel intensity, to name a few (Haralick, 1973; Shamir, 2010). It is however very important that features selected for use in downstream image classification approaches are relevant to the HCS assay, as inclusion of irrelevant or even poorly relevant features can comprise both the accuracy and efficiency of downstream classifications. This is particularly true for supervised machine learning based approaches (Kohavi, 1994; Shariff, 2010).

All screens presented in this thesis used image processing, segmentation and feature extraction scripts that were designed, optimized and executed within MATLAB® by a resident software engineer in the same research group. An automatic threshold was applied to all images on a per fluorescence channel basis, and these thresholds were re-evaluated for each screening replicate. Initially, various segmentation parameters (object size, shape, distribution, etc.) and various segmentation methods were explored using test images obtained from simulated experimental conditions. This was done in order to determine the best approach for identifying individual cells within images acquired in the 405 and 488 channels. These approaches were later refined using the data obtained from each screen replicate. Notably, features can either be developed *de novo* for a specific screen, or selected from large libraries of pre-existing features used in similar HCS assays (Shariff, 2010). In addition, there are a number of commercial and open source software solutions, each with their own advantages and drawbacks, that are capable of performing routine feature extraction (reviewed by Zanella, 2010). However given the available in-house expertise in computer vision and software engineering, a bespoke feature extraction approach was developed specifically for this study. This approach was implemented through MATLAB® and 17 features were extracted from the images acquired during the miRNA and compound screens presented in this study (Table 3.4). Fifteen of the 17 features were based on an HCS study that utilized a similar Tat-sensitive GFP reporter model to quantify HIV replication following siRNA-mediated knockdown (Genovesio, 2011). Two additional features (Cell Area and Infection Efficiency) relevant to the study were also included.

Table 3.4. Features extracted for image analysis of screen data (adapted from Genovesio, 2011)

Feature	Description	Biological relevance
Cell area*	Area of hoechst signal relative to size of an image	A low value indicates cell death
Infection efficiency *	Average number of GFP expressing cells divided by the cell count/ cell area score	A low value indicates suppressed HIV replication
Cell number	Number of cells	A low number indicates cell death
linkMinGFPAvg	Average of the minimum value of green fluorescent protein (GFP) along the line going from a cell to its neighbour.	A high value indicates the cell is in a syncytia formation
linkMinGFPSdtdev	Standard average of the minimum value of GFP along the line going from a cell to its neighbour	A high value indicates a mix of fused cells in syncytia formation and non-fused cells
linkLengthAvg	Average distance between two neighbouring cells	A high value means cells are spread
linkLengthSdtdev	Standard deviation of the distance between two neighbouring cells	A high value means an odd dispersion of cells (often happens in the case of cell death)
inTotalGFP	Integration of GFP over the image inside the boundaries of the precisely fitted experiment	A high value indicates infection measured on the spot
inIntNucleiAvg	Average intensity of cell nuclei inside the boundaries of the precisely fitted experiment	An irregular sample value compared to the control values means cell toxicity measured on the spot
inIntNucleiSdtdev	Standard deviation of intensity of cell nuclei inside the boundaries of the precisely fitted experiment	A high value means cell toxicity measured on the spot
inIntGFPAvg	Average intensity of GFP per cell inside the boundaries of the precisely fitted experiment	A high quantity of reporter per cell indicates infection measured on the spot
inIntGFPSdtdev	Standard deviation of GFP per cell on the precisely fitted experiment	A low value indicates a well-spread infection measured on the spot
outTotalGFP	Integration of GFP over the image around the boundaries of the precisely fitted experiment	A high value indicates infection on the border around the spot
outIntNucleiAvg	Average intensity of cell nuclei around the boundaries of the precisely fitted experiment	An irregular sample value compared to the control values means cell toxicity measured on the border around the spot
outIntNucleiSdtdev	Standard deviation of intensity of cell nuclei around the boundaries of the precisely fitted experiment	A high value means cell toxicity measured on the border around the spot
outIntGFPAvg	Average intensity of GFP per cell around the boundaries of the precisely fitted experiment	A high quantity of reporter per cell indicates infection measured on the border around the spot
outIntGFPSdtdev	Standard deviation of GFP per cell around the boundaries of the precisely fitted experiment	A low value indicates a well-spread infection measured on the border around the spot

* Features not described by Genovesio, 2011

Image processing, segmentation and feature extraction generally represent the most computationally intensive processes in an HCS workflow, and require high-end processing systems (Shamir, 2010). While simple segmentation and feature extraction scripts can be executed within seconds per image (e.g. Voronoi segmentation), more complex approaches utilising compound or abstract features (e.g. Active contours) can take hours to execute on a single image (Shariff, 2010). Processing of images acquired in a single miRNA replicate screen and extraction of 17 features from these images required ~ 1 month of processing time using a communal multicore MAC system running OSX (Apple Inc, USA).

3.6.3 Statistical analyses and data mining

The sheer size of datasets in combination with a requirement for complex statistical and data mining functionality can represent a major challenge in HCS (Bray, 2012; Zhang, 2012). A multitude of different approaches, strategies and software solutions have thus been specifically developed to address the challenges associated with downstream analysis of HCS data (Jackson, 2010; Zanella, 2010). Statistical analysis, data mining and hit selection were initially performed within MATLAB® by a resident software engineer but this approach was found to be impractical for long term screening applications, as it was not suited to biologists who were not well versed in computer programing. Limiting the requirement of programming expertise to automated image processing and feature extraction steps enabled biologists to undertake the data mining and hit selection processes. To facilitate this, a collaborative relationship with the Cell Screening Core at the University Medical Center Utrecht was established as they had developed a highly relevant tool called HCStratominer (HCSR). HCSR provided an easy-to-use interface with access to a virtual processing centre comprising >1000 cores that allows for on-the-fly statistical analysis, data visualization and data mining from large datasets.

For the screens described in this thesis, design of a statistical analysis and data mining pipeline was based on the use of HCSR and a 3-step HCS decision matrix proposed by Shun and colleagues (Shun, 2011). The first step was to determine the most appropriate data processing methods and define specific criteria for quality assessment and hit selection. The next step was to utilize a graphical review process to assess the quality of the HCS data and apply the necessary statistical adjustments (e.g normalisation, standardisation). This was done from the level of monitoring inter-replicate variation to the gating of individual experimental wells and features that were deemed to be substandard. Variables that did not meet predetermined minimum standards were either excluded from downstream analysis or corrected using analytical strategies (Quality control). The final step was to apply the relevant data reduction methods (when required) and hit selection criteria to the validated and processed HCS data. Together, these steps allowed for identification of reagents that produced phenotypes of interest within HCS datasets (hit selection).

HCS quality control

The large volumes of numerical data generated through HCS can be tainted by systematic and experimental errors thus distorting the quality of hit selection (Zhang, 2012). While such errors are easy to identify and correct in low throughput experimental setups, they are exponentially more cumbersome to identify and adjust in larger HCS-scaled datasets. Stringent quality control measures are thus required throughout the HCS experimental workflow (Zhang, 2008; Bray, 2012). A number of quality control guidelines and parameters have been described specifically for use in HTS/HCS (comprehensively reviewed in Zhang, 2008; Shun, 2011; Bray, 2012 and Zhang, 2012). The choice of quality control parameters should however be carefully considered in the context of each HCS assay and the available computing resources and expertise. The sequential stages in the quality control and data processing pipeline utilized in this study are discussed below.

The interactive data visualization tools within HCSR were used to first evaluate the quality of screening datasets and the performance of the HCS assay. Graphical renditions (scatter plots) of unprocessed average GFP intensity (inTotalGFP) and cell number (Total Cell Area) feature scores were generated for each experimental well, first at the scale of an entire screen (all replicates) and then at the level of individual experimental plates. These scatter plots were used to monitor a number of quality control parameters by visual inspection.

Firstly, the correct orientation of experimental plates was verified by confirming low GFP scores within well locations that corresponded to uninfected or positive control wells. Screen-level inTotalGFP plots were then used to confirm the consistent and significant separation of the major phenotypic controls (e.g NEG vs. POS) and the correct classification of the quality control-related phenotypic controls relative to NEG and POS controls (e.g. non-targeting miRNA reagent controls). Additionally the variability within the phenotypic distribution range of experimental treatments was also monitored at this stage in order to confirm that reagent-related variations in GFP-reporter activity were indeed prevalent within the dataset, and that a significant proportion of the experimental treatments had a functional impact on the HCS assay. Likewise screen-scale scatter plots relevant to the cell viability indicator, Total cell area, were used to confirm that there were no significant variations in cell viability between the phenotypic control samples and that experimental treatments exhibited a suitable range of variability related to the functional impact of the experimental treatments.

Plate level scatter plots were used for a side-by-side comparison of the phenotypic profiles of replicate experimental plates relative to inTotalGFP and Total cell area scores. Visual inspection of the variance between technical replicates on the same experimental plate allowed for the monitoring of possible edge effects through the confirmation that spatially separated technical replicates were not phenotypically distinct

from each other in terms of GFP-reporter activity and cell number. Controls wells that were found to be misclassified or outliers were excluded from downstream analysis. A number of different methods exist for the evaluation of HTS/HCS assay performance, including Z'-factor, strictly standardized mean difference (SSMD) and V-factor, to name a few (Bray, 2012). Of these, Z'-factor remains the most widely used, particularly in HTS. Z'-factor represents a statistical method to rate the performance of an HCS assay by evaluating how consistently, and by what margin, the positive and negative control well phenotypes are separated across multiple replicates of a screen. Z'-factor was automatically calculated for each experimental plate for both the miRNA and compound screens using HCSR. Z'-factor values > 0.5 are generally utilised as a cutoff for acceptable assay performance in HTS however due to the complex nature of phenotypic assays, Z' factor values <0.5 but greater than 0 are considered acceptable for statistically distinct positive and negative control treatments in HCS (Bray, 2012). The statistical significance of the variance between the positive and negative control phenotypes on each experimental plate were assessed by a Z'-factor value based on inTotalGFP (suitable values > 0) and Total cell area (suitable values < 0).

The visualization of inTotalGFP and Total cell area distributions for specific well locations across all experimental plates in a screen was used to monitor for specific positional biases (e.g row, column, well). These biases can result from defects in liquid handling equipment or image acquisition systems, and can result in a distorted representation of the data, specifically a high false discovery rate (FDR). Graphical representations of the average GFP intensity (inTotalGFP) and cell count scores for all experimental wells were also assessed on a per plate basis, to identify any non-random and global directional biases that might have been introduced during experimental procedures. These positional (well, column, row) biases can in theory be addressed using specialised intra-plate normalization techniques such as B-score normalisation, but such instances were not encountered within our datasets (Bray, 2012).

The next stage of the data processing pipeline following the inspection of the unprocessed data involved in the normalization of screening datasets. Normalization of feature scores is used to minimise the analytical noise caused by minor systematic errors, and to improve the detection of variations that result from experimental treatments by comparing them to a standardised baseline phenotype (Zhang, 2012). A number of different normalization methods can be applied to HCS data, including normalising against specific controls wells, sample wells and z-scoring (Bray, 2012). The choice of normalization method is dependent on the specific HCS assay, but all of these methods serve to improve the similarity of feature profiles for replicate experimental treatments located on different experimental wells/plates, and to 'tighten' the descriptive profiles of phenotypic controls across experimental plates. A number of normalization methods were evaluated within HSCR for each dataset and normalization against the negative controls was found to be the most useful approach for the majority of datasets tested. Normalised distribution profiles for each feature were then visualised and used to eliminate features that were not descriptive of the phenotypic assay or exhibited heavily

skewed distributions or missing values. The retained features were then either subjected to data reduction or utilised in a multivariate approach to hit selection. HCS generally results in the generation of multivariate data spread across numerous features. Data reduction reduces the dimensionality of this data by summarising the relationships (e.g through correlations) between features to create a smaller number of new and more relevant descriptors (Kaiser, 1958). Classical data reduction approaches used in HCS include principal component and factor analyses (Kaiser, 1958; Shariff, 2010).

Hit Selection

Identification of specific phenotypes of interest (hit selection) from numerical HCS data can be achieved using a number of different approaches including multivariate statistical analysis, machine learning based pattern recognition, and user defined selection criteria (Durr, 2007; Shamir, 2010). The choice of hit selection method can be limited by experimental design constraints and varying selection methods can in turn produce varying subsets of hits, even from the same dataset (Durr, 2007). For the purposes of this study, hit selection was focused primarily on the identification of reagents (miRNAs/compounds) that were able to either significantly suppress (hit class 1) or enhance (hit class 2) HIV replication in GHOST(3) cells, without nonspecific or detrimental effects on cell viability. A plethora of different combinations of hit selection criteria and methods were initially evaluated within HCSR using simulated test data and then screen data. From these, 4 methods were found to robustly facilitate the identification of the hit classes of interest within both the miRNA and compound datasets.

In the most basic method, referred to as ‘GFP-ranking’, HIV-suppressive hits were defined as reagents that exhibited a significant decrease in the normalized, combined inTotalGFP score (between replicates) relative to the negative control samples and a predetermined threshold (e.g 50% less GFP) (Figure 4.5). Likewise, HIV-enhancing hits were defined as reagents that exhibited a significant increase in the combined inTotalGFP score relative to the negative control samples and a predetermined threshold. The second approach utilized automated multidimensional-scaling (MDS) within HCSR, where pre-determined data reduction methods were applied to the feature scores in order to generate a maximum of 2 factors which best summarized the relationships between the available features. Experimental treatments that were statistically (p threshold) and phenotypically distant (manhattan distance) from the negative control samples were then selected for further analysis. From these reagents, HIV-suppressive hits were defined as reagents that exhibited a significant decrease in the average combined inTotalGFP score relative to the negative control samples. Likewise, HIV enhancing hits were thus defined as reagents that exhibited a significant increase in the average combined inTotalGFP score relative to the negative control samples. This method of hit selection based on the phenotypic distance of treatments from the negative controls using MDS is referred to as MDS-distance from negative (MDS-DFN).

PCA-based data reduction, specifically the use of Kaiser criterion, Bartlett scores and a maximum likelihood-based extraction method was also utilised in hit selection. Following PCA analysis, only factors that were adequately descriptive of the variation between the positive and negative control samples were retained for further analysis. These factors were then utilised in two different hit selection methods. The first is referred to as PCA-based on similarity to positive controls (PCA-STP) and was used to specifically identify reagents that were phenotypically (inverse manhattan distance) and statistically (p threshold) similar to the positive control phenotype. The final method relied on the use of the PCA-generated factors to identify experimental treatments that were phenotypically (manhattan distance) and statistically (p threshold) distant from the negative control wells. Reagents that met these criteria were then ranked by their combined inTotalGFP scores and HIV-suppressive or HIV-enhancing reagents were identified using specific cut-off thresholds as with 'GFP ranking'. This approach was referred to as PCA-based distance from negative analysis (PCA-DFN).

These four hit selection strategies were used in combination or isolation to identify reagents that produced phenotypes of interest in both the miRNA and compound screens presented in this study. The specific cut-off thresholds (p values, cell viability scores etc.) utilised for each method were selected based on individual datasets (e.g miRNA mimic or kinase compound library datasets). More relaxed selection criteria were specifically utilized in the miRNA screens to account for the high degree of complexity and potential variability in miRNA biology.

3.7 Hit Stratification

Functional HCS and HTS strategies can generate large numbers of hits with demonstrated functional relevance to the biological process of interest. These hit populations may then be stratified to identify and characterise systems biology scaled trends that underlie the functional phenotypes related to specific hit classes (e.g suppressed or enhanced HIV replication). The prediction/identification of the molecular targets (e.g miRNA-mRNA or chemical-protein) of reagents and the subsequent characterisation of specific regulatory pathways and molecular targets that are enriched for specific hit classes represents a general approach to HCS hit stratification that is used in many HCS pipelines (Brass, 2008; Genovesio, 2011). Hit stratification strategies specific to miRNA- and compound- based HCS are discussed below along with the specific hit stratification methods selected for inclusion in the HCS pipeline developed for this study.

miRNA screens

The interpretation/extrapolation of miRNA screening results beyond the basic phenotypic readouts of cellular assays (e.g. enhanced or suppressed HIV replication) is usually dependent on the identification of the functional targets of the miRNAs of interest and their subsequent characterization through enrichment and protein interaction analyses. The non-orthogonal nature of miRNA-target interactions however has made the accurate and cost effective characterisation of miRNA-target interactions very challenging, especially with regards to large subsets of miRNAs (Lemons, 2013). There are currently a number of computational (in silico) and experimental approaches available for the identification of miRNA targets (reviewed by Hausser, 2014) Briefly, quantitative transcriptomics (Linsley, 2007) and proteomics (Bargaje, 2012) approaches have both been utilised to correlate changes in mRNA and protein expression levels with the functional modulation of a single or small subset of miRNAs. These strategies have proven to be extremely useful in quantifying global cellular responses associated with the overexpression or suppression of a given miRNA but are ultimately unable to directly resolve miRNA-target interactions (Linsley, 2007; Bargaje, 2012). Alternatively, various biochemical methods like Photoactivatable-Ribonucleoside-Enhanced Crosslinking and Immunoprecipitation (PAR-CLIP) and the mir-TRAP system are able to identify specific miRNA-mRNA interactions through a series of cross-linking, immunoprecipitation and sequence verification steps (Hafner, 2010; Baigude, 2012). Additionally a number of 3' UTR reporter systems have also been developed in order to evaluate miRNA- target sequence binding efficiencies and to utilize these quantifications to verify predicted miRNA-target interactions (Krek, 2005). Each of these experimental methods have specific advantages and drawbacks but are all ultimately dependent on assaying the outcome of an experiment focused on a single miRNA (Hausser, 2014). These approaches are therefore generally not economically or practically suited to the identification of miRNA targets on a large scale.

Computational approaches on the other hand may incur little to no financial costs and are also less laborious and technically challenging compared to many of the experimental methods described above (Hausser, 2014). Computational miRNA target prediction is generally based on the use of specific algorithmic criteria such as seed sequence complementarity and the stability of RNA-RNA interactions to infer potential miRNA targets (Agarwal, 2015). This approach has proven to be a useful tool for the large scale prediction of putative miRNA target interactions and number of miRNA target prediction tools are freely available as web-based applications (summarised by Lemons, 2013). High false discovery rates and a lack biological context (e.g cell type specific interactions) have traditionally plagued early *in silico* prediction methods resulting in poor confidence in these methods (Alexiou, 2009). miRNA target prediction algorithms have however been constantly refined in order to improve their accuracy (Agarwal, 2015) and the integration of miRNA-prediction tools with curated databases of experimentally validated miRNA-target interactions and miRNA expression mapping tools have provided an added level of sophistication and quality to current miRNA target prediction

and pathway analysis tools (Vlachos, 2015). Considering that the average functional phenotypic miRNA screen is expected to yield between 30 and 200 hits per 900 miRNAs screened (Lemons, 2013) and that resources were limited for downstream validation experiments, an *in silico* miRNA target prediction and pathway analysis approach was implemented as part of the hit extrapolation strategy within the HCS pipeline. Specifically miRNA target prediction and pathway analysis was undertaken using the web-based tool, miRpath v.3 (Vlachos, 2015).

Compound screens

The extrapolation of higher-order functional data from compound screens utilizing well characterised and(or) clinically prescribed compounds represents a much simpler task when compared to similar miRNA-based analyses. The formulation of high confidence protein interaction networks for compounds with characterized functional targets can be readily achieved using a number of computational tools. On such tool, is the online resource, STITCH v.4.0. STITCH v.4.0 facilitates the construction of chemical-protein and protein-protein interaction networks based on published findings, online databases and experimental data and currently contains validated interactions for ~ 300 000 small molecules and 2.6 million proteins (Kuhn, 2008). STITCH 4.0 was thus chosen to serve as the hit stratification tool for compound screening in the HCS pipeline developed within this study.

3.8 Discussion

The optimisation and design principles described in this chapter were utilised to develop and successfully execute all miRNA and compound HCS described in this study. Notably, specific guidelines were established for the management of RNAi and compound libraries. A GHOST(3)-PSG3^{BAL} infection assay was selected and appropriate phenotypic controls were validated. Transfection, cell seeding, and sample processing experimental procedures were also optimised for HCS. Imaging parameters were verified by experimental simulations, and a functional data management, image analysis and data mining pipeline was also successfully implemented. Furthermore validated *in silico* approaches to hit stratification for both miRNA and compound screening datasets were established and integrated as part of a functional HCS pipeline.

The use of a Tat-sensitive reporter readout inherently limited the range of screens to miRNAs/compounds that affected early stages of HIV replication, up to the point of Tat-mediated transactivation. Thus reagents that may potentially impact later stages of infection (e.g Rev-dependent translation and budding) could not be resolved using this screening strategy. This issue was considered during the experimental design stage and could have been addressed by using infectious molecular clones (IMCs) that allow for multiple rounds of infection, in combination with a secondary infection assay similar to that described by Brass and colleagues (Brass, 2008). However, this was not possible

given the requirement of a BSL-3 facility for the use of IMCs. On a separate but related point, physiologically relevant cell types are best but many are not suited to HCS approaches (Gasparri, 2009). Primary macrophages and T lymphocytes are the most relevant cell types for HIV infection, however each of these cell types also present major challenges with regards to high content screening. T cells are generally non-adherent and difficult to transfect. Macrophages are more amenable to lipid-based transfection, however large variability and low efficiency rates with regards to macrophage infection render them unsuitable for phenotypic screening applications. The HOS-derived GHOST(3) cell line, while not as physiologically relevant as primary cell models, facilitated execution of RNAi-based experimental procedures with relative ease, and provided a cellular background that was proximal to progenitor lineages of both T cells and macrophages (Zhao, 2012).

The data presented in this chapter represents a functional guideline for the development of a high throughput phenotypic screening workflow. While the screening parameters described in this dissertation focus specifically on the use of an image- based approach to identify host miRNAs and compounds that modulate HIV replication, the HCS design and optimisation principles presented here can also be readily adapted to miRNA, siRNA, shRNA and compounds screens based on different biological models.

Chapter 4: HCS uncovers novel host miRNA-mediated modulation of HIV replication through the regulation of signalling networks that are functionally relevant to HIV

4.1 Introduction

In contrast to ~30 000 annotated human genes, there are currently only ~ 2000 annotated human miRNAs (Kozomara, 2014). Despite their relatively small number, these endogenous molecules are master regulators of almost all cellular processes, through their roles as molecular guides within the endogenous RNAi network (see Chapter 1 for a complete review of miRNA biology). Briefly, a single miRNA may govern the expression of multiple functionally related genes, and facilitate cross-talk between both coding and long noncoding RNA species (Yoon, 2014; Tan, 2015). Modulating the functional activity of a single miRNA can therefore result in complex physiological changes that are targeted to specific regulatory pathways and cellular processes (Tan, 2015). This non-orthogonal but functionally convergent nature of miRNA-target interactions has thus positioned many miRNAs as molecular switches that govern key biological processes including cellular proliferation (miR-21; Selcuklu, 2009), inflammation (miR-155; Faraoni, 2009) and G1/S cell cycle transitions (miR-17-5p; Cloonan, 2008) to name a few.

Genome-wide miRNA screening reagents provide researchers with a tool that is typically an order of magnitude smaller than traditional genome-wide siRNA libraries, and which also offers a potentially broader range of functional coverage which may not be readily achieved through single gene silencing strategies (Lemons, 2013). In addition most

miRNA reagent libraries are available in two formats, as collections of double-stranded miRNA mimics and single stranded miRNA inhibitors. miRNA mimics are synthetic replicates of mature endogenous miRNAs, while miRNA inhibitors function as molecular decoys that inhibit endogenous miRNA-target interactions (see Chapter 2). Ectopic expression of these molecules can thus be utilised to either enhance or suppress the functional activity of a specific endogenous miRNA(s), thereby allowing for a two-pronged screening approach to evaluate the functional relevance of specific miRNAs within a biological process of interest (Santhakumar, 2010).

Research into host-pathogen interactions has revealed that miRNAs are key mediators of viral infection with a number of host miRNAs reported to function as viral restriction or host-dependency factors (reviewed by Guo, 2014). A number of viruses have in turn also been reported to encode viral miRNAs of their own, that function to hijack the host RNAi network and promote viral replication (reviewed by Kincaid, 2012). Functional miRNA screens have been successfully utilized to identify a number of novel and broadly acting anti-viral host miRNAs in murine cellular models of infection (Santhakumar, 2010), as

well as human miRNAs that are relevant to influenza replication (Meliopoulos, 2012; Bakre, 2013), and even conserved functional targets among viral-encoded miRNAs (Cox, 2015). In addition to uncovering a wealth of novel information on complex signalling networks that govern host-viral interactions, miRNA-based HCS approaches have also demonstrated great potential for the identification of novel therapeutic targets. In fact, miRNAs themselves may be utilised as novel therapeutic agents (Lemons, 2013). Related to HIV, less than 30 host miRNAs have currently been described as functionally relevant for HIV replication, and a large-scale functional evaluation of the roles that host miRNAs play in the replication dynamics of HIV is absent (reviewed by Klase, 2012 and Barichievy, 2015). To address this shortfall, the GHOST(3)-PSG3^{BAL} infection assay and optimised HCS pipeline described in the previous chapter were used to screen a panel of miRNA mimics and inhibitors in order to characterize host miRNAs that significantly enhance or suppress HIV replication (Figure 4.1).

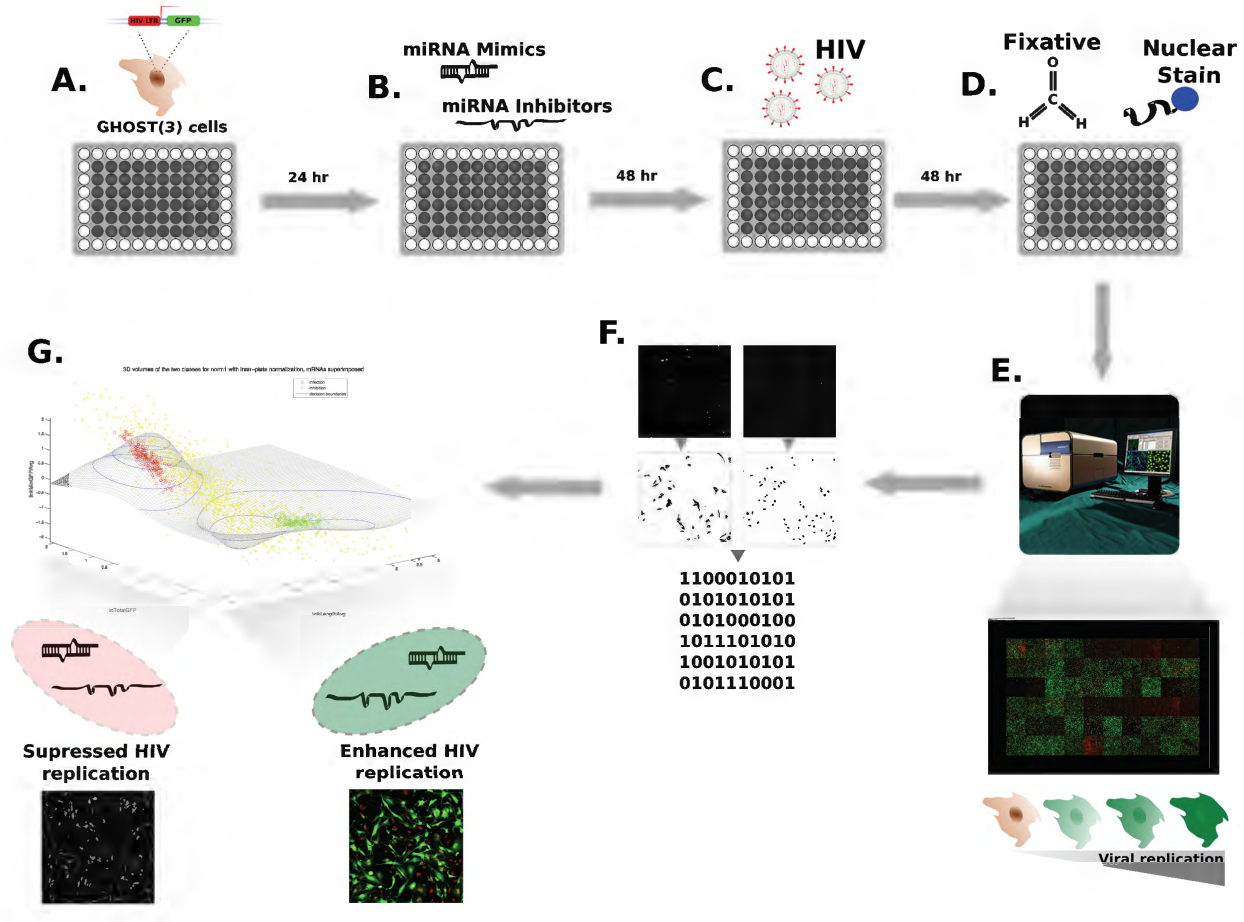

Figure 4.1 Validated miRNA-based HIV infection HCS pipeline

A) GHOST(3) reporter cells expressing a Tat-sensitive GFP reporter construct were seeded into the inner 60 wells of µClear® 96 well imaging plates (grey circles) and forward transfected 24 hours later, **B)** with a 25 nM final concentration of miRNA mimics or inhibitors. **C)** 48 hours post-transfection cells were transduced with PSG3^{BAL} (HIV) at an MOI of 0.5, **D)** 48 hours post-

infection cells were fixed with formaldehyde solution and nuclei were counterstained with 2 nM of Hoechst, **E)** Four FOVs were acquired per well in both the 405 (Hoechst) and 488 (GFP) channels using an automated microscope system. GFP expression positively correlated with HIV replication, **F)** The acquired images were processed and 17 subcellular measurements (features) were extracted from each image in order to convert image-based data to numerical data, **G)** Statistical analyses, quality control filtering and data mining strategies were applied to the numerical dataset to identify miRNA reagents that significantly enhanced or suppressed HIV replication relative to control samples.

4.2 Results

A total of 1239 miRNA mimics and 1245 miRNA inhibitors mimics were screened in duplicate across 126 experimental plates. A reconstructed image of a single experimental plate is presented in Figure 4.2 below. Uninfected control wells and siCD4-treated control wells were collectively utilized to define a positive control phenotype for image analysis (Figure 4.2). Approximately 7500 individual transfections reactions were manually executed along with ~6500 individual HIV infection reactions and ~7500 fixation/nuclear staining reactions. More than 60 000 images were acquired over ~70 hours of imaging time, and these images were then catalogued, processed and analysed over several months (see Chapter 3). miRNA screening results were separated into mimic and inhibitor datasets for image analysis. This was done to try and improve the hit recovery rate for miRNA inhibitors which generally produce much more subtle phenotypic effects. However, the overarching aim of identifying miRNA mimics and inhibitors that enhanced or repressed HIV replication remained.

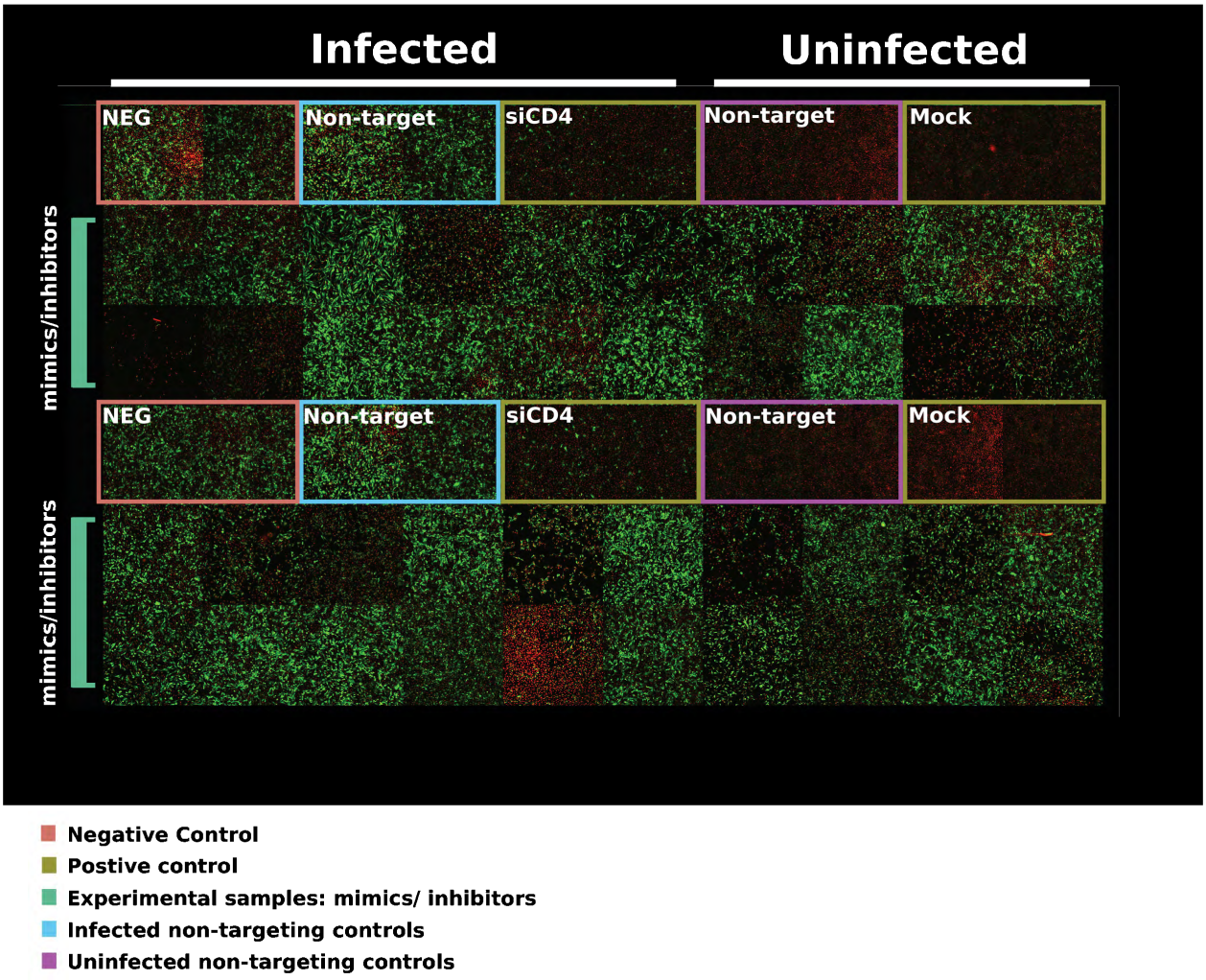

Figure 4.2 miRNA screen experimental plate layout

A single composite image comprised of reconstructed images acquired in both the 405 (Hoechst) and 488 (GFP) channels is shown. Each well is represented by 4 FOVs. The black border represents the outer 36 wells that were not utilized for experimental reactions. Duplicate experimental control wells were located on rows B and E of each experimental plate and experimental samples (mimics/ inhibitors) were were always located on rows C, D, F and G. GFP reporter signal (green), nuclei stained with Hoechst (red).

4.2.1 HCS Quality Control

Visual inspection of graphical data outputs in HCstratomineR were utilised to perform a number of quality control verification steps. Briefly, cellular assay performance was quantified by Z' factor analysis using the 'inTotalGFP' and 'Total Cell Area' feature scores. An 'inTotalGFP' Z' factor value > 0.1 and a negative 'Total Cell Area' Z' factor were indicative of acceptable assay performance. Plate rotations and well-specific

biases were also evaluated by distributions plots of ‘inTotalGFP’ and ‘Total Cell Area’ feature scores for all experimental wells/ plates. Individual datasets were generated for miRNA mimics and inhibitors for each replicate (n=2) and replicate datasets were analysed within a single screening experiment.

4.2.1.1 Mimics

The unprocessed ‘Total Cell Area’ scores (cell count parameter) demonstrated no clear variation between the phenotypic control samples, including the positive and negative controls and the internal infected and uninfected controls (Figure 4.3A). This was confirmed by the recovery of negative Z’ factor values for all experimental plates. Experimental treatments demonstrated a greater level of variation, indicative of miRNA mimic -associated effects on cell density (Figure 4.3A). The unprocessed ‘inTotalGFP’ scores (primary reporter assay feature) demonstrated a clear and significant variation between positive and negative control samples (Figure 4.3B). In addition, uninfected non-targeting miRNA controls as well as infected non-targeting miRNA control samples exhibited similar phenotypic classifications compared to their respective controls (Figure 4.3B). A Z’ factor range between 0.3-0.6 was recovered for all experimental plates indicative of assay performance and data quality that was suitable for downstream analysis. To be clear, there was a significant difference between positive and negative control wells, based on total GFP expression. Similarly, wells containing virus and non-targeting controls showed similar GFP expression to virus only wells, and these were significantly different from wells containing only non-targeting controls (Figure 4.3A ii). Distribution of the uninfected phenotypic controls confirmed that none of the experimental plates were acquired in the wrong orientation and well location based analysis (‘Frequent hitter’ analysis) confirmed that systematic errors had not significantly impacted the inTotalGFP-related phenotypic readout within experimental plates (Figure 4.3C). Controls wells were observed to consistently produce specific and distinct GFP expression phenotypes, while experimental treatment wells did not (Figure 4.3C). In addition, no biased directional (column, row) or well-specific effects on GFP expression were observed across experimental well locations. The quality of the data obtained from the miRNA mimic screens was thus deemed to be acceptable for further analysis.

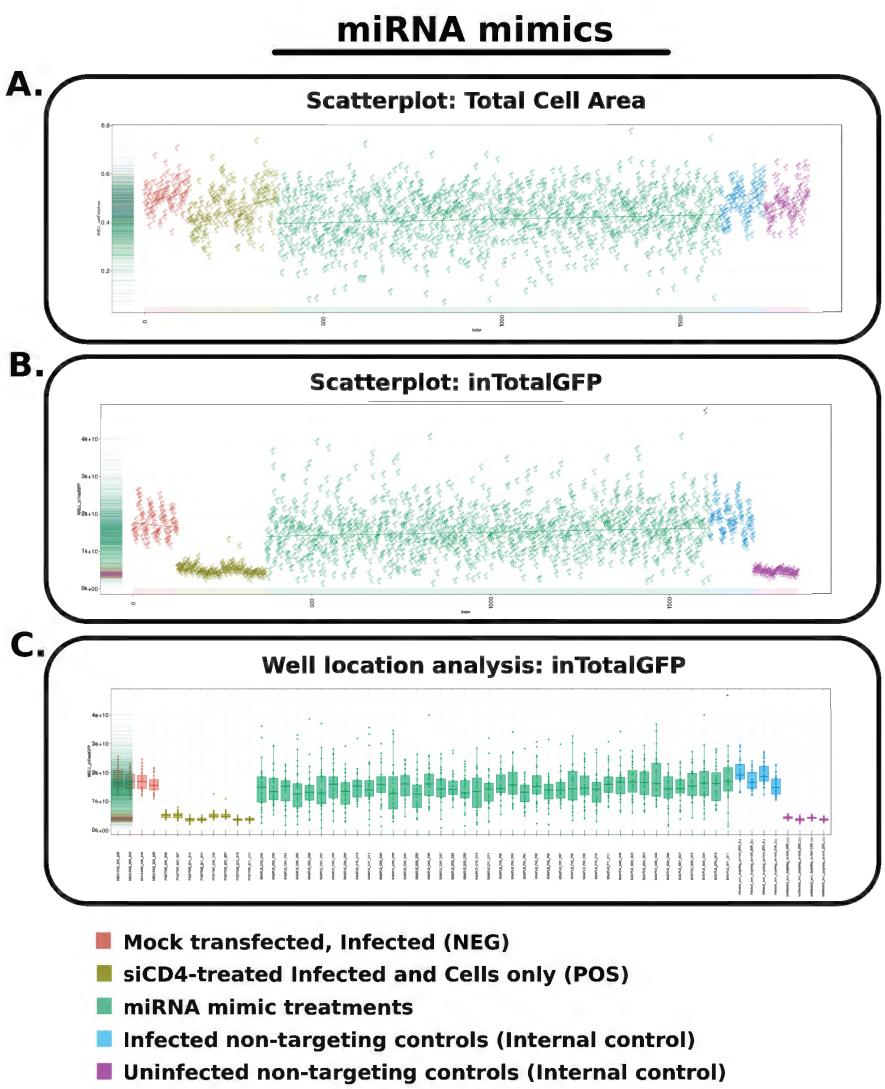

Figure 4.3 Quality control for miRNA mimic screen data.

A) Scatter plot of unprocessed 'Total Cell Area' scores for all experimental wells across two replicates. Significant variations in cell count were observed within experimental treatments (green), but not for experimental controls (red, yellow, blue, purple). **B)** Scatter plot of the unprocessed 'inTotalGFP' scores for all experimental wells (controls and treatments) across two replicates. A significant variation in GFP intensity was observed within miRNA treatments, and positive (yellow) and negative (red) controls exhibited discrete distributions which were recapitulated by infected (blue), and uninfected (purple) non-targeting miRNA controls. **C)** Visualization of frequent-hitter (Well-based) analysis by box plots revealed no directional or well specific biases for 'inTotalGFP' scores for experimental treatment wells, while control wells consistently exhibited distinct visual profiles.

4.2.1.2 Inhibitors

As with the miRNA mimic dataset, unprocessed ‘Total cell area’ scores demonstrated no clear variation between phenotypic control samples for the miRNA inhibitor dataset and this was confirmed by the recovery of negative Z’ factor values for all experimental plates. However, the miRNA inhibitor-treated samples demonstrated little to no variation, indicating a low incidence of treatment-associated effects on cell viability (Figure 4.4A). The unprocessed ‘inTotalGFP’ scores demonstrated a clear and significant variation between the positive and negative control samples as expected (Figure 4.4B) and this was confirmed by a Z’ factor range between 0.2 and 0.8, which was recovered for all experimental plates. In addition the uninfected and infected samples containing non-targeting miRNA controls exhibited similar phenotypes compared to positive and negative controls samples respectively (Figure 4.4B). miRNA inhibitor-treated samples again however displayed a poor GFP distribution range suggesting that, by in large, miRNA inhibitor treatments had no significant effects on GFP-reporter activity. Well location-based analysis also confirmed that technical errors had not significantly impacted the phenotypic readout across experimental plates (Figure 4.4C). Thus while the overall quality of the GHOST(3) miRNA inhibitor assay was acceptable, the dataset exhibited a limited phenotypic range.

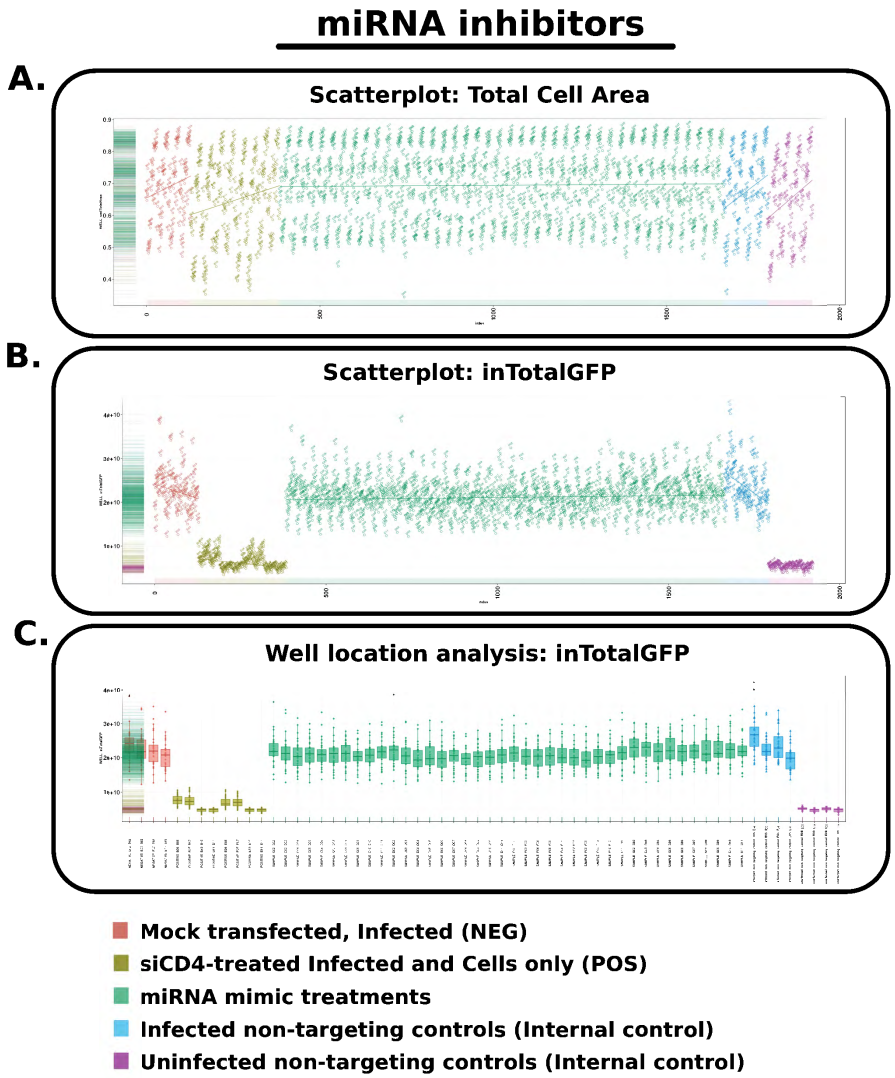

Figure 4.4 Quality control for miRNA inhibitor screen data.

A) Scatter plot of the unprocessed Total cell area scores for all experimental wells (controls and treatments) across two replicates. No significant variations were observed within experimental treatments (green) or between experimental controls (red, yellow, blue, purple). **B)** Scatter plot of the unprocessed 'inTotalGFP' scores for all experimental wells (controls and treatments) across two replicates. Significant variations in GFP intensity were observed between experimental controls (positive (yellow), negative (red), infected (blue), and uninfected (purple) non-targeting miRNA controls). **C)** Visualization of frequent-hitter analysis by box plots based on inTotalGFP revealed no directional or well specific biases for experimental treatment wells, while control wells consistently exhibited distinct visual profiles.

4.2.2 Normalisation and Feature retention

Features scores were normalized against negative control wells on a per plate basis. Normalized features trends were then evaluated through HCSR visualization tools and only certain features were retained for downstream analysis (feature reduction). Features that contributed to an accurate assessment of cell count/viability (Figure 4.5A), and features that distinguished between positive and negative control phenotypes (Figure 4.5B) were retained. In addition experimental treatment wells were confirmed to exhibit feature-specific distribution trends suggestive of a broad phenotypic range. Where applicable, specific data reduction methods were applied using PCA- or MDS-based data transformations (see *Hit Selection* in Chapter 3), and screen hits were then selected using different hit selection criteria.

Similar distribution plots were generated and evaluated for all features and these distributions contributed to the selection of features for data reduction and hit selection.

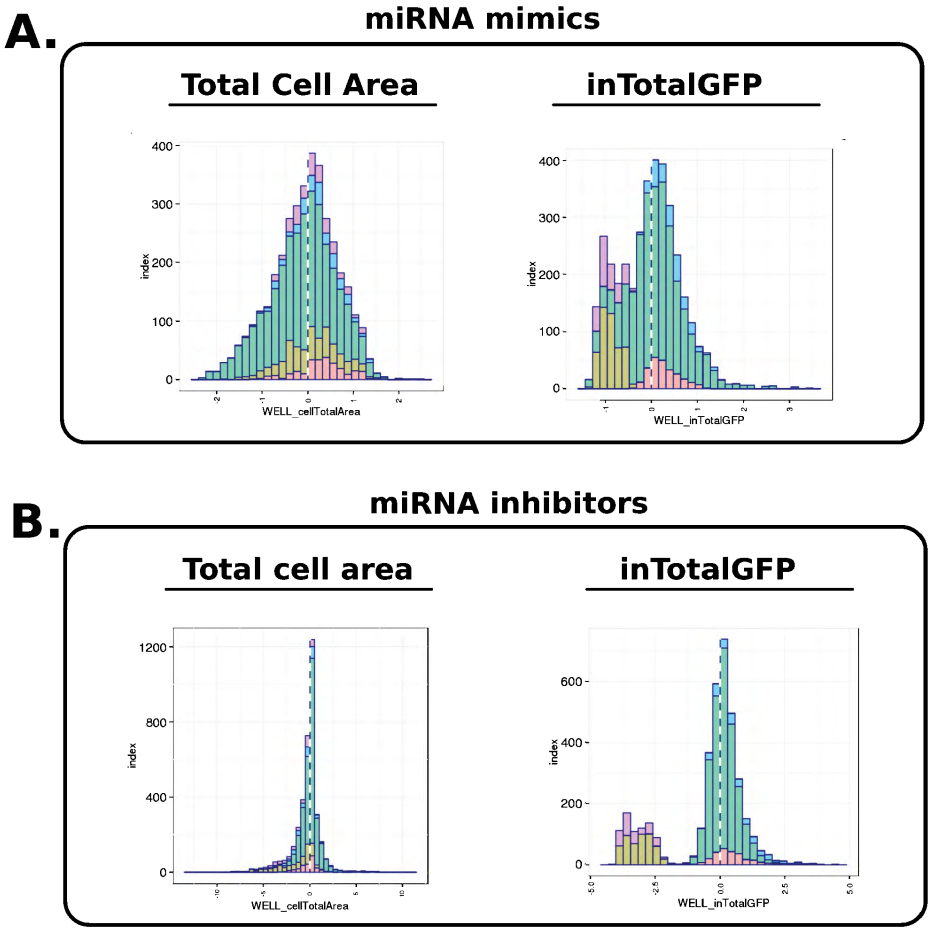

Figure 4.5 Normalised feature score distribution plots for mimic and inhibitor datasets

A) Distribution plots from mimic dataset, **Total cell area** distributions revealed a uniform distribution for all experimental treatments with no significant variations between positive (yellow) and negative control (red) samples. Additionally the majority of experimental treatments were observed to overlap with the distribution range of the experimental control samples, the **inTotalGFP** feature exhibited non-uniform and bimodal distribution patterns across all experimental treatments with clear variation between the positive (yellow) and negative (red) control samples as well as the infected (blue) and uninfected (purple) non-targeting miRNA control samples. Experimental treatments (green) samples were widely distributed across and beyond both the negative and positive control sample ranges. **B)** Distribution plots from inhibitor dataset. **Total cell area** distributions revealed a uniform distribution for all experimental treatments with no significant variations between positive (yellow) and negative control (red) samples. Additionally the majority of experimental treatments (green) overlapped with the distribution range of the experimental control samples, the **inTotalGFP** feature exhibited non-uniform and bimodal distribution patterns across all experimental treatments with clear variation between the positive (yellow) and negative (red) control samples as well as the infected (blue) and uninfected (purple) non-targeting miRNA control samples. Experimental treatments (green) samples exhibited a uniform distribution within the negative control sample range. Distribution median (Dashed vertical line)

4.3 Hit Selection

miRNA mimics and inhibitors that either enhanced or suppressed $PSG3^{BAL}$ replication within GHOST(3) cells were recovered by multiple hit selection methods (see Chapter 3, *Hit selection methods*). Briefly, where applicable data reduction by either multidimensional scaling (MDS) or principal component analysis (PCA) was utilized to generate factors which summarised the relationships between specific sets of features (Figure 4.6 A). Only factors that were descriptive of the phenotypic variation between the positive and negative control phenotypes were then applied to hit selection (Figure 4.6 B). The phenotypic distance between experimental treatments was calculated using either the positive (-STP) or negative (-DFN) controls as reference points and a phenotypic distance threshold ($p<0.1$) was used to identify putative hits (Figure 4.6 C). All miRNA mimics and inhibitors that resulted in a >60% decrease in cell viability ('Total cell area') compared to negative control wells were excluded from hit selection and GFP-related thresholds were applied to generate final hit lists. Notably, while HIV-suppressive and HIV replication -enhancing miRNA mimics were readily recovered by different hit selection methods, miRNA inhibitors that induced significant functional effects on HIV replication were not.

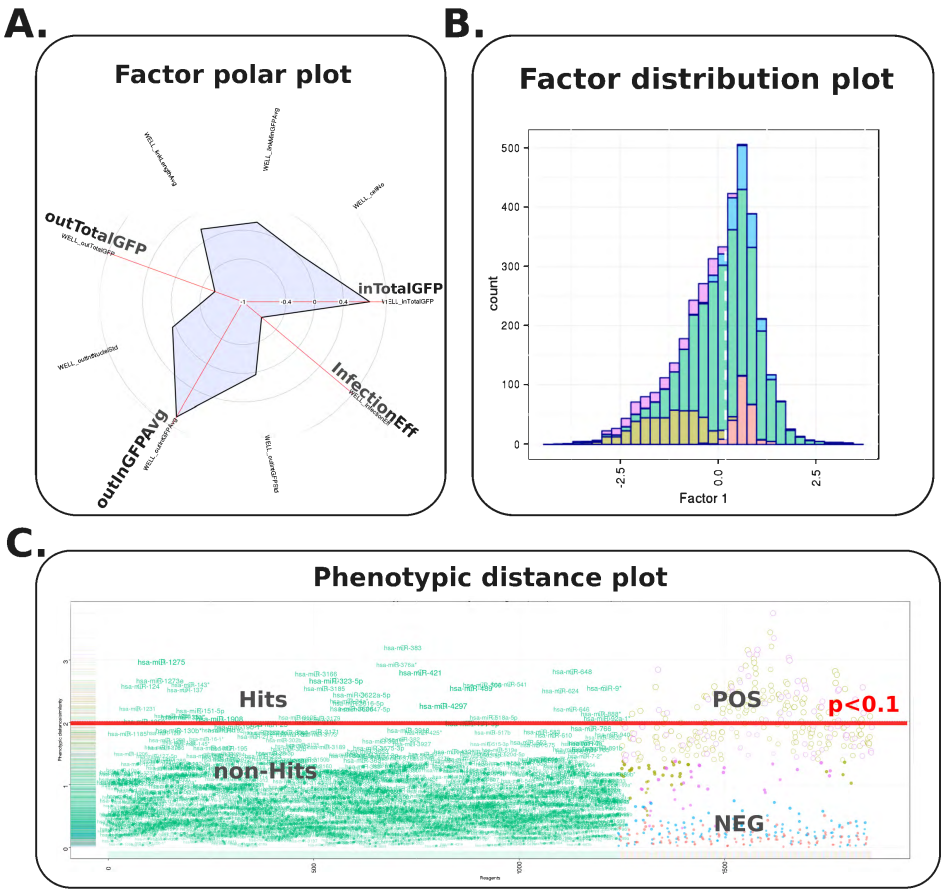

Figure 4.6 Data reduction-based hit selection

A) Polar plot summarising the correlative relationships between specific features. **B)** Data distribution plot generated for the factor present in (A), a non-uniform and bimodal distribution pattern was observed for all experimental treatments with clear variation between the positive (yellow) and negative (red) control samples as well as the infected (blue) and uninfected (purple) non-targeting miRNA control samples, Experimental treatments (green) samples were widely distributed across the negative and positive control sample ranges. **C)** Distance plot, the phenotypic distance of all experimental treatments are plotted in reference to the negative controls (NEG), experimental treatments that exhibited significant phenotypic distance from the negative controls in both replicates (average p<0.1) were classified as putative hits.

4.3.1 Suppressed HIV replication

Mimics

GFP ranking identified 46 miRNA mimics that resulted in a >55% reduction in GFP-reporter signal compared to negative control wells. The percentage of total reagents (all mimics) identified as hits (hit rate) using this approach was thus 3.7%. Two-factor PCA-DFN hit selection recovered 17 HIV-suppressive miRNA mimics (hit rate = 1.3%) that

were phenotypically distinct from negative control wells ($p<0.1$) and which also resulted in a >55% reduction in GFP-reporter signal as compared to negative control wells. PCA-STP hit selection using the same 2 factors resulted in identification of 12 miRNA mimics (hit rate = 0.96%) that were phenotypically similar ($p<0.1$) to positive control wells. None of the hits recovered by PCA-STP were recovered by PCA-DFN, and only 3 of the 12 hits recovered by PCA-STP were also recovered by GFP ranking (hsa-mir-940, hsa-mir-650 and hsa-mir-192), see Figure 4.7 below. PCA-STP thus resulted in identification of 9 unique hits. 16 of the 17 hits recovered by PCA-DFN were also recovered by GFP ranking, with hsa-mir-646 being the only unique hit identified by PCA-DFN (Figure 4.7). In contrast to PCA-DFN, 28 of the 46 hits recovered by GFP ranking were unique to that hit selection method (Figure 4.7). Only PCA-STP and GFP ranking hit lists were retained for further analysis, owing to the high number of unique hits identified by each method.

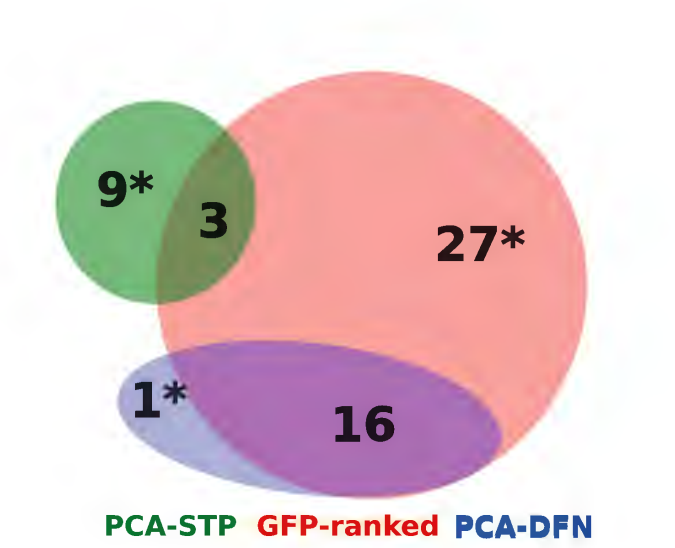

Figure 4.7 Overlap in HIV-suppressive hits recovered by different hit selection methods.

Number of miRNA mimics recovered as HIV-replication suppressing agents by 'GFP ranking', 'PCA-DFN' and 'PCA-STP' hit selection methods, * denotes number of unique hits identified by each method.

The majority of hits identified by GFP ranking were randomly validated by visual inspection (Figure 4.6). Variable but consistently significant phenotypes of suppressed HIV replication (reduced GFP expression) were observed right from top ranked hits (Figure 4.8A) down to the lowest ranked hit, hsa-mir-1231 (Figure 4.8B). Variations in cell number were also observed, and many hits exhibited lower cell numbers compared to negative controls although always within an acceptable range (>40%, Figure 4.8). These observations further validated GFP ranking as a functional hit selection method within the GHOST(3)-PSG3^{BAL} assay.

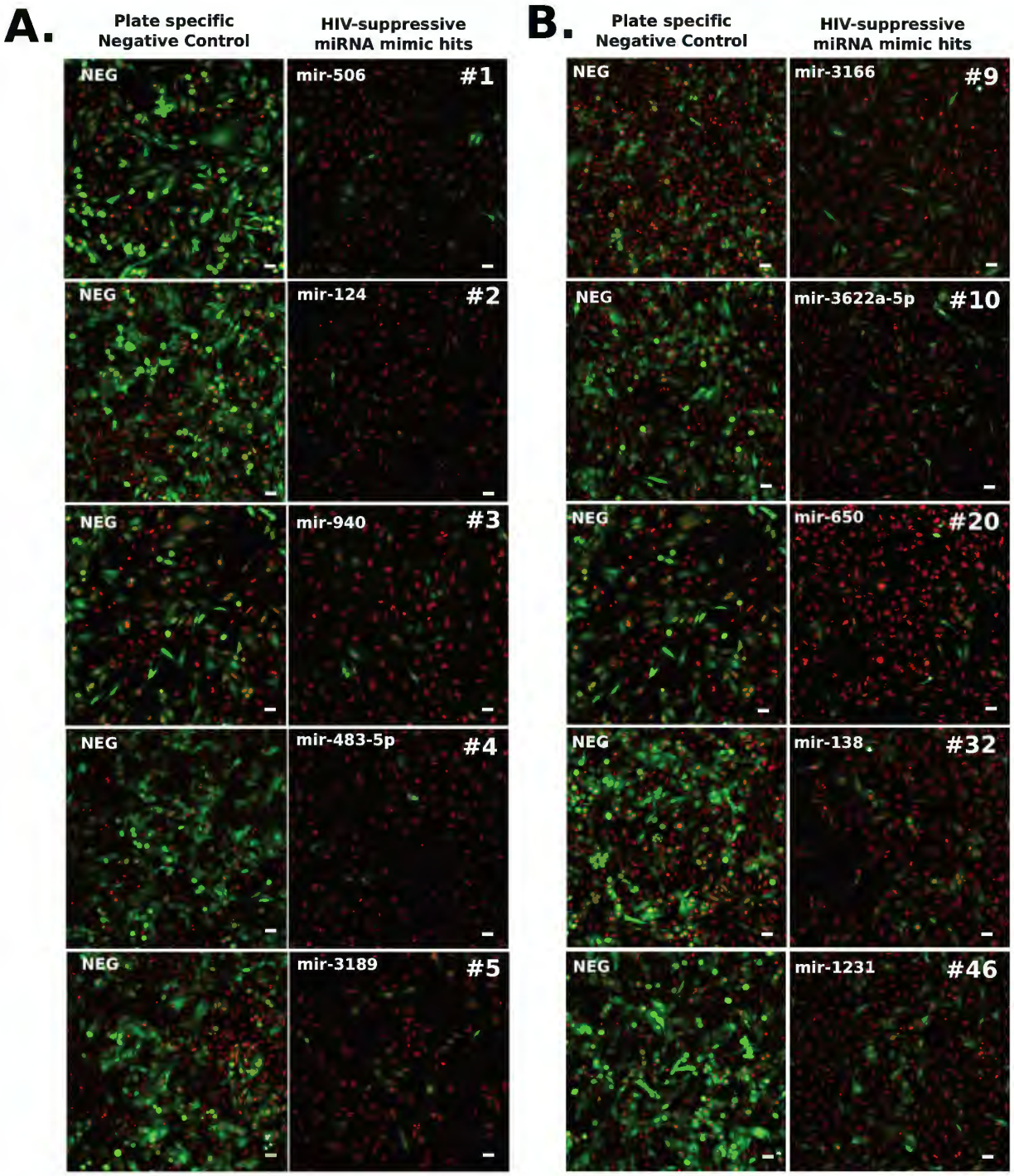

Figure 4.8 Visual inspection of GFP ranking-derived miRNA mimic hits for suppressed HIV replication

A) Top 5 miRNA mimic hits identified by GFP ranking hit selection as compared to negative control images (NEG) acquired from the same plate. **B)** Lower ranked miRNA mimic hits identified by GFP ranking as compared to NEG. Images represent unprocessed composite images acquired in the 405 and 488 channels. GFP-reporter signal (green), nuclei stained with Hoechst (red), scale bars = 20 μm.

All hits recovered by PCA-STP hit selection were evaluated by visual inspection (Figure A4.1, Appendix IV). Two hits were excluded from further analyses following visual inspection as they did they did not adequately represent a suppressed HIV phenotype (Figure A4.1, Appendix IV). In general, hits identified by PCA-STP showed suppressed HIV replication albeit at a more subdued level compared to those identified by GFP ranking. Seven hits obtained from PCA-STP and all 46 hits obtained by GFP ranking were retained for further analysis. Taken together, HCS therefore identified 53 miRNA mimics, that when exogenously expressed, resulted in suppressed HIV replication (Table A4.1, Appendix IV).

Inhibitors

Quality control data initially suggested a potentially weak functional effect for miRNA inhibitor treatments and this was confirmed by multiple hit selection methods including PCA-DFN, GFP ranking, MDS-DFN, PCA-STP and sample-orientated variations of these methods (e.g PCA based on phenotypic distance from sample medians). Even when selection criteria were significantly relaxed (e.g. variations in GFP reporter activity >25% relative to sample medians or negative controls), few significant hits were identified (<5). Furthermore the majority of hits identified by these methods did not meet acceptable visual inspection criteria. In total, 4 miRNA inhibitors were identified that resulted in either reduced GFP reporter activity or a reduction in the percentage of infected cells relative to negative control wells (Figure 4.9). No rankings were provided for these hits as they were not identified by a single selection method, and these miRNAs were not included in downstream pathway analysis.

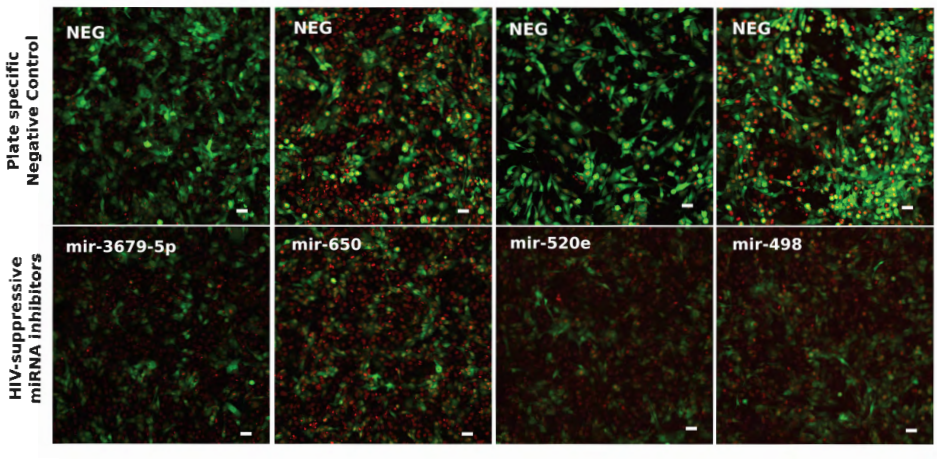

Figure 4.9 Visual profiles of miRNA inhibitor hits identified by multiple hit selection methods

Consistent phenotypes related to decreased GFP-reporter activation and(or) reduced numbers of infected cell were observed for this hit class. Images represent unprocessed composite images

acquired in the 405 and 488 channels. GFP-reporter signal (green), nuclei stained with Hoechst (red), scale bars = 20 µm.

4.3.2 Enhanced HIV replication

Having identified miRNA mimics that suppressed HIV replication, similar methods were then used to identify mimics that enhanced HIV replication. MDS-DFN identified 6 miRNA mimics (hit rate = 0.48%) that were phenotypically distinct from negative control wells ($p < 0.1$), and which resulted in >70% increase in GFP reporter signal (mir-378*, mir-141*, mir-2277-5p, mir-3679-3p, mir-4318 and mir-200*). PCA-DFN recovered 4 miRNA mimics (hit rate = 0.32%), while GFP ranking classified 28 miRNA mimics (hit rate = 2.2%), including all of the hits identified by both other methods. Visual inspection of these hits revealed three consistent phenotypic trends: enhanced infection rates (e.g. mir-2277-5p), enhanced GFP-reporter activity (mir-378*) or both (mir-200b*). In contrast to the reduced cell numbers that were observed for many of the HIV suppressive hits, HIV enhancing miRNA mimics did not exhibit any noticeable effects on cell viability (Figure 4.10). However, a trend of aberrant cell morphology (shape or size) was noted for many HIV enhancing hits, such as mir-891b (rank #9) and mir-34c-3p (rank #28). Overall, 28 miRNA mimics identified by GFP ranking were thus retained for further investigation and pathway analysis (Table A4.2, Appendix IV). Notably, none of the miRNA inhibitor treatments were recovered as HIV-replication enhancing hits.

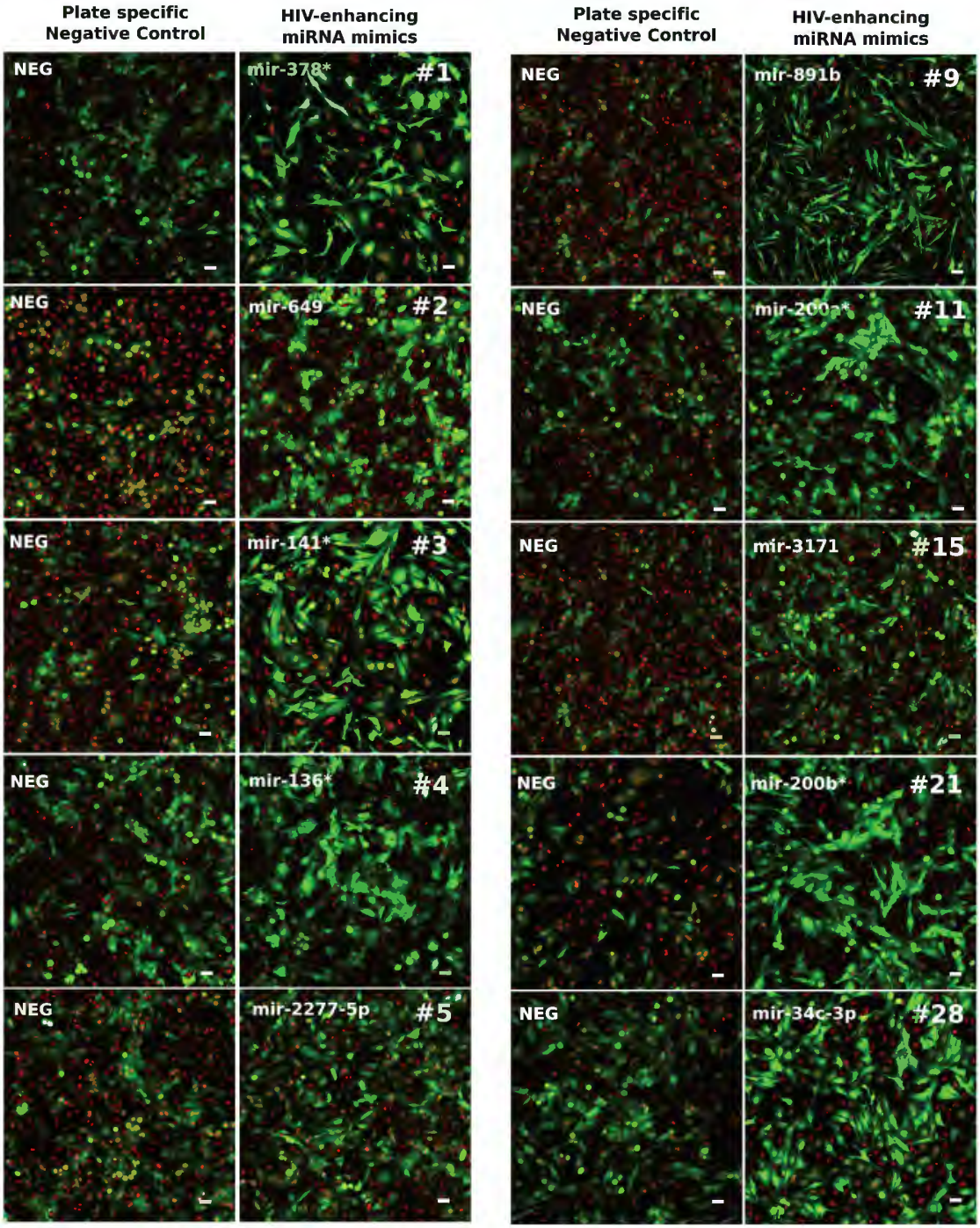

Figure 4.10 Visual profiles of HIV replication-enhancing miRNA mimic hits identified by GFP ranking hit selection.

Consistent phenotypes related to increased GFP-reporter activation and(or) increased numbers of infected cell were observed for the miRNA mimics identified by this method. Images represent unprocessed composite images acquired in the 405 and 488 channels. GFP-reporter signal (green), Nuclei stained with Hoechst (red), scale bars = 20 µm.

4.4 Hit triage

High content image analysis and data mining recovered 53 miRNA mimics and 4 miRNA inhibitors that suppressed HIV replication. Similarly, 27 miRNA mimics were found that enhance HIV replication. Together, this gave a total of 84 host miRNAs that are functionally relevant for HIV replication, thereby expanding the current repertoire of HIV-modulating miRNAs by more than 2 fold (Figure 4.11).

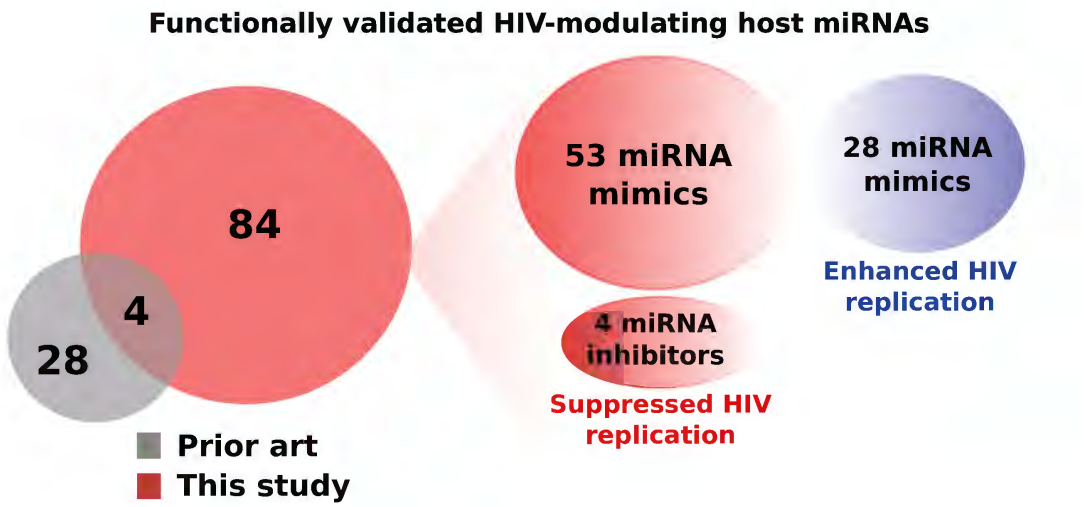

Figure 4.11 Summary of contribution to current knowledge on HIV replication modulating human miRNAs

4.4.1 miRNA hits and prior art

Four of the miRNA hits described here (hsa-miR-124-3p, hsa-miR-138-5p, hsa-miR-378a-5p, hsa-miR-19b-2-5p) were previously demonstrated to functionally modulate HIV replication (reviewed by Barichievy, 2015). Specifically, miR-138 was predicted to target multiple sites in the HIV genome corresponding to Env, Pol and Tat mRNAs (Houzet, 2012). miR-378 was predicted to target Vpu (Hariharan, 2005), miR-19b was predicted to target the Tat-associated PCAF/p300 complex (Triboulet, 2007), and miR-124-3p (previously miR-124a) was described to increase HIV replication through suppression of TASK1 (Farberov, 2015). While the HIV suppressive phenotype recovered for miR-138 supported previous findings (Houzet, 2012), the remaining phenotypes did not. This suggests that alternative mechanisms of miRNA action may be modulating HIV replication, within the confines of the assays described in this study. Notably, only 2 of the recovered hits (miR-138 and miR-378) were described to directly target sites on the HIV genome (Hariharan, 2005; Houzet, 2012). Furthermore, miRDB-based (mirdb.org) miRNA binding analysis revealed that none of the recovered miRNA were predicted to

interact with the humanised GFP variant (GenBank U50963.1) expressed by GHOST(3) cells. These observations would suggest that the majority of enhanced or suppressed HIV replication phenotypes recovered by HCS were a result of miRNA-mediated effects on HIV replication and not as a result of miRNA-mediated modulation of GFP mRNA.

Chemokine C-C motif ligand 4 (CCL4/MIP1ß), a well characterized antagonist of CCR5 and HIV replication (Guan, 2002), is also an experimentally validated target of miR-378-5p (Skalsky, 2012). Thus miRNA-378-5p suppression of CCL4 may account for the enhanced HIV replication phenotype in this study. Likewise, a number of experimentally validated targets of miR-19b-2-5p are enriched within the TGFß and cell cycle pathways, and current literature have posited these to be highly relevant to HIV replication, thus suggesting alternative by which miR-19b-2-5p may influence HIV replication (Table A4.4, Appendix IV). The HIV replication enhancing function of miR-124-3p was previously related to its' ability to downregulate TASK1, a viral restriction factor (VRF) which disrupts Vpu-mediated virion release (Farberov, 2015). TarBase analysis of miR-124-3p targets revealed a low association score for TASK1 (KCNK3), with only microarray expression data to support the miR-124/TASK1 association. In contrast, one of the highest scored targets for miR-124-3p, confirmed by immunoprecipitation, was the TAR RNA binding protein (TRBP1). TRBP1 facilitates HIV replication through inhibition of the antiviral activity of PKR (Sanghvi, 2011), thus supporting the HIV-suppressive phenotype recovered for this miRNA in the current study. In addition, a number of other host miRNAs previously associated with HIV replication were either identified as HIV-suppressive hits but excluded due to toxicity (miR-15a and miR-92a-1), or were recovered as HIV-enhancing hits using more relaxed selection criteria (miR-125b, miR-150, miR-204, miR-382). The recovery described here of a number of host miRNAs also previously shown to modulate HIV replication validates the robustness and fidelity of this study, and provides confidence that the novel host miRNA-HIV interactions may be similarly robust.

A poor concordance was observed between miRNA hits recovered by HCS and miRNAs previously reported to be differentially expressed following HIV infection (summarised in Hayes, 2011). However, this was expected because i) there are cell type-specific miRNA expression patterns noted by many independent expression-based studies (see Chapter 1), and ii) differential expression of a miRNA is not necessarily indicative of its functional relevance within a given biological model (Salmena, 2011). Furthermore the HCS hit recovery model utilised in this study did not specifically exclude miRNAs based on tissue or cell-type expression patterns in order to characterise all host miRNAs with the potential to modulate HIV replication, not simply those expressed in HIV susceptible cell lines (e.g T lymphocytes, macrophages). With that in mind, it was nonetheless surprising that none of the 19 host miRNAs which regulate CD4 or the 15 host miRNAs which target CCR5 (as described using Tarbase v7.0) were recovered as HIV-suppressive hits in this study. This suggests that the level of CD4/CCR5-specific post-transcriptional repression mediated by each of these miRNAs is not sufficient to functionally inhibit HIV entry. This is plausible given that, i) GHOST(3) cells have been engineered to express

elevated levels of both CD4 and CCR5 receptors, and ii) host miRNAs have been described to target on average ~ 300 different host genes.

Interestingly, a number of miRNA hits identified in this study were correlated with other models of viral infection, including Influenza virus and HCV. Specifically, miR-491 and miR-654 suppress Influenza virus replication in MDCK cells (Liu, 2010), and both of these miRNAs were recovered as HIV-suppressive hits by HCS (Table A4.1, Appendix IV). In addition, miR-491 has been shown to suppress HCV replication in cultured hepatoma cells, in a PI3K-dependent manner (Ishida, 2011). Ectopic expression of a miR-34c-3p mimic enhanced Influenza virus replication in cultured cells (Bakre, 2013), and an enhanced viral replication phenotype was also recovered for HIV in this study. miR-141, which was recovered as an HIV replication-enhancing hit, is upregulated by Influenza infection and associated with viral-mediated regulation of TFGß signalling (Lam, 2013). This same miRNA is also induced by enterovirus infection and is required for viral propagation through the inhibition of host translation (Ho, 2011). In contrast to the reported attenuation of Influenza replication by miR-136 (Zhao, 2015), the current HCS recovered miR-136 exclusively in association with enhanced HIV replication (Table A4.2, Appendix IV). The HIV suppressive hit, miR-124, was described to be epigenetically silenced by HCV infection (Zeng, 2012), while the HIV suppressive hit, miR-138, was found to regulate CDK13, a host factor essential for Influenza virus replication (Bakre, 2013). miR-192 was recovered as an HIV-suppressive hit which has also been described as a tumor suppressor that negatively regulates ZEB2 and nucleotide excision repair (NER) processes in response to P53 induction (Kim, 2011; Xie, 2011). Suppression of NER processes has been linked to carcinogenic viruses such HTLV-I and HCV but a direct role for miR-192 in viral infection has yet to be elucidated (Xie, 2011). Additionally miR-192 has been described to regulate cycle progression, promoting P53-dependent G_1 and G_2 cell cycle arrest (Bo, 2008; Georges, 2008). The results of this study therefore represent the first account of a functional role for miR-192 in the modulation of HIV replication. These observations further bolster confidence in the novel findings of this study, and suggests that a specific subset of host miRNAs may exhibit pan-viral modulating activity although this warrants further investigation.

4.4.2 miR-200 and miR-34 families and HIV

Strikingly, 3 of the 5 members from the miR-200 family, namely hsa-miR-141-5p, hsa-miR-200a-5p and hsa-miR-200b-5p, were recovered as hits for the enhanced viral replication phenotype, while a fourth member, hsa-miR-200c, was marginally excluded based on hit selection criteria. Analysis of their sequences revealed a high degree of homology (90%) between miR-200a-5p, miR-200b-5p and miR-141-5p but not miR-200c-5p (Figure 4.12A), and mirPath analysis revealed 8 genes that were regulated by all three miRNAs (Figure 4.12B). STITCH 4.0 protein-protein interaction analysis revealed a significant ($p<0.05$) KEGG enrichment for both P53 and cell cycle associated factors for these genes (Figure 4.12C), and gene ontology (GO) analysis revealed a

significant ($p<0.05$) correlation with 'enzyme linked receptor protein signaling pathway' and 'regulation of DNA replication'. This was unsurprising given the previous association of miR-200 family members and P53 (Kim, 2011).

The miR-200 family consists of two separate polycistronic pri-miRNA transcripts, miR-200a/200b/429 and miR-141/200c, which regulate epithelial to mesenchymal transition (EMT) and tumour metastasis by targeting the transcription factors ZEB1 and ZEB2(reviewed by Mongroo, 2010). As mentioned, the miR-200 family have also been implicated as P53-regulated miRNAs (Kim, 2011) that negatively regulate WNT signalling leading to EGFR-directed anti-cancer therapy resistance(Mongroo, 2010). While miRNAs of the miR-200 family were previously described to be downregulated in murine models of HIV-associated nephropathy (Cheng, 2013), there has until now been no functional data supporting a direct relationship between the miR-200 family and HIV replication. The results of this study therefore posit a novel functional role for this miRNA family in HIV replication, potentially through P53 signalling, cell cycle regulation and(or) ZEB1/2 (Kim, 2011; Figure 4.12).

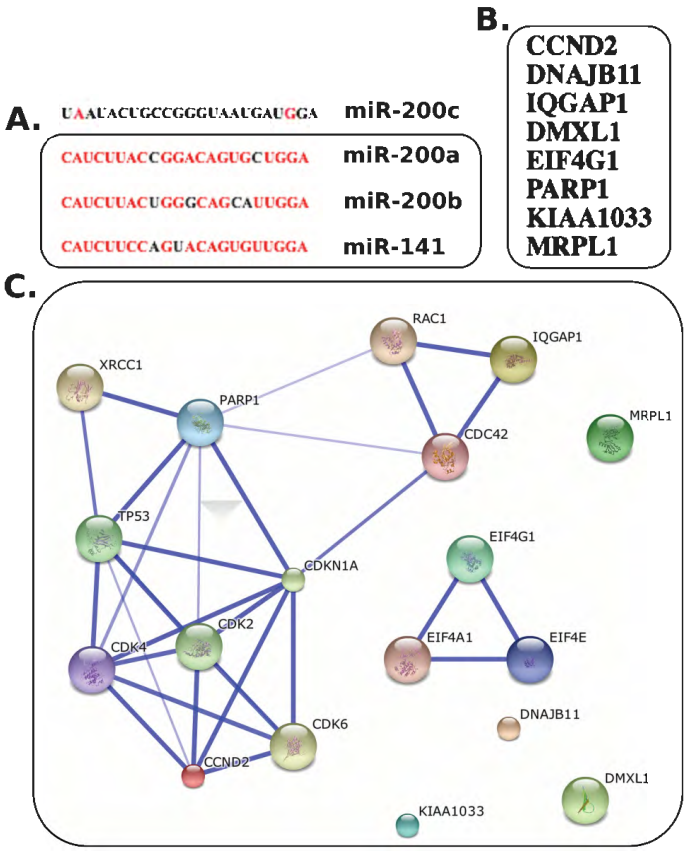

Figure 4.12 miR-200 family associated with enhanced HIV replication.

A) Alignment of miR-200a-5p, miR-200b-5p, miR-141-5p and miR-200c-5p sequences with mismatches shown in black. **B)** Host factors regulated by miR-200a-5p, miR-200b-5p and miR-

141-5p. **C)** Protein interaction map for common gene targets of miR-200a-5p, miR-200b-5p and miR-141-5p.

The miR-34 family of miRNAs (miR-34a/b/c) have been well characterised as tumour suppressors that are direct targets of P53 transcriptional activity, and which regulate a myriad of host factors to suppress cellular proliferation and induce apoptosis in response to DNA damage and other genotoxic stressors (reviewed by Hermeking, 2010). miR-34a-3p was recovered as an HIV suppressive hit by HCS, while miR-34c-3p was recovered as an HIV replication enhancing hit. The molecular mechanisms associated with miR-34c-3p function have not been completely elucidated but it may act in part through suppression of eIF4E (Liu, 2015) and modulation of Myc (reviewed by Cannell, 2010). miR-34a-3p modulates macrophage activation, TGFß-mediated apoptotic signals (Guennewig, 2013), and also negatively regulates XIAP, ß-catenin and the negative regulator of ß-catenin, AXIN2 (Tarbase v7.0). In addition, mir-34a-3p has been implicated as a critical mediator of the P53/P63-OCT4 axis associated with human cell transformation (Ng, 2014). While 'miR-34a' has been described to be induced by Tat and promote LTR activation through suppression of SIRT1 (Zhang, 2012), this has been associated with miR-34a-5p and not the -3p arm of the miR-34a precursor (Guennewig, 2013). Likewise, no functional association between miR-34c-3p and HIV replication has been described in the current literature, although ectopic expression miR-34c-3p was found to significantly enhance Influenza virus replication, potentially through upregulation of Polo-Like kinase 1 (PLK; Bakre, 2013). The results of this study represent the first account of experimental evidence establishing a functional role for miR-34a-3p and miR-34c-3p in the modulation of HIV replication.

4.4.3 Top ranked hits

miR-506 was the top ranked hit by GFP expression for suppressed HIV replication (Figure 4.8) and miRpath analysis revealed 89 experimentally validated targets for this miRNA. In addition miR-506 was shown to be downregulated in chronically infected PBMCs, although a direct functional association between HIV replication and miR-506 was not described (Hayes, 2011). Protein-protein interaction analysis of the experimentally validated targets of miR-506 revealed a significant enrichment for Erbb (EGFR)-mediated signalling (Figure 4.13) and this was confirmed by KEGG analysis ($p>0.05$). Of interest, the second highest ranked HIV-suppressive hit, miR-124, was previously also identified as a critical regulator of EGFR-mediated control of cell cycle (Uhlmann, 2012).

The top ranked hit recovered for enhanced HIV replication was miR-378-5p (Figure 4.10), for which mirPath analysis revealed 441 experimentally validated targets. Protein interaction and subsequent KEGG analysis revealed a significant ($p<0.05$) enrichment for factors associated with RNA transport and endocytosis.

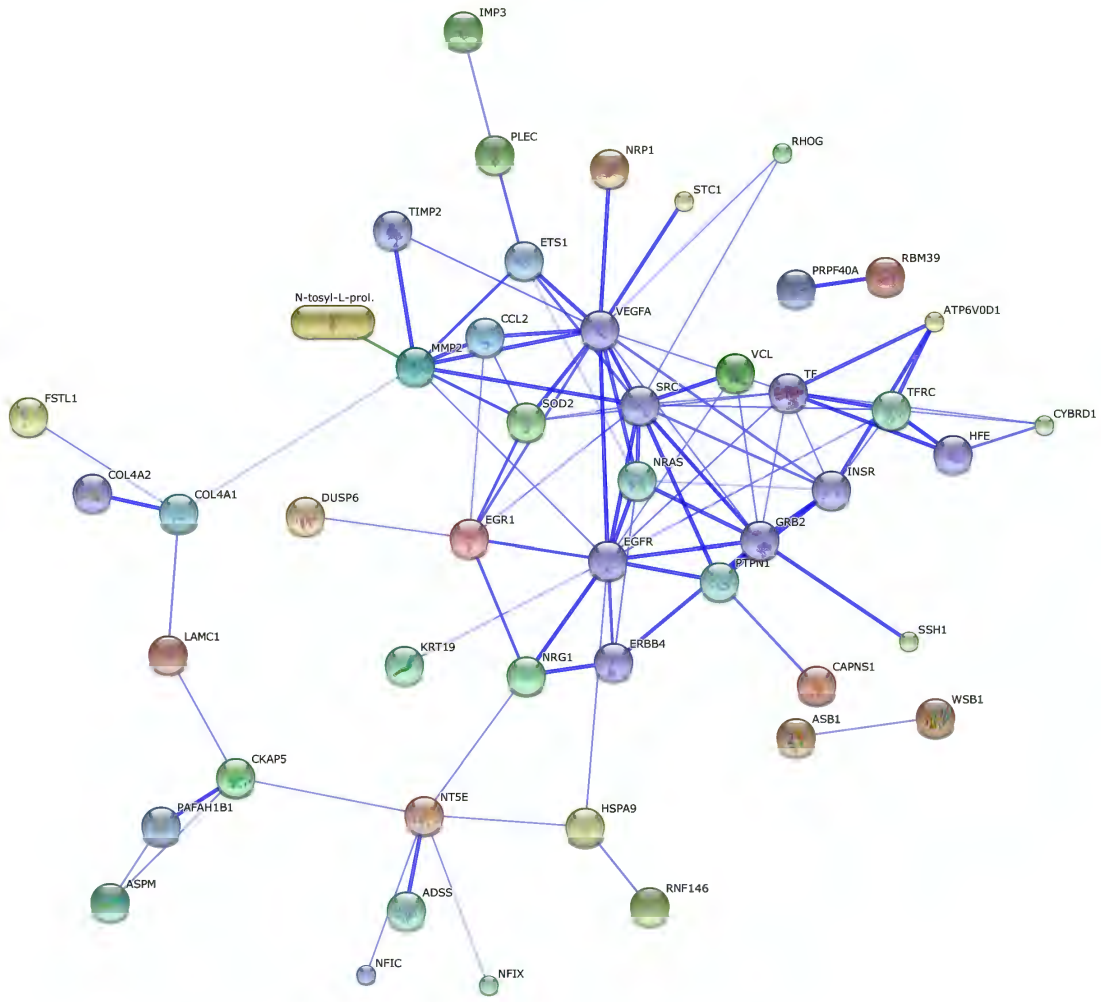

Figure 4.13 Protein interaction network for miR-506 and its associated targets

Protein interactions were predicted using STITCH 4.0 and derived from various sources including, genomic context, high throughput experiments, and conserved co-expression. Thickness of lines indicates the strength of the predicted interaction.

4.5 Pathways analysis

Given the relatively large size of the recovered hit pool (~90 reagents), miRNA-target prediction and pathway analyses were used to ratify the data and identify functional trends. mirPath, a web-based miRNA pathway analysis tool, was utilized to identify specific functional pathways enriched within each of the hit classes. miRNA names were based on miRBASE v.20 nomenclature and those miRNA sequences that were excluded from the miRBASE v.20 database were also excluded from pathway analysis. miRPath analysis was based on experimentally validated miRNA-target interactions listed in Tarbase v.7.0, or using microT-CDS v.5.0 target prediction when experimentally validated targets were not available (Vlachos, 2015).

Fifty-two of the 53 miRNAs (mimics) associated with suppressed viral replication were used in pathway analysis and experimentally validated targets were available for 34 of these. The total number of experimentally validated targets per miRNA ranged from between 25 genes (for mir-483-5p) to 1962 genes (for mir-124, now mir-124-3p), with an average of ~300 genes per miRNA. Likewise, twenty-seven of the 28 miRNAs (mimics) associated with enhanced viral replication were retained during pathway analysis. Experimentally validated targets were available for 22 of these, with target number per miRNA ranging from 3 for mir-3679-3p to 1769 for mir-22-3p. Pathway analysis yielded 62 functional pathways that significantly ($p<0.05$) correlated with miRNA target genes recovered for the suppressed HIV replication phenotype (Table A4.3, Appendix IV) and 48 functional pathways that significantly ($p<0.05$) correlated with the enhanced HIV replication phenotype (Table A4.4, Appendix IV). These pathways were ranked according to the number of miRNAs associated with each pathway and the top 30 pathways recovered for the suppressed (Figure 4.14) and the enhanced (Figure 4.15) HIV replication phenotypes are presented below.

‘Proteoglycans in cancer’ was revealed as the highest ranked pathway associated with the suppressed HIV replication phenotype (48 miRNAs targeting 138 genes). ‘Pathways in cancer’ was ranked second (48 miRNAs targeting 252 genes) and ‘Focal Adhesion’ third, with 48 miRNAs targeting 138 genes (Figure 4.14). A large overlap (~90%) was observed for the miRNAs associated with each of these pathways, and 40-56% overlap in the genes associated with each pathway was also noted.

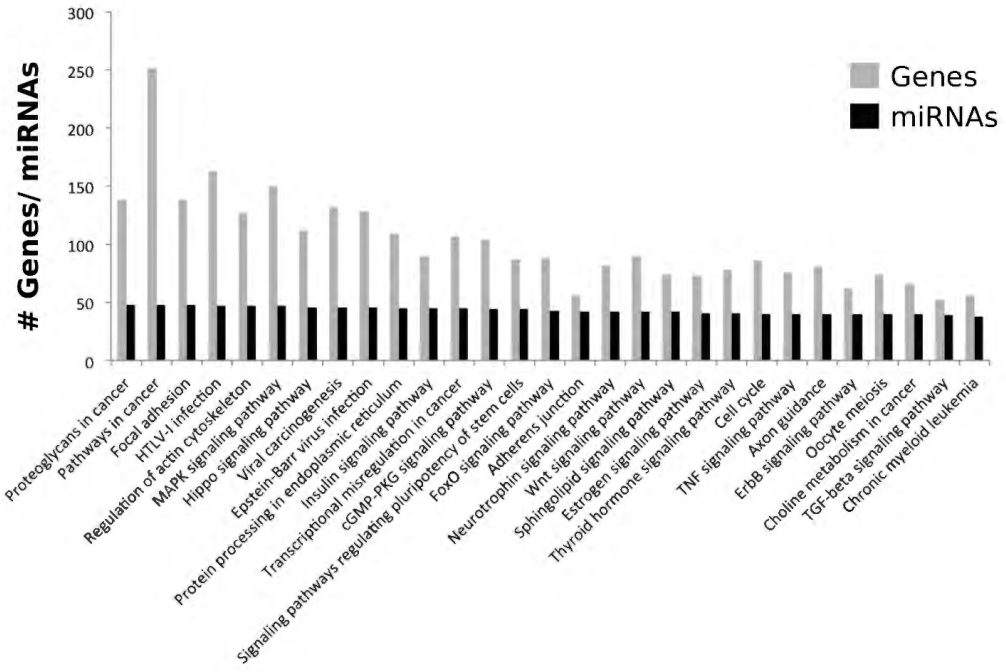

Figure 4.14 Top 30 functional pathways associated with suppressed HIV replication.

Pathways were identified by mirPath v.3.0 and ranked according to the number of miRNA hits associated with each pathway.

The PI3K signalling pathway was the highest ranked pathway associated the enhanced HIV replication phenotype with 26 miRNAs targeting 124 genes (Figure 4.15). ‘Proteoglycans in cancer’ was ranked second (24 miRNAs targeting 96 genes) and ‘Focal Adhesion’ third, with 24 miRNAs targeting 96 genes (Figure 4.15).

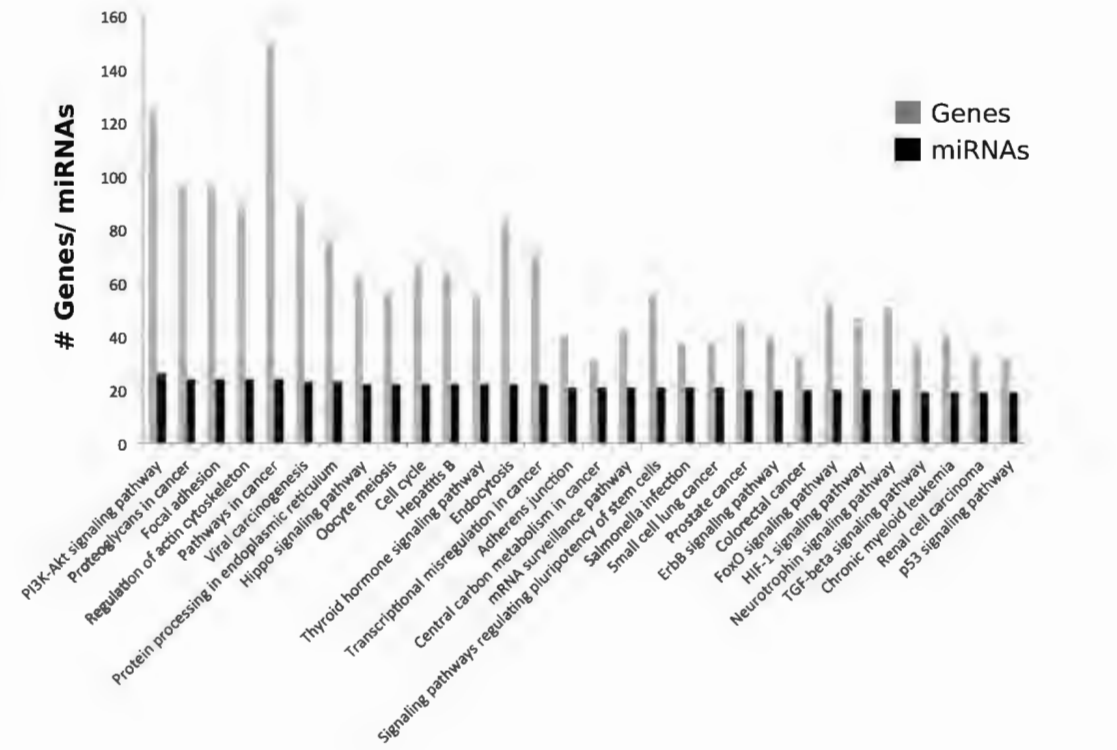

Figure 4.15 Top 30 functional pathways associated with enhanced HIV replication.

Pathways were identified by mirPath v.3.0 and ranked according to the number of miRNA hits associated with each pathway.

4.5.1 Pathways associated with both enhanced and suppressed HIV replication

Interestingly, pathway analysis recovered 38 functional pathways which were enriched within both ‘suppressed’ and ‘enhanced’ HIV replication phenotypes (Table 4.1). These findings posit the cellular networks associated with these pathways as central mediators of HIV-host interactions. Unsurprisingly a number of these pathways have well characterized functional relevance to HIV replication and viral infection in general including the Erbb, TGFß, P53 and WNT signalling pathways (Brass, 2008; Konig, 2008; Friedrich, 2011). Contrastingly, mirPath analysis also recovered pathways which have not been well characterised with regards to HIV replication, including the hippo signalling pathway, thus placing these as potentially novel mediators of HIV-host interactions. A comparison of the functional targets identified for suppressed and enhanced HIV replication within a single pathway also provided an ideal opportunity to recover specific miRNA targets preferentially associated with each HIV replication phenotype, and this comparison was completed for the viral carcinogenesis, cell cycle, regulation of actin cytoskeleton and hippo signalling pathways.

Table 4.1 Functional pathways associated with both enhanced and suppressed HIV replication

Functional pathways recovered by mirPath*	
Adherens junction	Neurotrophin signaling pathway
Bacterial invasion of epithelial cells	Oocyte meiosis
Bladder cancer	p53 signaling pathway
Cell cycle	Pancreatic cancer
Central carbon metabolism in cancer	Pathways in cancer
Chronic myeloid leukemia	Prion diseases
Colorectal cancer	Prostate cancer
ECM-receptor interaction	Protein processing in endoplasmic reticulum
Endometrial cancer	Proteoglycans in cancer
Epstein-Barr virus infection	Regulation of actin cytoskeleton
ErbB signaling pathway	Renal cell carcinoma
Fatty acid biosynthesis	Shigellosis
Focal adhesion	Signaling pathways regulating pluripotency of stem cells
FoxO signaling pathway	Small cell lung cancer
Glioma	TGF-beta signaling pathway
Hepatitis B	Thyroid hormone signaling pathway
Hippo signaling pathway	Transcriptional misregulation in cancer
Insulin signaling pathway	Viral carcinogenesis
Melanoma	Wnt signaling pathway

*pathways are listed alphabetically

Viral carcinogenesis

Pathway analysis recovered 46 HIV-suppressive miRNAs (Table A4.5, Appendix IV) and 23 HIV replication enhancing miRNAs (Table A4.6, Appendix IV) which regulate host factors enriched within the viral carcinogenesis pathway. To date, this represents the most comprehensive list of host miRNAs that functionally modulate HIV replication, potentially through regulation of host factors classically associated with both viral replication and carcinogenesis (Wang, 2015). Carcinogenesis refers to the process whereby a normal cell is systematically re-programmed at the genetic, epigenetic and cellular level by specific mutations or environmental factors, ultimately resulting in uncontrolled cell division and escape from apoptosis (Hanahan, 2011). In addition, certain viruses can also transform host cells into a cancerous state and this process is known as viral carcinogenesis (Butel, 2000; Chen, 2014). A number of carcinogenic human viruses have been described including HCV, HBV, Epstein-Barr virus (EBV), Human papilloma virus (HPV), HTLV-I and Kaposi's sarcoma-associated herpesvirus (KSHV). Furthermore, viral infections are estimated to account for 15-20% of all cancers globally (Bregnard, 2014). HIV has traditionally been indirectly associated with cancer phenotypes as HIV-mediated depletion of the immune response results in a higher

susceptibility to carcinogenic pathogens like KSHV and HPV (reviewed by da Silva, 2011). However, it has also been suggested that HIV infection itself may indeed be oncogenic (Nakai-Murakami, 2007; reviewed by Pierangeli, 2015). mirPath analysis revealed a strong concordance between host factors enriched within HCV, HBV, EBV, HPV, HTLV-I and KSHV infection and the miRNA hits recovered by HCS (Figure A4.2, Appendix IV). The high degree of overlap in functional targets between such 'true' oncogenic viruses and HIV supports the 'viral cooperation' model of tumorigenesis (reviewed by da Silva, 2011), and is also indicative of the highly conserved mechanisms exploited by various human viruses (Wang, 2015).

Indeed, the majority of the protein targets recovered for enhanced HIV replication hits were also associated with suppressed viral replication hits (Figure A4.2). In addition, 18 host proteins were exclusively associated with enhanced viral replication hits (Table A4.7, Appendix IV) including JAK1 and STAT5B, while 59 host factors were exclusively associated with suppressed HIV replication hits (Table A4.8, Appendix IV) including Protein Kinase-R (PKR), BAD, Retinoblastoma protein (Rb), IκBα, NFKß, Lyn and PCAF. All of these proteins have been previously associated with HIV replication and therefore represent strong functional targets related to miRNA-mediated modulation of HIV replication. PKR is activated by P53 following HIV infection and directly interacts with Tat, thereby suppressing Tat-mediated transcription (Clerzius, 2011; Yoon, 2015). HIV Nef suppresses the proapoptotic activity of BAD via p21 activated kinase (PAK) in a PI3K-dependent manner (Wolf, 2001), while the induction of Rb (RB1) in HIV-infected monocytes has been associated with resistance to apoptosis and enhanced cell survival in response to immune activation (Gekonge, 2012). The SRC kinase Lyn, facilitates CCR5-mediated activation of ERK and TNFα production in macrophages, in response to HIV gp120 (Tomkowicz, 2006). P300/CBP-associated factor (PCAF) is a well characterised coactivator of Tat transcriptional activity (Zeng, 2005) that is also a documented target for miRNA-mediated modulation of HIV replication (Triboulet, 2007). IκBα and NFKß signalling are linked to viral persistence and resistance to apoptosis in HIV-infected monocytes and macrophages (reviewed by Le Douce, 2010). JAK1 was recovered by genome-wide siRNA screening as a putative HIV-HDF (Zhou, 2008) and STAT5 protein is downregulated in response to HIV infection (Pericle, 1998). A number of HLA variants (HLA-B, HLA-C, HLA-F) were also identified within the suppressed viral replication hits, and miRNA-mediated regulation of HLA-C in particular has been associated with the natural restriction of HIV replication (Kulkarni, 2011). Finally, HDACs have well described effects on HIV latency and transcriptional activation of the HIV LTR (reviewed by Shirakawa, 2013).

Cell Cycle

Pathways analysis recovered 46 HIV-suppressive miRNA hits (Table A4.9, Appendix IV) and 22 HIV replication enhancing miRNA hits (Table A4.10, Appendix IV) associated with regulation of cell cycle. Similarly to the trend previously observed for viral

carcinogenesis, approximately 90% of proteins associated with *enhanced* HIV replication hits were also associated with *suppressed* viral replication hits, and only 7 host proteins were exclusively associated with enhanced viral replication hits (Table A4.11, Appendix IV). In contrast, 27 host factors were exclusively associated with suppressed HIV replication hits (Table A4.12, Appendix IV).

In support of previous HIV-related findings (Brass, 2008; reviewed by Friedrich, 2011; Romani, 2015) P53 and its associated factors (HDM2, Retinoblastoma protein (Rb), various CDKs (CDK1,2 4,6), Cdc25A, PCNA, Wee-1, the mini chromosome maintenance (MCM) complex and 14-3-3 were also identified here, either for enhanced or suppressed HIV replication phenotypes (Figure 4.16). Notably, regulation of the ATM/ATR- CHK1/CHK2 DNA damage signalling cascade was recovered for enhanced replication and not suppressed viral replication (Figure 4.16). ATR-mediated activation of CHK1 specifically, has been associated with the DNA-binding activity of Vpr and Vpr-induced cell cycle arrest (Lai, 2005; Bregnard, 2014). miRNA-regulation of SMAD4 was also recovered exclusively for the enhanced HIV replication hits (Figure 4.16). SMAD4 directly interacts with HIV Tat to inhibit LTR transactivation and Tat-mediated transcription (Coyle-Rink, 2002; Abraham, 2003). Two members of the Inhibitors of CDK4 (INK4) family of cyclin-dependent kinase inhibitors (CKIs), namely CDKN2A (p16) and CDKN2D (p19), were exclusively associated with suppressed HIV replication hits (Figure 4.16). The INK4 family of CKIs specifically regulate the activity of CDKs 4 and 6, and inhibition of CDK6 specifically inhibits HIV reverse transcription through regulation of the cell cycle via VRF and SAMHD1 (Pauls, 2014). Similarly, proliferating cell nuclear antigen (PCNA) was exclusively associated with suppressed HIV replication hits (Figure 4.16). PCNA expression correlates with HIV infection in mononuclear phagocytes (Fischer-Smith, 2004), and was also shown to be upregulated in response to HIV gp120 (Singhal, 2000). Finally multiple components of the anaphase promoting complex (ANAPC 1,4,13) as well as cyclins B1 (CCNB1) and D3 (CCND3) were also exclusively associated with suppressed HIV hits. ANAPC is associated with site selection during HIV integration (Ocwieja, 2011), while CCNB1 directly interacts with Tat in order to influence cell cycle (Zhang, 2012), and CCND3 interacts with CDK6 to inhibit the activity of SAMHD1 and promote HIV replication in primary macrophages (Ruiz, 2015). Interestingly, no clear bias was observed towards factors associated with a specific cell cycle stage (Figure 4.16) even though HIV replication has been reported to result in G_2M cell cycle arrest (reviewed by Bregnard, 2014). These findings suggest that specific networks of host miRNAs, including those described by this study, are capable of modulating HIV replication through regulation of cell cycle related factors, including P53. Notably, a large overlap was observed between the miRNA hits enriched for cell cycle and those enriched within the ‘viral carcinogenesis’ pathway.

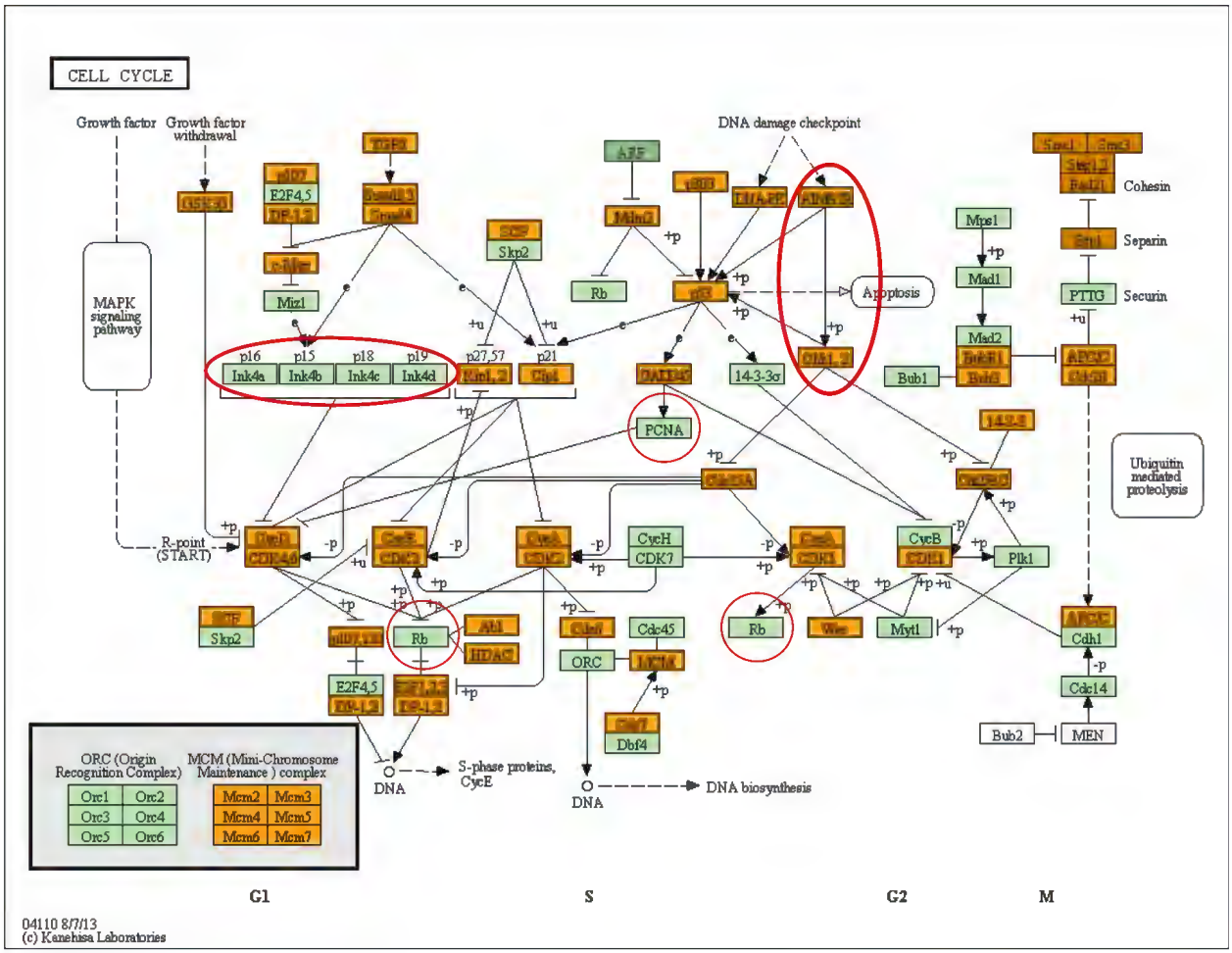

Figure 4.16 miRNA targets associated with cell cycle pathways and enhanced HIV replication.

Host genes targeted by miRNA hits (orange), host genes not targeted by miRNA hits (green), viral proteins (white), selected proteins differentially regulated for HIV-suppression phenotype (red ring).

Actin cytoskeleton

A number of functional pathways uncovered by mirPath were inherently associated with processes related to cytoskeletal remodelling, including 'Regulation of actin cytoskeleton', 'Adherens junctions' and 'Bacterial invasion of epithelial cells'. The host factors associated with these pathways were best summarised within the 'Regulation of actin cytoskeleton' pathway (Figure A4.3, Appendix IV). Briefly, miRNA modulation of receptor (e.g EGFR, TGFRβ) and cytoplasmic kinase (e.g src, c-abl) driven signaling cascades (e.g MEK/ERK, PI3K/AKT, MAPK) that are typically associated with various processes such as endocytosis, actin-mobilization and intracellular trafficking, were found to be enriched within both the suppressed and enhanced HIV replication hit pools (Figure A4.2, Appendix IV). 60 host factors were exclusively recovered for the

suppressed HIV replication phenotype (Table A4.13, Appendix IV) including, APC, ROCK1, MAP2K1, MAPK3 while 24 host factors were recovered for the enhanced HIV replication phenotype only, including ARHGEF4, PDGFß, VAV2 and VAV3 (Table A4.14, Appendix IV). Many of these proteins have also been described to mediate cytoskeletal interactions during early stages of HIV infection, including viral entry and nuclear trafficking (reviewed by Stolp, 2011). mirPath analysis recovered 45 HIV-suppressive miRNA hits (Table A4.15, Appendix IV) and 25 HIV replication enhancing miRNA hits that were associated with the 'Regulation of actin cytoskeleton' pathway (Table A4.16, Appendix IV). The results of this study therefore represent the first body of experimental work to functionally relate discrete subsets of host miRNAs associated with cytoskeletal rearrangements to the modulation of HIV replication.

Hippo signalling pathway

Unlike many of the other functional pathways recovered by mirPath analysis, functional significance of the Hippo signalling pathway with regards to viral infection and HIV replication remains poorly characterised (Larsson, 2013). The Hippo signalling cascade was first described in *Drosophila Melanogaster* where it was shown to control cell growth and apoptosis in organ size regulation (reviewed by Pan, 2010). In humans the pathway is comprised of a core kinase cascade that causes phosphorylation of YAP/TAZ and its cytoplasmic retention by 14-3-3 as part of contact inhibition and stress-induced apoptosis in mammalian cells (Pan, 2010). Dysregulation of hippo kinase activity and the nuclear accumulation of YAP/TAZ generally results in the expression of anti-apoptotic proteins like survivin (Pan, 2010; Vigneron, 2010). Conversely the specific nuclear association of YAP with p73 results in expression of proapoptotic genes like PUMA. Forty-six HIV-suppressive miRNA hits (Table A4.17, Appendix IV) and 22 HIV replication enhancing miRNA hits (Table A4.18, Appendix IV) were collectively linked to the regulation of 175 genes associated with the Hippo signalling pathway. Similarly to previous analyses, approximately 90% of the host factors recovered were common between both enhanced and suppressed HIV replication hit lists. Only 6 host genes were exclusively recovered for enhanced HIV replication hits (Table A4.19, Appendix IV), while 55 host genes were exclusively recovered for suppressed HIV replication (Table A4.20, Appendix IV) including the central kinases Mst1/2, SAV1 and their binding proteins RASSF6 and RASSF1 (Figure 4.17). These host factors have previously not been directly associated with HIV replication and these findings thus suggest a potentially novel role for the hippo central kinase cascade in the regulation of HIV replication.

The Hippo signalling cascade intersects with many additional pathway members including transcriptional coactivators of YAP, TEAD homologs, TCF/LEF associated factors, Smad4, as well as a number of genes associated with the WNT and BMP signalling pathways (Figure 4.17). Genes associated with P53 signalling including TP73 and TP53BP2 were uncovered for suppressed HIV hits only (Figure 4.17). Collectively,

these genes are important as many have established roles in the HIV life cycle. WNT signalling negatively regulates HIV replication (reviewed by Al-Harthi, 2012) and Nef has been posited as a potential antagonist of WNT signalling that competes for ß-catenin receptor binding (Weiser, 2013). Tat downregulates transcription of BMP receptor 2 (Caldwell, 2006) and P73 negatively regulates the transcriptional and apoptotic effects of Tat in human astrocytes (Saunders, 2005). Contrastingly, the role of the hippo kinase cascade and the differential regulation of YAP/TAZ transcriptional activity in response to HIV infection remains poorly characterised. Chronic HIV infection correlates with increased expression of CTLA4 and induction of the transcriptional repressor, BLIMP-1 in CD8+ cells and this may occur through CTLA4-mediated activation (reviewed by Larsson, 2013). The results of the work presented here suggest, for the first time, that there is a direct role for the Hippo central kinase cascade, YAP/TAZ, and their associated transcriptional coactivators in the differential modulation of HIV replication (Figure 4.17). In addition given that many other pathways associated with cellular proliferation and apoptosis are widely exploited by many other human viruses, the hippo signalling pathway may also be similarly involved. Thus, the Hippo signalling -associated host miRNAs identified by HCS and described here represent a unique target list involved in a host pathway previous unassociated with HIV replication.

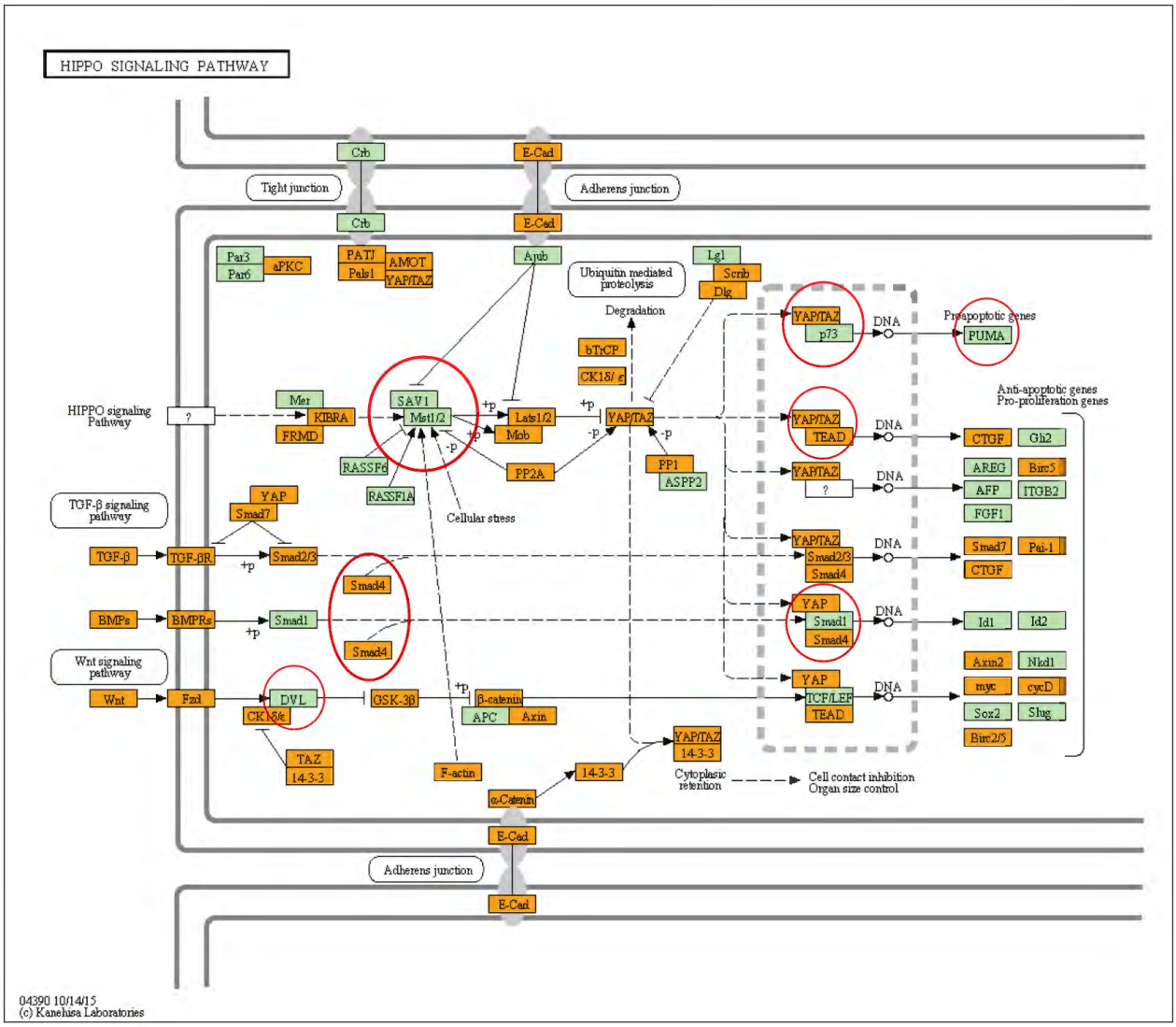

Figure 4.17 Enhanced HIV replication miRNA hit targets associated with the Hippo and intersecting signalling pathways.

Host genes targeted by miRNA hits (orange), host genes not targeted by miRNA hits (green), viral proteins (white), selected proteins differentially regulated for HIV-suppression phenotype (red ring).

4.5.2 Pathways associated exclusively with enhanced HIV replication

The enhanced HIV replication phenotype yielded 10 unique pathways (Table 4.2) including the PI3K/AKT, HIF-1 and spliceosome pathways. Considering that miRNA-induced perturbation of these pathways resulted exclusively in enhanced HIV replication, this would suggest that specific host factors/signals within these pathways may exert an inhibitory effect on HIV replication. The functional relevance of PI3K signalling has been well characterised for a number of viruses (reviewed by Ehrhardt, 2009). The pathway

has also been specifically linked to alternative splicing of HIV transcripts (Hillebrand, 2014), and signalling events related to HIV entry (Herbein, 2010). The relevance of the of the HIF-1 and spliceosome pathways are discussed in greater detail below.

Table 4.2 Functional pathways associated exclusively with enhanced HIV replication phenotypes

Functional pathways recovered by mirPath	
PI3K-Akt signaling pathway	Spliceosome
Endocytosis	Lysine degradation
mRNA surveillance pathway	Alanine, aspartate and glutamate metabolism
Salmonella infection	2-Oxocarboxylic acid metabolism
HIF-1 signaling pathway	Glycosaminoglycan biosynthesis - keratan sulfate

Spliceosome

Modulation of host RNA splicing machinery by HIV has been well characterised (reviewed by Stoltzfus, 2006) and was also discussed in Chapter 1. Briefly, various members of the Ser-Arg (SR) and heterogeneous ribonucleoproteins (hnRNPs) family have been associated with splicing of HIV transcripts, and suppression of such factors, like CDK13, lead to increased viral replication (Berro, 2008). Furthermore, spliceosome-associated processes, including the host mRNA surveillance pathway, which was also recovered for the enhanced HIV replication phenotype, have been described to naturally restrict retroviral replication (reviewed by Mocquet, 2015), including that of HIV (Liu, 2011). HCS and pathway analysis revealed 18 host miRNAs (Table 4.3) targeting 57 genes within the spliceosome pathway including various hnRNPs, SR proteins, specific spliceosome-related small nuclear RNAs, and their associated proteins (Figure 4.18). These findings represent the first account of a subset of host miRNAs that specifically enhance HIV replication, potentially through modulation of spliceosome-associated factors.

Table 4.3 HIV replication-enhancing miRNA hits associated with the Spliceosome pathway

miRNA (mirBase v.20)	
hsa-miR-1260a	hsa-miR-378a-5p
hsa-miR-1260b	hsa-miR-4318
hsa-miR-136-3p	hsa-miR-550a-3p
hsa-miR-141-5p	hsa-miR-576-3p
hsa-miR-188-5p	hsa-miR-587
hsa-miR-200a-5p	hsa-miR-625-3p
hsa-miR-22-3p	hsa-miR-668-3p
hsa-miR-3171	hsa-miR-675-3p
hsa-miR-335-3p	hsa-miR-891b

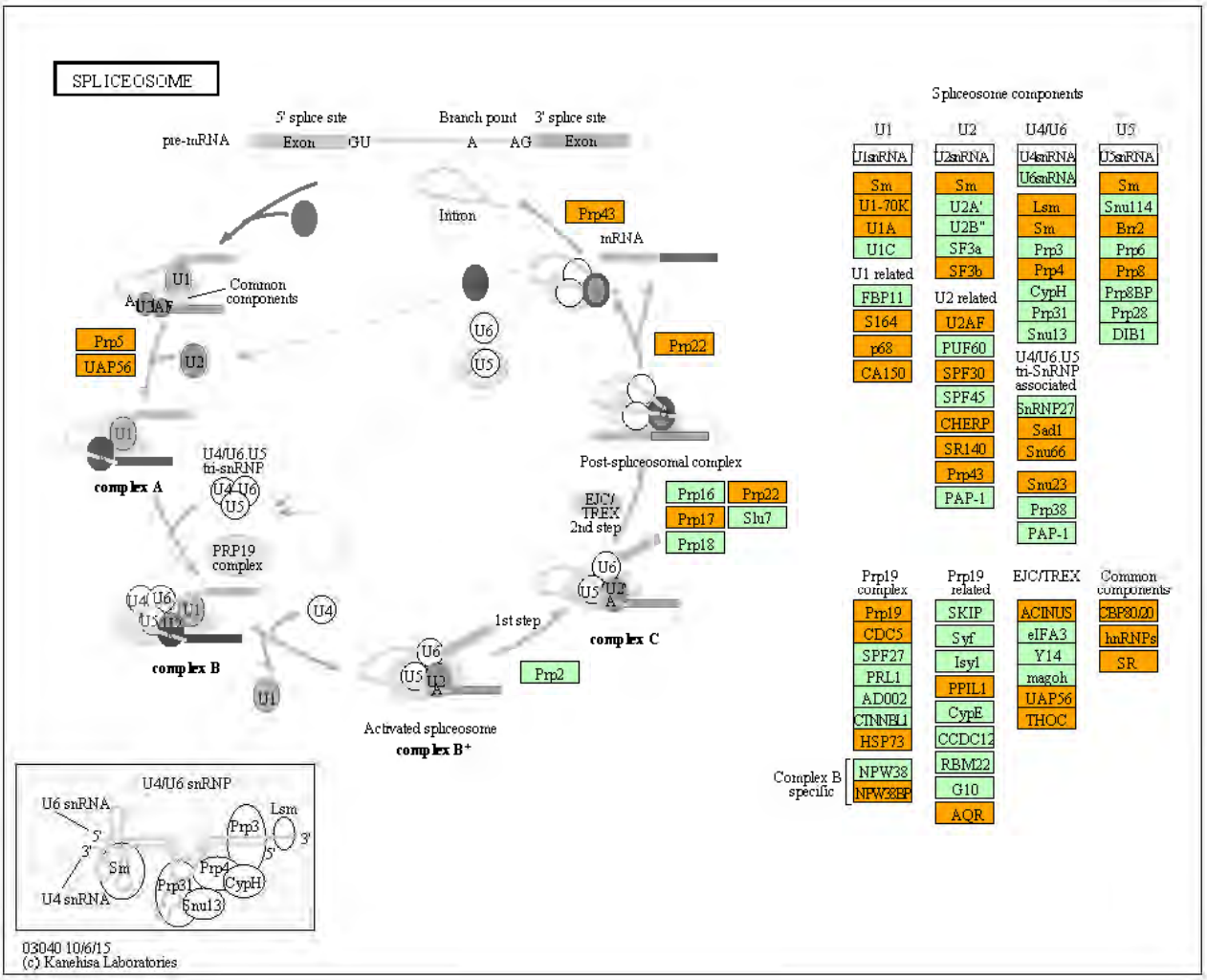

Figure 4.18 miRNA targets associated with Spliceosome pathway and enhanced HIV replication.

Host genes targeted by miRNA hits (orange), host genes not targeted by miRNA hits (green).

HIF-1 signalling pathway

HIF-1 is a heterodimeric transcription factor comprised of two subunits, HIF-1α and HIF-1ß (reviewed by Semenza, 2007). HIF-1α is negatively regulated by a prolyl hydroxylase domain protein (PHD) under normal cellular conditions, but this suppression is relieved in response to various environmental stressors, including hypoxia. Through its interaction with transcriptional coactivators like p300 and Creb binding protein (CBP), HIF-1 is able to regulate the transcription of hundreds of genes, including many genes related to cellular proliferation and apoptosis (Semenza, 2007). HIF-1 signalling is induced in response to a Vpr-mediated oxidative stress response, and has also been linked to persistent HIV infection in macrophages (Deshmane, 2011; Barrero, 2013).

Additionally, activation of the HIF-1 signalling pathway results in the upregulation of stromal cell-derived factor 1 (SDF-1) a well characterised inhibitor of HIV entry and replication (Bleul, 1996; Xiang, 2004). HCS and pathway analysis recovered 20 host miRNAs (Table 4.4) targeting 47 genes enriched within the HIF-1 and oxidative stress signalling pathway (Figure 4.19). In support of the previous association between HIV and HIF-1 signalling, these findings represent the first description of a specific subset of host miRNAs that functionally enhance HIV replication, potentially through the HIF-1 signalling pathway.

Table 4.4 HIV replication-enhancing miRNA hits associated with the HIF-1 pathway

miRNA (mirBase v.20)	
hsa-miR-1260a	hsa-miR-34c-3p
hsa-miR-1260b	hsa-miR-378a-5p
hsa-miR-1271-5p	hsa-miR-3938
hsa-miR-141-5p	hsa-miR-4318
hsa-miR-188-5p	hsa-miR-550a-3p
hsa-miR-19b-2-5p	hsa-miR-576-3p
hsa-miR-218-1-3p	hsa-miR-587
hsa-miR-22-3p	hsa-miR-625-3p
hsa-miR-3171	hsa-miR-668-3p
hsa-miR-335-3p	hsa-miR-891b

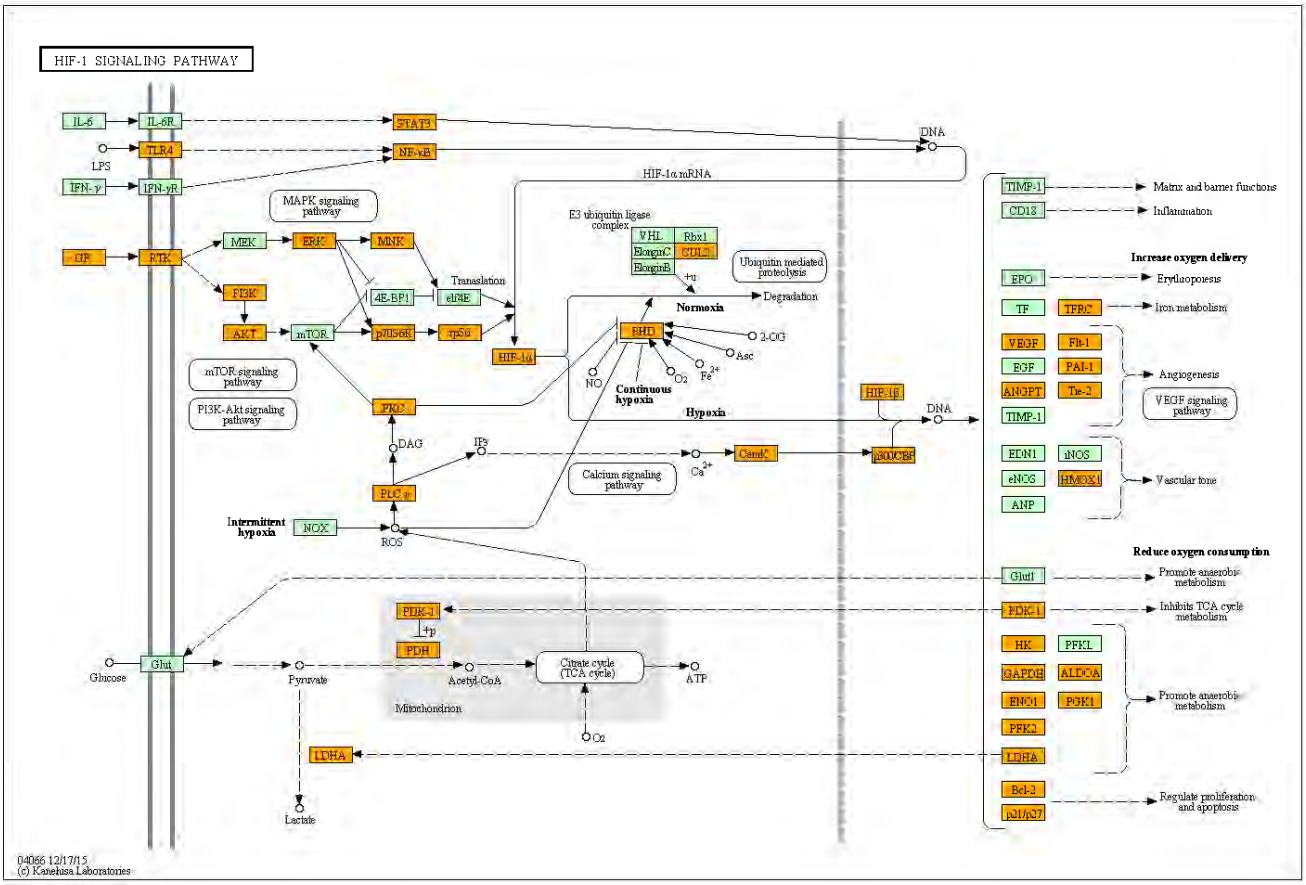

Figure 4.19 miRNA targets associated with HIF-1 signalling pathway and enhanced HIV replication.

Host genes targeted by miRNA hits (orange), host genes not targeted by miRNA hits (green), viral proteins (white).

4.5.3 Pathways associated exclusively with suppressed HIV replication

Twenty-four functional pathways were exclusively associated with the suppressed HIV replication phenotype (Table 4.5) including the MAPK, mTOR, TNF and sphingolipid signalling pathways. The functional relevance of the MAPK signalling pathway has been extensively characterised for HIV replication (Jacqué, 1998). Likewise the mTOR (Nicoletti , 2011) and TNF (Westendorp, 1995) signalling pathways have also been previously associated with HIV replication, while sphingolipids have been described mediate a number of processes associated with HIV entry and HIV-mediated signal transduction (reviewed by Rawat, 2005). Surprisingly, while the BER (Espeseth, 2011) and NHEJ (Genovesio, 2011) DNA repair pathways have been previously associated with HIV replication by functional genomic screens, only the homology directed repair (HDR) pathway was recovered by mirpath analysis as being exclusively associated with

the suppressed HIV replication phenotype and this finding is discussed in greater detail below.

Table 4.5 Functional pathways associated exclusively with suppressed HIV replication phenotype

Functional pathways recovered by mirPath	
Acute myeloid leukemia	HTLV-I infection
Arrhythmogenic right ventricular cardiomyopathy (ARVC)	MAPK signaling pathway
Axon guidance	mTOR signaling pathway
cGMP-PKG signaling pathway	N-Glycan biosynthesis
Choline metabolism in cancer	Non-small cell lung cancer
Estrogen signaling pathway	Progesterone-mediated oocyte maturation
Fatty acid elongation	Sphingolipid metabolism
Fatty acid metabolism	Sphingolipid signaling pathway
Fc gamma R-mediated phagocytosis	Thyroid cancer
Glycosaminoglycan biosynthesis - chondroitin sulfate / dermatan sulfate	Thyroid hormone synthesis
GnRH signaling pathway	TNF signaling pathway
Homologous recombination	Vasopressin-regulated water reabsorption

Homology directed repair

A number of viral lifecycles, including that of HIV, are dependent on manipulation of host DNA damage repair pathways, and deregulation of host P53 signaling networks that determine cell fate in response to DNA damage (reviewed by Chen, 2014 and Bregnard, 2014).

The homologous DNA repair (HDR) pathway is a host DNA repair process generally associated with the repair of double strand breaks (DSBs) following resectioning of damaged DNA into 3' single strand structures that then 'invade' a homologous DNA strand, using it as a template for the repair process (reviewed by Jasin, 2013). Fifteen host miRNAs associated with suppressed HIV replication (Table 4.6) were reported to regulate 21 host proteins involved in the homologous repair of DSBs (Figure 4.20). Specifically, factors involved in resectioning (RAD50, Nbs1), strand invasion (RAD51, RPA, BRCA2) and resolution of the adjoining strands (BLM, TOP3) correlated with suppressed HIV replication (Figure 4.20). This functional association of HDR, specifically the activity of RAD51, with HIV replication supported previous findings (Nakai-Murakami, 2006; Cosnefroy, 2012). Specifically, enhanced activation of RAD51 and DNA repair suppressed HIV infection through inhibition of HIV integrase (Cosnefroy, 2012), while Vpr-induced DNA damage in turn enhanced activation of RAD51 and HDR (Nakai-Murakami, 2007). In addition, a number of other host DNA damage repair pathway genes were also shown to be required for HIV replication by multiple independent

siRNA-based screens (Brass, 2008; Konig, 2008, Zhou, 2008, Espeseth, 2011). Notably, the miRNAs uncovered in this study represent a novel subset that are associated with HDR and HIV replication (Table 4.6; Figure 4.20).

Table 4.6 HCS miRNA hits associated with HDR

miRNA (mirBASE v.20)*	
hsa-miR-124-3p	hsa-miR-383-5p
hsa-miR-1295a	hsa-miR-4256
hsa-miR-192-5p	hsa-miR-4270
hsa-miR-2110	hsa-miR-4314
hsa-miR-3179	hsa-miR-497-5p
hsa-miR-3190-5p	hsa-miR-889-3p
hsa-miR-342-5p	hsa-miR-940
hsa-miR-3616-5p	

*miRNAs ordered numerically

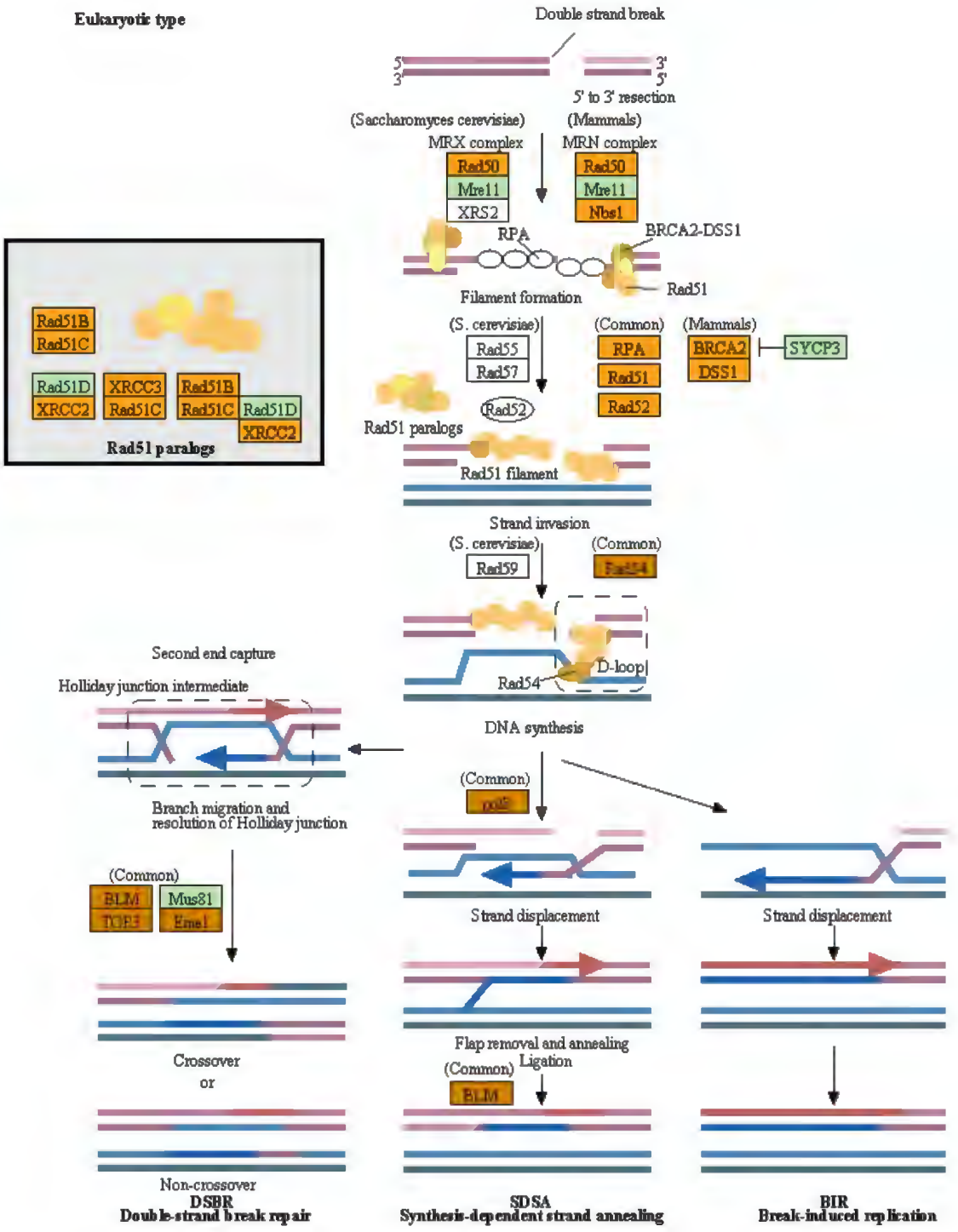

Figure 4.20 HCS miRNA hit targets that are enriched within the HDR pathway.

Host genes targeted by HCS miRNA hits (orange). Host genes not targeted by HCS miRNA hits (green).

4.6 HIV infection promotes a cancer-like phenotype in GHOST(3) cells

A rigorous bioinformatics-based investigation revealed some common 'functional outputs' with regards to pathways recovered by mirPath analyses for miRNAs associated with functional modulation of HIV replication. These included evasion of apoptosis, regulation of cell cycle and host DNA repair pathways, as well as modulation of signalling pathways associated with cellular proliferation (e.g MAPK, PI3K, TNF, Erbb). A number of these processes are functionally relevant to cancer-like phenotypes and a possible link between HIV infection and cancer was further underscored by enrichment of multiple tissue-specific carcinomas as well as recovery of the viral carcinogenesis pathway by mirPath analysis. The viral carcinogenesis pathway in particular revealed a high degree of overlap between HIV and a number of oncogenic viruses, specifically in terms of their host-pathogen interaction profiles (Figure A4.2, Appendix IV).

The HDR pathway was exclusively recovered for suppressed HIV replication and signaling networks classically associated with the host cell response to DNA damage were enriched within many of the recovered pathways. HIV integrase and Vpr have both been associated with the induction of double strand DNA breaks and activation of the host DNA damage response (Craigie, 2001; Nakai-Murakami, 2007). Furthermore, HIV infection has previously been described to promote aberrant cell survival in both cultured cell lines and primary macrophages in response to DNA damage-inducing agents and other forms of genotoxic stress (Col, 2005; reviewed by Cummins, 2013), potentially through the P53-inhibitory effects of viral Tat and Nef proteins (Greenway, 2002; Col, 2005). Finally, HIV gp120 has also been well characterized as an activator of apoptotic signalling pathways through its interaction with various cell surface receptors, although these apoptotic signals are counterbalanced by the pro-survival activity of specific viral (e.g Vpr) and host (e.g MAPK) proteins (Cummins, 2013).

Inhibition of P53 and aberrant cell survival in spite of high levels of DNA damage are molecular phenotypes associated with hallmarks of cancer (reviewed by Hanahan, 2011). The close functional relationship between cancer-like molecular phenotypes and HIV replication posited by HCS pathway analysis is thus well supported by prior art although this relationship has not yet been specifically characterised in GHOST(3) cells. A series of validation experiments were thus undertaken to further evaluate the potential relationship between HIV infection and cancer-like phenotypes in cultured GHOST(3) cells, specifically in relation to DNA damage.

4.6.1 HIV infection deregulates P53 transcriptional activity

The tumour suppressor P53 is widely regarded as the 'gatekeeper' of genome integrity and cell survival as a result of its ability induce to apoptosis or cell cycle arrest in response to various environmental stresses including DNA damage (reviewed by Levine, 2009). P53 is specifically inactivated in many cancers, and by many viruses, resulting in abnormal cell survival and proliferation despite high levels of DNA damage and genomic instability (Chen, 2014). The *CDKN1A* gene, which encodes p21, is a direct transcriptional target of P53 and p21 is a well characterised downstream effector of P53-mediated cell cycle arrest and apoptosis (Nowsheen, 2012).

qPCR analysis revealed that *TP53* transcript levels were significantly downregulated following HIV infection of GHOST(3) cells both at 24 hpi (46%) and 48 hpi (89%; Figure 4.19A, $p<0.05$). Likewise a corresponding 70% and 79% downregulation was observed for *CDKN1A* at 24 hpi and 48 hpi respectively (Figure 4.19B). These findings suggest that HIV infection functionally inhibits P53 at the transcriptional level and that this effect, together with the reported P53-inhibitory effects of viral proteins like Tat and Nef, together contribute to suppressed transcriptional activity of P53 and its transcriptional target CDKN1A (Figure 4.21). As mentioned previously, dysregulation of TP53 signalling is one of the hallmarks of cancer and these findings thus support the notion that HIV infection may induce a cancer-like phenotype in GHOST(3) cells.

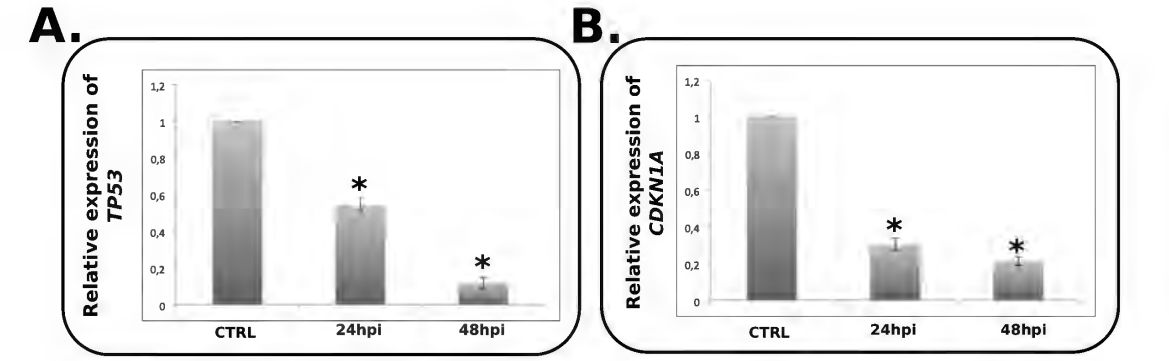

Figure 4.21 Relative *TP53* and *CDKN1A* expression levels in response to HIV infection.

qPCR analysis showing **A)** relative TP53 expression 24 and 48 hpi in infected GHOST(3) cells, and **B)** relative CDKN1A expression levels 24 hpi and 48 hpi in infected GHOST(3) cells. Expression levels were normalized against the reference gene *HPRT*, * = $p<0.05$, n=3.

4.6.2 Stable or *de novo* HIV infection as a determinant of GHOST(3) cell survival in response to DNA damage

Another hallmark of cancer is aberrant cell survival in spite of high levels of DNA damage (Hanahan, 2011). Double strand breaks (DSBs) represent one of the most lethal forms of genotoxic stress and even single unrepaired break can lead to dire consequences including mutagenesis and cell death (reviewed by Nowsheen, 2012). DSBs are readily detected by DNA damage sensors such as the MRN complex, which then activates Ataxia Telangiectasia Mutated (ATM) or Ataxia Telangiectasia and Rad3 Related (ATR) kinases leading to histone protein H2AX serine 139 phosphorylation (γ-H2AX) at sites proximal to the DSB (Kuo, 2008; Nowsheen, 2012). Activated γ-H2AX then recruits DNA repair factors to DSB sites (Kuo, 2008). γ-H2AX foci thus represent biomarkers for DSBs, where a single foci is generally representative of a single DSB (Kuo, 2008). The effect of HIV infection on GHOST(3) cell survival in response to DNA damage was assessed by indirect immunofluorescence and imaging following chemically-induced DSBs, and γ-H2AX was used to visualize DNA damage (Figure 4.22). Such damage was induced by VP16 (Etoposide) which is a topoisomerase II inhibitor that causes stalled replication forks and accumulation of DSBs, which eventually result in P53-mediated cell cycle arrest and apoptosis (Arriola, 1999; Jamil, 2015).

ICC revealed that GHOST(3) cells naturally exhibit multiple γ-H2AX foci per cell indicative of persistent DNA-damage or stalled replication forks, which are a common phenotype in immortalised cell lines (Figure 4.22). A 24 hour treatment with 10 μM Etoposide resulted in a significant increase in γ-H2AX foci but did not have a significant effect on cell viability (Figure 4.22). In contrast, 48 hour treatment with 10 μM Etoposide resulted in significantly elevated levels of γ-H2AX foci as compared to the untreated controls (Figure 4.22) and a corresponding broad cytotoxicity (>95% loss of cell viability). HIV infection alone generally resulted in moderately elevated levels of γ-H2AX foci, especially in infected cells, as compared to untreated control cells (Figure 4.22). This was in agreement with previous findings which demonstrated that Vpr induces DSBs (Nakai-Murakami, 2007), but also suggested that HIV exposure may induce DSBs in bystander cells not stably infected by HIV.

A highly noteworthy phenotype was observed when viral infection and Etoposide treatment were combined. GHOST(3) cells infected with HIV for 24 hours that were then treated with 10 μM Etoposide for 24 hours showed higher levels of γ-H2AX as compared to untreated control cells, with only a moderate effect on cell viability (Figure 4.22). A similar experiment using HIV-infected GHOST(3) cells but treated with 10uM Etoposide for 48 hours resulted in the highest level of γ-H2AX foci observed for any treatment, yet cell viability still generally exceeded ~20% (Figure 4.22). Intriguingly, the surviving population was dominated by cells exhibiting high levels of LTR transactivation (Figure 4.22), suggesting that integrated virus is able to protect host cells from additional lethal

DNA damage. This protective phenotype was readily reversed when the order of reagents was changed such that GHOST(3) cells received 10uM Etoposide for 24 hours prior to infection for 24 hours. In this case, broad scale cytotoxicity was observed (Figure 4.22). Likewise, simultaneous exposure of GHOST(3) cells to HIV and Etoposide (10 μM) for 48hr exhibited a similar cytotoxic effect as a 48 hr Etoposide only treatment (Figure 4.22).

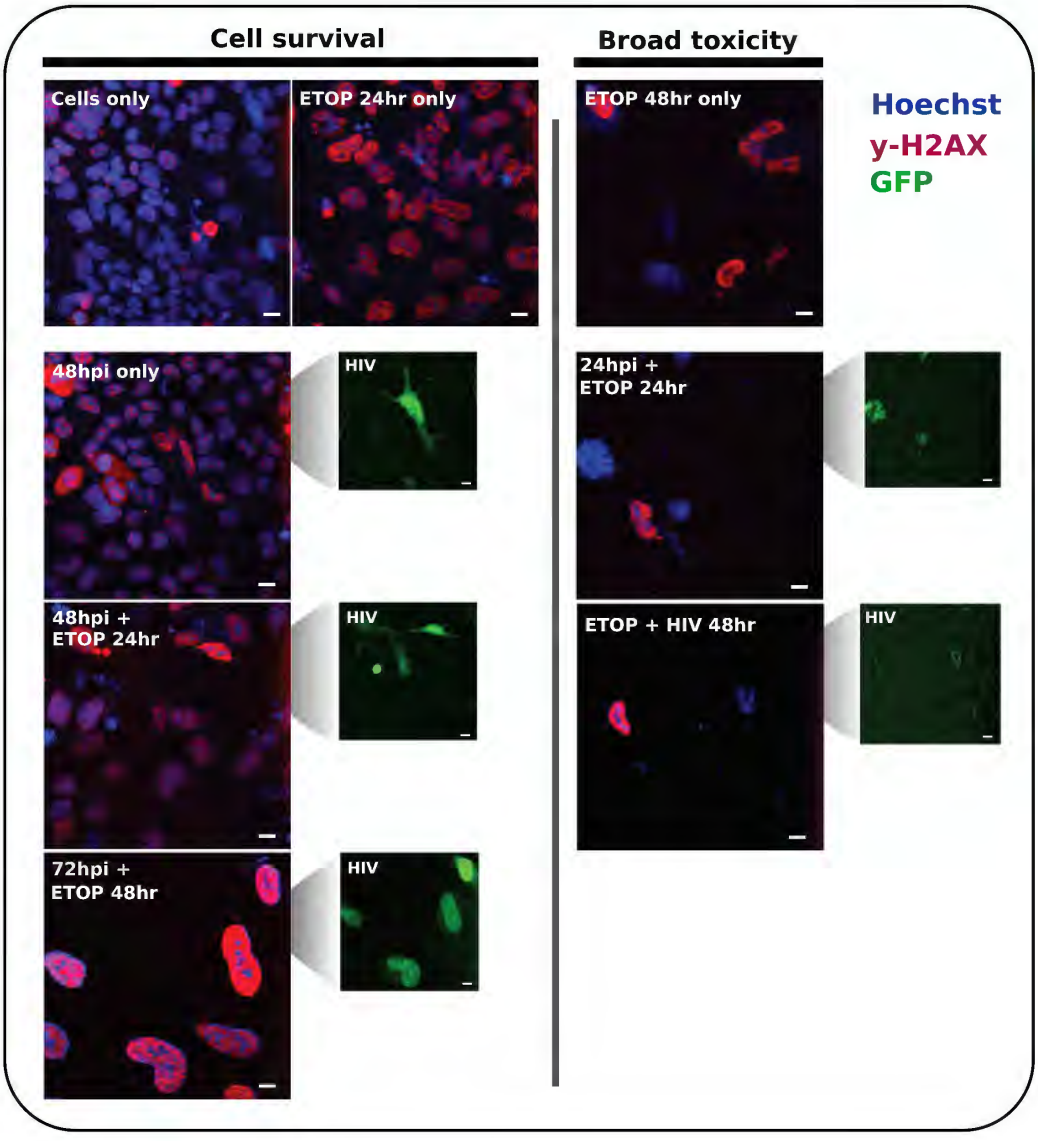

Figure 4.22 GHOST(3) cell survival in response to HIV infection and chemically-induced DNA damage.

Survival of GHOST(3) cells in response to Etoposide only or infection only treatment, or in response to HIV infection followed by 24 or 48 hours of Etoposide treatment, or simultaneous treatment with both HIV and Etoposide. Nuclei counterstained with Hoechst (blue), activated γ-

H2AX (red), activated LTR-GFP reporter (green). Images represent overlays of single FOVs, acquired at 40x from the 405, 488 and 550 excitation channels. Scale bars = 10μm.

ICC-based validation experiments thus revealed two contrasting effects on GHOST(3) cell viability in response to DNA damage and HIV infection. Firstly, exposing GHOST(3) cells to Etoposide either prior to or during HIV infection sensitized cultured cells towards apoptosis (Figure 4.22). This effect was clearly related to HIV exposure, as the same Etoposide treatment conditions (10μM, 24hrs) did not induce broad scale cytotoxic effects in the absence of virus (Figure 4.22). The induction of DNA damage has previously been described to enhance HIV replication, specifically integration (Koyama, 2013), thus suggesting that these pro-apoptotic phenotypes may involve more complex mechanisms associated with the consequences of Etoposide treatment rather than just the induction of DSBs alone. Furthermore, DNA damage induced by Etoposide can be repaired within 3hr in cultured cells following the withdrawal of Etoposide (Arriola, 1999), thus suggesting that the apoptotic effect related to HIV exposure was likely initiated within the first 3 hours of virus addition, implicating early interaction events between HIV virions and the host cell. This would posit the HIV entry process, and specifically the interaction between HIV gp120 and cell surface proteins, as a prime candidate for the apoptotic 'trigger' associated with this phenotype.

Secondly, while prolonged Etoposide treatment (48hr) was highly toxic in HIV-naive GHOST(3) cells, stably infected GHOST(3) cells exposed to the same treatment course were significantly more resistant to Etoposide-induced apoptosis, despite exhibiting extremely high levels of DNA damage (Figure 4.22). This observation thus provides direct evidence that stable or chronic HIV infection promotes an aberrant cell survival phenotype in GHOST(3) cells. This is line with previous findings which reported HIV-mediated attenuation of apoptosis in response to both Etoposide and UV -induced DNA damage in T cells and primary macrophages (Schindler, 2005; Cummins, 2013). The observation that similar phenotypes were recovered in primary PBMCs and macrophages, again suggests that the GHOST(3) infection assay is able to robustly recapitulate critical and physiologically relevant HIV-associated molecular phenotypes. These findings thus, in addition to confirming the functional trends recovered by HCS and pathway analysis, also posit that functional associations and miRNA hits recovered by HCS are indeed physiologically relevant.

4.6.3 Transcriptional activity of P53 may influence HIV-DNA damage associated cell survival phenotypes

Etoposide has previously been described to inhibit the P53-suppressor, HDM2, at both the protein and transcriptional level, resulting in nuclear localisation and transcriptional activation of P53, as denoted by an upregulation of *CDKN1A* (Arriola, 1999).

Additionally, Nef-mediated destabilization of P53 transcriptional activity enhanced cell survival in response to UV-induced DSBs (Greenway, 2002). qPCR analysis was thus used to evaluate the potential role of P53 transcriptional activity in relation to the phenotypes described in Figure 4.22 above. In accordance with previous data (Figure 4.21) *TP53* expression analysis revealed a significant downregulation of *TP53* 24 hours after HIV infection (~40%) which was similar to that observed for 3hr (~42%) and 24hr (~49%) Etoposide treatments (Figure 4.23A). A 24hr HIV exposure followed by 24 hr Etoposide treatment (10μM) also exhibited a significant downregulation of *TP53* (~28%), while a 3hr Etoposide treatment administered 24hr post-infection did not exhibit a significant ($p>0.05$) effect on *TP53* expression levels (Figure 4.23A).

An evaluation of *CDKN1A* expression levels for the same set of treatments revealed that 3hrs of Etoposide treatment did not have a significant effect on *CDKN1A* transcript levels, although 24hrs of Etoposide treatment resulted in a significant 250% increase in *CDKN1A* transcript levels (Figure 4.23B). In accordance with previous results, *CDKN1A* was confirmed to be significantly downregulated (~38%) 24hr post infection, while cells infected with HIV for 24 hrs and then exposed to Etoposide for 24 hrs showed significant (~60%) upregulation in *CDKN1A* (Figure 4.21B). Likewise *CDKN1A* was observed to significantly upregulated by ~240% following a short (3hr) Etoposide treatment of HIV-infected cells (Figure 4.23B).

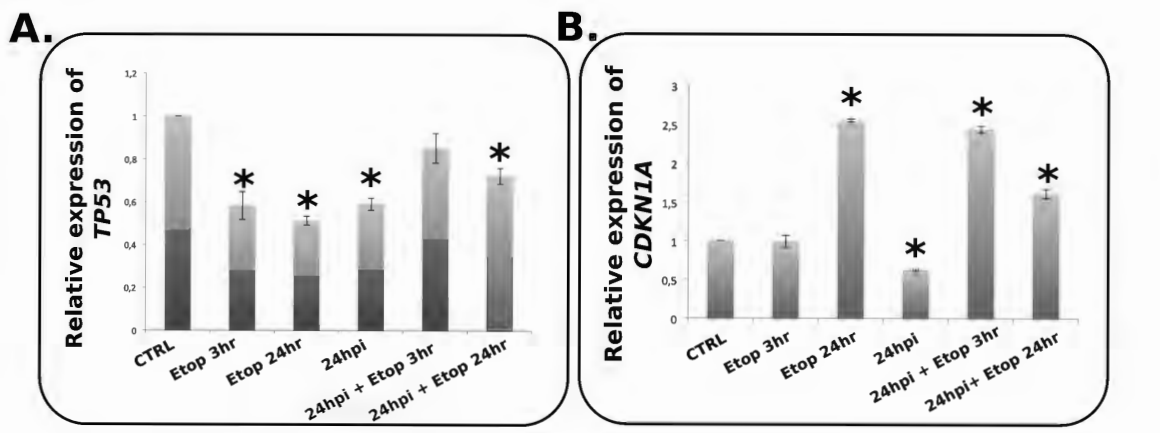

Figure 4.23 Relative *TP53* and *CDKN1A* expression levels in response to combinations of HIV infection and Etoposide treatment.

qPCR analysis of mRNA transcript levels on GHOST(3) cells exposed to Etoposide alone or, HIV alone, as well as HIV-infected cells exposed to Etoposide for various time courses. **A)** Relative *TP53* expression and **B) r**elative *CDKN1A* expression. Expression levels were normalized against the reference gene *HPRT*, * = $p<0.05$, n=3.

qPCR analysis of *TP53* and *CDKN1A* expression levels in response to HIV infection and chemically-induced DNA damage revealed that 24hrs of Etoposide treatment was able to significantly induce *CDKN1A* expression levels, through a process independent of *TP53* transcription. This is in line with previous findings that describe elevated *CDKN1A* expression following Etoposide treatment (Arriola, 1999; Jamil, 2015). Intriguingly, while 3hrs of Etoposide treatment alone did not induce a significant increase in *CDKN1A* expression, the same treatment in a population of infected GHOST(3) cells resulted in a 2.4 fold increase in *CDKN1A* expression compared to untreated cells, and a ~3 fold increase compared to the 24 hpi treatment.

Notably, P53 transcriptional activity is actively suppressed during HIV infection (Figure 4.23B, Greenway, 2002) suggesting that Etoposide treatment partially alleviates HIV-mediated suppression of P53 transcriptional activity, resulting in a rapidly amplified transcriptional response. In addition, the 're-activation' of P53 transcriptional activity in response to Etoposide treatment of infected cells may contribute to the moderate toxicity observed (Figure 4.22).

Intriguingly, the variations in *CDKN1A* expression did not correspond with concordant variations in *TP53* expression highlighting that the interaction of these factors is complex and multi-layered, occurring at transcriptional and translational levels. Activation of P53 transcriptional activity, through the inhibition of HDM2 by Nutlin-3 treatment (10μM, 24hr; Vassilev, 2004) *prior* to HIV exposure did not have a significant impact on HIV replication or cell viability (Appendix IV, Figure A4.4), suggesting that simply elevating levels of P53 prior to HIV exposure may not be enough to sensitise GHOST(3) cells to apoptosis or significantly impact HIV replication. In accordance with the prior art these data suggest that HIV-mediated modulation of P53 transcriptional activity plays an important role in aberrant cell survival phenotypes recovered in response to DNA damage following HIV infection (reviewed by Cummins, 2013). These findings thus further support the cancer-like phenotype

4.7 LincRNA-p21 plays a role in the modulation of HIV replication and GHOST(3) cell survival in response to DNA damage

LincRNA-p21 was first described as a P53-induced long noncoding transcript which was actively transcribed in response to chemically-induced DNA damage (Huarte, 2010). LincRNA-p21 acts as a pro-apoptotic factor that mediates transcriptional repression of hundreds of P53 target genes through its association with heterogeneous nuclear ribonucleoprotein K, hnRNP-K (Huarte, 2010). Given the close association between P53 transcriptional activity and many of the functional trends and phenotypes recovered by miRNA-based HCS, specifically those related to DNA damage and apoptosis, an evaluation of lincRNA-p21 with regards to HIV infection was undertaken.

LincRNA-p21 transcript levels were first evaluated by qPCR analysis and a significant ($p<0.05$) downregulation of 43% was observed 48 hours after infection (Figure 4.24). This suggested that LincRNA-p21 may be functionally relevant to HIV replication but the influence of Nef-mediated P53 inhibition could not be discounted. Thus to explore possible functional associations between LincRNA-p21 and the HIV replication phenotypes recovered by HCS, an *in silico* approach was adopted to identify putative miRNA binding sites within the human LincRNA-p21 transcript. This analysis yielded 409 putative miRNA binding sites that were then filtered against HCS hits recovered for both enhanced and suppressed HIV replication phenotypes. This list was then filtered to identify only miRNAs that contained more than one binding site within the LincRNA-p21 sequence, as the presence of multiple binding sites for a single miRNA on a single transcript is generally indicative of a higher likelihood for a functional miRNA-target interaction (Grimson, 2007; Bartel, 2009).

Interestingly only 4 HCS hits met these criteria and all four of these miRNAs were exclusively recovered for suppressed HIV replication (Figure 4.25). An evaluation of the locations for these miRNA binding sites also revealed an interesting trend whereby they appeared to be clustered within specific regions of the LincRNA-p21 transcript (Figure 4.25A). The first of these 'functional clusters' comprised of a 150nt region (0nt-150nt) which contained 4 putative binding sites, two for miR-637 and 1 each for miR-3189 and miR-654-5p (Figure 4.25A). The second 'functional cluster' was a 100nt region (1600-1700nt) which contained a single binding site for each of the four miRNA hits. In addition, visual inspection confirmed a strong HIV-suppressive phenotype for each of the mimic treatments associated with these 4 miRNAs (Figure 4.25B). The lincRNA-p21 hnRNP-K binding domain is located within the first 780 bp at the 5' end of the transcript and this region is highly conserved between both mouse and human LincRNA-p21 transcripts (Huarte, 2010). It is therefore possible that the miRNA-lincRNA-p21 phenotypes presented here may in fact be associated with miRNA-mediated modulation of the interaction between LincRNA-p21 and its binding partners, including hnRNP-K.

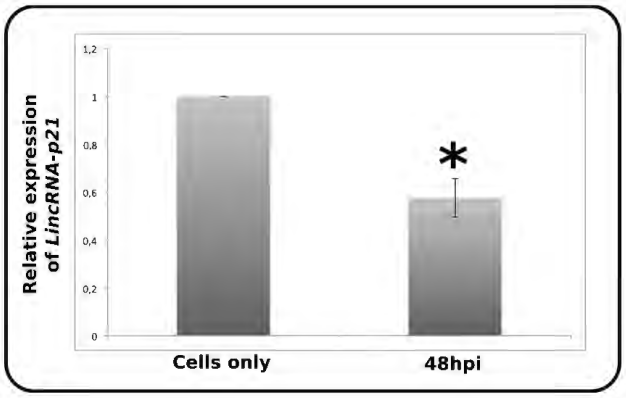

Figure 4.24 Relative *LincRNA-p21* expression levels in response to HIV infection.

qPCR analysis of LincRNA-p21 transcript levels 48hr post infection. Expression levels were normalized against the reference gene *HPRT*, * = $p<0.05$, n = 3.

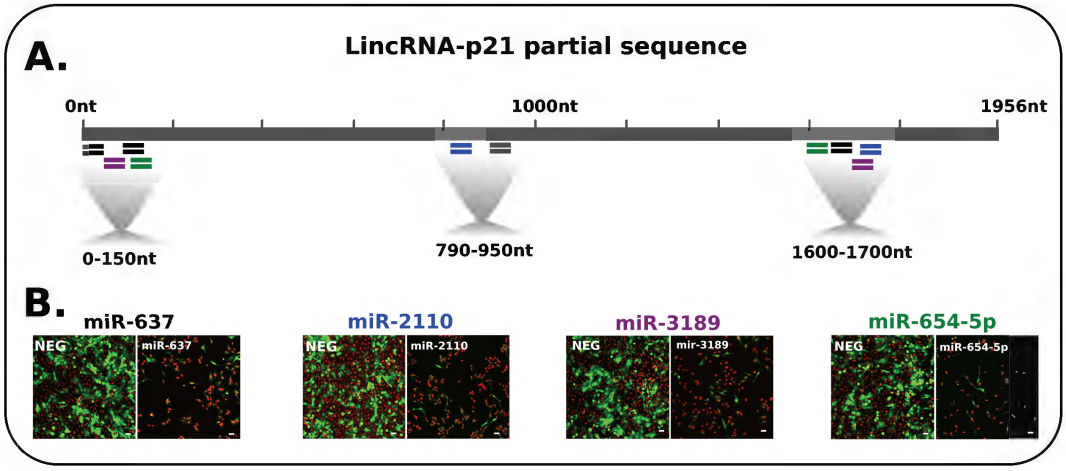

Figure 4.25 Putative associations between lincRNA-p21 and miRNA HCS hits

A) Predicted miRNA binding sites that map to various regions of the human lincRNA-p21 transcript, and which correspond to HIV-suppressive HCS hits. '=' denotes a single miRNA binding site, miR-637 (black), miR-2110 (blue), miR-3189 (purple), miR-654-5p (green). **B)** Visual profiles of miRNA mimic treatments recovered by HCS for each of the mimics in A. Plate-specific negative control images are included on the left of each miRNA treatment image. Images represent overlays of images acquired from a single FOV in the 405 and 488 channels, nuclei counterstained with Hoechst (red), LTR-GFP reporter activity (green). Images acquired at 20x, scale bars = 20μm.

These findings suggest a potential role for LincRNA-p21 in HIV replication, where miRNA-mediated modulation of LincRNA-p21 targeted to specific, concise regions may strongly inhibit HIV replication (Figure 4.25). miRNA-lincRNA interactions can result in a broad range of functional effects including lincRNA cleavage, modifications to the secondary structure of lincRNAs, perturbations of lincRNA binding dynamics, as well as cross-talk between lincRNAs and mRNAs which may fine tune gene expression (Salmena, 2011; Yoon, 2014).

Although a more comprehensive investigation into the proposed miRNA-lincRNA-p21 interactions is clearly required to definitively validate these interactions, some additional experimental data was generated. Specifically, siRNA-mediated knockdown of lincRNA-p21 was used to identify whether the observed HIV-suppressive phenotypes were related to functional silencing of lincRNA-p21. A 25 nM siRNA treatment resulted in significant downregulation (83%, $p<0.05$) of lincRNA-p21 transcript levels 24 hours post transfection (Figure A.4.5, Appendix IV). However, microscopy revealed that this did not have a significant effect on HIV replication in si-lincRNA-p21 transfected/infected GHOST(3) cells as compared to infected control cells (Figure 4.26). Interestingly though, siRNA-treatment *did* have a significant effect on cell viability in response to si-lincRNA-p21 transfected/Etoposide treated cells (10μM, 48hr). In this case, siRNA-mediated

knockdown of lincRNA-p21 attenuated the cytotoxic phenotype previously noted for this treatment (Figure 4.22, Figure 4.26).

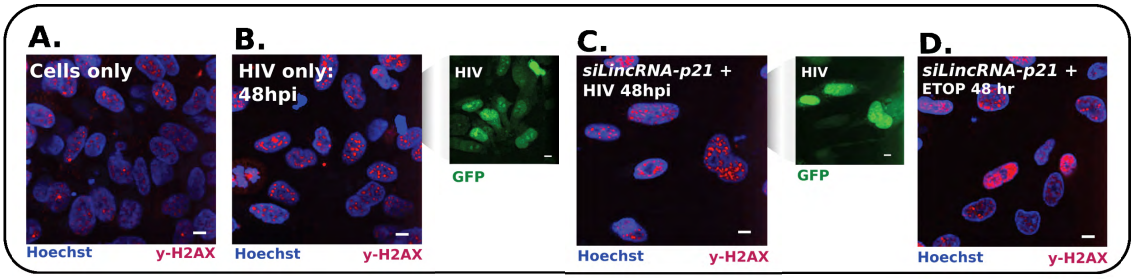

Figure 4.26 Effects of siRNA-mediated knockdown of lincRNA-p21 on HIV replication and GHOST(3) cell survival.

A) Untreated cells, **B)** Cell infected with HIV for 48 hours, MOI=0.5., **C)** Cells transfected with 25nM si-lincRNA-p21 (25nM) for 24 hours, then infected with HIV for 48 hours, MOI=0.5., **D)** Cells transfected with 25nM si-lincRNA-p21 for 24 hours, then Etoposide treated for (10μM, 48 hours). Nuclei counterstained with Hoechst (blue), activated y-H2AX (red), activated LTR-GFP reporter (green). Images represent overlays of single FOVs, acquired at 40x from the 405, 488 and 550 excitation channels. Scale bars = 10μm.

Overall, as the functional silencing of lincRNA-p21 by siRNAs did not impact HIV replication, this suggested that the phenotypes recovered for miRNAs predicted to bind lincRNA-p21 may be due to modification of the lincRNA's protein/DNA/RNA binding interactions, and not simply its degradation. Furthermore, the enhanced GHOST(3) cell survival phenotype observed for si-lincRNA-p21 transfected/Etoposide treated cells reinforces the role of lincRNA-p21 in DNA-damage-induced apoptosis. In the context of pathogenic infection, such as that of HIV, these data also revealed that viral manipulation of host non-coding RNAs is a powerful mechanism to avoid a terminal outcome such as apoptosis.

4.8 Validation of HCS miRNA hits against an X4-tropic HIV variant

The depletion of $CD4^+$ T cell populations during late stages of chronic HIV infection have been associated with a switch in HIV co-receptor usage and emergence of X4-tropic viral strains that utilise CXCR4 co-receptors as opposed to CCR5 (Gorry, 2005). Co-receptor binding by HIV gp120 results not only in fusion events, but also in the activation of downstream signalling cascades which prime host cells, making them more permissive to HIV replication (Wu, 2009). A panel of 6 HIV-suppressive and 2 HIV replication enhancing miRNA mimics were thus screened against the X-4 tropic viral variant, HIV Gag-iGFP (Hubner, 2007), in order to determine whether viral tropism was a discriminating factor in the phenotypes recovered for these specific miRNA mimics by

HCS. As with HCS, GHOST(3) cells were transfected with a 25 nM final concentration of miRNA mimics 48 hour prior to infection and cells were fixed, stained and imaged 48 hpi (Figure 4.27). An siRNA targeted to the CD4 receptor was utilized as a positive control for suppressed HIV replication, while a mock transfection was utilised as a negative control (Figure 4.27A). HIV Gag-iGFP was identified as a syncytia-inducing strain, as indicated by large multinucleate cellular bodies, which were also positive for GFP expression (Figure 4.27A). Syncytia are induced by specific variants of Env, the cell surface expression of which, results in membrane fusion events between neighbouring cells (Watkins, 1997).

The highest ranked HIV-suppressive hit recovered by HCS, miR-506, significantly inhibited both syncytia formation and GFP signal output (Figure 4.27B). Likewise, similar effects were observed for miR-637 and miR-124-3p (Figure 4.27B). Furthermore, in accordance with the phenotype recovered by HCS, exogenous expression of miR-2110 resulted in a cytotoxic phenotype where the majority of surviving cells were not positive for GFP (Figure 4.27B). Exogenous expression of miR-138 on the other hand exhibited an opposing effect, where only HIV-infected cells seemingly survived (Figure A4.6 A, Appendix IV). In contrast to its HIV-suppressive effect on $PSG3^{BAL}$ infection, miR-193-3p treatment did not have a significant effect on HIV Gag-iGFP replication (Figure A4.6 A, Appendix IV).

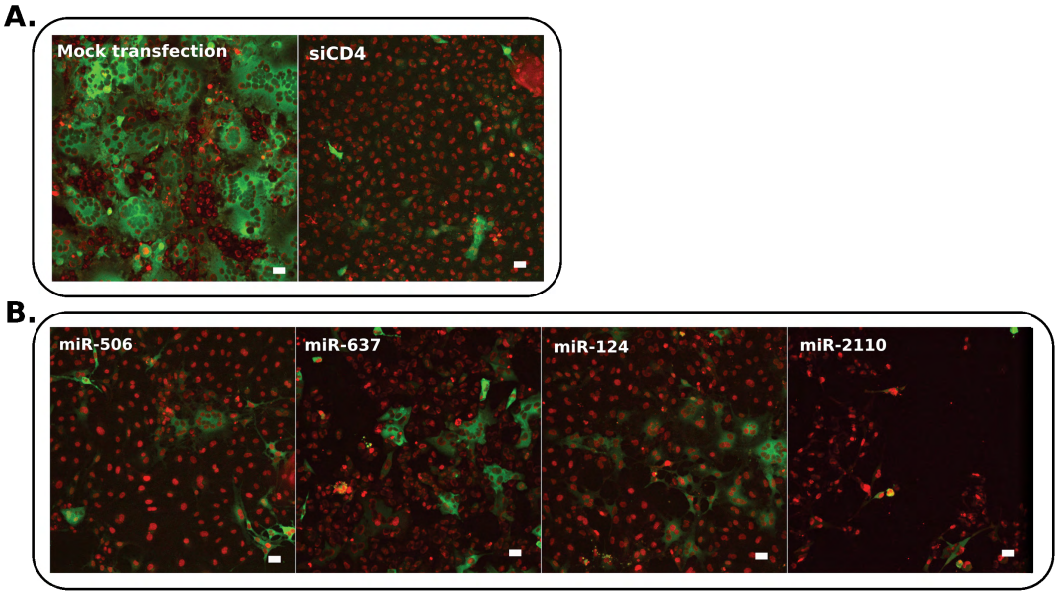

Figure 4.27 HIV-suppressive miRNA hits with conserved anti-HIV activity against an X4-tropic HIV variant.

A) Phenotypic control experiments included mock transfected/infected GHOST(3) cells (left), and siCD4-treated/infected GHOST(3) cells (right), **B)** Examples of HIV-suppressive hits recovered by HCS with demonstrated activity against the X4-tropic variant HIV Gag-iGFP. Images represent overlays of single FOVs acquired at 20x in the 405 and 488 excitation channels. Nuclei counterstained with Hoechst (red), HIV Gag-iGFP/ LTR reporter (green), scale bars = 20 µm.

These data suggest that a CCR5-related mechanism was at play for the HIV-suppressive phenotypes recovered for both miR-138-5p and miR-193-3p. Four of the 6 HIV-suppressive miRNA hits evaluated exhibited more broadly-acting anti-HIV activity, i.e. against both R5 and X4 -tropic HIV variants, suggesting that their mechanism of action is independent of viral tropism. Likewise, the HIV replication-enhancing miRNA mimic hit, miR-34c-3p, exhibited a similar phenotype following X4-tropic HIV infection, while miR-1200 exhibited a higher rate of syncytia formation as compared to negative controls (Figure A4.6 B, Appendix IV). These findings thus confirmed pan-tropic HIV replication modulating activity for the majority of miRNAs evaluated, but also suggested that at least a small proportion of miRNA hits recovered by HCS may be sensitive to HIV viral tropism. A more comprehensive investigation of the impact of viral tropism on the phenotypes recovered by HCS is thus warranted and will likely be pursued in future projects.

4.9 Discussion

HCS recovered 53 miRNA mimics and 4 miRNA inhibitors as potential VRFs while 28 miRNA mimics were revealed to specifically enhance HIV replication. Additionally subsequent validation experiments suggested that the majority of these HIV replication modulating effects may be independent of HIV viral tropism. miRNA target prediction and subsequent pathway analysis recovered 62 functional pathways associated with suppressed HIV replication, and 48 functional pathways associated with enhanced HIV replication. Of these, 38 functional pathways were associated with both replication phenotypes. Furthermore, 23 function pathways were exclusively associated with suppressed HIV replication and 9 exclusively with enhanced HIV replication. Details of selected pathways are described in Figure 4.28.

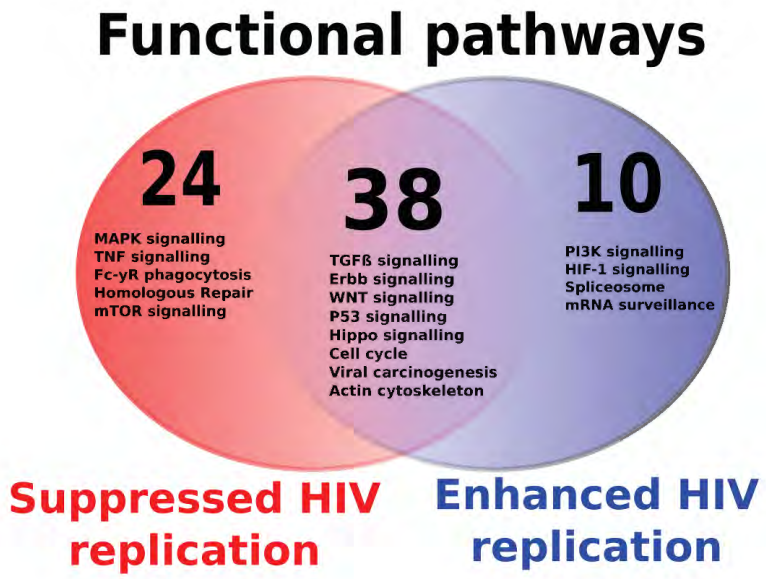

Figure 4.28 Functional pathways associated with enhanced and suppressed HIV replication.

A total of 70 functional pathways were recovered by mirPath analysis. A panel of 38 pathways were recovered for both enhanced and suppressed HIV replication phenotypes, while 24 pathways were associated exclusively with suppressed viral replication, and 10 pathways exclusively with the enhanced viral replication phenotype. Selected pathways of interest are presented for each panel.

Viral carcinogenesis was one of the broader functional processes recovered by mirPath analysis and included a number of specific host signalling cascades and functional outcomes (Figure A4.2, Appendix IV). The high degree of overlap between host factors associated with viral carcinogenesis and those associated here with HIV infection suggests that the virus itself may elicit certain carcinogenic properties within infected cells, or that HIV replication is highly dependent on overlapping molecular cues and signalling events. Characterisation of host miRNAs that are able to modulate viral replication through the regulation of functional pathways associated with viral carcinogenesis could be a lucrative research avenue for the discovery of host miRNAs with anti-HIV therapeutic potential (Wang, 2015). This study has specifically identified 47 host miRNAs that directly affect HIV replication and which target host factors enriched within the viral carcinogenesis pathway. Therefore, these miRNAs may also have therapeutic benefit across a broader range of viral pathogens.

The highest ranked pathway recovered by mirPath analysis for HIV suppressive miRNAs, ‘proteoglycans in cancer’ (reviewed by Connell, 2013) was also the second highest ranked hit recovered for the enhanced HIV replication phenotype. This pathway revealed a high degree of overlap with ‘viral carcinogenesis’ in terms of associated miRNAs, implicated genes and relevant signalling cascades. Of particular interest, a number of the membrane-bound proteoglycans associated with this pathway (e.g. heparan and chondroitin sulfate proteoglycans) were shown to physically interact with

HIV gp120 and p17 in order to mediate HIV binding, entry and activation of T cells (Bobardt, 2004; Poiesi, 2008). This suggests a similar set of interactions occurred in the HCS described here. Likewise 'regulation of the actin cytoskeleton' was also recovered by pathway analysis for both enhanced and suppressed viral replication phenotypes and revealed a high degree of overlap with 'proteoglycans in cancer' and functional pathways associated with bacterial entry and endocytic processes. The miRNA hits associated with these pathways are therefore also likely related to the modulation of cellular signals and re-arrangements of the actin cytoskeleton that are required for HIV entry and nuclear localization of the HIV RTC (see Chapter 1). Indeed, these same factors may also modulate bacterial infection in human cells, underscoring the convergent evolution of intracellular pathogens.

While most of the recovered signalling pathways have previously been widely associated with viral infection and even HIV replication specifically (Brass, 2008; Friedrich, 2011), the role of Hippo signalling in HIV infection remains poorly characterised and mostly unknown (Larsson, 2013). Hippo signalling has classically been associated with the regulation of apoptosis in response to contact inhibition and other environmental cues (reviewed by Pan, 2010) and thus aligns very well with the functional trend observed for other signalling pathways recovered here by mirPath analysis. The Hippo signalling pathway was recovered for both enhanced and suppressed viral replication phenotypes, portending its importance to HIV replication. Notably, data analysis revealed differential regulation of factors specifically associated with the hippo central kinase cascade and transcriptional activity of the Hippo effector proteins YAP/TAZ. This suggests that YAP/TAZ may either directly or indirectly influence transactivation of the HIV LTR. Intriguingly a recent study published only last year demonstrated that KSHV infection enhances the activation and transcriptional activity of YAP/TAZ (Liu, 2015). In the current study pathway analysis posited that KSHV and HIV may employ highly similar mechanisms of host subversion (Figure A4.2, Appendix IV). Furthermore, Vpr regulates the ability of 14-3-3 proteins to interact with their binding partners (Kino, 2005) and 14-3-3 has been well characterized as the cytoplasmic 'anchor' for inactivated YAP/TAZ (Pan, 2010). These findings thus support a model whereby HIV infection may modulate the Hippo signalling pathway in order to regulate the transcriptional activity of YAP/TAZ, and where Vpr is able to subvert Hippo-induced cytoplasmic retention of YAP/TAZ by interacting with 14-3-3 (Figure 4.29). Thus, the findings of this study, for the first time, propose a direct relationship between host miRNAs associated with the Hippo signalling pathway and HIV replication.

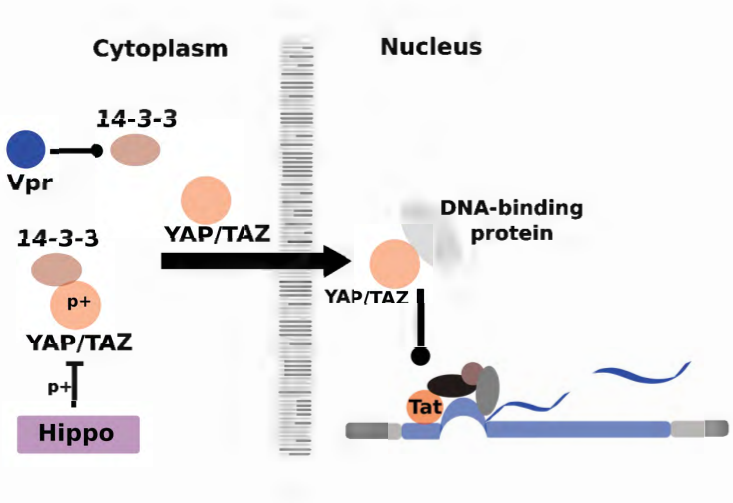

Figure 4.29 Proposed model for Hippo signalling in HIV replication

Typically, YAP/TAZ and 14-3-3 are negatively regulated via Hippo signalling. HIV infection dysregulates Hippo signalling to promote nuclear localisation of YAP/TAZ, in part through the interaction of Vpr with 14-3-3 in the cytoplasm, as well as association of YAP/TAZ with specific DNA-binding partners in the nucleus to modulate HIV LTR activation. miRNA hits recovered for both enhanced and suppressed HIV replication phenotypes directly regulate Hippo kinases, YAP/TAZ, 14-3-3 and the transcriptional coactivators of YAP/TAZ. Circular arrowheads indicate an hypothetical interaction with likely but unknown biological effect.

The homologous recombination directed repair (HDR) pathway was recovered exclusively for the suppressed HIV replication phenotype, implying that dysregulation of host DNA repair processes related to double strand breaks (DSBs) *prior* to HIV exposure may inhibit viral replication. Integration of the HIV genome into that of its host occurs via HIV integrase-mediated DSBs and subsequent ligation which in turn is mediated by host DNA repair machinery (see Chapter 1). Vpr has also been shown to induce DSBs and activation of the ATM/ATR-CHK host DNA damage response, specifically HDR and Rad51 activation (Nakai-Murakami, 2007). In addition the non-homologous end joining (NHEJ) and BER DNA repair pathways have previously been implicated in HIV replication by functional genomic screens (Espeseth, 2011; Genovesio, 2011). Ectopic expression of the Tat-interacting protein, Pur-alpha, suppressed Rad51 foci formation in response to DSBs, while expression of Tat was found to enhance Rad51 expression and HDR in response to DSBs (Wang, 2008). The human DNA damage response is closely related to cell cycle and P53-mediated signalling and both these functional pathways were also recovered by mirPath analysis. Current knowledge has thus positioned the host DNA repair pathway as a critical juncture in HIV-host interactions and this was confirmed by miRNA-based HCS and pathway analysis. Fifteen HDR-related miRNAs were recovered by HCS and a number of Rad51 homologs were enriched as validated targets of those. These miRNAs may therefore represent potential therapeutic agents that are able to inhibit HIV replication through modulation of HDR and

further posit HDR and Rad51 as potential targets for the treatment of HIV (Cosnefroy, 2012).

Importantly, experimental validation confirmed a functional relationship between the DNA damage response and HIV replication in GHOST(3) cells which was initially predicted by mirPath analysis. In accordance with prior art, HIV infection induced a cancer-like survival phenotype in cultured cells in response to lethal levels of chemically-induced DSBs. Surprisingly, priming of GHOST(3) cells with a DNA damage-inducing agent either prior to or during HIV exposure dramatically sensitized host cells towards apoptosis in response to HIV. This HIV-specific toxicity phenotype was further deduced to be associated with viral entry. Furthermore, miRNA-mediated modulation of the DNA damage-associated long noncoding transcript, lincRNA-p21, was proposed as a novel mechanism related to specific 'suppressed HIV replication' phenotypes recovered by HCS, with these phenotypes presumably resulting from miRNA-mediated perturbation of lincRNA-p21 transcriptional and(or) protein binding activity.

The EGFR-mediated signaling cascade was also prevalent within many of the larger functional networks uncovered by pathway analysis. The Erbb signalling pathway specifically was also identified within the top 30 pathways associated with both suppressed and enhanced HIV replication phenotypes (Table A4.3; A4.4). EGFR signalling has been well characterised in many carcinomas where constitutive activation of Erbb signalling results in aberrant cellular proliferation and resistance to apoptosis (reviewed by Normanno, 2006). In addition, nuclear localisation of EGFR (nEGFR) has been shown to promote enhanced DNA damage repair and resistance to both radiation and chemotherapeutic-based treatment strategies through its association with DNA-PKs (Liccardi, 2011). Furthermore, EGFR signalling has been associated with the entry strategies of many viruses, including influenza, where RNAi-mediated suppression of EGFR was demonstrated to inhibit viral entry and replication (Meliopoulos, 2012). Of particular relevance, the rearrangement and subsequent activation of receptor tyrosine kinases (RTKs), like EGFR, within the cell membrane in response to influenza attachment was found to induce downstream signals that were required for viral entry by endocytosis, ultimately resulting in accumulation of viral particles and RTKs within late endosomes (Meliopoulos, 2012). Similar roles for EGFR signalling have also been described for other viruses including hCMV, HCV and vaccinia virus (reviewed by Grove, 2011). In terms of HIV replication, Env, Nef and Tat have been predicted to directly interact with a number of host factors enriched within the Erbb signalling pathway (Evans, 2009). In addition Tat upregulates *TGF-alpha* production in an EGF-dependent manner (Nabell, 1994), while Gag expression inhibits EGFR degradation resulting its accumulation within late endosomes which correlated with enhanced MAPK signalling (Valiathan, 2004). Despite all this data, the functional relevance of EGFR signalling during early stages of HIV infection and its potential role in the HIV-induced DNA damage response are not well characterised, although it seems likely that EGFR-mediated signalling may play a similar role in HIV entry as described for other viruses. This is particularly significant given that the current study has now identified a unique

subset of host miRNAs that are able to functionally modulate HIV replication, at least in part, through regulation of the Erbb signalling pathway.

Notably, the panel of HIV replication modulating miRNAs described in this study likely do not represent an exhaustive list of host miRNAs that are capable of modulating HIV replication. Indeed, the use of the GHOST(3) assay limited the scope of this study to factors that influence HIV replication upto the point of LTR transactivation only. A functional evaluation of host miRNAs that specifically impact the later stages of the viral replication cycle would thus, in combination with the findings of this study, provide a more comprehensive overview of the HIV-modulating capacity of the human miRNAome. The poor functional performance of miRNA inhibitor panels is a common trend that has been well documented and is likely also a contributing factor to the poor characterization of human miRNAs that function as HIV-HDFs. A more intensive validation and optimisation approach geared specifically at miRNA inhibitor uptake and functional impact would thus be advisable for all future screening projects. Specifically the use of methodologies like RNAseq and qPCR may be utilised to validate the efficacy of miRNA inhibitor positive control reagents.

Conclusion

Many years of research have posited miRNAs as critical mediators of the molecular interface between pathogen and host, and these small regulatory molecules have also been described to exhibit broad functional control over almost all cellular processes (reviewed by Huang, 2011; Tan, 2015). A number of studies have reported perturbations in host miRNA expression profiles in response to HIV infection but the functional relevance of these variations and the potential of each host miRNA to modulate replication dynamics of HIV have not been well characterized. Indeed, less that 30 host miRNAs have been described to functionally modulate replication (reviewed by Barichievy, 2015). In addition, HCS has emerged as a powerful tool delineate functional relevance of the host miRNAome within various cellular models of pathology, including viral infection (Santhakumar, 2010; Meliopoulos, 2012; Lemons, 2013). The principal aim of this study was therefore to utilise a HCS-based approach to characterize the functional relevance of host miRNAs in HIV replication.

This study represents the first known description of a large scale functional screen to identify specific host miRNAs that modulate HIV replication and its findings have, i) successfully demonstrated the utility of a novel HCS pipeline developed for this study, ii) led to the identification of 85 novel host miRNAs that regulate HIV (Figure 4.30) and iii) facilitated the identification of 70 host functional processes and pathways upon which HIV replication is highly dependent and thus potentially susceptible to therapeutic intervention (Figure 4.30). Specifically, this study has identified 53 host miRNAs as novel potential VRFs and 5 host miRNAs as potential HDFs. Furthermore, 28 host miRNAs were specifically identified that enhance HIV replication. Notably, novel functional roles

were uncovered for the miR-200 family of miRNAs and the Hippo signalling pathway as potential mediators of HIV-host interactions. Normal activity of the PI3K, spliceosome, mRNA surveillance and HIF-1 functional pathways were associated with suppression of HIV replication. Conversely successful HIV replication was found to be highly dependent on the normal activity of HDR, MAPK, TNF and mTOR pathways.

Furthermore, HIV-modulating miRNAs recovered by this study constitute valuable intellectual property which could be exploited for commercial purposes. Specifically, HIV-suppressive miRNAs recovered by this study may be exploited as therapeutic agents for prevention and(or) treatment of HIV infection. HIV replication-enhancing miRNAs on the other hand may provide a valuable clinical resource for the activation and eradication of latent viral reservoirs, or serve as functional tools to increase yields of virus in cell culture-based vaccine production models. Finally, a number of functional pathways and miRNA targets identified in this study are also prevalent targets of pharmaceutical agents used to treat various pathologies. Many of these compounds may thus also exhibit anti-HIV properties and represent prime candidates for drug repurposing as novel ARVs. The overall outcomes of this study therefore represent a significant and novel contribution to current HIV research efforts, and will likely also provide a platform for many future studies on HIV-host interactions.

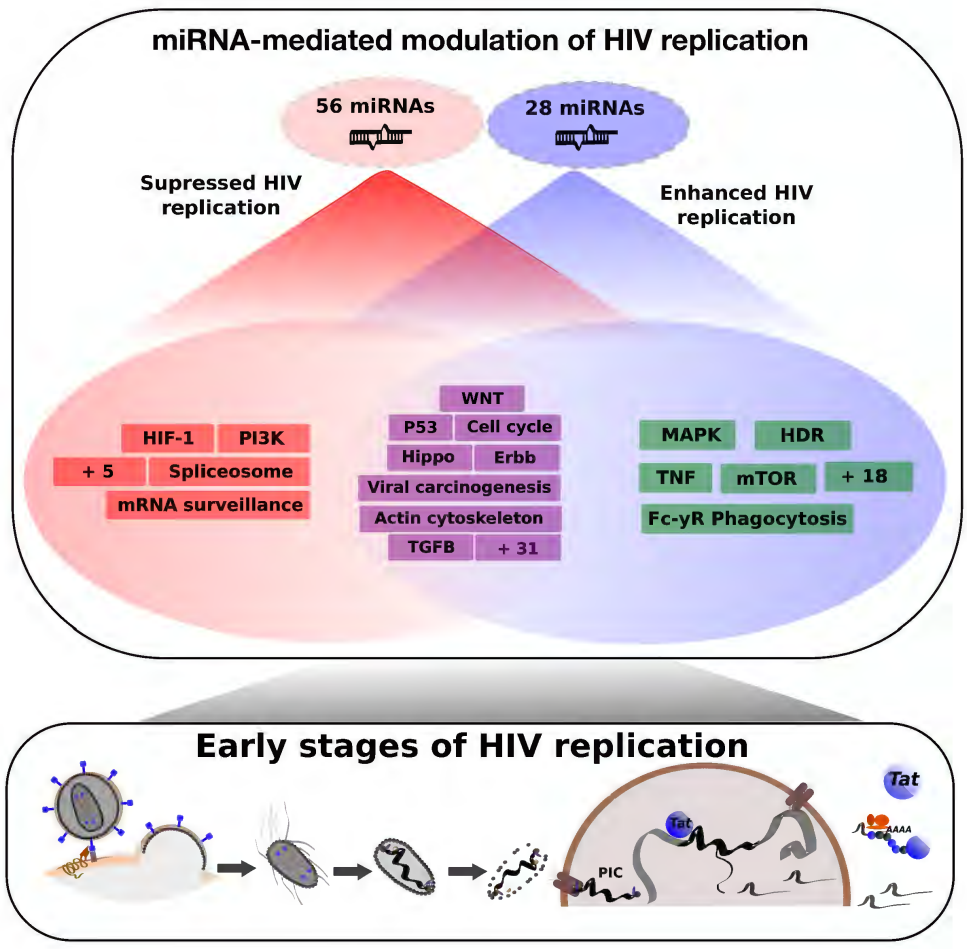

Figure 4.30 Summary of HCS and pathway analysis

HCS identified 53 host miRNAs that suppressed viral replication and 28 host miRNAs that enhanced HIV replication. Of these, 9 functional pathways were associated exclusively with the natural suppression of HIV replication (red blocks) and 23 functional pathways were found to support HIV replication (green blocks). In addition, 39 functional pathways were associated with both enhanced and suppressed viral replication phenotypes (purple blocks).

Chapter 5: miRNA-informed HCS uncovers novel anti-HIV activity for pharmaceutical compounds and reveals novel functional targets associated with HIV replication

5.1 Background

HCS and pathway analysis recovered 88 host miRNAs that potentially regulate >5000 host genes across 70 functional pathways to influence HIV replication (Chapter 4). The relatively large number of hits recovered and potential complexity and cost associated with a comprehensive miRNA-target validation approach (discussed in Chapter 3) prompted pursuit of an alternative hit validation strategy. To this end, a series of orthogonal compound-based validation screens were undertaken to determine whether small molecule inhibitors targeted to specific functional processes recovered by mirPath analysis (Chapter 4) could i) recapitulate the observed miRNA-related HIV replication phenotypes, and ii) identify novel anti-HIV therapeutic applications for these compounds

Many of the functional processes recovered by mirPath analysis converged on HIV-mediated subversion of host pathways related to cellular proliferation, apoptosis, DNA damage repair and cell cycle (see Chapter 4). In addition a high number of host factors related to viral carcinogenesis were recovered thus portending a close relationship between HIV infection and a cancer-like molecular phenotype in infected GHOST(3) cells. This relationship was subsequently confirmed by experimental data demonstrating deregulated P53 transcriptional activity and aberrant cell survival in response to DNA damage in HIV-infected GHOST(3) cells, as compared to uninfected controls (Chapter 4).

The summation of these observations suggested that modulation of cancer-associated functional targets may potentially impact the replication dynamics of HIV. Thus, the HCS workflow utilised in Chapter 4 was specifically adapted for compound-based screening (see Chapter 3) that included a panel of small molecule inhibitors, and a number of FDA-approved chemotherapeutic compounds, to assess their anti-HIV activity.

These screens were executed in three formats referred to as ‘pre-HIV exposure’, ‘post-HIV exposure’ and’ Drug Only’ (Figure 5.1). The divergent effects observed for Etoposide treatment administered either *prior to* or *following* HIV exposure was the primary motivation for these different screening formats as it revealed that the phenotypic outcome of pharmaceutical intervention may vary between pre- and post-HIV exposure treatments.

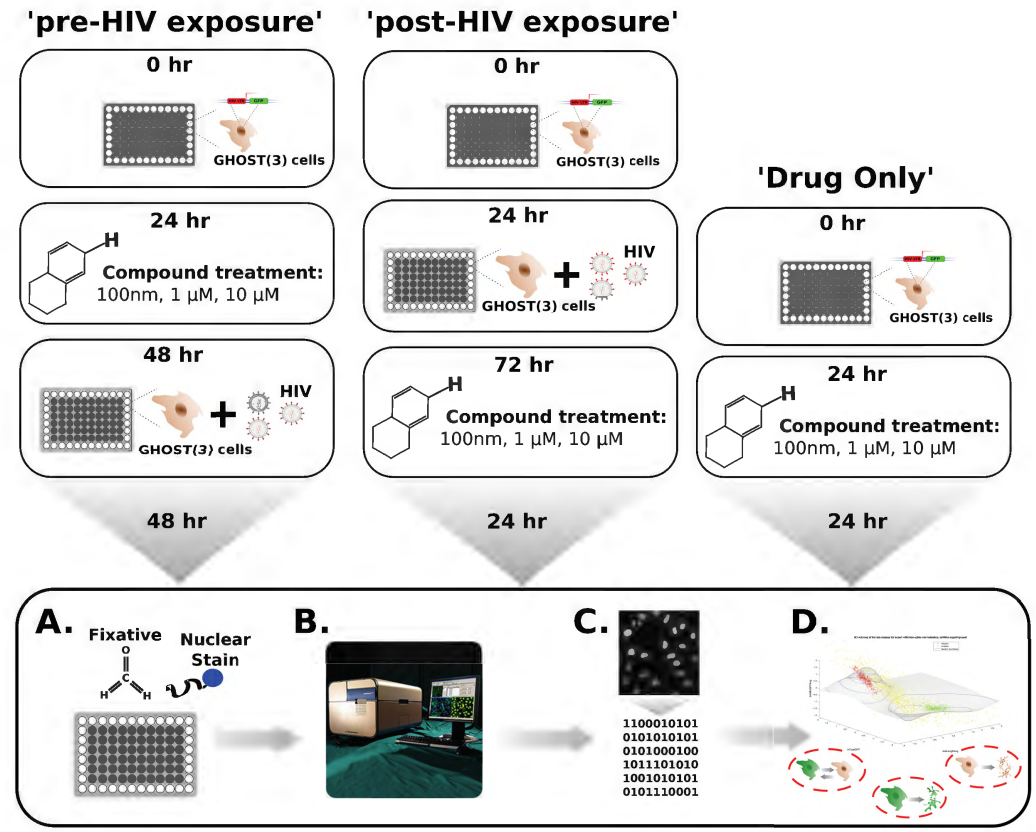

Figure 5.1 Experimental plan for compound screening formats

GHOST(3) cells were seeded in µClear 96 well plates at a density of 5000 cells/well at 0 hr for all screen formats. Cells were treated with drugs 24hr post-seeding for **pre-HIV exposure** screens. Cells were then exposed to $PSG3^{BAL}$ for 48hr before being processed for imaging. In the **post-HIV exposure** screen format, 24hr following seeding, cells were exposed to $PSG3^{BAL}$ for 48hr. Cells were then treated with compounds for 24hr before sample processing. In the **Drug Only** screen format, cells were treated with compounds for 24hr before being processed for imaging. **A)** Cells were fixed in 4% PFA and nuclei were counterstained with Hoechst. **B)** Plates were imaged on the IXU system, 4 FOVs were acquired per well at 20x for the 405 and 488 excitation channels. **C)** Images were transformed into numerical data through feature extraction, and **D)** the numerical data was processed and analysed within the HCStratomineR data mining tool to identify compounds that produced phenotypes of interest.

Two targeted compound libraries (Kinase Inhibitor set and Oncology set) comprising a total of 293 small molecules were screened at three concentrations each (100nM, 1µM and 10 µM) across the three screening formats. This allowed for characterization of the following functional classes of small molecules: i) those that protect host cells against HIV infection or suppress HIV replication when administered prior to HIV exposure, ii) those that suppress HIV replication within cells stably infected by HIV, iii) those that

sensitise host cells to apoptosis specifically in response to HIV exposure/infection, and iv) those that can no longer induce apoptosis due to the presence of HIV (Figure 5.2). Approximately 11 000 individual experimental wells, including ~7000 individual infection reactions, were prepared by hand, and more than 90 000 images were acquired and analysed to identify small molecules of interest.

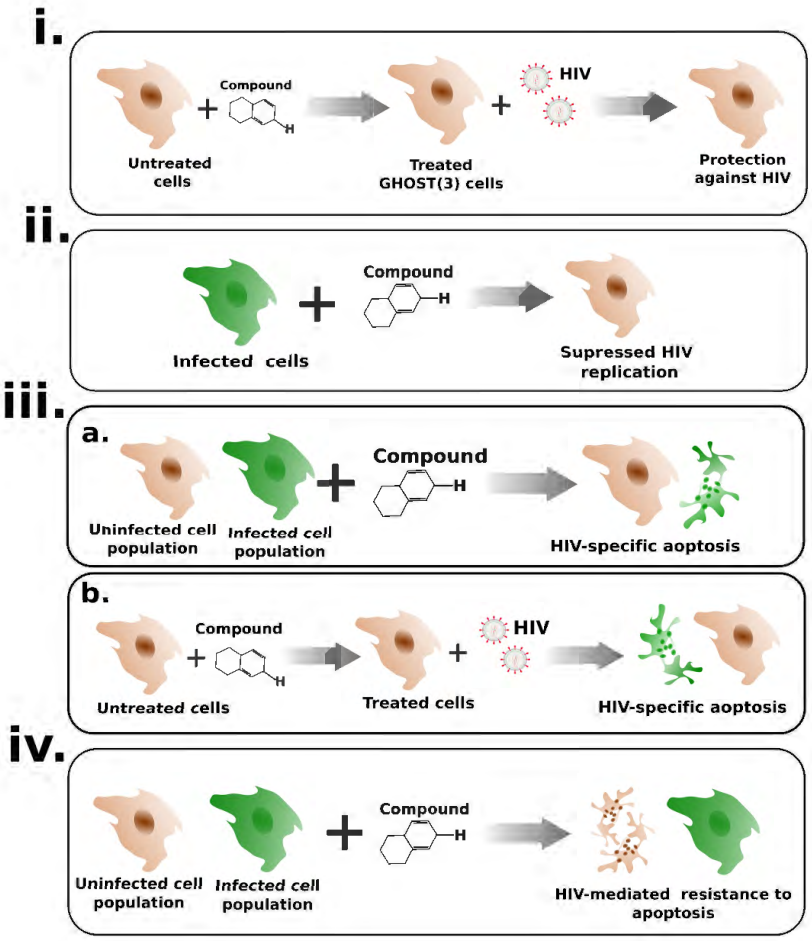

Figure 5.2 Functional hit classes identified by small molecule drug screening and high content image analysis.

i) Small molecules that protect host cells against HIV infection in the **pre-HIV exposure** screen format. **ii)** Small molecules that suppress LTR activation in the **post-HIV exposure** screen format. **iii) a.** Small molecules that were not toxic in the **drug only** screen but exhibited toxicity in the **post-HIV exposure** screen format. **b.** Small molecules that were not toxic in the **drug only** screen format but sensitized cells to apoptosis following HIV exposure in the **pre-HIV exposure** screen format. **iv)** Compounds that exhibited toxic effects in the **drug only** screen format but not in the **pre- or post-HIV exposure** screen formats. HIV infected cells (green), uninfected cells or HIV suppressed phenotypes (brown).

5.2 Results

5.2.1 HCS quality control

As with miRNA screen-derived data, visual inspection of graphical data outputs in HCstratomineR were utilised to perform a number of quality control verification steps for the various compound screens. Briefly, where applicable performance of the cellular assay was quantified by Z' factor analysis using 'inTotalGFP' and 'Total Cell Area' feature scores. In addition, plate rotations and well-specific biases were evaluated by distribution plots of 'inTotalGFP' and 'Total Cell Area' feature scores for all experimental wells/plates. Individual datasets were generated for each replicate (n=2 for Drug only screens and n=3 for all other screens), from each screen format, across each drug concentration (100nM, 1μM, 10μM) and for each compound library. Replicate datasets were then analysed for a single screening experiment with each concentration, screen format and drug panel treated as separate screens during image analysis. GHOST(3) cells treated with an appropriate dilution of DMSO only were utilized as negative controls. Similarly to the screen discussed in Chapter 3, Maraviroc and Raltegravir (ARV) treatments (10 μM) were utilized here as positive phenotypic controls for suppressed HIV replication.

Distribution plots for the 10 μM Kinase Inhibitor drug panel screen in the 'pre-HIV exposure', 'post-HIV exposure' and 'drug only' formats are presented and discussed below, while corresponding plots for the Oncology drug panel screen are presented in Appendix V in the interest of brevity. The pre-HIV exposure kinase datasets revealed no significant variation between positive and negative controls as a function of average cell density per well (Total Cell Area), with a negative Z' factor range obtained for all experimental plates (Figure 5.3 A). Experimental treatment wells exhibited a broad distribution below the average distribution range of phenotypic controls, implying that specific compound treatments may have had a negative effect on cell viability (Figure 5.3A). Well location-based analysis spanning all experimental plates and replicates revealed that no plate rotations or well-specific directional biases had impacted the cell seeding step (Figure 5.3B), and all positive and negative control well locations exhibited a consistent and tight distribution range across all experimental plates and replicates.

Most of the experimental well locations exhibited distribution trends similar to that of the phenotypic control well locations, but a number of experimental well locations also exhibited broad distributions indicative of functional effects of specific compounds on cellular density/viability (Figure 5.3B). Scatterplots based on 'inTotalGFP' scores revealed significant variability between distribution ranges of the negative and positive phenotypic controls across all replicates, and this was confirmed by an acceptable Z' factor range of between 0.3-0.5 for all experimental plates (Figure 5.3B). In addition experimental treatments exhibited broad distribution ranges exceeding the upper and lower distribution limits of negative control wells (Figure 5.3C). This suggested that a

number of experimental treatments had variable effects on GFP reporter signal output. Well location-based analysis confirmed consistent and distinct distribution ranges for well locations corresponding to the positive and negative controls (Figure 5.3 D). No directional biases or plate rotation-related effects were noted and a number of well locations corresponding to specific experimental treatments exhibited broad distribution ranges suggestive of fluctuations in the GFP reporter activity related to treatment with specific compounds (Figure 5.3D).

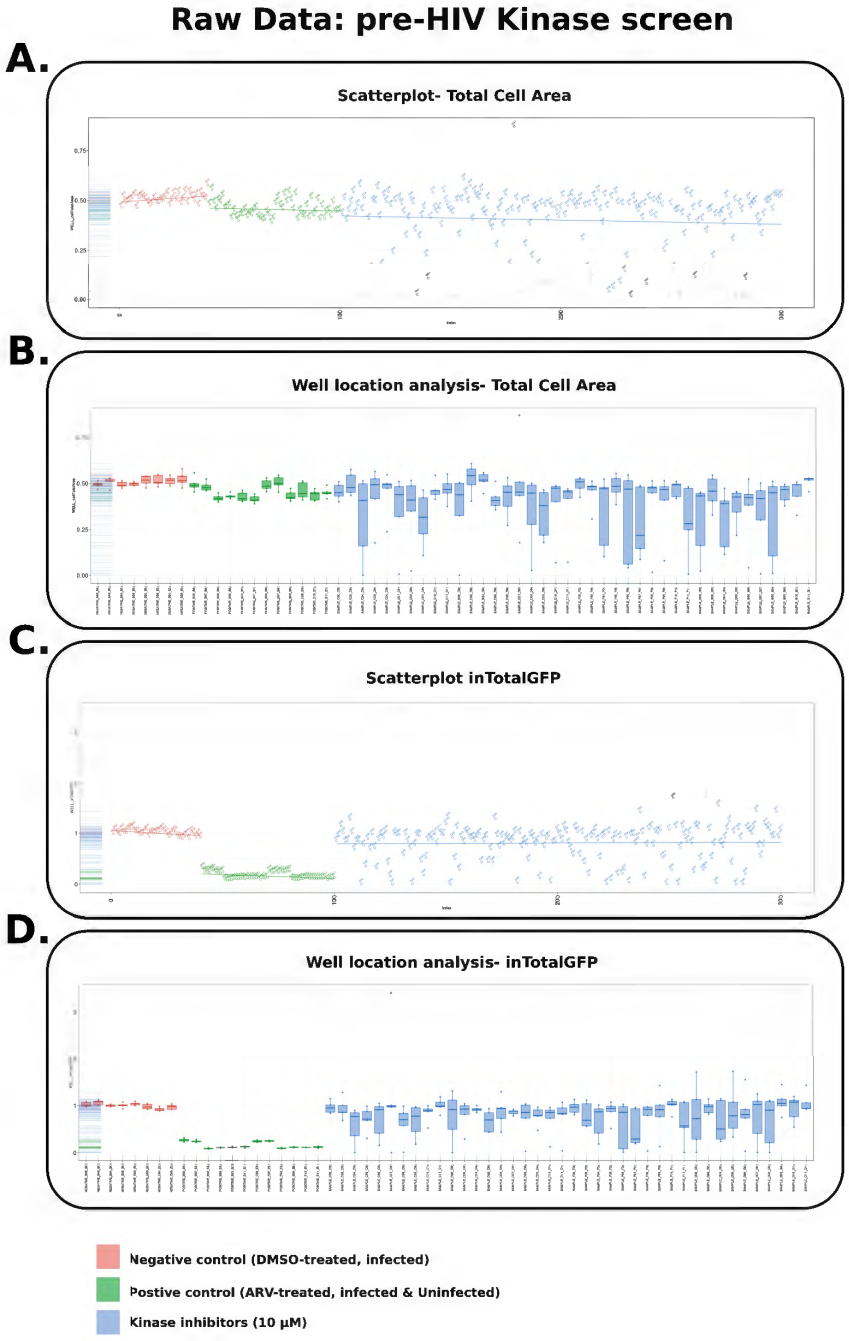

Figure 5.3 Unprocessed data distribution plots for all replicates of 'pre-HIV exposure' Kinase Inhibitor panel (10µM).

A) Scatterplot representing the distribution of individual experimental controls and treatments across three screen replicates in relation to the extracted Total Cell Area feature scores. No significant variability in Total Cell Area was noted between positive (green) and negative (red) controls. Experimental treatments (blue) exhibited a broad distribution range that extended beyond the lower limits of phenotypic controls suggesting strong treatment-related effects on cell density. **B)** Box plot representing the average Total Cell Area scores obtained for specific well locations across all experimental plates and replicates. Negative (red) and positive (green) control well locations exhibited consistent distribution ranges that were not distinct from each other. Well locations corresponding to experimental treatments exhibited broader distribution ranges. **C)** Scatterplot representing the distribution of individual experimental control and treatment wells across three screen replicates in relation to the extracted 'InTotalGFP' feature scores. Positive (green) and negative (red) controls exhibited distinct distribution ranges from each other. Experimental wells (blue) exhibited broader distribution ranges beyond the lower limits of negative controls suggestive of treatment-related effects LTR reporter activity. **D)** Box plot representing the average 'InTotalGFP' scores obtained for specific well locations across all experimental plates and replicates. Negative (red) and Positive (green) control well locations exhibited consistent and distinct distribution ranges. Well locations corresponding to experimental treatments exhibited broader distribution ranges.

The second dataset, that of the post-HIV exposure screen, showed negative Z' factor values for experimental plates in relation to Total Cell Area feature scores. These values were not as high as those obtained for the pre-HIV exposure dataset, suggesting a higher level of variability was present between positive and negative control phenotypes in the post-HIV exposure screen (Figure 5.4A). This variance was however non-significant (based on Z' factor values). An acceptable Z' factor range between 0.3 and 0.7 was obtained for all experimental plates in relation to 'InTotalGFP' scores. This was confirmed by visual inspection of the data distribution trends, which revealed a clear separation between positive and negative controls as well as a broad distribution range for experimental treatments (Figure 5.4 C). Well location-based analysis confirmed that directional biases and plate rotations had not impacted the dataset, and phenotypic control well locations exhibited consistent and tight distributions (Figure 5.4D). Notably, the effect of compounds treatments as a function of distribution range was not as prominent in the post-HIV exposure screen format compared to the pre-exposure dataset (Figure 5.3), suggesting that HIV infection may attenuate the general functional impact of compound treatments with regards GFP reporter activity and (or) cell viability.

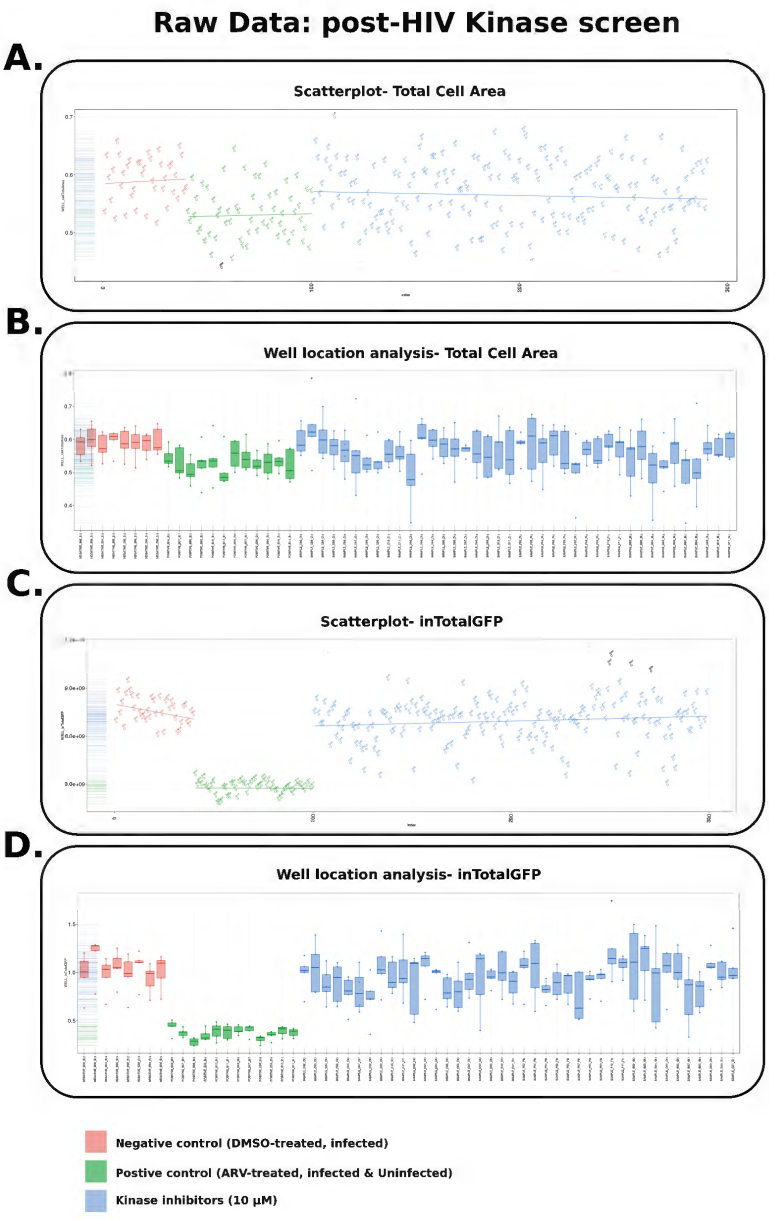

Figure 5.4 Unprocessed data distribution plots for all replicates of 'post-HIV exposure' Kinase Inhibitor panel (10µM).

A) Scatterplot representing the distribution of individual experimental controls and treatments across screen replicates in relation to the extracted Total Cell Area feature scores. The positive (green) and negative (red) controls exhibited noticeable but non-significant variation in their respective distribution ranges. Experimental wells (blue) exhibited a broad distribution range suggestive of treatment-related effects on cell density. **B)** Box plot representing average Total Cell Area scores obtained for specific well locations across all experimental plates and replicates. Negative (red) and positive (green) control well locations exhibited consistent and tight distribution ranges. Well locations corresponding to experimental treatments exhibited broad distribution ranges. **C)** Scatterplot representing the distribution of individual experimental control and treatment wells across screen replicates in relation to the extracted 'InTotalGFP' feature

scores. Positive (green) and negative (red) controls exhibited distinct distribution ranges. Experimental wells (blue) revealed broader distribution ranges, mostly beyond the lower limits of the negative controls suggestive of negative treatment-related effects on LTR reporter activity. **D)** Box plot representing average lnTotalGFP scores obtained for specific well locations across all experimental plates and replicates. Negative (red) and positive (green) control well locations exhibited consistent and distinct distribution ranges. Well locations corresponding to experimental treatments exhibited broader distribution ranges exceeding those of the negative controls.

For the last compound screen, that of the Drug Only dataset, Total Cell Area distribution plots were utilised to monitor general data distribution trends (Figure 5.5A) and to confirm that plate rotations and directional biases had not impacted individual datasets (Figure 5.5B).

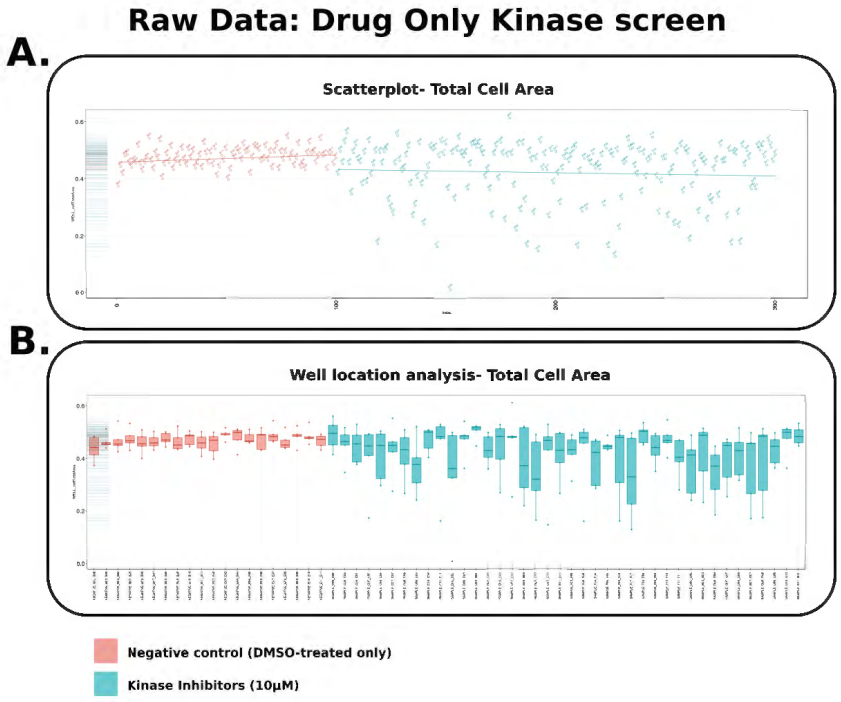

Figure 5.5 Unprocessed data distribution plots for all replicates of 'Drug Only' Kinase inhibitor panel (10μM) based on Total Cell Area feature scores

A) Scatterplot representing the distribution of individual negative controls and treatments across three screen replicates in relation to the extracted Total Cell Area feature scores. Negative controls (red) did not differ in their distribution ranges. Experimental treatments (green) exhibited a broad distribution range. **B)** Box plot representing the average Total Cell Area scores obtained for specific well locations across all experimental plates and replicates. Negative control well locations (red) exhibited consistent and tight distribution ranges irrespective of their positions on experimental plates. Well locations corresponding to experimental treatments (green) exhibited broad distribution ranges, with no clear pattern or bias.

Overall, similar distribution trends were observed for all 10 μM datasets (Appendix V, Figures A5.1-A5.3), with the exception that a larger number of compounds exhibited strong cytotoxic effects on GHOST(3) cell viability in the 'pre-HIV exposure' and 'drug only' screen formats. As with the Kinase Inhibitor panel dataset however, this effect was attenuated in the post-HIV exposure screen format (Appendix V). In addition, data quality including Z' factor analysis and visual inspection of data distribution profiles were verified for all screening-derived datasets.

5.2.2 Normalisation and feature retention for hit selection

Extracted feature scores were normalized against those of the negative controls on a per plate basis for all compound screens. Normalized feature plots were then evaluated by visual inspection to identify features that were descriptive of the variability between positive and negative control phenotypes for 'pre-HIV exposure' and 'post-HIV exposure screens'. All features acquired in the Hoechst channel were considered for 'Drug only' toxicity analysis. Features which did not meet these criteria, or exhibited missing values, or skewed distributions, were excluded from subsequent analyses.

A general dose response phenotype was observed for normalized Total Cell Area and InTotalGFP feature plots for all three compound concentrations (10 μM, 1 μM and 100 nM) across all screen formats and for both drug panels. Normalized feature plots recovered for the Kinase Inhibitor drug panel screens are presented in Figure 5.6 as an example. Briefly, a number of compounds exhibited significant effects on cell density (Figure 5.6A) and GFP reporter signal output (Figure 5.6B) at the 10 μM concentration as evident by the non-uniform distribution patterns recovered for experimental treatments (blue bars). This effect was noticeably diminished at 1 μM (reduced variability within experimental treatment distributions) and was mostly abrogated at 100 nM treatments, as evident by the uniform distribution patterns recovered for experimental treatments and Negative controls (Figure 5.6). This concentration-dependent response was best exemplified by the Total Cell Area plots obtained for the Drug Only screen format (Figure 5.6C).

In addition, normalized Total Cell Area feature plots revealed overlapping distribution patterns for positive and negative controls at each of the concentrations screened in both pre- and post-HIV exposure formats (Figure 5.6A). Conversely normalized InTotalGFP plots revealed a clear bimodal distribution and separation of positive and negative controls across all screen formats and treatment concentrations (Figure 5.6B). Initially, the 10 μM InTotalGFP distribution plots for both the pre- and post-HIV exposure formats were noticeably 'left-shifted' with respect to the median cut off in each plot, with this effect most pronounced in the post-HIV treatment (Figure 5.6B). This was attributable to a single compound that was highly autofluorescent thus resulting in an elevated and outlying GFP signal readout which distorted the distribution of these plots (Figure 5.6B). As a further point of interest, the 10 μM post-HIV experimental treatments

exhibited a significantly more uniform distribution when compared to the 10 µM pre-HIV experimental treatments, implying that HIV infection may in general attenuate the functional impact of compounds on cell viability (Figure 5.6A). Overall, similar trends were recovered for the normalized Oncology drug panel feature plots and these are presented in Appendix V, Figure A5.4.

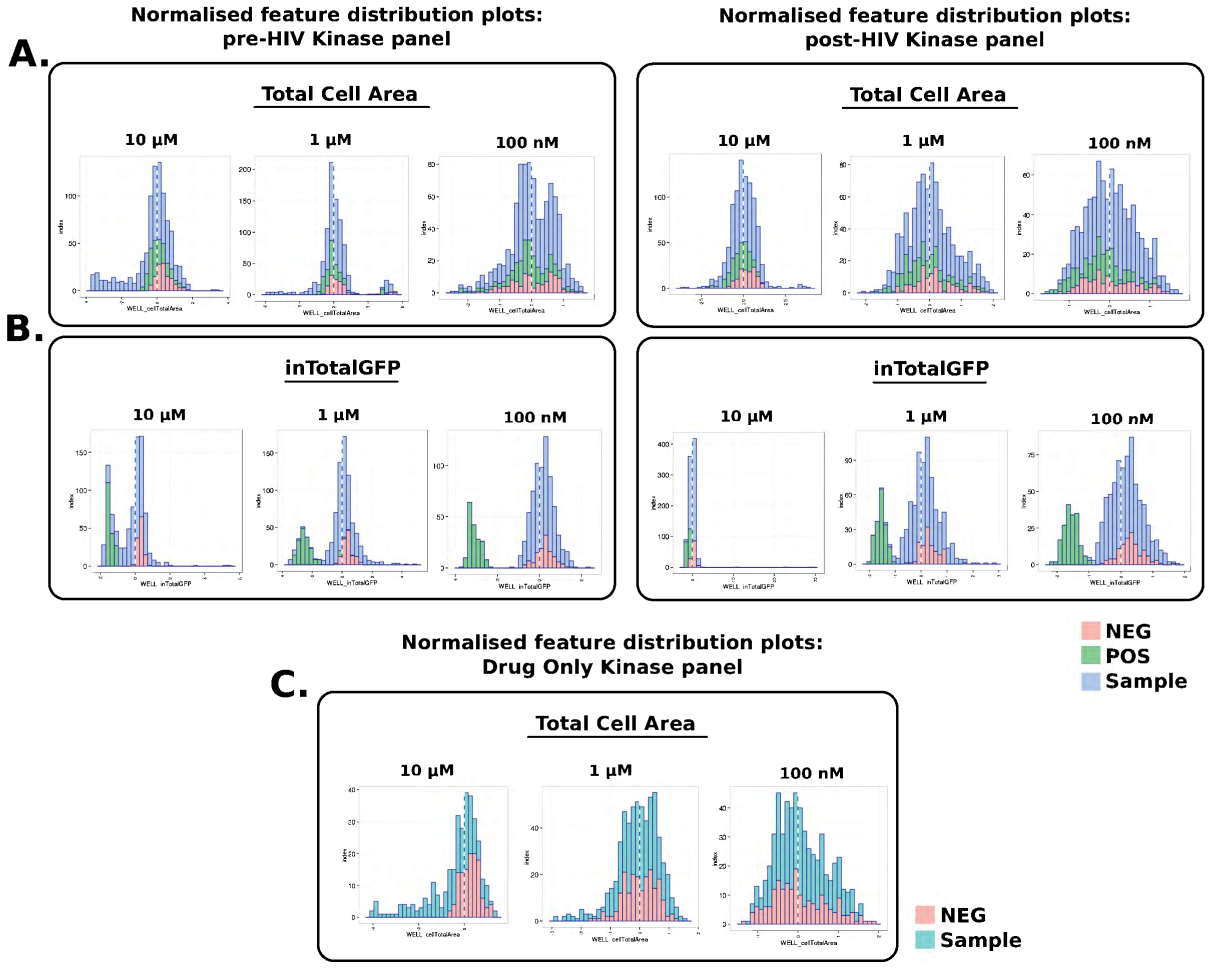

Figure 5.6 Normalized feature plots for Kinase Inhibitor drug panel screens

A) Normalized Total Cell Area distribution plots for pre-HIV and post-HIV treatment screens at 10 µM, 1 µM and 100 nM compound concentrations. **B)** Normalized InTotalGFP distribution plots for pre-HIV and post-HIV treatment screens at 10 µM, 1 µM and 100 nM compound concentrations. **C)** Normalized Total Cell Area distribution plots for Drug only screens at 10 µM, 1 µM and 100 nM compound concentrations. DMSO only controls (NEG), ARV-treatments (POS), Experimental treatments (sample).

5.2.3 Hit Selection and triage

Normalized feature scores were subjected to MDS or PCA-based data reduction in order to create factors that best summarised the relationships between them. Unique factors were generated for each screening dataset although they followed a general trend with regards to the screen format. Factors utilized in analysis of the Kinase Inhibitor drug panels screened at 10 μM are presented in Appendix V, Figure A5.5 as an example. Factor-based analysis was then applied to experimental datasets and either PCA-DFN or MDS-DFN based hit selection methods were applied to identify compounds that produced phenotypes of interest (Figure 5.2). Briefly, the combined phenotypic distance scores between replicates were used to define compounds that exhibited phenotypic profiles which were significantly ($p<0.05$) distant from negative controls. These compounds were then ranked by combined InTotalGFP scores, to identify compounds that suppressed LTR activity (>50%), or by combined Total Cell Area scores to identify compounds that were highly toxic (Combined Total Cell Area score < 0.1).

The pre-HIV and post-HIV exposure screen formats thus allowed for identification of i) compounds that could suppress HIV LTR activity, and ii) compounds that were toxic in either screen format. The 'Drug only' screen format allowed for establishment of baseline toxicity effects for all compounds, and the toxic hits recovered by this screen format were used in a comparative analytical approach to differentiate between compounds that were broadly cytotoxic and those that had toxic effects specifically in response to HIV exposure/infection (HIV-specific toxicity). In addition identification of compounds that were highly toxic in the 'Drug only format' but not in the HIV exposure screen formats allowed for the recovery of compounds whose natural apoptotic activity was attenuated by HIV infection (Mitigated toxicity).

The hits recovered for each drug panel were then combined to obtain discrete lists of compounds related to each functional class of interest (Figure 5.7). Briefly, high content image analysis recovered 8 unique compounds which significantly suppressed LTR reporter activity in the 'pre-HIV exposure' screen format (Figure 5.7, Red), and 5 compounds that exclusively suppressed reporter activity in the 'post-HIV exposure' screen format (Figure 5.7, Blue). Only four compounds (Ponatinib, SNS-032 and two versions of Flavopiridol) suppressed HIV replication in both the pre-HIV exposure and post-HIV exposure screen formats. Six compounds were recovered for the mitigated toxicity phenotype and 2 of these, NVP-TAE684 and Dactinomycin, were also recovered as HIV-suppressive hits in the 'post-HIV exposure' screen format (Figure 5.7, Grey). The largest number of hits was recovered for the HIV-specific toxicity phenotype where 28 compounds were found to specifically sensitize host cells to apoptosis in response to HIV exposure/infection (Figure 5.7, Green). Four of these 28 compounds were also recovered as HIV-suppressive hits in the post-HIV exposure screen format, namely A-674563, SNS-032 and both versions of Flavopiridol.

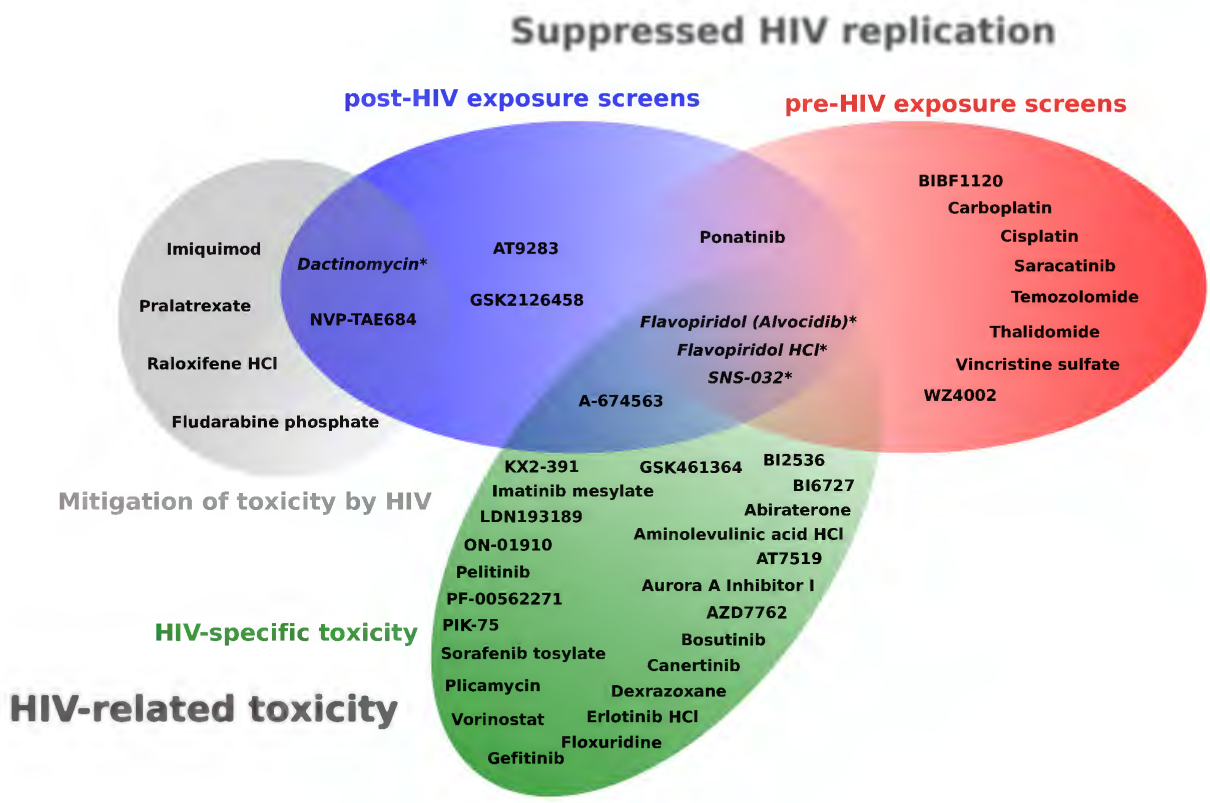

Figure 5.7. Compound screen hits recovered by HCS and grouped by phenotypic class

Suppressed HIV replication hits

Visual inspection was utilized to confirm the recovered hit classifications and examples of HIV-suppressive hit phenotypes from the pre- and post-HIV exposure screen formats are presented in Figure 5.8 below. Briefly, Ponatinib suppressed HIV replication in both screens, while BIBF1120 and Temozolomide were recovered as hits exclusively for the pre-HIV screen format (Figure 5.8 A-D). Likewise A-674563 and NVP-TAE684 were recovered as HIV-suppressive hits in the post-HIV exposure screen format only (Figure 5.8 E & F).

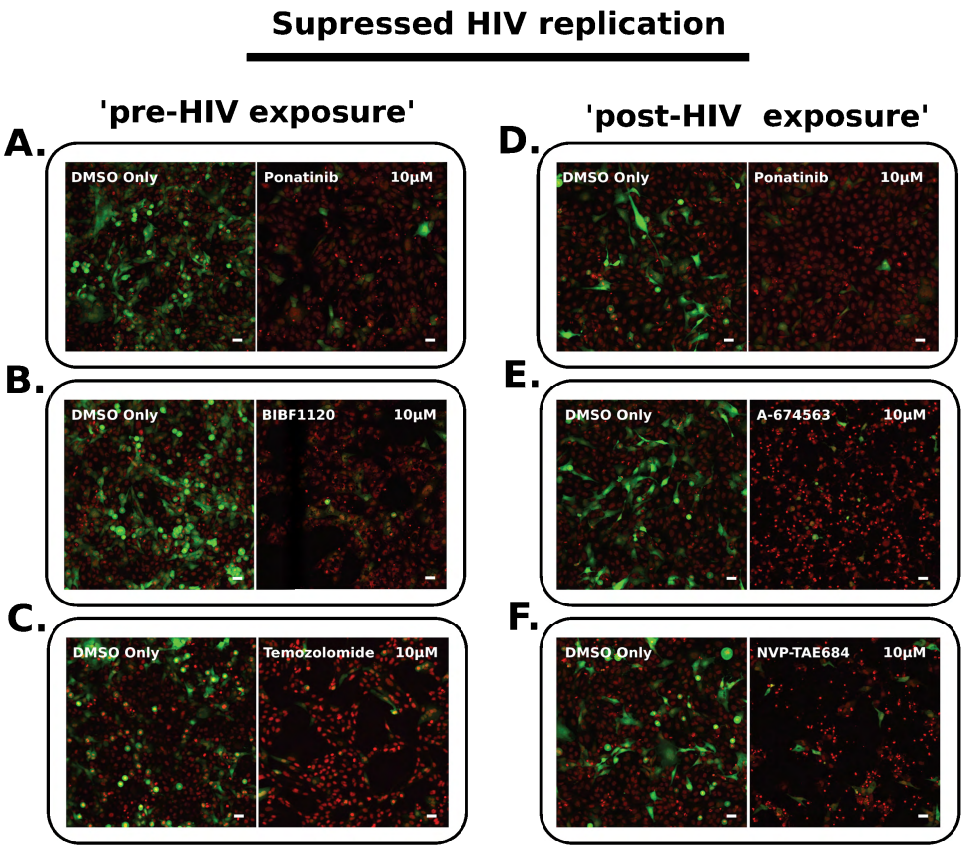

Figure. 5.8 Examples of HIV-suppressive compounds recovered by HCS for pre- and post-HIV exposure treatments.

Hits characterised within this functional class exhibited significantly reduced GFP expression compared to the appropriate plate-specific negative control (DMSO only). **A-C**: HIV-suppressive phenotype recovered for the pre-HIV exposure screen format. **D-E**: HIV-suppressive phenotype recovered for the post-HIV exposure screen format. 'DMSO only' images were obtained from a negative control well on the same experimental plate as the compound treatments. Images represent an overlay of acquisitions from the 405 and 488 excitation channels from a single FOV. GFP/LTR activation (green), nuclei counterstained with Hoechst (red). Scale bars = 20 μm.

Ponatinib was one of the most promising novel anti-HIV drug candidates recovered by HCS as it exhibited significant suppression of HIV replication in both the pre- and post-HIV exposure screen formats with little to no effect on GHOST(3) cell viability (Figure 5.8 A & D). Ponatinib is a potent inhibitor of the oncogenic BCR-ABL fusion protein that has also been described to inhibit SRC kinases and various receptor kinases including PDGFR, VEGFR and FGFR (Frankfurt, 2013). Ponatinib received accelerated approval from the FDA in 2012 but is currently limited to treatment of patients who cannot be treated with other tyrosine kinase inhibitors (TKIs), including patients with malignancies harbouring a T315I TKI resistance mutation (Gainor, 2015). The significant HIV-suppressive activity of ponatinib suggests an important role for BCR, ABL and SRC kinase signalling activity in progressive HIV replication, Indeed, SRC kinases have been previously associated with cell to cell transfer of HIV from dendritic cells to T

lymphocytes and the subsequent endocytic processes governing viral entry (Gilbert, 2007). Likewise ABL kinases have been implicated as HDFs which mediate actin rearrangements during HIV entry, specifically the membrane fusion step (Harmon, 2010). This is also supported by miRNA pathway analysis which identified regulation of the actin cytoskeleton and a number of cytoplasmic kinases as functional targets associated with miRNA-mediated modulation of HIV replication (Chapter 4).

While the HIV-entry associations described for Ponatinib targets may explain the associated phenotype in the pre-HIV-exposure screen format, the HIV-suppressive effect of Ponatinib in the post-HIV exposure screen format cannot be explained by inhibition of viral entry. Instead, this latter phenotype suggests a potential role for BCR, ABL and SRC kinases in transactivation of the viral LTR or alternatively, that the HIV-suppressive activity of Ponatinib may be related to its functional effect on other targets, including viral proteins. BIBF1120, also known as Nintedanib (marketed as Vargatef) is an FDA-approved kinase inhibitor with documented activity against VEGFR, PDGFR and FGFR (Hilberg, 2008). Notably these specific receptor kinases are also targets of Ponatinib, suggesting a potentially conserved mechanism of action related to inhibition of these receptor kinase signaling cascades and the suppressed viral replication phenotypes recovered for both Ponatinib and BIBF1120 (Figure 5.7). Temozolomide on the other hand is an FDA-approved DNA alkylating agent that induces DNA damage and apoptosis in a mismatch repair-dependent manner (Zhang, 2012). Notably, the apoptotic activity of Temozolomide is antagonised by HDR, specifically the activity of RAD51 and BRCA2 (Quiros, 2011) which were all implicated in miRNA-mediated suppression of HIV replication (Chapter 4). Furthermore, Temozolomide has previously been described to enhance the chemotherapeutic activity of BCR-ABL inhibitors (Milano, 2009), thus suggesting that it may also represent a promising candidate for combination therapy with Ponatinib or BIBF1120 for the suppression of HIV replication.

A-674563 is an AKT inhibitor (Okuzumi, 2010) which induces caspase-3/9 activation and apoptosis through functional inhibition of AKT and sphingosine kinase 1 (Xu, 2016). TAE684, also known as NVP-TAE684, was first described as an inhibitor of the ALK1 receptor tyrosine kinase (RTK), which is associated with the TGFß signalling pathway (Galkin, 2007). In addition, Leucine-rich repeat kinase 2 (LRRK2) was described as a functional target of TAE684 activity (Smith, 2005). Exclusive recovery of both A-674563 and TAE684 in the post-HIV exposure screening format suggests that AKT and TGFß -mediated signalling is more relevant for sustained transactivation of the HIV LTR following viral integration as opposed to earlier stages of the viral life cycle. Notably, the TGFß signaling pathway and many of its associated factors were also recovered by miRNA pathway analysis (Chapter 4).

Suppressed HIV replication hits below 10 μM

Only 4 compounds were observed to exhibit significant HIV-suppressive activity at 1 μM (Figures 5.9 and 5.10) while no compounds were found to be effective at 100 nM. Three of these compounds, (SNS-032, Flavopiridol HCl and Flavopiridol) were highly toxic in the 10 μM screens, but exhibited HIV-suppressive phenotypes with attenuated cytotoxicity at 1 μM (Figure 5.9). SNS-032 is a CDK inhibitor with documented efficacy against CDK9 and is currently under phase I clinical investigation (Chen, 2009). Flavopiridol, also known as Alvocidib, is a pan-CDK inhibitor currently under phase II clinical trials for the treatment of various lymphomas. Flavopiridol, has been previously shown to suppress HIV replication through inhibition of CDK9/P-TEFb (Chao, 2000), and both SNS-032 and Flavopiridol have been reported to exhibit similar IC50s for inhibition of CDK9 (Ali, 2009; Chen, 2009). It is therefore plausible that both the HIV-suppressive and toxic phenotypes recovered for these compounds across all screen formats are related to inhibition of host transcriptional processes, specifically CDK9 (P-TEFb)-mediated transcription, which is also required for stable activation of the HIV LTR (Chao, 2000). The two variants of Flavopiridol provided within the Kinase Inhibitor drug panel were located on separate experimental plates and their concordant recovery by high content analysis further highlights the robustness and fidelity of the analytical approach used as well the technical accuracy with which experimental treatments were prepared.

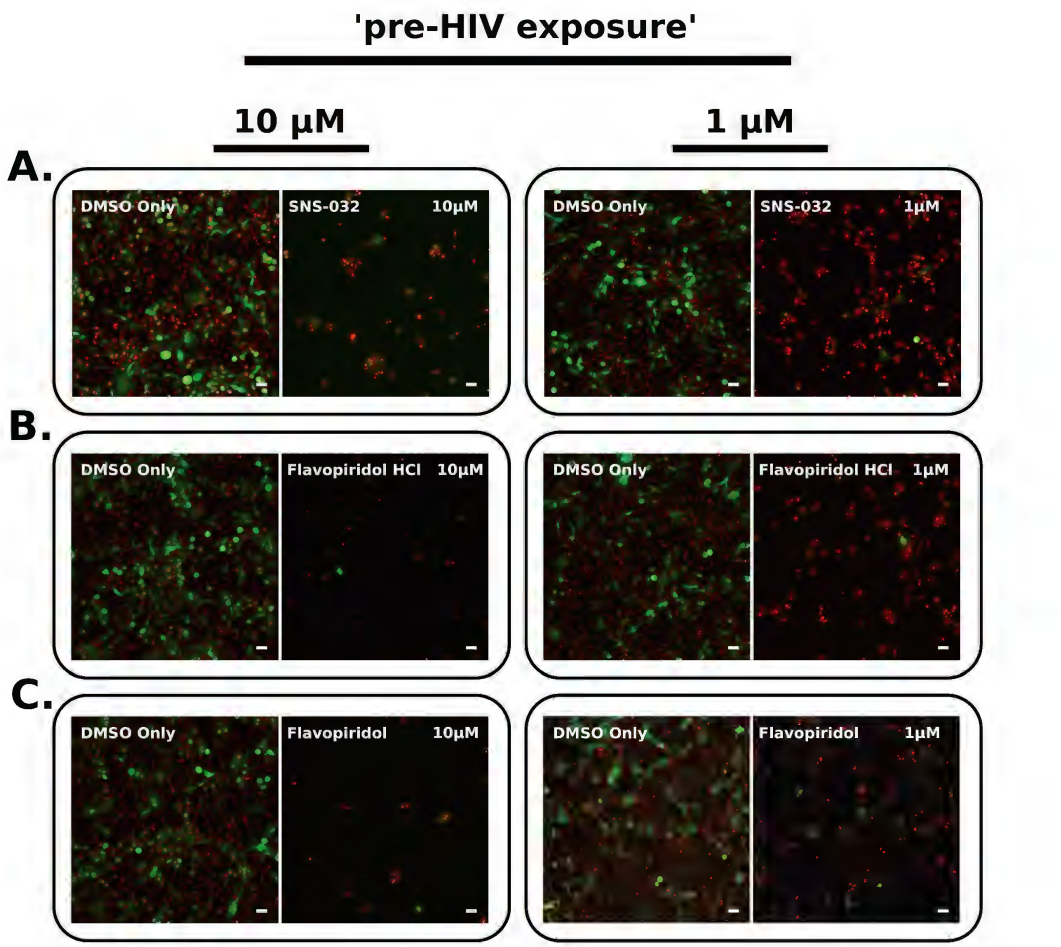

Figure. 5.9 Compounds with anti-HIV activity at 1 µM.

A) Cytotoxic (10 µM) and HIV-suppressive (1 µM) phenotypes recovered for SNS-032 treatment in the pre-HIV exposure screen format. **B)** Cytotoxic (10 µM) and HIV-suppressive (1 µM) phenotypes recovered for Flavopiridol HCl treatment in the pre-HIV exposure screen format. **A)** Cytotoxic (10 µM) and HIV-suppressive (1 µM) phenotypes recovered for Flavopiridol (Alvocidib) treatment in the pre-HIV exposure screen format. DMSO only images were obtained from a negative control well on the same experimental plate as the compound treatments. Images represent an overlay of acquisitions from the 405 and 488 excitation channels from a single FOV. GFP/LTR activation (green), nuclei counterstained with Hoechst (red). Scale bars = 20 µm.

The fourth compound that exhibited anti-HIV activity at 1 µM was Dactinomycin which is a DNA-intercalating, RNA synthesis inhibitor originally isolated from *Streptomyces* bacteria and which has received FDA-approval as a chemotherapeutic agent (reviewed by Bensaude, 2011). In addition, Dactinomycin treatment induces DSBs and γ-H2AX activation (Bensaude, 2011). In connection with HIV, Dactinomycin primes T cell populations for reactivation of latent viral reservoirs in response to TNF stimulation (Shishido, 2012). Intriguingly, the same study also demonstrated that while Dactinomycin enhanced LTR activation in latent reservoirs it exhibited an opposing, inhibitory effect on LTR activity in actively infected cell populations (Shishido, 2012).

Furthermore these HIV-replication modulating phenotypes were independent of the transcription-inhibiting effects of Dactinomycin suggesting an alternative unknown mechanism of action associated with the observed phenotypes (Shishido, 2012). The results obtained by HCS revealed a strong concordance with the phenotypes reported by Shishido and colleagues (Shishido, 2012), as Dactinomycin treatment suppressed HIV replication in the post-HIV exposure screen format (Figure 5.10), and induced modest but significant LTR activation in the HIV-naive Drug Only screen format, albeit with high levels of toxicity (Figure 5.10). These observations suggest that the molecular mechanisms associated with HIV replication in primary T lymphocytes may be conserved within the GHOST(3)-PSG3^{BAL} infection assay, thus further strengthening confidence in the HCS-recovered hits.

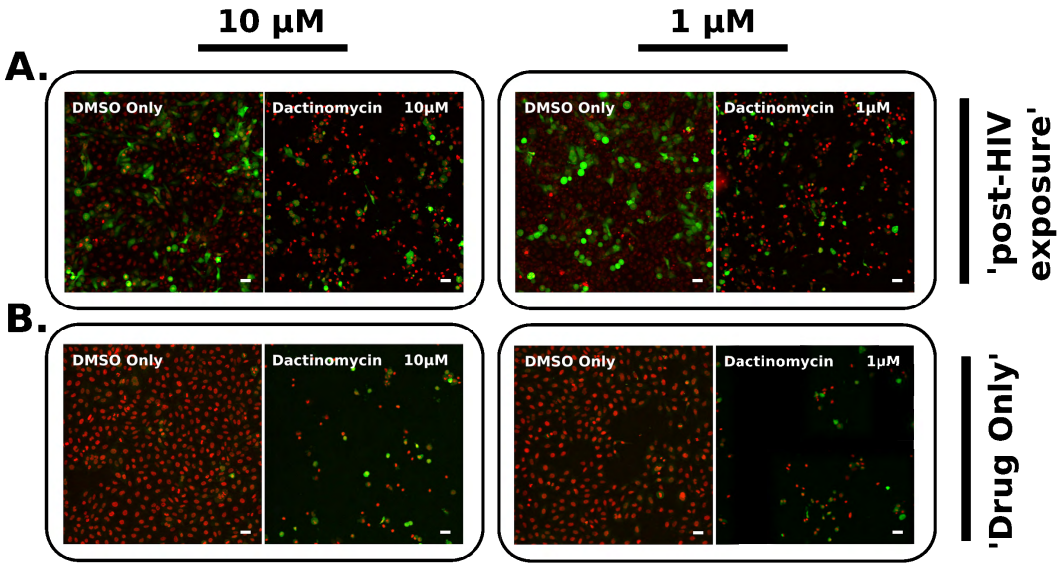

Figure. 5.10 Effects of Dactinomycin treatment in Drug Only and post-HIV exposure screen formats.

A) Dactinomycin-induced suppression of HIV replication in 10 µM and 1 µM post-HIV treatments. **B)** Dactinomycin induced toxicity and LTR-GFP stimulation in 10 µM and 1 µM Drug Only treatments. DMSO only images were obtained from a negative control well on the same experimental plate as the compound treatments. Images represent an overlay of acquisitions from the 405 and 488 excitation channels from a single FOV. GFP/LTR activation (green), nuclei counterstained with Hoechst (red). Scale bars = 20 µm.

Dactinomycin has also previously been described to suppress HPV replication, reverse HPV-mediated suppression of P53, and promote apoptosis in HPV infected cells through nuclear accumulation and transcriptional activation of P53 (Hietanen, 2000). Given the highly similar host interaction profiles described for HIV and HPV infection by miRNA pathway analysis, it is likely that the same P53-related mechanisms may contribute to Dactinomycin-associated HIV phenotypes recovered by HCS, particularly those related

to cell survival. Indeed similar cell survival phenotypes were also recovered for the DNA damage inducing agent Etoposide in the Drug Only, post-HIV and pre-HIV treatments with the exception that Etoposide did not suppress HIV replication in the 'post-HIV' treatment (Chapter 4). Like Dactinomycin, Etoposide promotes nuclear localization and activation of P53, via suppression of MDM2 (Arriola, 1999). The apoptotic phenotypes induced by both Dactinomycin and Etoposide in HIV-naive GHOST(3) cell populations are thus likely dependent on P53. Inactivation of P53 during HIV infection by both Nef-dependent and independent mechanisms (Greenway, 2002; Schindler, 2005), including downregulation of *TP53* transcript levels (Chapter 4), is therefore likely a contributing factor in the Mitigated Toxicity phenotypes recovered for many post-HIV treatments, including that of Dactinomycin and Etoposide. Furthermore, P53 has been described to activate the HIV LTR (Sawaya, 1998) suggesting that activation of the GHOST(3) LTR-GFP reporter construct in the 'Drug Only' Dactinomycin treatment may also be associated with enhanced P53 transcriptional activity.

HIV-specific toxicity

The largest contingent of hits was comprised of compounds that sensitized or 'primed' host cells towards apoptosis in response to HIV exposure or infection. Examples of 3 compounds that induced HIV-specific toxicity in the pre-HIV exposure screen format are presented in Figure 5.11 below. Briefly, in the pre-HIV exposure screen format, cells exposed to 10 μM of Pelitinib (Figure 5.11A), Abiraterone (Figure 5.11B) or A-674563 (Figure 5.11C) showed significant cytotoxicity, as denoted by diminished Hoechst signal (i.e. lower cell numbers), compared to relevant plate-specific negative controls (Figure 5.11). Notably, this highly cytotoxic phenotype was not recovered for the same compounds in the Drug Only screen format (Figure 5.11). These data clearly suggested that certain compounds, when applied in isolation are not toxic to cells, but when added prior to HIV infection, lead to apoptosis of the HIV-infected cells only.

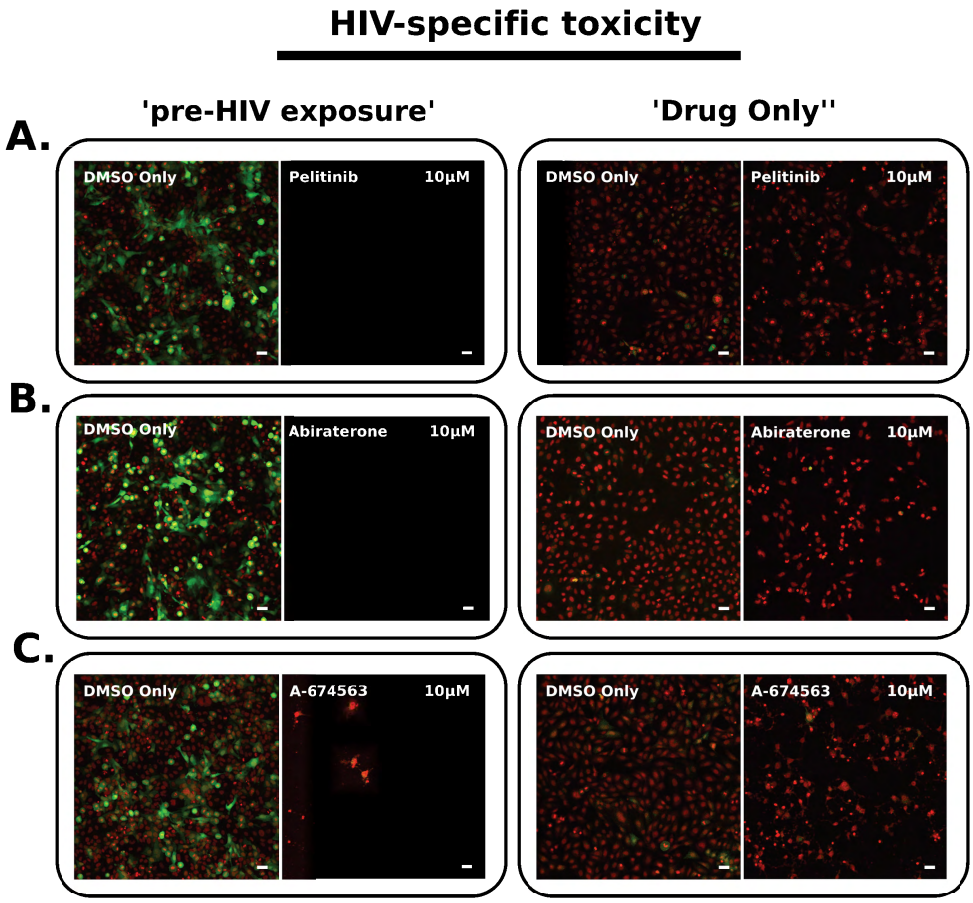

Figure. 5.11 Example of compound hits associated with HIV-specific toxicity in the pre-HIV exposure screen format.

A) 10 μM Pelitinib treatment resulted in significant cytotoxicity in the pre-HIV exposure format but not in the Drug Only format. **B)** Similarly 10 μM Abiraterone treatment resulted in significant cytotoxicity in the pre-HIV exposure format but not in the Drug Only format, and the same was observed for **C)** 10 μM A-674563 treatment. DMSO only images were obtained from a negative control well on the same experimental plate as compound treatments. Images represent an overlay of acquisitions from the 405 and 488 excitation channels from a single FOV. GFP/LTR activation (green), nuclei counterstained with Hoechst (red). Scale bars = 20 μm.

As mentioned previously, A-674563 is an inhibitor of AKT signalling, while Pelitinib is an irreversible EGFR inhibitor that is currently under phase II clinical trials with documented activity against SRC, STAT3, AKT and ERK1/2 (Nunes, 2004). Abiraterone (marketed as Zytiga) is an FDA-approved inhibitor of the enzyme 17 alpha-hydroxylase/C17,20 lyase (CYP17A1) and functions as an antagonist of androgen receptor (AR) signalling for the treatment of prostate cancer (Schweizer, 2012). The nuclear localisation and transcriptional activation of AR promotes cell survival and proliferation, and may be activated in an androgen-independent manner through RTK-mediated (e.g HER-2) signalling via MAPK, AKT and JAK/STAT cascades (Bennett, 2010). Functional

inhibition of host factors associated with pro-survival signalling pathways like ERBB, MAPK and AKT may therefore sensitise host cells to apoptosis in response to HIV infection. Compounds that exhibit these phenotypic trends may prime host cells into a pro-apoptotic or stressed state where the genotoxic stress associated with HIV infection then irreversibly initiates an apoptotic response which cannot be subverted by a non-established viral infection.

HIV-induced cell survival

Small molecules that exhibited significant cytotoxic effects in the Drug Only screen format but not the post-HIV exposure screen format were of particular interest, as these contrasting cytotoxic outcomes suggest that HIV is able to specifically subvert the pro-apoptotic activity of these small molecules. Only six small molecules were recovered for this functional class by HCS and two of these, NVP-TAE684 and Dactinomycin (Figure 5.10), also suppressed HIV replication in the post-HIV exposure screen format. Two examples of hits relevant to this functional class are represented in Figure 5.12 below. Briefly, significant cytotoxic effects of both Fludarabine phosphate and NVP-TAE684 were readily denoted by diminished Hoechst signal (i.e. lower cell numbers) in the Drug Only screen format (Figure 5.12 A & B). However, the same treatment time and compound concentrations exhibited significantly diminished cytotoxic effects when administered 48hr after HIV exposure (Figure 5.12 A & B). These data clearly suggest that HIV is able to mitigate or subvert, perhaps even lessen, the cytotoxic effects of specific compounds already present in the cellular environment when the virus begins its infection cycle.

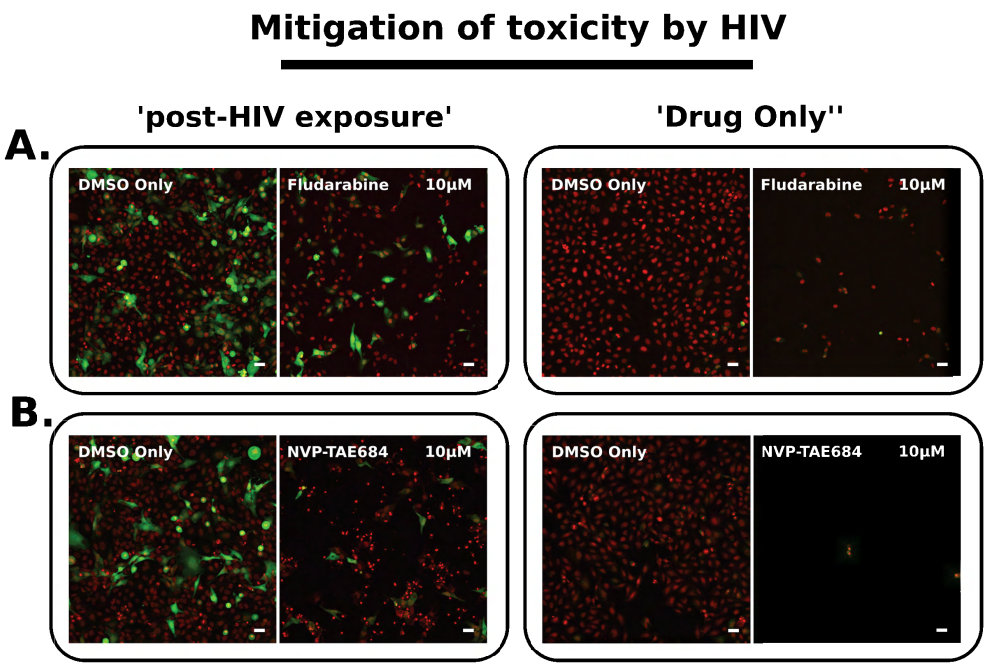

Figure. 5.12 Example of compound hits associated with HIV-mitigated toxicity in the post-HIV exposure screen format.

A) 10 µM Fludarabine treatment resulted in significant cytotoxicity in the Drug Only treatment but not in the post-HIV screen format. **B)** Similarly, 10 µM NVP-TAE684 treatment resulted in significant cytotoxicity in the Drug Only treatment but not in the post-HIV screen format. DMSO only images were obtained from a negative control well on the same experimental plate as compound treatments. Images represent an overlay of acquisitions from the 405 and 488 excitation channels from a single FOV. GFP/LTR activation (green), nuclei counterstained with Hoechst (red). Scale bars = 20 µm.

Fludarabine is an FDA-approved nucleoside analog, marketed as Oforta, which is traditionally used for the treatment of various lymphomas (Christopherson, 2014). This drug is incorporated into the DNA of actively dividing cells and results in inhibition of transcription, accumulation of DNA breaks, as well as nuclear and mitochondrial localisation of activated P53 (Christopherson, 2014). As mentioned previously NVP-TAE684 inhibits ALK and TGFß-mediated signalling (Galkin, 2007). These findings suggest that HIV is able to subvert apoptotic signals mediated through the P53 and TGFß signalling pathways and this is in accordance with miRNA HCS data which recovered a close functional relationship between these specific pathways and the modulation of HIV replication. Additionally these findings also lend further support the proposed role of HIV-induced downmodulation of P53 transcriptional activity in the aberrant cell survival phenotypes previously noted for Etoposide treatment following HIV infection (Chapter 4).

5.2.4 Pathway analysis

Based on the hits selected from the various screen formats, compound-protein and protein-protein interaction analyses were then performed in order to evaluate higher-order processes associated with each functional class of hits. These enrichment and interaction analyses were performed using the online analysis tool STITCH 4.0 (Kuhn, 2008).

pre-HIV exposure

STITCH analysis recovered interactions between CDKs 1, 2, 4, 5, 7 and 9 in association with the HIV suppressive phenotype in the pre-HIV exposure screen format (Figure 5.13). Specifically, the posttranslational modification of a number of CDKs by CDK7 and vice versa was recovered. This is in accordance with the central role of CDK7 in the CDK-activating complex (CAK), which regulates cell cycle progression (Obaya, 2002) and has also been implicated as Tat-associated factor that mediates LTR transactivation (Cujec, 1997). These findings thus posit the pharmacological inhibition of multiple CDKs as a potential strategy for the treatment of HIV and has recovered specific small molecules that are eble to exert anti-HIV effects through this specific mechanism of action (Figure 5.13). In addition the inhibition of EGFR-SRC signalling and VEGFA and the activation of PTGS2 were also associated with the HIV suppressive phenotype by STITCH analysis. VEGFA has been described to be upregulated in response to HIV infection (Korgaonkar, 2008), while PTGS2 has been implicated as an inhibitor of HIV replication (Whitney, 2011). The functional inhibition of EGFR-SRC signaling was strongly implicated in miRNA-based modulation of HIV replication by HCS (Chapter 4) and the potential role of EGFR in HIV replication is discussed in greater detail in section 5.2.5. KEGG analysis revealed a significant ($p<0.05$) enrichment for the cell cycle, VEGFR, ERBB, adherens junction, endocytosis and MAPK signalling pathways, along with regulation of the actin cytoskeleton. All of these functional pathways were also found to be enriched by pathway analysis for miRNA mimics that suppressed HIV replication (Chapter 4). This observation further highlights the significant concordance between certain functional targets identified by miRNA screening and the pharmacological activity of specific small molecules that both suppress HIV replication. Notably, as these targets were all identified in a pre-HIV exposure format, their effect on HIV is likely exhibited early on during infection positing these molecules as prime candidates for post-exposure prophylaxis.

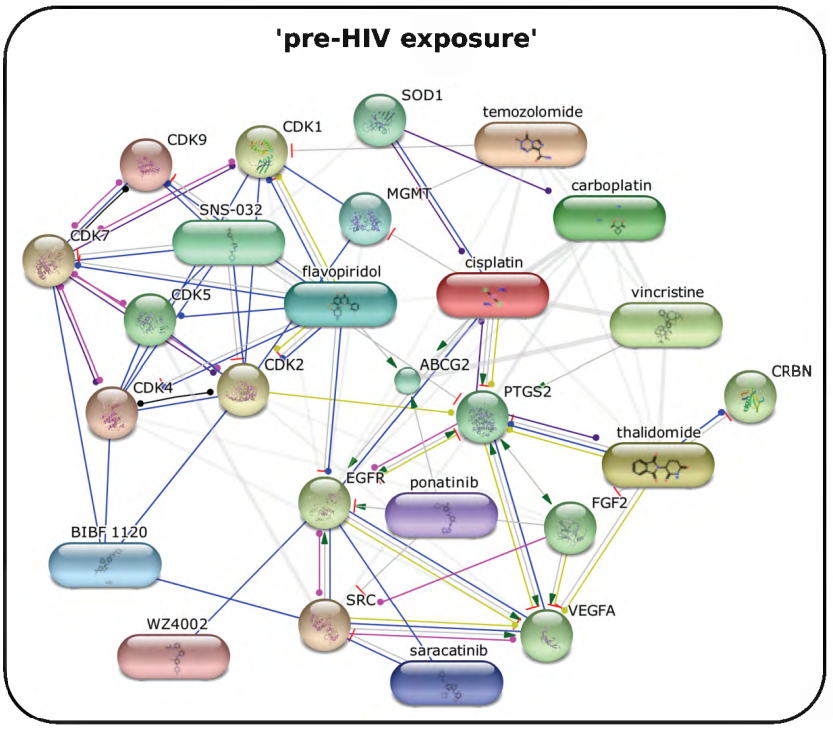

Figure 5.13 STITCH analysis for pre-HIV exposure compound hits

The pharmacological inhibition of, and molecular interactions between, various CDKs as well as a signalling network comprised of EGFR, SRC, VEGFA and PTGS2 were the most prominent functional clusters recovered for compounds hits associated with suppressed HIV replication in the pre-HIV screen format. Posttranslational modification (pink), activation (green arrowhead), inhibition (flat red arrowhead), catalysis (purple), binding (blue), effect on gene expression (yellow), interaction (grey).

In addition Ponatinib, Flavopiridol and Cisplatin stimulate expression of Breast Cancer Resistance Protein (BCRP), also known as ABCG2 (Figure 5.13). The ATP-binding cassette (ABC) family of transporters regulate absorption and bioavailability of small molecules including lipids and drugs (reviewed by Szakacs, 2008). BCRP is specifically induced by Tat in T lymphocytes (Zhou, 2016), and elevated BCRP expression has been linked to AIDS progression and failure of ARV treatment (Wang, 2003; Zhang, 2014). Furthermore, ABCG2 has been described as a direct transcriptional target of EGFR (Huang, 2011). Together, these findings posit BCRP-mediated drug resistance as an additional potential mechanism of HIV-induced cell survival in response to toxic compounds. However, while Cisplatin, Ponatinib and Flavopiridol may represent viable candidates for drug repurposing as novel anti-HIV therapeutics, these compounds are susceptible to BCRP-mediated drug resistance. Taking a cue from HIV-specific regimens, a combination therapy that includes BCRP-inhibition, may provide a more effective long-term treatment strategy.

post-HIV exposure

In the post-HIV exposure format, STITCH analysis again recovered CDKs 1, 2, 4, 5, 7 and 9 as well their interaction with CCND1 and either the activation or posttranslational modification of P53 (Figure 5.14). The posttranslational modification of P53 is intrinsically related to its stability, nuclear localization and transcriptional activity (reviewed by Meek, 2009). Notably the posttranslational modification of P53 transcriptional activity was implicated in the aberrant cell survival phenotype recovered for Etoposide treatments in Chapter 4. EGFR-mediated signalling occupied a significantly less prominent role in the post-HIV treatment as compared to the pre-HIV treatment, suggesting that EGFR-mediated signals may be more relevant during the earlier stages of viral replication i.e. prior to stable LTR transactivation. STITCH analysis also suggested that inhibition of P53 posttranslational modification by CDKs may exert a strong influence on LTR transactivation in stably infected cells. If so, these interactions represent potentially attractive targets for therapeutic intervention. Indeed, Tat has been proposed to interact with cyclin-CDK complexes including CDKs 2, 7 and 9, and pharmacological inhibition of CDKs has previously been proposed as a potential strategy to inhibit HIV replication (Maddukuri, 2003). However, the majority of compounds recovered by this study have not been directly or specifically associated with suppressed HIV replication, meaning additional data is required to gain confidence in these connections. In contrast, KEGG analysis revealed a significant ($p<0.05$) enrichment for the cell cycle, P53, Wnt and MAPK signalling pathways which were also recovered by miRpath analysis (Chapter 4). This latter piece of data once again generates confidence in the use of orthogonal assays to identify HIV-related host functional pathways that provide novel therapeutic targets.

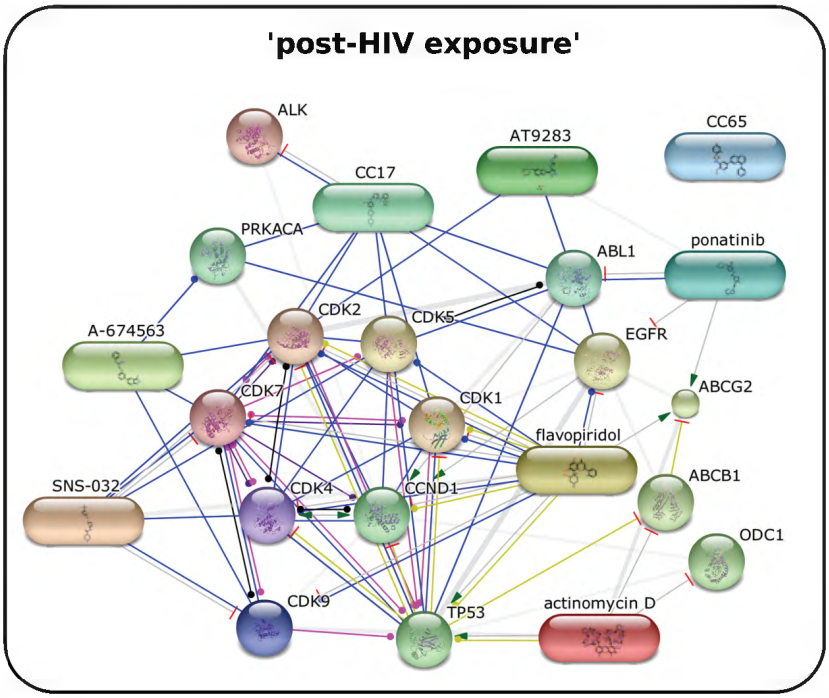

Figure 5.14 STITCH analysis for post-HIV exposure compound hits

The pharmacological inhibition of, and molecular interactions between, various CDKs, CCND1 and P53 comprised the most prominent functional cluster associated with suppressed HIV replication in the post-HIV exposure screen format. Notably, a signalling network comprised of EGFR, SRC, VEGFA and PTGS2 were the most prominent functional clusters recovered. Posttranslational modification (pink), activation (green arrowhead), Inhibition (flat red arrowhead), catalysis (purple), binding (blue), effect on gene expression (yellow), interaction (grey).

HIV-specific toxicity

The most conserved mechanism associated with the HIV-specific toxicity phenotype was related to pharmacological inhibition of RTKs (ERBBs, PDGFRs, KIT, RET, FLT3) which exhibited convergent downstream interactions with cytoplasmic kinases such as BCR, LCK, ABL1 and SRC (Figure 5.15). The functional inhibition of these RTKs and(or) the inhibition of their binding to each other correlated with HIV-induced toxicity. Notably, LCK (P56) activity is modulated by gp120 (Hubert, 1995), and LCK has also been linked to Tat-mediated regulation of NF-kß and apoptosis (Manna, 2000). The fact that the majority of these compounds only exhibited HIV-specific toxicity in the pre-HIV exposure screen format further suggests that these toxic phenotypes are associated with a host cell ‘priming effect’. In other words, pharmacological inhibition of RTK signalling cascades seems to sensitize host cells to apoptosis, specifically in response to HIV exposure. Further investigation is required in order to determine exactly which stage of the viral life cycle, and which viral proteins may serve as the ‘trigger’ for such an apoptotic switch. In addition, the large scale toxic effects recovered for these compound

treatments, compared to negative control images, appear to extend beyond only the infected cell population (Figure 5.11). This represents an interesting outcome that may be related to the broad-scale pyroptotic responses in uninfected bystander cells which is induced by stalled HIV replication in infected cells (Doitsh, 2014). Again, validation of such a relationship requires further investigation. Overall, the compounds recovered for the HIV-specific toxicity phenotype may constitute promising therapeutic candidates, for the prevention of *de novo* infections during chronic HIV infection, and also as post-exposure prophylactic treatments to counteract the establishment of viral reservoirs following acute exposure to HIV. Finally, KEGG analysis revealed a significant ($p<0.05$) enrichment for the ERBB, focal adhesion, endocytosis, cytokine-cytokine, adherens junction and MAPK signalling pathways. The recovery of these specific pathways supports the role of RTK-mediated signalling in the survival of compound-treated cells exposed to HIV. The KEGG results also suggest that actin-associated rearrangements, potentially during viral entry, may serve as the molecular triggers for apoptosis, although further investigation will be required to fully elucidate these phenotypes.

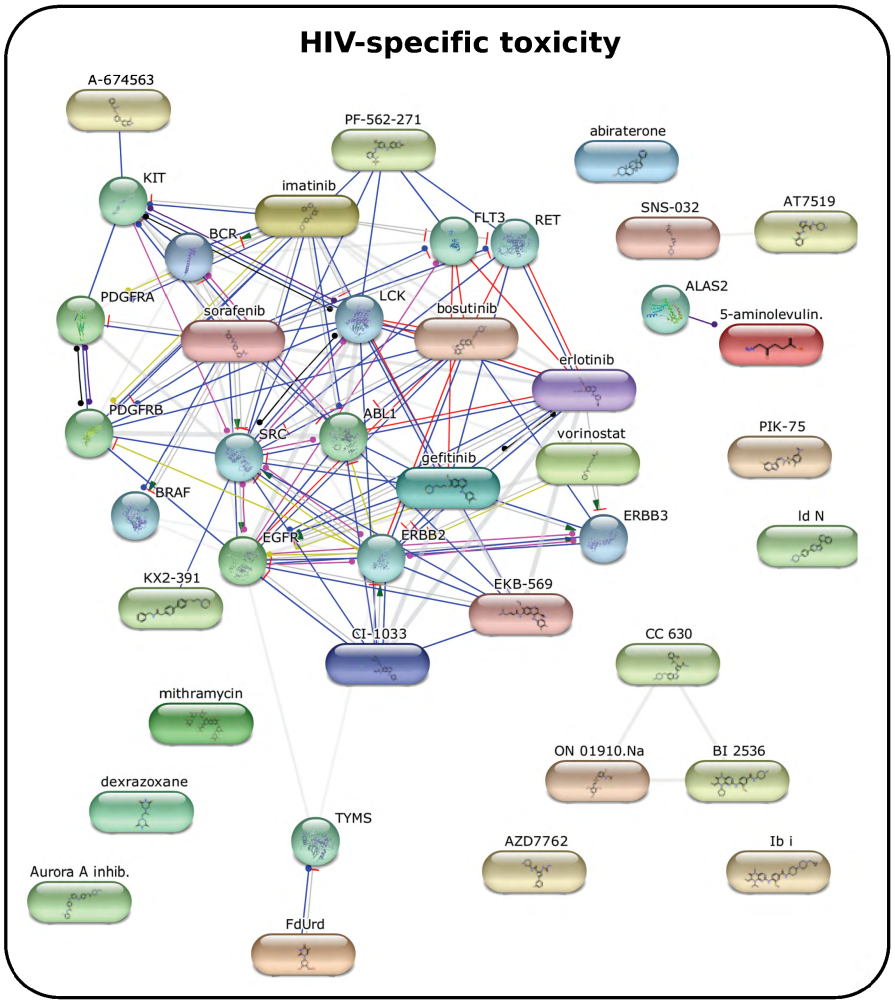

Figure 5.15 STITCH analysis for HIV-specific toxicity-associated compound hits

The pharmacological inhibition of a number of RTKs and their convergent signalling through cytoplasmic kinases was highly enriched within this hit class. Posttranslational modification (pink), activation (green arrowhead), inhibition (flat red arrowhead), catalysis (purple), binding (blue), effect on gene expression (yellow), interaction (grey).

The prosurvival effect of stable HIV replication in cell types such as macrophages has been described as a major barrier to the eradication of viral reservoirs by conventional therapeutic strategies (Cummins, 2013). The panel of HCS hits recovered for the HIV-specific toxicity hit class thus represent a potentially valuable therapeutic resource for combination therapy as these compounds have been demonstrated to specifically sensitize host cells towards apoptosis in response to HIV.

Mitigated toxicity

KEGG analysis revealed a significant ($p<0.05$) enrichment for Toll-like receptor, Hepatitis C, JAK/STAT and Influenza A-associated signalling pathways for compounds related to the mitigated toxicity phenotype (Figure 5.17). Enrichment of pathways associated with Influenza A and Hepatitis C suggest that the mitigated toxicity phenotype may be conserved between various human viruses, warranting further investigation. In addition STITCH analysis suggested that HIV is able to overcome apoptosis induced by the activation of TLRs and P53 and the inhibition and(or) posttranslational modification of STAT3, IL6, AKT and ESR. IL6 mediates anti-apoptotic activity through upregulation of MCL1 (Lin, 2001), and inhibition of STAT3 promotes apoptosis in various malignancies (Siddiquee, 2008). Furthermore, inhibition of TLR8 has been linked to enhanced apoptotic effects through negative regulation of the ERK1/2 and NF-kß signaling cascades (Tang, 2015). Given the strong relationship between these factors and HIV-mediated regulation of apoptosis, these interactions may also play a role in HIV-induced apoptosis during the later stages of viral replication and represent therapeutically relevant targets specifically in long-lived viral reservoirs like macrophages.

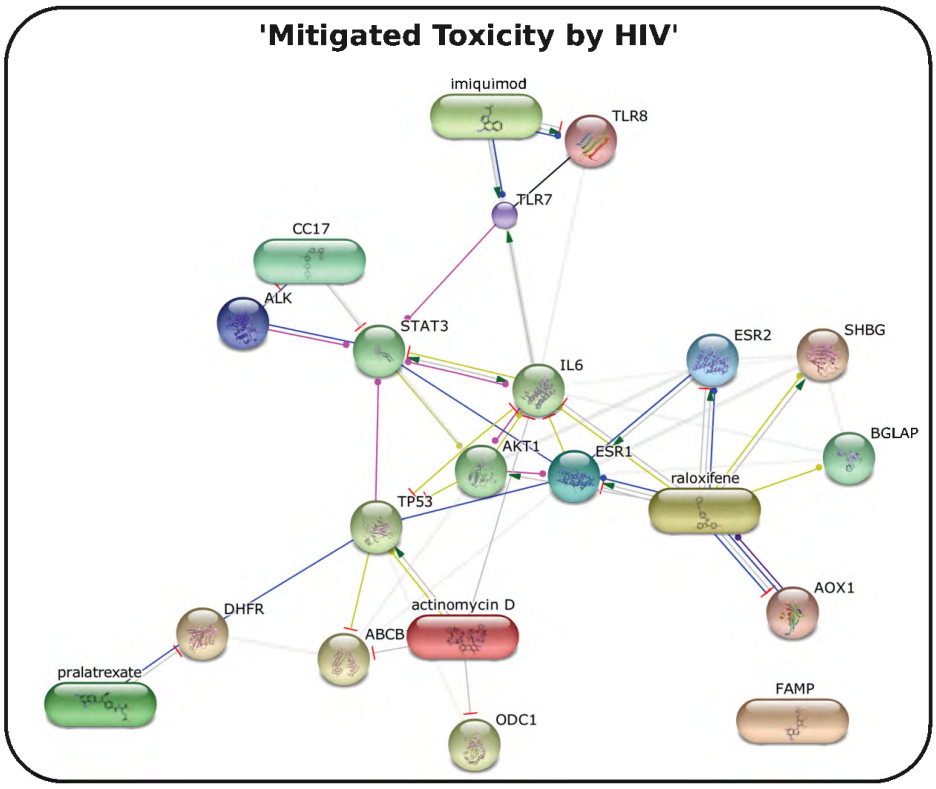

Figure 5.17 STITCH analysis for compound hits associated with the mitigated toxicity phenotype

RTK and cytoplasmic kinase-associated drug targets were noticeably omitted from this hit class, while inhibition of STAT3, IL6 and TLR signalling were identified as target points that HIV could overcome to promote cell survival, potentially through a P53-related process. Posttranslational modification (pink), activation (green arrowhead), inhibition (flat red arrowhead), catalysis (purple), binding (blue), effect on gene expression (yellow), interaction (grey).

5.2.5 Potential role for EGFR during the early stages of viral replication

Small molecule inhibitors of RTKs, including EGFR, and their associated cytoplasmic effector kinases featured prominently in the compound hits and enrichment analyses for the HIV-specific toxicity and pre-HIV exposure screen formats (Figure 5.13 and Figure 5.15). Based on this, potential relationships between EGFR and HIV replication were thus explored.

Microscopy revealed higher EGFR (ERBB1) expression levels in uninfected control treatments as compared to infected samples, with EGFR levels observed to be significantly diminished 24 hpi and even more so at the 48 hpi time point (Figure 5.18A). Conversely qPCR analysis revealed *EGFR* transcript levels to be non-significantly upregulated 24 hpi, with a significant ($p<0.05$) 2 fold upregulation noted at the 48 hpi

time point (Figure 5.18B i). These observations suggest that EGFR protein and transcript levels are differentially modulated at distinct time points following HIV infection. Surprisingly, in contrast to immunofluorescence data, Western Blotting revealed a significant ($p<0.05$) upregulation of cytoplasmic EGFR 9hr (60%) and 24hr (200%) post-infection (Figure 5.16B ii). In accordance with immunofluorescence data however, Western Blotting also confirmed a significant ($p<0.05$) downregulation of cytoplasmic EGFR 48 hpi (Figure 5.18B ii). Similar trends were recovered for EGFR levels detected from whole cell lysate (Appendix V, Figure A5.6 A), while only a degraded EGFR-product was clearly detectable in the nuclear fractions from all experimental samples (Appendix V, Figure A5.6 B).

A possible explanation for the discordance between ICC and Western Blot analyses at specific time points following infection is that antibody binding sites may have been occluded in the 24 hpi time point and were thus not accessible for detection by immunofluorescence. The dissociation steps associated with sample processing for Western Blot analysis would, in contrast, have exposed this binding site. In addition, the discordance between EGFR transcript and protein levels 48 hpi by HIV suggests either a translational block or rapid degradation of EGFR at this time point, but additional data is required to confirm this.

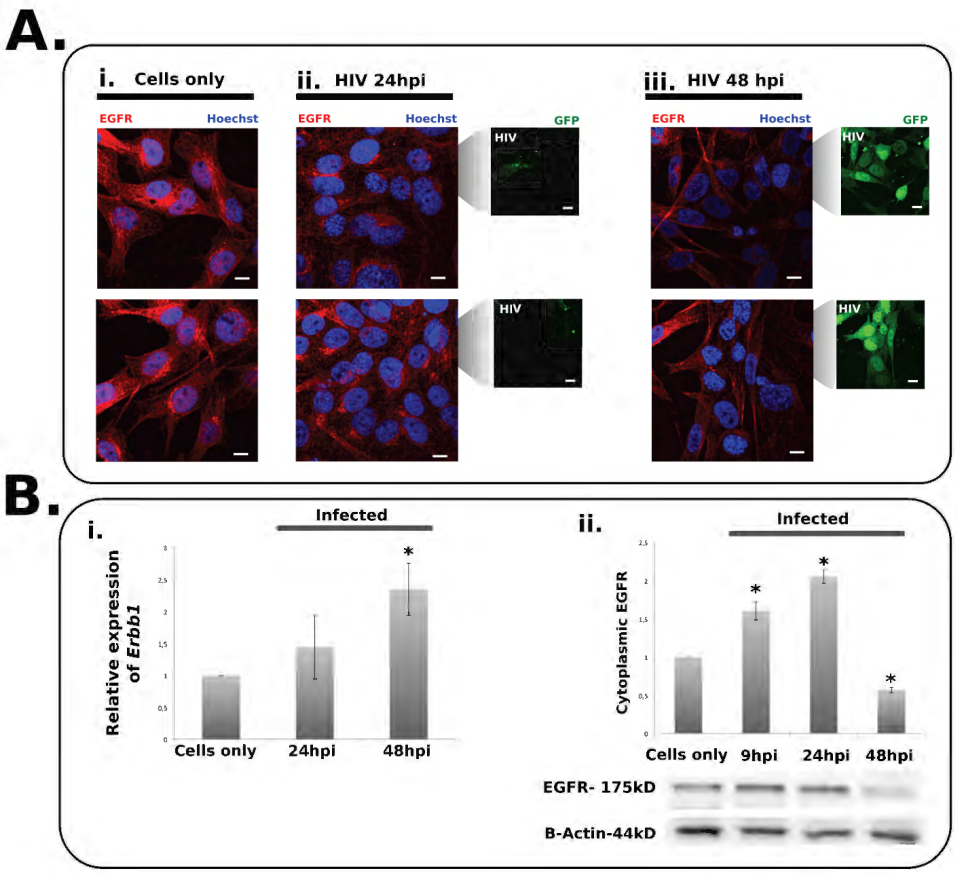

Figure 5.18 Modulation of EGFR following HIV infection

A) EGFR-specific immunocytochemistry, EGFR expression and localisation i) in untreated GHOST(3) cells, ii) cells observed 24 hpi with HIV or iii) 48 hpi with HIV. Nuclei stained with Hoechst (blue), anti-EGFR (red), scale bars = 15μM. Frames represent independent FOVs **B)** Quantification of EGFR expression by i) qPCR analysis showing *EGFR* expression levels 24 hpi and 48 hpi relative to *HPRT* expression (n=3, *= $p<0.05$), and ii) Western Blot analysis showing relative EGFR expression 9, 24 and 48 hpi as compared to untreated control cells. ß-Actin was used a loading control, * = $p<0.05$.

Upregulation of EGFR protein levels 9 hpi suggests that HIV entry and infection events *preceding* viral integration, which typically occur ~16 hpi, may result in either stabilization or direct upregulation of EGFR. This effect appears to be potentiated following viral integration as EGFR levels increase further at 24 hpi. Notably, the discrepancy in EGFR detection levels between immunofluorescence and Western Blot datasets at 24 hpi also suggests that an EGFR binding interaction that is relevant to HIV replication may be at play during this early time point. This would be in accordance with previous findings that have reported the colocalization of viral particles and RTKs within late endosomal structures following Influenza A, HCV and hCVM infection (Grove, 2011; Meliopoulos, 2012). These observations thus suggest a potential role for EGFR during the early stages of HIV infection, up to and including 24 hpi.

Strikingly, EGFR levels are significantly downregulated (as detected by both ICC and Western Blotting) at 48 hpi thus suggesting that EGFR activity may be dispensable during the later stages of infection that correspond with stable transactivation of the HIV LTR and subsequent GFP expression (Figure 5.16). These results are in strong agreement with STITCH analysis, which suggested that RTK-mediated signalling may play important roles in determining the outcome of successful HIV infection (Figure 5.13) and the propagation of a prosurvival cellular response during early stages of infection (Figure 5.15). This hypothesis is supported by data showing that HIV is able to both enhance the stability of EGFR and induce EGFR-mediated activation of pro-survival signalling pathways (Valiathan, 2004). Finally, a number of miRNAs that target factors associated with the EGFR signalling pathway were recovered as HIV-replication modulating hits during primary miRNA screens, thereby providing further evidence of a role for EGFR-mediated signalling during early stages of viral replication.

5.2.6 Validation of anti-HIV compound phenotypes against X4 tropic viral variants

An additional validation of the potential physiological relevance of phenotypes recovered by HCS was undertaken by evaluating the anti-HIV activity of a small subset of compound hits against an X4 tropic HIV variant. Six compound hits were validated against the X4-tropic variant, HIV Gag-iGFP. A simple validation approach was employed utilising the pre-HIV exposure experimental format only. GHOST(3) cells were

treated with either DMSO only (negative control), Raltegravir (positive control for suppressed replication) or specific compounds for 24 hours prior to HIV exposure at an MOI of 0.5.

Raltegravir treatment significantly reduced syncytia formation, suppressed LTR-reporter activation, as well as virus-related GFP production as compared to the negative control phenotype (Figure 5.19 A & B). Treatment with a SRC-kinase inhibitor, Saracatinib, emulated the phenotypes recovered by HCS, resulting in minimal toxicity and suppressed HIV replication (Figure 5.19C). AT7519, which was recovered as an HIV-specific toxicity hit by HCS, again revealed enhanced toxicity in response to HIV exposure, but also exhibited a strong HIV-suppressive phenotype akin to that of Raltegravir treatment in the surviving cell population (Figure 5.19D). Likewise A-674563, which exhibited HIV-specific toxicity in the pre-HIV exposure screen format and HIV-suppressive activity in the post-HIV exposure screen format, also resulted in high levels of HIV-specific toxicity with the surviving cells seemingly protected against HIV infection (Figure 5.19E). GSK2126458 which was recovered as an HIV-suppressive hit in the post-HIV exposure screen format by HCS, revealed a strong HIV-specific toxicity response to HIV Gag-iGFP exposure (Figure 5.19F).

Intriguingly, both of the EGFR inhibitors, WZ4002 and Gefitinib, which exhibited HIV-suppressive and HIV-specific toxicity phenotypes respectively in HCS, did not exhibit similar divergent phenotypes compared to negative controls in X4-tropic validation experiments (data not shown). This suggests that R5- and X4-tropic HIV variants may utilise/initiate discrete downstream signaling effectors that promote distinct vulnerabilities to therapeutic intervention, with EGFR activity likely being specifically required by R5-tropic viruses. In addition this observation also suggests that the anti-HIV activities recovered for both WZ4002 and Gefitinib by HCS, may be related to viral entry.

Overall, the observation that the majority of compounds tested against the X4 variant recapitulated the anti-HIV activity initially recovered by HCS, suggests that there are also a number of common vulnerabilities between R5 and X4 HIV variants. It is therefore likely that a greater number of compounds hits recovered by HCS may also exhibit pan-antiviral activity against both X4 and R5-tropic variants of HIV, although this remains to be tested. Clearly, a more extensive validation of all compound hits recovered by HCS, may yield further information on discrete host-pathogen interactions and therapeutic vulnerabilities specifically associated with HIV viral tropism.

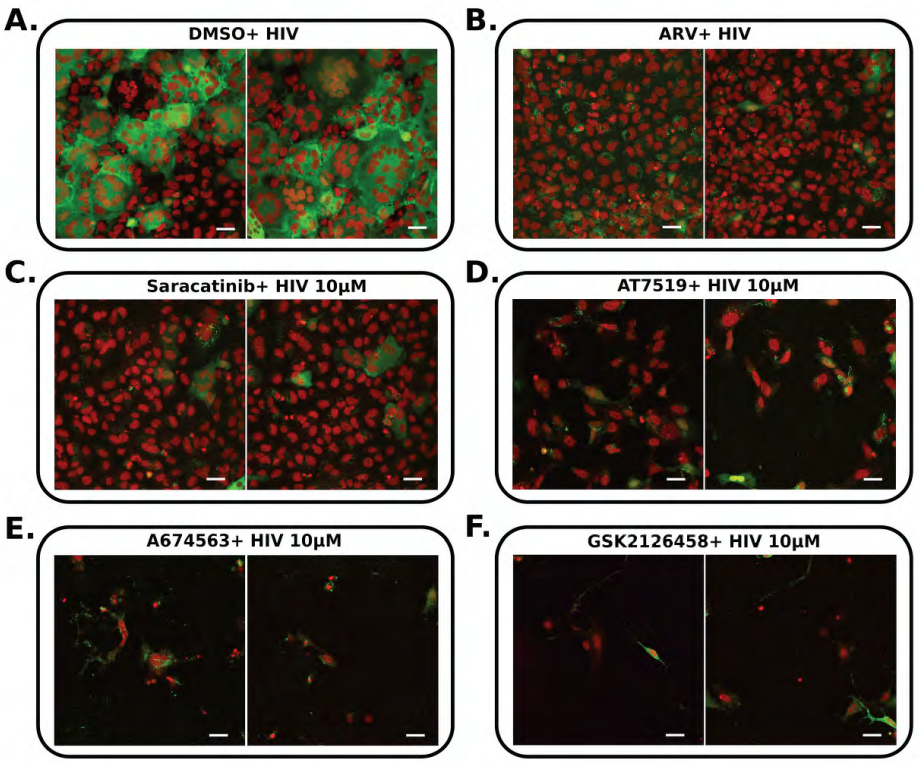

Figure 5.19 Compound hit activity against an X4-tropic viral strain in GHOST(3) cells

GHOST(3) phenotypes associated with 10 µM compound treatments prior to X4-tropic HIV exposure for 48 hours. **A)** DMSO-treated/HIV-infected controls, **B)** Raltegravir-treated/HIV-infected controls, **C)** Saracatinib-treated/HIV-infected, **D)** AT7519-treated/HIV-infected, **E)** A-674563-treated/HIV-infected, **F)** GSK2126458-treated/HIV-infected cells. Images represent overlays acquired from a single FOV at 40x, LTR-reporter (green), nuclei counterstained with Hoechst (red), scale bars = 20 µm.

Closer inspection of the HIV-suppressive phenotypes recovered for Saracatinib (Figure 5.20), A-674563 (Appendix V, Figure A5.7 A) and AT7519 (Figure A5.7 B) revealed the presence of punctate GFP spots either on the cell surface or within the cytoplasm of cells that did not exhibit activation of the LTR reporter or a syncytial phenotype (Figure 5.20). These GFP 'spots' are indicative of the capsid-linked GFP molecules generated by HIV Gag-iGFP virions, and a similar phenotype was observed for the majority of cells that received Raltegravir treatment (Figure 5.20). Given that Raltegravir inhibits HIV integration specifically, this implies that Saracatinib may also prevent HIV integration, or possibly even earlier stages of the HIV replication cell cycle following viral entry. The number of GFP spots recovered for cells treated with Saracatinib was noticeably attenuated in comparison to the number of spots acquired per cell for Raltegravir treatment (Figure 5.20). This implies that fewer virions were able to enter cells in the presence of Saracatinib and/or that virions which did enter the cell were inhibited prior to or at HIV integration (Figure 5.20). Together, this suggests a multiple inhibitory effect for Saracatinib at various stages during the HIV replication cycle. The HIV-specific toxicity

phenotypes recovered for A-674563 (Appendix V, Figure A5.7 A) and AT7519 (Appendix V, Figure A5.7 B) also suggest that these phenotypes are similarly related to either viral entry or integration. Further kinetic and temporally-focused validation experiments are required to delineate these phenotypes.

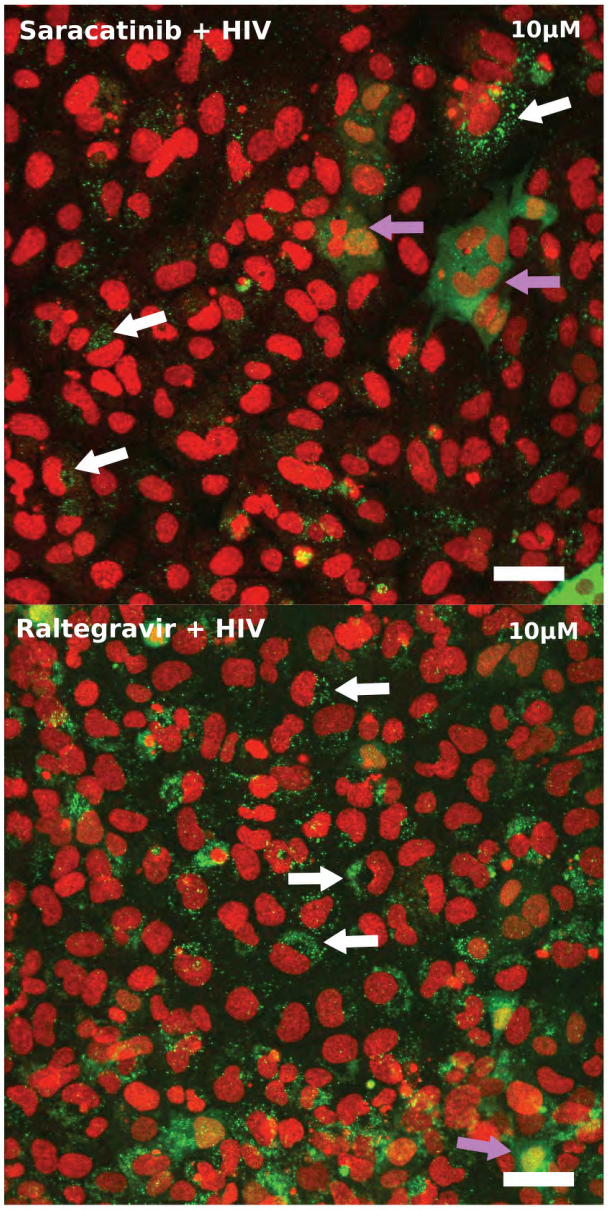

Figure 5.20 Enlarged images from HIV-tropism validation experiments

Upper) 10 µM Saracatinib-treated/HIV-infected cells. **Lower)** 10 µM Raltegravir-treated/HIV-infected cells. White arrows indicate examples of cells where HIV capsid/virions are present in either the cytoplasm on at the surface of cells that are not stably infected with HIV. Pink arrows indicate examples of stably infected cells. Images represent overlays acquired from a single FOV at 40x, non-integrated virus (punctate green spots)/ integrated HIV (diffuse green), nuclei counterstained with Hoechst (red), scale bars= 20 µm.

5.2.7 Conclusion

The principle aim of the compound screens conducted here was to determine whether functional inhibition of certain molecular targets recovered by primary miRNA screening could be recapitulated by a targeted panel of small molecules. Indeed, compound-based screening revealed a high level of concordance with many of the functional pathways and specific targets initially recovered by the primary miRNA screen. This observation bolsters confidence in the HIV-host interactions proposed by miRNA pathway analysis, and posits miRNA-advised secondary compound screening as a robust validation strategy.

In addition, a combined overview of miRNA and small molecule-based HCS data suggests a convergence on RTK-mediated signalling, and its direct downstream effectors, as a central vulnerability during early HIV replication which could be exploited for therapeutic gain. Intriguingly, this could occur either via inhibition of HIV replication or by priming host cells such that they undergo apoptosis following exposure to HIV. The use of multiple screening formats also highlighted a clear distinction between phenotypic outcomes as a function of the timing of compound addition (either before or after stable HIV infection). Furthermore, distinct and prioritised therapeutic targets could be identified for each case, which may not have been possible if one format had been used throughout (Figure 5.21).

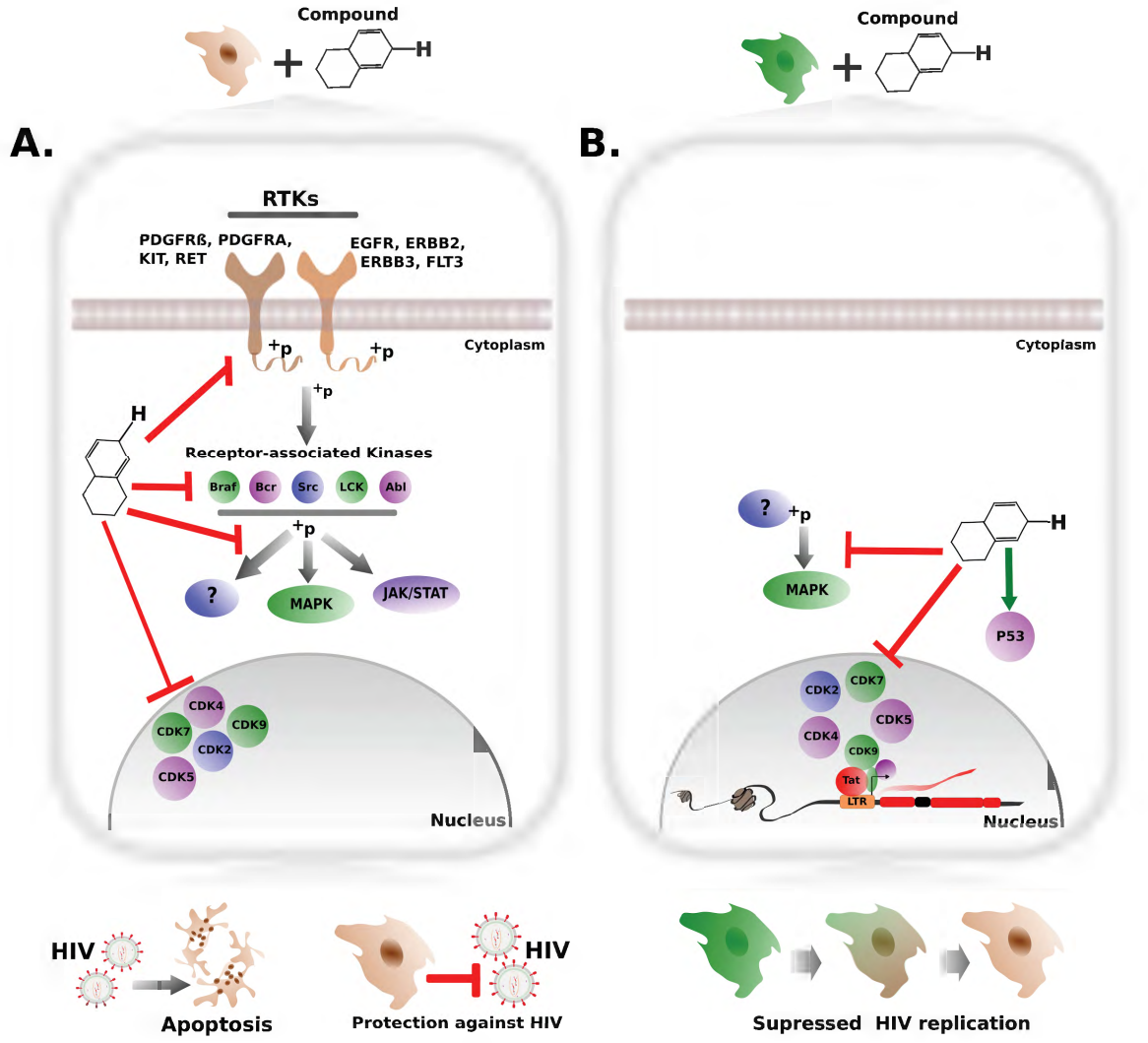

Figure 5.21 Prioritised host targets for treatment of HIV infection

Targets recovered for experimental formats where A) host cells were treated with relevant compounds prior to HIV exposure, or B) stably infected populations of host cells were treated with relevant compounds.

A strong concordance between previously described phenotypes related to HIV replication was also noted for a number of compounds (e.g. Flavopiridol, Dactinomycin). However, the majority of compound-related phenotypes characterised here represent the first description of their potential anti-HIV properties. This body of work therefore represents a significant contribution to potential anti-HIV therapies directed against endogenous, i.e. host targets. Furthermore, as a large number of the compounds recovered here have either already obtained FDA-approval or are currently under clinical investigation, repurposing them for use as novel anti-HIV therapies is highly feasible.

Overlapping functional targets and phenotypic outputs related to specific miRNAs and small molecules also represent a potentially valuable resource, as such miRNA/compound combinations could complement current therapeutic regimens. For example, Tarbase v7.0 identified hsa-miR-491-5p as the highest scored experimentally validated miRNA regulator of SRC-kinase and a miR-491-5p mimic was identified as an HIV hit suppressive by HCS. In addition miR-491-5p mediated suppression of SRC kinase in a bone marrow-derived cell line similar to that of the GHOST(3) parental cell line (Balakrishnan, 2014). Together, these findings strongly support the anti-HIV activity of miR-491-5p via regulation of SRC kinase in GHOST(3) cells.

A number of other compounds, including Ponatinib and Saracatinib, that also suppress SRC kinase activity showed similar HIV-suppressive phenotypes. Perhaps then, miR-491-5p is able to augment or mimic the function of these FDA-approved drugs. Indeed, analogous relationships were identified for several miRNA mimics and compounds that both suppressed HIV replication. SNS-032 and miR-192-5p suppress CDK1 protein levels (Hafner, 2010), while miR 193-3 targets CDK1, CDK7 and CCND1 (Chen, 2010; Helwak, 2013, Balakrishnan, 2014) as do Flavopiridol and SNS-032. In addition, miR-138-5p and miR-124 suppress CCND1 (Karginov, 2013) and CDK2 (Nakamachi, 2009) respectively, and these proteins are also targeted by A-674563 and SNS-032. The miRNA to targeted compound HCS approach presented in this study therefore represents a valuable strategy to identify alternative/complementary miRNA-based therapies with the same functional effect as commercially available drugs.

It should also be noted that the poor concordance between compound effects observed for 10 μM screens and treatments at lower concentrations was in accordance with data from the Broad Institute's Cancer Cell Line Encyclopedia (CCLE) database (Barretina, 2012). The average IC_{50} for pharmaceutical agents in GHOST(3) parental cells, HOS, was ~8 μM (Barretina, 2012), implying that concentrations > 8μM may be required to induce observable functional effects within populations of cultured GHOST(3) cells. This hypothesis is supported by the HCS data presented in this study, which revealed that only a single compound, Dactinomycin, was able to induce concordant anti-HIV phenotypes at both 10 μM and 1 μM concentrations (Figure 5.10). The majority of drug-induced toxicity effects in the Drug Only screen format were also observed to be significantly diminished, or absent at the lower concentrations screened (Figure 5.6). Intriguingly, Etoposide (which was included in the Oncology compound library set) did not induce a toxic phenotype in response to pre-treatment with HIV as observed in the experimental work described in the previous chapter. Given the poor long-term stability of many compounds, even at -20˚C, it is plausible that this aliquot of Etoposide was no longer efficacious.

Similarly to the miRNA screens, functional readouts from the compounds screens presented in this study were limited to the identification of compounds that could impact HIV replication up to the point of LTR transactivation. However, the novel multi-format screening approach utilised here, significantly expanded the use of the GHOST(3) assay system and was extremely useful in the discrimination of specific compound-induced effects that may have been missed by traditional single format screens. The application of such a 'three-pronged' screening approach may thus prove equally useful in various other models of pathogenic infection.

In conclusion, the compound-based screens described within this chapter effectively validated many of the HIV-host interactions identified by miRNA screening, and also demonstrated the significant utility of the established HCS pipeline for screening small molecules and compounds. The data generated by these screens have contributed a significant amount of new knowledge to HIV-host interactions and have revealed novel HIV-associated functionality for many FDA-approved therapies, which could be readily repurposed for the treatment of HIV. Finally, the novel multi-format screening approach and retrospective comparison of miRNA and compound phenotypes to identify miRNA-based alternative therapies, represent potentially valuable approaches for future drug discovery efforts.

Chapter 6: Concluding Remarks

Two decades since its discovery, HIV remains a disease for which there is neither a cure nor vaccine. The estimated cost associated with lifetime HIV treatment for a single patient is ~560 000 US dollars (Nakagawa, 2015), and this is a limiting factor to treatment accessibility in many developing regions hardest hit by the HIV/AIDS pandemic, including South Africa (UNAIDS, 2014). In addition, a number of drug-resistant variants of HIV have been identified (Wittkop, 2011) thereby necessitating the development of novel HIV therapies which are not only more cost-effective but also provide a stronger barrier against viral escape by simple mutagenesis. Host-directed therapy thus represents an attractive research avenue for the discovery of novel therapeutic strategies against HIV, but this approach also requires comprehensive knowledge of HIV-host interactions in order to identify suitable therapeutic targets. The combination of high throughput screening and RNAi interference technologies have emerged as powerful tools to delineate complex biological systems, including host-pathogen interactions (Lemons, 2013). Functional genomics screens specifically, have previously led to the identification of over 1000 host genes as novel host dependency factors (HDFs) that were required for successful HIV replication (Brass, 2008; Konig, 2008; Zhou, 2008). In comparison, the roles of the noncoding component of the human genome, including the host miRNAome, in modulation of HIV replication has remained comparatively poorly characterized (Barichievy, 2015).

The principal aims of this study were to establish, optimise and then utilise a high content phenotypic screening (HCS) workflow in order to characterise host miRNAs that were functionally relevant to HIV replication. To this end, a cell-based assay was optimised and validated for high throughput processing and bespoke image analysis and data mining pipelines were developed to facilitate efficient quantification of HIV replication from image-based datasets (Chapter 3). A panel of 1239 miRNA mimics and 1245 miRNA inhibitors were screened in duplicate in order to identify host miRNAs that could either significantly enhance or suppress HIV replication (see Chapter 4). A total of 7 560 individual experimental reactions yielded ~ 60 000 images, which following image analysis and data mining recovered 84 host miRNAs that were functionally relevant to HIV replication. Specifically, 53 mimics suppressed HIV replication and 28 miRNA mimics significantly enhanced HIV replication. In addition, 4 miRNA inhibitors also exhibited anti-HIV activity. These findings represent the largest single contribution to current knowledge on host miRNAs that functionally modulate HIV replication (Barichievy, 2015), and have expanded the number of host miRNAs demonstrated to functionally modulate HIV replication by well over two-fold.

miRNA-based therapeutics have recently gained a lot of momentum, and ongoing clinical evaluations of the first-in-class miRNA mimic-based therapy, MRX34 (Bouchie, 2013) and the first miRNA inhibitor-based therapy, Miravirsen (Janssen, 2013), suggest that these modalities may become increasingly relevant as new technologies enabling

their targeted delivery continue to evolve. The HIV-suppressive miRNA mimics recovered by HCS may therefore represent valuable therapeutic agents that could potentially either complement or replace current ARV therapies. Similarly, the miRNAs associated with enhanced viral replication phenotypes may prove useful in the activation of latent reservoirs of HIV. Additionally HIV-replication enhancing agents may prove valuable in improving viral protein yields for cell culture-based vaccine production and other commercial research applications.

An *in silico* approach to miRNA target validation and pathway analysis recovered a number of host pathways and processes previously associated with HIV replication (Chapter 4), but for which potential miRNA-mediated regulators were previously unknown. The outcomes of this study have thus, for the first time, provided specific panels of hosts miRNAs related to these host pathways with demonstrated HIV replication-modulating capabilities. Notably, these miRNAs have experimentally validated targets enriched within functional pathways previously associated with HIV replication including the MAPK, PI3K, TNF, cell cycle, P53 and DNA damage repair pathways to name a few. Pathway analysis also recovered novel HIV relevance for host pathways such as the Hippo signaling pathway, where the Hippo central kinase cascade and its downstream transcriptional effectors YAP/TAZ were implicated in miRNA-mediated modulation of HIV replication. Subsequent validation experiments also revealed novel HIV-related functional relevance for the long noncoding transcriptional target of P53, lincRNA-p21. Specifically, lincp21 was posited as a potential host factor associated with miRNA-mediated suppression of HIV replication, and the outcome of cell survival in response to DNA damage.

Furthermore, pathway analysis suggested a central convergence in processes associated with the evasion of apoptosis, regulation of cellular replication and modulation of host DNA repair factors. These molecular processes are typically associated with carcinogenesis and subsequent validation experiments demonstrated deregulated P53 transcriptional activity and aberrant cell survival in response to Etoposide-induced DNA damage in stably infected cells. This was in accordance with previous descriptions of oncogenic effects associated with HIV infection in various cellular models including primary macrophages (reviewed by Cummins, 2013). The concept of HIV preventing apoptosis in infected cells may at first seem counterintuitive given that HIV pathogenesis is known to result in the death/depletion of host T cell populations (Doitsh, 2014). This apoptotic effect has been further demonstrated to occur in both productively infected cells, through caspase-3 activation (Garg, 2006), and in abortive infections through caspase-1 activation and pyroptosis (Doitsh, 2014). However, during the early stages of viral infection (0-48 hpi) preceding virion release and apoptosis, HIV requires host cells to survive in order to produce sufficient amounts of virions and viral proteins. Many of these viral proteins, such Vpr, may induce genotoxic responses (e.g. DSBs) within infected host cells, especially at high concentrations (Andersen, 2006). HIV would therefore need to actively mitigate innate apoptotic responses induced by HIV replication events in order to prevent premature termination

of viral replication as a result of host cell death. This theory is supported by data showing viral subversion of key host factors associated with the apoptotic response, such as Nef-induced destabilization of P53 (Greenway, 2002).

Current knowledge thus suggests that HIV infection may induce a transient protective phenotype within infected T cells until sufficient levels of viral proteins are produced where increasing levels of genotoxic stress eventually overwhelm or release HIV-mediated subversion of apoptosis. A similar replicative strategy has also been noted for other intracellular pathogens including *Brucella abortus*, which promotes apoptosis in human macrophages, but only after sufficient periods of bacterial replication (Cha, 2013). Furthermore longer-term aberrant cell survival phenotypes have been described for HIV-infected primary macrophages and monocyte populations in response to DNA damage-induced apoptosis, suggesting that this cancer-like survival phenotype is highly conserved for HIV infection but may vary in duration in a cell-type specific manner (Cummins, 2013).

Strikingly however, validation experiments also revealed a potential vulnerability in the HIV replicative cycle which was related to the differential cell survival phenotypes recovered for Etoposide treatments. Specifically, while stably infected cells were resistant to Etoposide-induced apoptosis, the priming of host cells with Etoposide prior to or during HIV exposure resulted in broad cytotoxic effects that were specific to HIV treatments. The HIV infective state of a host cell was thus identified as a major determinant of cell survival in response to DNA damage and this suggested that HIV may exhibit temporally distinct phenotypic responses to host-directed therapeutic intervention. These findings posited the priming approach as a potentially effective strategy to counteract *de novo* HIV infection.

A secondary compound-based screening approach was selected to validate the pathway associations recovered by miRNA-based HCS and to further explore the divergent cell survival phenotypes associated with HIV exposure either prior to or following establishment of stable HIV infection. The newly established HCS workflow was adapted for compound screening (Chapter 3) and a novel multi-format screening and comparative analytical approach was utilised to screen 392 small molecules directed to the functional targets recovered by miRNA-based HCS (Chapter 5). Compounds generated anti-HIV phenotypes including those that induced apoptosis specifically in response to HIV infection/exposure and those that could suppress HIV replication in stably infected cells or prime host cells to resist HIV replication. Compound-based HCS recovered a total of 41 compounds that exhibited anti-HIV activity at a hit rate of ~10%, which would ordinarily be considered extremely high but in this case served as a validation of the utility of miRNA-based screening in advising targeted drug discovery. Interestingly, HIV was also observed to effectively attenuate the apoptotic activity of a specific subset of compounds, but only when compound treatments were administered to cell populations with an established HIV infection. In addition, a number of compounds were also found to prime uninfected host cells towards apoptosis specifically in response

to HIV exposure. These findings confirmed the phenotypes recovered for Etoposide-based validation experiments presented in Chapter 4, and recovered a number of novel functional targets which may be exploited to limit the spread of *de novo* HIV infection.

Drug-target interaction and enrichment analyses revealed a strong concordance between the anti-HIV phenotypes recovered by compound screening and functional targets recovered by miRNA-based HCS (Figure 6.1). Notably tyrosine kinase receptor-mediated signalling and its associated downstream effectors emerged as a central functional target for the modulation of HIV replication and HIV-associated cell survival by targeted pharmacological inhibition. Specific clusters of functional targets were also prioritized for the priming of HIV-naive cells to apoptosis in response to HIV exposure, suppression of HIV replication in stably infected cells and suppression of HIV replication or infection in HIV-naive cell populations primed with specific compounds. Given that the majority of compounds described to exhibit anti-HIV activity by this study are either under clinical investigation, or have already been granted FDA-approval, this positions these compounds as ideal candidates to be repurposed as anti-HIV therapies. Furthermore, convergent functional targets and phenotypic effects on HIV replication described for specific compounds and miRNAs suggests that these miRNAs could either be complementary therapies utilized to lower functional drug concentrations, or replacement therapies with similar functional properties as commercially available drugs. Further investigation is required to confirm that the HIV-associated phenotypes recovered for these compounds are not related to off-target effects on viral proteins.

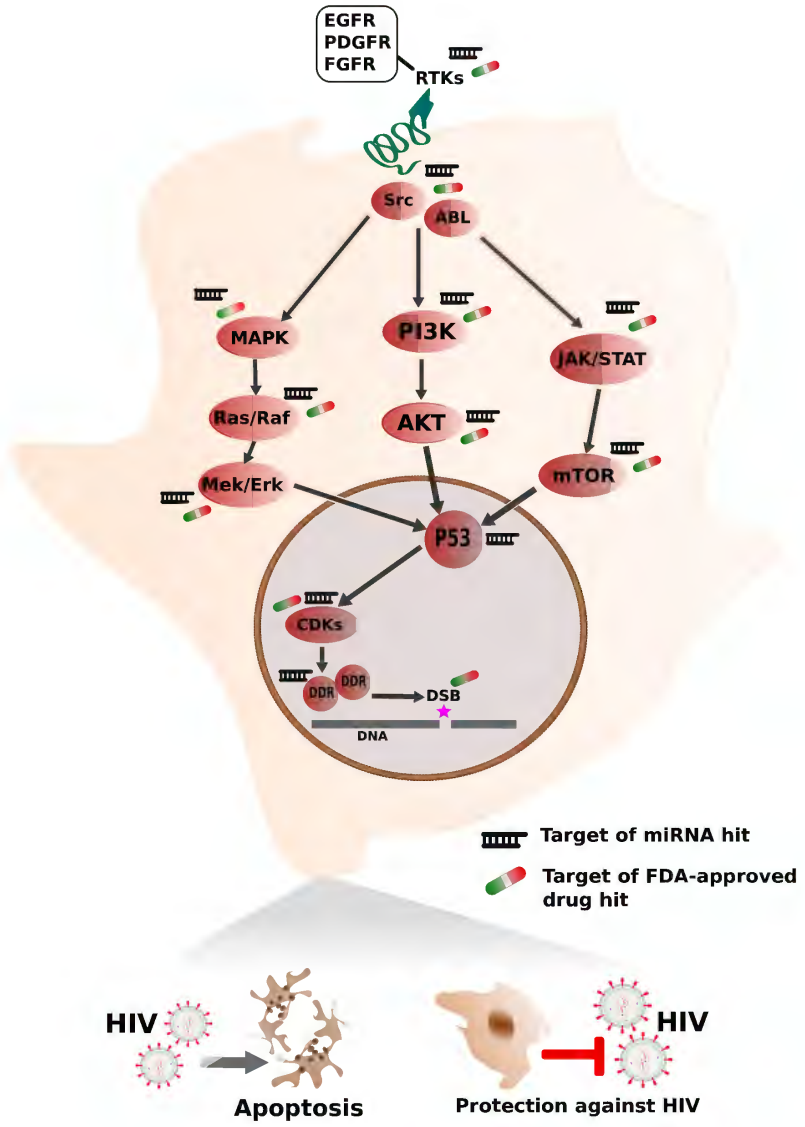

Figure 6.1 Concordance between miRNA and compound based HCS

Example of concordance between miRNA and compounds based HCS where functional targets that exhibited anti-HIV activity in the form of suppressed viral replication or HIV-specific toxicity are presented, double strand breaks (DSB).

In summation, this study has established a robust HCS workflow, which has been demonstrated to be suitable for both RNAi and compound-based phenotypic screening. Additionally, the outcomes of the miRNA screens presented here represent a significant novel contribution to current knowledge on HIV-host miRNA interactions, and have uncovered novel putative HIV-based therapeutic applications for a large panel of host miRNAs. Furthermore a cancer-like molecular phenotype was characterized in HIV-infected cells populations, which may be therapeutically relevant and exploitable during the early stages of HIV infection. The multiformat compound screening approach was also able to identify novel anti-HIV activity for a number of therapeutically-relevant compounds, and identified specific temporally discrete functional clusters that may be

exploited for the treatment and(or) prevention of HIV replication. Comparative analysis between miRNA and compounds screens revealed a number of miRNAs that may potentially be utilised as alternative or complementary therapies to specific commercially active drugs. The findings of this study may thus contribute to the development of future therapies against HIV, and represents a substantial contribution towards current knowledge on HIV-host interactions.

Appendices

Appendix 2

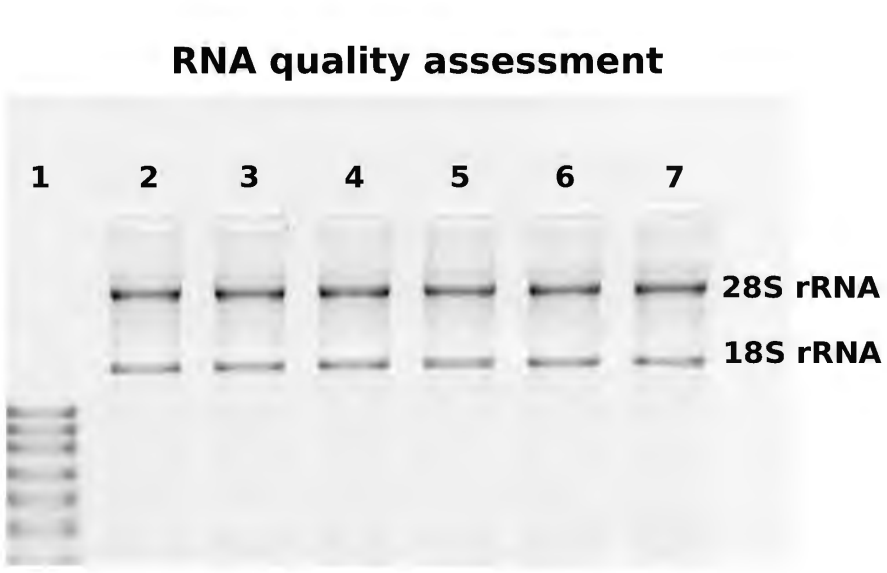

Figure A2.1 Example of RNA quality evaluation by electrophoresis

RNA isolated from GHOST(3) cells and evaluated prior to utilisation in cDNA synthesis. Acceptable RNA quality as is indicated by intact 28S and 18S bands. 1) RNA ladder, 2) GHOST(3) cells only, 3) GHOST(3) cells 24 hpi, 4) GHOST(3) cells 48 hpi, 5) GHOST(3) cells-siCD4, 6) GHOST(3) cells- siHuR, 7) GHOST(3) cells-LincRNA-p21. 1 µg of RNA loaded per sample/well.

Table A2.1 List of compounds in Oncology FDA-approved compound library

Methotrexate	Daunorubicin hydrochloride	Vorinostat
Busulfan	Streptozocin	Estramustine phosphate sodium
Thioguanine	Arsenic trioxide	Capecitabine
Mercaptopurine	Azacitidine	Exemestane
Mechlorethamine hydrochloride	Cladribine	Gefitinib
Allopurinol	Ifosfamide	Erlotinib hydrochloride
Dactinomycin	Cisplatin	Fulvestrant
Chlorambucil	Tretinoin	Arimidex
Thiotepa	Teniposide	Letrozole
Melphalan	Doxorubicin hydrochloride	Celecoxib
Triethylenemelamine	Bleomycin sulfate	Zoledronic acid
Altretamine	Paclitaxel	Dasatinib
Quinacrine hydrochloride	Decitabine	Everolimus
Aminolevulinic acid hydrochloride	bendamustine hydrochloride	Pazopanib HCl
Fluorouracil	Etoposide	Imatinib mesylate
Plicamycin	Dexrazoxane	Lapatinib ditosylate
Pipobroman	Tamoxifen citrate	Nilotinib
Cyclophosphamide	Pentostatin	Sorafenib tosylate
Mitomycin	Sirolimus	Lenalidomide
Floxuridine	Carboplatin	Ixabepilone
Hydroxyurea	Valrubicin	Raloxifene hydrochloride
Uracil mustard	Oxaliplatin	Abiraterone
Mitotane	Mitoxantrone	Sunitinib (free base)
Dacarbazine	Amifostine	Depsipeptide
Methoxsalen	Fludarabine phosphate	pralatrexate
Vinblastine sulfate	Temozolomide	Vismodegib
Cytarabine hydrochloride	Imiquimod	PF-2341066
Thalidomide	Carmustine	AG-013736
Vincristine sulfate	Clofarabine	Carfilzomib
Megestrol acetate	Vinorelbine tartrate	Vandetanib
Procarbazine hydrochloride	Topotecan hydrochloride	Vemurafenib
Lomustine	Gemcitabine hydrochloride	Cabazitaxel
Nelarabine	Irinotecan hydrochloride	Bortezomib
Pemetrexed Disodium	Docetaxel	

Table A2.2 List of compounds in Kinase Inhibitor compound library*

BMS-599626 (AC480)	SNS-032 (BMS-387032)	WYE-125132
Erlotinib HCl	AZD7762	SB 431542
Gefitinib (Iressa)	Aurora A Inhibitor I	Linifanib (ABT-869)
Neratinib (HKI-272)	Barasertib (AZD1152-HQPA)	AEE788 (NVP-AEE788)
PD153035 HCl	CCT129202	Afatinib (BIBW2992)
Pelitinib (EKB-569)	ENMD-2076	Lapatinib Ditosylate (Tykerb)
Vandetanib (Zactima)	MLN8237 (Alisertib)	JNJ-7706621
WZ3146	Telatinib (BAY 57-9352)	WYE-687
WZ4002	PHA-680632	BEZ235 (NVP-BEZ235)
WZ8040	SNS-314	GSK1059615
Axitinib	VX-680 (MK-0457, Tozasertib)	AG-490
BIBF1120 (Vargatef)	ZM-447439	Tofacitinib citrate (CP-690550 citrate)
BMS 794833	AS703026	Crenolanib (CP-868596)
NVP-BHG712	AZD6244 (Selumetinib)	GSK1838705A
Cediranib (AZD2171)	AZD8330	KX2-391
OSI-420 (Desmethyl Erlotinib)	BIX 02188	NVP-BSK805
CYC116	BMS 777607	PCI-32765 (Ibrutinib)
R935788 (Fostamatinib disodium, R788)	CI-1040 (PD184352)	PF-00562271
Imatinib (Gleevec)	PD318088	DCC-2036 (Rebastinib)
Imatinib Mesylate	PD0325901	LDN193189
KRN 633	PD98059	Flavopiridol hydrochloride
Masitinib (AB1010)	U0126-EtOH (UO126 EtOH)	AS-604850
MGCD-265	LY2228820	WAY-600
Motesanib Diphosphate	BIRB 796 (Doramapimod)	TG101209
Amuvatinib (MP-470)	SB 202190	GDC-0980 (RG7422)
OSI-930	SB 203580	A-769662
Pazopanib HCl	VX-702	TAK-901
Sorafenib (Nexavar)	VX-745	AMG 900
Sunitinib Malate (Sutent)	GDC-0879	ZM 336372
TSU-68	CX-4945	PH-797804
Foretinib (GSK1363089, XL880)	PLX-4720	AZD8931
Danusertib (PHA-739358)	RAF265 (CHIR-265)	Tivozanib (AV-951)
AT9283	SP600125	Ki8751
Saracatinib (AZD0530)	Phenformin hydrochloride	Vatalanib dihydrochloride (PTK787)
Bosutinib (SKI-606)	AS-605240	Ponatinib (AP24534)
Dasatinib (BMS-354825)	GDC-0941	SU11274
Nilotinib (AMN-107)	LY294002	Flavopiridol (Alvocidib)

Quercetin (Sophoretin)	PIK-293	Hesperadin
NVP-ADW742	PIK-90	Raf265 derivative
Quizartinib (AC220)	PIK-93	AZ 960
Tandutinib (MLN518)	TG100-115	Mubritinib (TAK 165)
KW 2449	TGX-221	PP242
CI-1033 (Canertinib)	XL147	Apatinib (YN968D1)
CP-724714	XL765	CAL-101 (GS-1101)
Regorafenib (BAY 73-4506)	ZSTK474	PIK-294
JNJ-38877605	AZD8055	BI6727 (Volasertib)
PF-04217903	Everolimus (RAD001)	BIX 02189
Crizotinib (PF-02341066)	Ku-0063794	BKM120 (NVP-BKM120)
Cyt387	Rapamycin (Sirolimus)	IC-87114
SGX-523	Temsirolimus (Torisel)	Deforolimus (Ridaforolimus)
TAE684 (NVP-TAE684)	WYE-354	KU-55933
SB 525334	PP-121	GSK2126458
R406	PIK-75	PI-103
R406(free base)	CHIR-99021 (CT99021)	GSK1120212 (Trametinib)
XL-184 free base (Cabozantinib)	Indirubin	WP1130
BI 2536	SB 216763	TAK-733
GSK461364	KU-60019	AZD5438
HMN-214	MK-2206 dihydrochloride	OSI-027
ON-01910	LY2603618 (IC-83)	NU7441(KU-57788)
AT7519	AT7867	A-674563
BS-181 HCl	PF-05212384 (PKI-587)	AS-252424
PD 0332991 HCl	AZD1480	PF-04691502
PHA-793887	CCT128930	
Roscovitine (Seliciclib, CYC202)	LY2784544	
Enzastaurin (LY317615)	A66	

* Alternate compound name or commercial name indicated within brackets

Appendix 3

A3.1 miRNA library reconstitution

Briefly, all 96 well master plates containing lyophilized pellets were centrifuged at 500 x g for 5 minutes at 4 °C in a Microfuge 22R refrigerated benchtop microcentrifuge (Beckman Coulter Incorporated, USA) before use. 250 µL of 1x Dharmacon™ siRNA buffer (GE Healthcare, USA) was dispensed per well into all wells of a master plate, excluding columns 1 and 12 . The contents of each well were mixed by repeat pipetting (100 µL volume three times) and the plates were then sealed with Rotilabo® AllumaSeal II™ sterile adhesive seals (Carl Roth GmbH + Co. KG, Germany), and placed on a Stuart® SSM5 microtitre plate shaker (medium setting) for 30 minutes at room

temperature (Bibby Scientific Limited, UK). The master plate was re-centrifuged at 500 x g for 5 minutes at 4 °C, the seal was removed and the contents of each well were mixed by repeat pipetting (50 µL volume three times). A volume of 50 µL was then aspirated from each well and 15 µL of each reagent was dispensed into corresponding wells in each of 3 pre-labelled daughter plates. The daughter plates and the master plate were then sealed with Rotilabo® AllumaSeal II™ sterile adhesive seals (Carl Roth GmbH + Co. KG, Germany) and placed into storage at - 20 ˚C. Plates and individual wells had to be sealed in order to prevent reagent loss and cross-contamination during long term storage. Rotilabo® AllumaSeal II™ sterile adhesive seals (Carl Roth GmbH + Co. KG, Germany) seals were specifically selected for plate storage due to their increased stability at low temperatures thus facilitating library storage at -80 ˚C and transport on dry ice should this be required at any stage. Likewise, Corning® 96 Well Clear V-Bottom Polypropylene microplates (Corning®, UK) were selected as the daughter plate type due to their increased stability at -80 ˚C as compared to standard polystyrene microplates. miRNA master and daughter plates were stored in dedicated non-cycling freezers at -20 ˚C. Reconstitution and daughtering of the entire miRIDIAN library was staggered and completed over the course of a week. Master and daughter plates were always centrifuged at ~500 x g for 5 minutes at 4 °C prior to use.

A3.2 Compound libraries

As with the miRNA library, all master and daughter plates removed from storage were always briefly centrifuged at ~500 x g for 5 minutes at 4 °C prior to use. All compound library dilution, re-formatting and daughtering steps were completed by hand using Lambda™ Plus 12 channel micropipettes (Corning®, UK) in a BSL-2 biosafety cabinet.

A3.3 Cell seeding protocol

Cell seeding was the first experimental step in the screening workflow of both miRNA and compound screens. The process of seeding a relatively constant volume and density of cells across multiple 96 well experimental plates was achieved by first detaching GHOST(3) cells from their culture vessels and resuspending them in a low volume of culture media. The number of cells present was calculated using a TC10™ automated cell counter (Bio-Rad, USA), to ensure consistency of cell counting across multiple seeding events and to reduce the time spent on this step. The required cell dilution was generated in an appropriate volume in a sterile Pierce® reagent reservoir (Thermo Fisher Scientific, USA), and dispensed across experimental plates using a multichannel micropipette. The reagent reservoir was agitated by hand and the solution was always repeat pipetted before each aspiration step.

When a multiwell plate (room temperature) is placed into an incubator, a transient temperature gradient is created from outside of the plate to the inner wells as the plate reaches 37 ˚C. This temperature gradient can result in differential cell attachment

patterns across the wells of a multiwell plate which can in turn distort downstream experimental readouts (Lundholt, 2003). All experimental screen plates were therefore incubated at room temperature for ~ 20 mins prior to being placed in a cell culture incubator. This allowed cells to settle evenly across all experimental wells thus mitigating the potential effects of resulting temperature gradients on cellular densities. GHOST(3) cells were seeded at a constant density of 5000 cells/well for miRNA screens and 6000 cells/well for compound screens. Specific seeding volumes were selected for both miRNA and compound screens in order to minimise downstream liquid handling steps. For example, by seeding GHOST(3) cells in 80 µL of culture media for the miRNA screens, the volume of media in each well did not need to be adjusted prior to the transfection step. In addition to reducing the required treatment time this design principle also reduced the overall cost of the screen by reducing the number of filtered micropipette tips required. During large-scale screens, omission a single pipetting step from a workflow process can have a huge impact on the requirement of consumables and can therefore also affect the total cost of the screen. This design principle was applied to all screening-related experimental steps where possible.

A3.4 HCS GHOST(3)-PSG3^{BAL} infection protocol

PSG3^{BAL} viral stocks were diluted in infection media and then dispensed into a sterile reagent reservoir. Culture media was removed from each well on an experimental plate using a multichannel micropipette. 50 µL of HIV-naive infection media was added to each uninfected control well using a single channel micropipette. 50 µL of diluted PSG3^{BAL} solution was dispensed into all infected control wells and all experimental wells using a multichannel micropipette. The reagent reservoir was agitated by hand before each dispensing step. Infection reactions utilized in both miRNA and compound screens were executed in final reaction volumes of 50 µL, in order to increase the probability of virion to cell contact events. GHOST(3) cells were exposed to PSG3^{BAL} at an MOI of 0.5 for both miRNA and compound screens and cell cultures were always exposed for 48 hours before the infectious media was removed.

A3.5 HCS liquid handling practices

All liquid transfer steps following cell seeding were carefully executed so as not to disturb adherent cells at the bottom of each experimental well (Figure A3.1) by following specific aspiration (Figure A3.1 A) and dispensing (Figure A3.1 B) techniques.

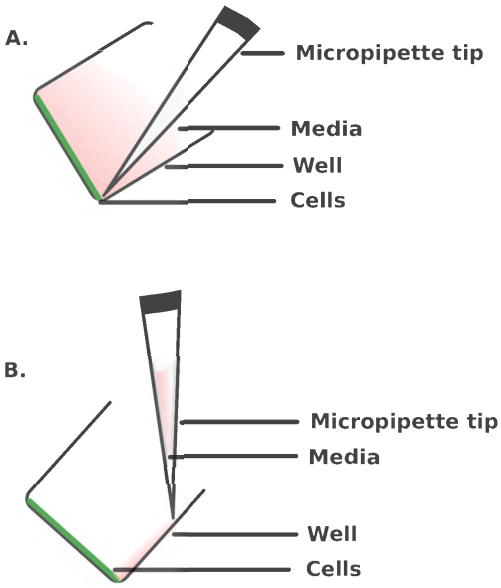

Figure A3.1 Aspiration and dispensing techniques utilized in HCS workflow.

A) Solutions were aspirated from wells by angling the experimental plate and positioning micropipette tips at the bottom each well. B) Solutions were dispensed into experimental wells by angling the experimental plate and placing the micropipette tip against the wall of the well.

A3.6 GHOST(3) infection assay validation

GHOST(3) infection time course in order to determine suitable infection time point for HCS assay. 48hpi was observed to be the shortest time course that produced significant reporter activation following infection.

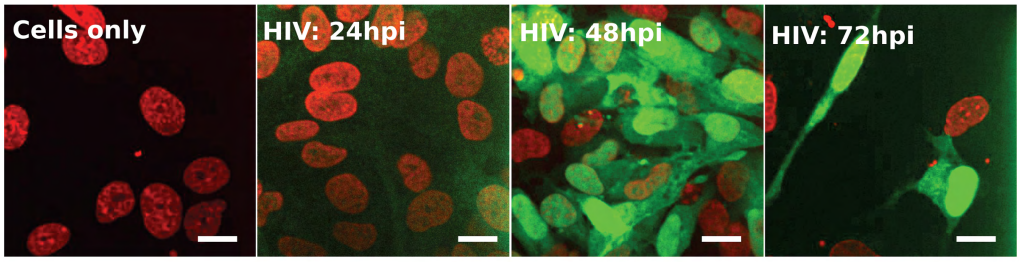

Figure A3.2 GHOST(3) reporter signal relative to infection time course

GFP-reporter signal readout in uninfected cells (cells only), 24hr post infection, 48hr post infection and 72hr postinfection. Cells infected at MOI of 0.5 with $PSG3^{BAL}$. GFP-reporter signal (green), nuclei stained with Hoechst (red), scale bars = 10 μm.

Appendix 4

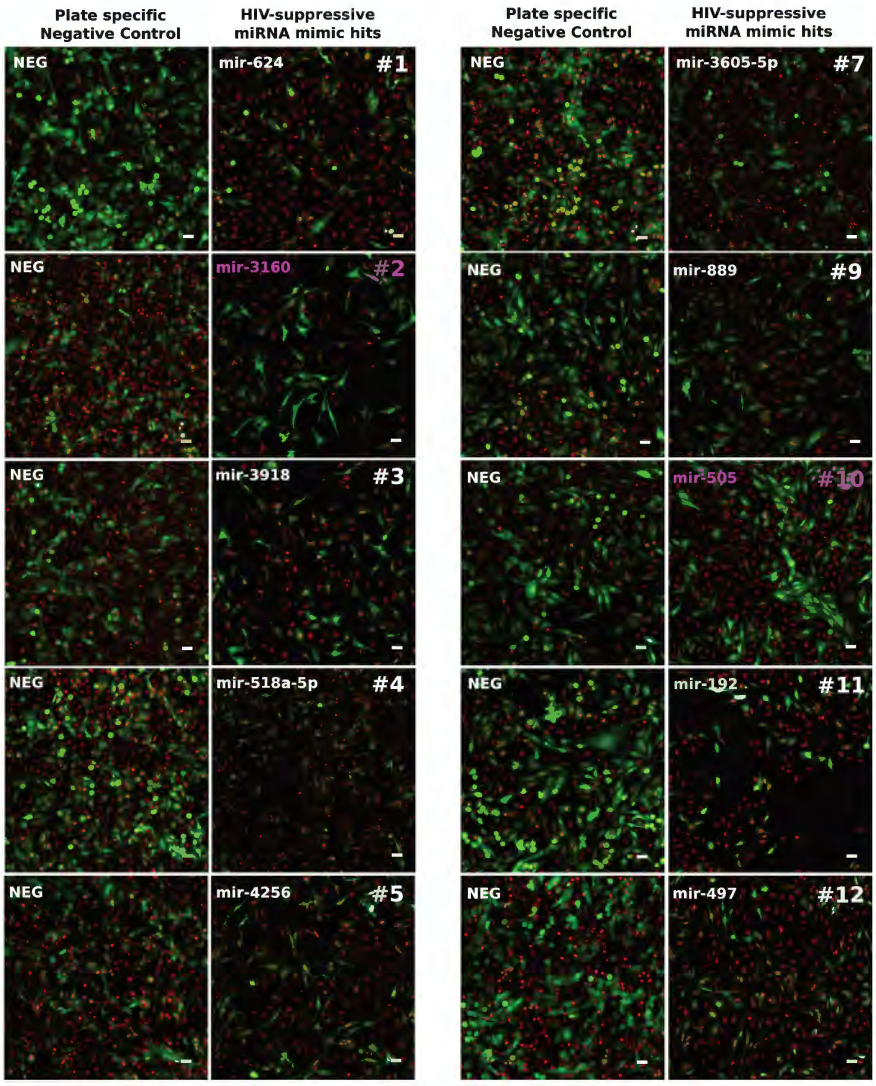

Figure A4.1 Visual profiles of HIV-suppressive hits identified by PCA-STP hit selection.

Hits that did not exhibit desirable phenotypes following visual inspection were excluded from further analysis (pink miRNA name and rank). Images represent unprocessed composite images acquired in the 405 and 488 channels. GFP-reporter signal (green), nuclei stained with Hoechst (red), scale bars = 20 μm.

Table A4.1 HIV replication suppressing miRNA mimic hitlist *

hsa-miR-1185	hsa-miR-3616-5p
hsa-miR-1231	hsa-miR-3622a-5p
hsa-miR-124	hsa-miR-3647-5p
hsa-miR-1250	hsa-miR-3691
hsa-miR-1269	hsa-miR-383
hsa-miR-127-5p	hsa-miR-3918
hsa-miR-1270	hsa-miR-3927
hsa-miR-1273e	hsa-miR-4256
hsa-miR-1295	hsa-miR-4270
hsa-miR-1306	hsa-miR-431*
hsa-miR-135b*	hsa-miR-4314
hsa-miR-138	hsa-miR-450b-3p
hsa-miR-145*	hsa-miR-483-5p
hsa-miR-192	hsa-miR-491-5p
hsa-miR-193b*	hsa-miR-497
hsa-miR-2110	hsa-miR-506
hsa-miR-3166	hsa-miR-518a-5p
hsa-miR-3173	hsa-miR-520d-5p
hsa-miR-3179	hsa-miR-624
hsa-miR-3189	hsa-miR-637
hsa-miR-3190	hsa-miR-650
hsa-miR-3192	hsa-miR-654-5p
hsa-miR-3200-3p	hsa-miR-671-3p
hsa-miR-342-5p	hsa-miR-889
hsa-miR-34a*	hsa-miR-892b
hsa-miR-3605-5p	hsa-miR-940
hsa-miR-3616-3p	

*mirBase v16.0 nomenclature

Table A4.2 HIV replication enhancing miRNA mimic hitlist*

hsa-miR-378*	hsa-miR-3171
hsa-miR-649	hsa-miR-1260b
hsa-miR-141*	hsa-miR-1271
hsa-miR-136*	hsa-miR-587
hsa-miR-2277-5p	hsa-miR-1260
hsa-miR-3679-3p	hsa-miR-335*
hsa-miR-3938	hsa-miR-200b*
hsa-miR-668	hsa-miR-675*
hsa-miR-891b	hsa-miR-22
hsa-miR-4318	hsa-miR-576-3p

hsa-miR-200a*	hsa-miR-19b-2*
hsa-miR-218-1*	hsa-miR-1308
hsa-miR-188-5p	hsa-miR-550*
hsa-miR-625*	hsa-miR-34c-3p

*mirBase v16.0 nomenclature

Table A4.3 Pathways enriched for suppressed HIV replication

Pathway	Number of genes	Number of miRNAs
Proteoglycans in cancer	138	48
Pathways in cancer	252	48
Focal adhesion	138	48
HTLV-I infection	163	47
Regulation of actin cytoskeleton	127	47
MAPK signaling pathway	150	47
Hippo signaling pathway	112	46
Viral carcinogenesis	132	46
Epstein-Barr virus infection	128	46
Protein processing in endoplasmic reticulum	109	45
Insulin signaling pathway	90	45
Transcriptional misregulation in cancer	107	45
cGMP-PKG signaling pathway	104	44
Signaling pathways regulating pluripotency of stem cells	87	44
FoxO signaling pathway	88	43
Adherens junction	56	42
Neurotrophin signaling pathway	82	42
Wnt signaling pathway	90	42
Sphingolipid signaling pathway	74	42
Estrogen signaling pathway	73	41
Thyroid hormone signaling pathway	78	41
Cell cycle	86	40
TNF signaling pathway	76	40
Axon guidance	81	40
ErbB signaling pathway	62	40
Oocyte meiosis	74	40
Choline metabolism in cancer	66	40
TGF-beta signaling pathway	52	39
Chronic myeloid leukemia	56	38
Prostate cancer	67	38

Bacterial invasion of epithelial cells	57	38
Hepatitis B	94	38
Glioma	44	38
Fc gamma R-mediated phagocytosis	59	38
ECM-receptor interaction	55	37
Renal cell carcinoma	48	37
Pancreatic cancer	54	35
Melanoma	49	35
Arrhythmogenic right ventricular cardiomyopathy (ARVC)	42	35
p53 signaling pathway	45	35
GnRH signaling pathway	59	35
Progesterone-mediated oocyte maturation	64	34
Small cell lung cancer	60	34
Shigellosis	46	34
Colorectal cancer	50	33
mTOR signaling pathway	48	33
Endometrial cancer	42	33
Central carbon metabolism in cancer	42	33
Acute myeloid leukemia	44	32
Bladder cancer	32	31
Non-small cell lung cancer	41	31
Vasopressin-regulated water reabsorption	30	30
Thyroid hormone synthesis	44	29
Sphingolipid metabolism	30	29
N-Glycan biosynthesis	32	27
Thyroid cancer	22	24
Prion diseases	15	22
Fatty acid metabolism	29	22
Fatty acid elongation	15	15
Homologous recombination	21	15
Glycosaminoglycan biosynthesis - chondroitin sulfate / dermatan sulfate	15	12
Fatty acid biosynthesis	7	8

Table A4.4 Pathways enriched for enhanced HIV replication

KEGG pathway	#genes	#miRNAs
PI3K-Akt signaling pathway	124	26
Proteoglycans in cancer	96	24
Focal adhesion	96	24
Regulation of actin cytoskeleton	88	24
Pathways in cancer	149	24
Viral carcinogenesis	89	23
Protein processing in endoplasmic reticulum	76	23
Hippo signaling pathway	63	22
Oocyte meiosis	56	22
Cell cycle	66	22
Hepatitis B	64	22
Thyroid hormone signaling pathway	54	22
Endocytosis	83	22
Transcriptional misregulation in cancer	70	22
Adherens junction	41	21
Central carbon metabolism in cancer	31	21
mRNA surveillance pathway	42	21
Signaling pathways regulating pluripotency of stem cells	55	21
Salmonella infection	37	21
Small cell lung cancer	37	21
Prostate cancer	45	20
ErbB signaling pathway	40	20
Colorectal cancer	32	20
FoxO signaling pathway	53	20
HIF-1 signaling pathway	47	20
Neurotrophin signaling pathway	51	20
TGF-beta signaling pathway	36	19
Chronic myeloid leukemia	41	19
Renal cell carcinoma	33	19
p53 signaling pathway	31	19
Insulin signaling pathway	59	19
Wnt signaling pathway	57	19
Pancreatic cancer	36	18

Spliceosome	57	18
Melanoma	32	18
Epstein-Barr virus infection	82	18
Glioma	33	17
Bacterial invasion of epithelial cells	35	17
Shigellosis	32	17
Lysine degradation	22	16
Endometrial cancer	24	16
ECM-receptor interaction	33	14
Bladder cancer	21	14
Alanine, aspartate and glutamate metabolism	17	13
Prion diseases	12	12
2-Oxocarboxylic acid metabolism	10	8
Glycosaminoglycan biosynthesis - keratan sulfate	7	7
Fatty acid biosynthesis	2	3

Table A4.5 HIV-suppressive miRNA hits associated with viral carcinogenesis*

hsa-miR-1185-5p	hsa-miR-3200-3p	hsa-miR-520d-5p
hsa-miR-1231	hsa-miR-342-5p	hsa-miR-624-3p
hsa-miR-124-3p	hsa-miR-34a-3p	hsa-miR-650
hsa-miR-1269a	hsa-miR-3605-5p	hsa-miR-654-5p
hsa-miR-127-5p	hsa-miR-3616-3p	hsa-miR-671-3p
hsa-miR-1270	hsa-miR-3616-5p	hsa-miR-889-3p
hsa-miR-1273e	hsa-miR-3622a-5p	hsa-miR-892b
hsa-miR-1306-3p	hsa-miR-3691-5p	hsa-miR-940
hsa-miR-135b-3p	hsa-miR-3918	
hsa-miR-138-5p	hsa-miR-4256	
hsa-miR-192-5p	hsa-miR-4270	
hsa-miR-193b-5p	hsa-miR-431-3p	
hsa-miR-2110	hsa-miR-4314	
hsa-miR-3166	hsa-miR-450b-3p	
hsa-miR-3173-3p	hsa-miR-483-5p	
hsa-miR-3179	hsa-miR-491-5p	
hsa-miR-3189-3p	hsa-miR-497-5p	
hsa-miR-3190-5p	hsa-miR-506-3p	

hsa-miR-3192-5p	hsa-miR-518a-5p	

*miRNA (mirBASE v.20), miRNAs are ranked numerically

Table A4.6 HIV replication enhancing miRNA hits associated with viral carcinogenesis*

hsa-miR-1260a	hsa-miR-34c-3p
hsa-miR-1260b	hsa-miR-378a-5p
hsa-miR-1271-5p	hsa-miR-3938
hsa-miR-136-3p	hsa-miR-4318
hsa-miR-141-5p	hsa-miR-550a-3p
hsa-miR-188-5p	hsa-miR-576-3p
hsa-miR-200a-5p	hsa-miR-587
hsa-miR-200b-5p	hsa-miR-625-3p
hsa-miR-218-1-3p	hsa-miR-649
hsa-miR-22-3p	hsa-miR-668-3p
hsa-miR-3171	hsa-miR-891b
hsa-miR-335-3p	

*miRNA (mirBASE v.20), miRNAs are ranked numerically

Table A4.7 miRNA targets exclusively associated with enhanced viral replication that also coincide with members of the viral carcinogenesis pathway

Gene symbols (KEGG identifiers)			
CCNE2	HIST1H4L	H2BFM	SRF
CHEK1	HPN	HDAC6	STAT5B
DNAJA3	JAK1	HDAC8	TRAF3
GTF2A2	PIK3R1	HIST1H4A	
GTF2H1	PIK3R3	SP100	

Table A4.8 miRNA targets exclusively associated with viral carcinogenesis and suppressed HIV replication

Gene symbols (KEGG identifiers)			
ATF4	GRB2	HIST1H4E	PIK3CA
ATF6B	GTF2H2	HIST1H4H	PIK3CB
BAD	GTF2H3	HIST1H4J	PIK3R5
CCNA1	HDAC10	HIST2H2BE	PSMC1
CCND3	HDAC11	HIST2H4A	RANBP1
CCR8	HDAC5	HLA-B	RB1
CDC42	HIST1H2BB	HLA-C	RBL2
CDKN2A	HIST1H2BF	HLA-F	SKP2
CREB1	HIST1H2BH	KAT2A	SND1

CREB3	HIST1H2BI	KAT2B	SNW1
CREB3L1	HIST1H2BJ	KRAS	TBPL1
DLG1	HIST1H2BL	LYN	TRAF2
EGR2	HIST1H2BO	MAPK3	TRAF5
EGR3	HIST1H4B	NFKB1	USP7
EIF2AK2	HIST1H4C	NFKBIA	

A.

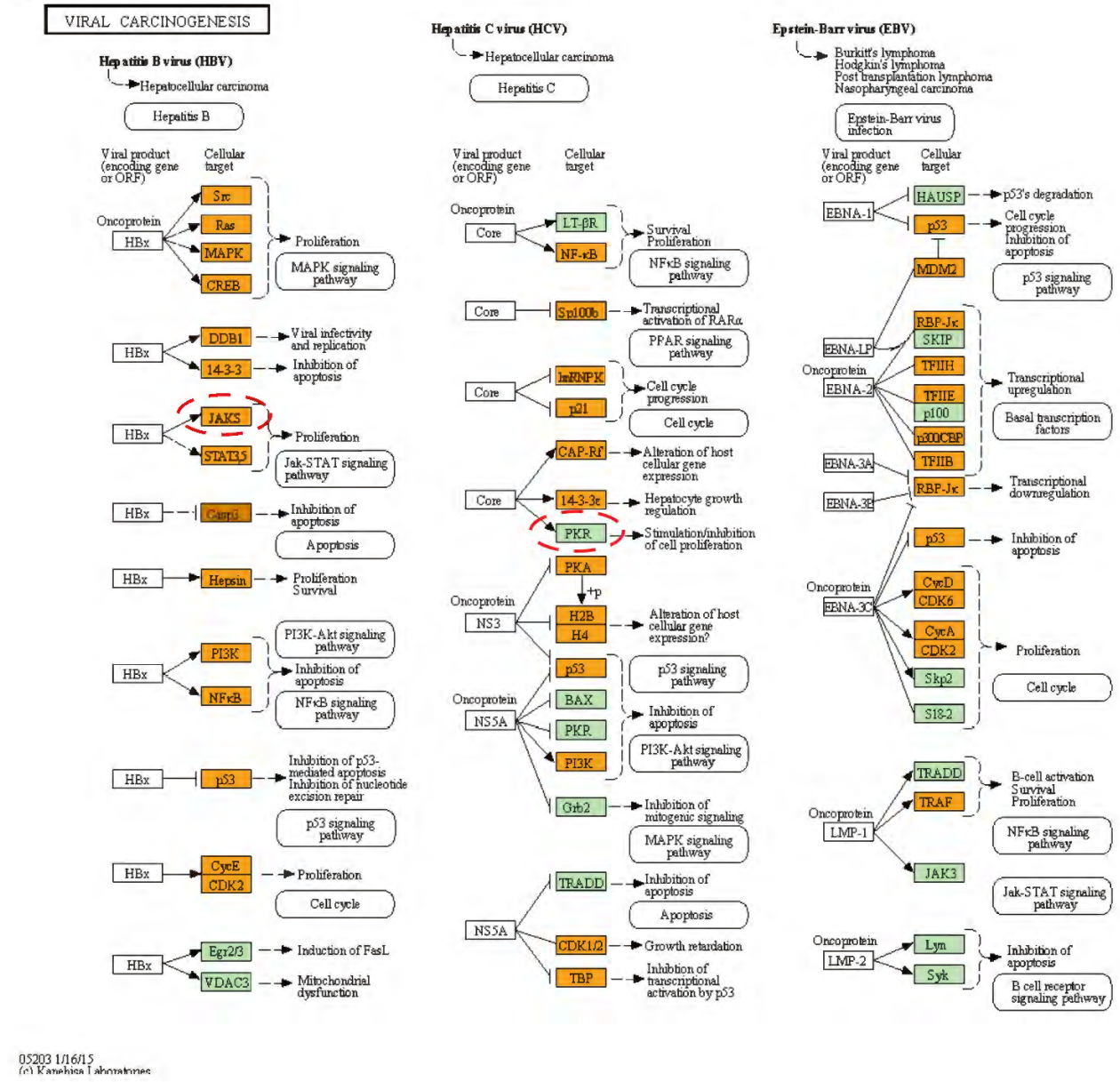

B.

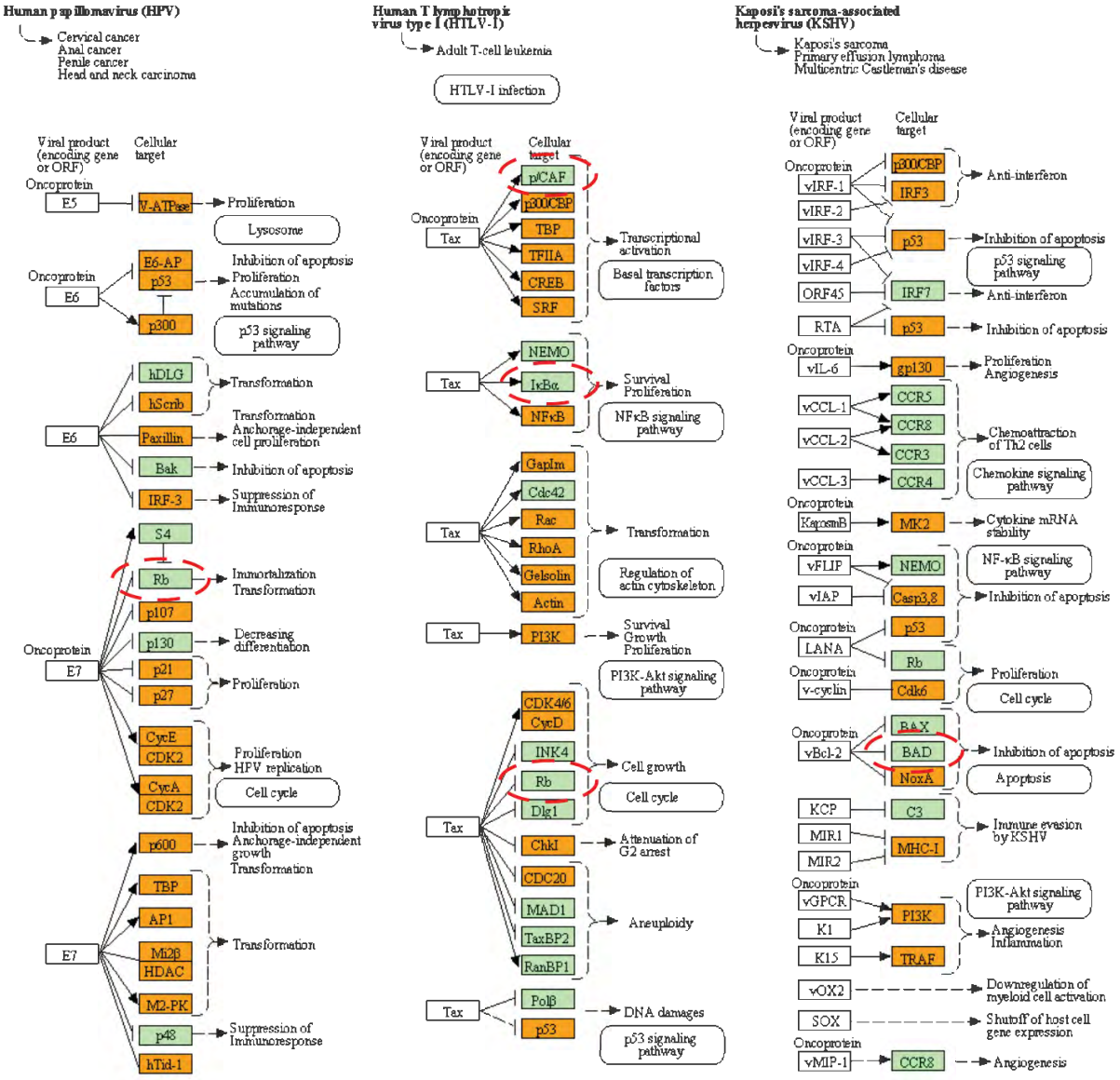

Figure A4.2 miRNA targets associated with viral carcinogenesis and enhanced HIV replication.

A) Summary of viral-host interactions relevant to HCV, HBV and EBV. **B)** Summary of the viral-host interactions relevant to HPV, HTLV-I and KSHV. Host genes targeted by miRNA hits (orange), host genes not targeted by miRNA hits (green), viral proteins (white), proteins differentially targeted by HIV-suppressing miRNAs (red ring).

Table A4.9 HIV-replication suppresive miRNA hits associated with cell cycle

miRNA (mirBase v.20)*		
hsa-miR-1231	hsa-miR-431-3p	hsa-miR-4314
hsa-miR-124-3p	hsa-miR-3190-5p	hsa-miR-450b-3p
hsa-miR-127-5p	hsa-miR-3192-5p	hsa-miR-483-5p
hsa-miR-1270	hsa-miR-3200-3p	hsa-miR-491-5p
hsa-miR-1295a	hsa-miR-342-5p	hsa-miR-497-5p
hsa-miR-1306-3p	hsa-miR-34a-3p	hsa-miR-506-3p
hsa-miR-135b-3p	hsa-miR-3605-5p	hsa-miR-518a-5p
hsa-miR-138-5p	hsa-miR-3616-3p	hsa-miR-520d-5p
hsa-miR-145-3p	hsa-miR-3616-5p	hsa-miR-624-3p
hsa-miR-192-5p	hsa-miR-3622a-5p	hsa-miR-650
hsa-miR-193b-5p	hsa-miR-3691-5p	hsa-miR-654-5p
hsa-miR-2110	hsa-miR-3918	hsa-miR-671-3p
hsa-miR-3166	hsa-miR-3927-3p	hsa-miR-889-3p
hsa-miR-3173-3p	hsa-miR-4256	hsa-miR-892b
hsa-miR-3179	hsa-miR-4270	hsa-miR-940
hsa-miR-3189-3p		

Table A4.10 HIV-replication enhancing miRNA hits associated with cell cycle

miRNA (mirBase v.20)	
hsa-miR-378a-5p	hsa-miR-1271-5p
hsa-miR-141-5p	hsa-miR-891b
hsa-miR-22-3p	hsa-miR-576-3p
hsa-miR-34c-3p	hsa-miR-200a-5p
hsa-miR-188-5p	hsa-miR-218-1-3p
hsa-miR-335-3p	hsa-miR-19b-2-5p
hsa-miR-550a-3p	hsa-miR-668-3p
hsa-miR-625-3p	hsa-miR-3171
hsa-miR-1260b	hsa-miR-200b-5p
hsa-miR-4318	hsa-miR-3938
hsa-miR-1260a	hsa-miR-136-3p

Table A4.11 miRNA hits exclusively associated with cell cycle and enhanced HIV replication

Gene symbols (KEGG identifiers)			
ATR	CDC6	CUL1	TFDP2
CCNE2	CHEK1	SMAD4	

Table A4.12 miRNA hits exclusively associated with cell cycle and suppressed HIV replication

Gene symbols (KEGG identifiers)			
ANAPC1	CDC14B	FZR1	PTTG2
ANAPC13	CDC27	MAD2L1	RB1
ANAPC4	CDKN2A	MAD2L2	RBL2
CCNA1	CDKN2D	ORC1	SKP2
CCNB1	DBF4	ORC5	TFDP1
CCND3	E2F4	PCNA	TTK
CDC14A	E2F5	PTTG1	

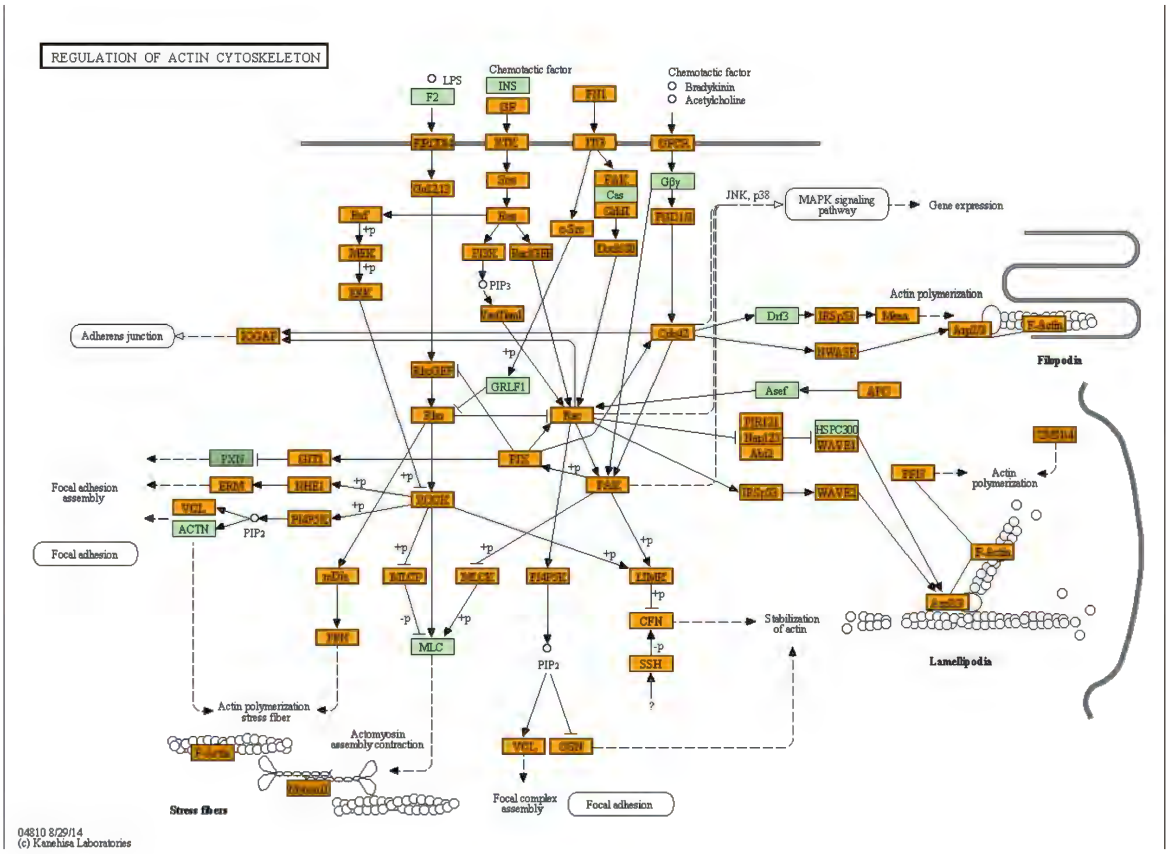

Figure A4.3 Cytoskeletal-associated functional processes enriched for miRNA hits that suppress HIV replication.

Regulation of the actin cytoskeleton including signalling cascades related to focal adhesions, stress fibres, cellular extensions and adherens junctions. Genes targeted by miRNA hits (orange), genes not targeted by miRNA hits (green), bacterial protein (white).

Table A4.13 miRNA hits exclusively associated with regulation of actin cytoskeleton and suppressed HIV replication

Gene symbols (KEGG identifiers)		
APC	FGF18	MYLK
ARAF	FGF23	MYLK4
ARHGEF1	FGF7	NCKAP1
ARPC4	FGFR1	PAK3
ARPC5L	GNA12	PIK3CA
BDKRB1	GNA13	PIK3CB
BDKRB2	ITGA1	PIK3R5
CDC42	ITGA10	PIP4K2C
CHRM2	ITGA3	PIP5K1B
CYFIP2	ITGAL	PPP1CA
DIAPH2	ITGAX	PPP1R12B
DOCK1	ITGB3	PTK2
F2R	ITGB4	RAC2
FGD1	KRAS	ROCK1
FGF1	LIMK1	RRAS
FGF10	LIMK2	RRAS2
FGF11	MAP2K1	SLC9A1
FGF12	MAPK3	SSH2
FGF14	MYL2	TIAM1
FGF16	MYL9	WASL

Table A4.14 miRNA hits exclusively associated with regulation of actin cytoskeleton and enhanced HIV replication

Gene symbols (KEGG identifiers)	
ARHGEF4	ITGA7
ARPC1A	ITGA8
ARPC2	ITGAE
CYFIP1	PAK4
DIAPH3	PAK7
EZR	PDGFB
FGF13	PIK3R1
FGF20	PIK3R3
FGF9	RDX
FGFR2	VAV2
GIT1	VAV3
GNG12	WASF1
ITGA2	

Table A4.15 HIV-suppressive miRNA hits associated with regulation of the actin cytoskeleton pathway*

hsa-miR-1231	hsa-miR-431-3p	hsa-miR-483-5p
hsa-miR-124-3p	hsa-miR-3190-5p	hsa-miR-491-5p
hsa-miR-127-5p	hsa-miR-3192-5p	hsa-miR-497-5p
hsa-miR-1270	hsa-miR-3200-3p	hsa-miR-506-3p
hsa-miR-1295a	hsa-miR-342-5p	hsa-miR-518a-5p
hsa-miR-1306-3p	hsa-miR-34a-3p	hsa-miR-520d-5p
hsa-miR-135b-3p	hsa-miR-3605-5p	hsa-miR-624-3p
hsa-miR-138-5p	hsa-miR-3616-3p	hsa-miR-650
hsa-miR-145-3p	hsa-miR-3616-5p	hsa-miR-654-5p
hsa-miR-192-5p	hsa-miR-3622a-5p	hsa-miR-671-3p
hsa-miR-193b-5p	hsa-miR-3691-5p	hsa-miR-889-3p
hsa-miR-2110	hsa-miR-3918	hsa-miR-892b
hsa-miR-3166	hsa-miR-3927-3p	hsa-miR-940
hsa-miR-3173-3p	hsa-miR-4256	
hsa-miR-3179	hsa-miR-4270	
hsa-miR-3189-3p	hsa-miR-4314	

*miRNA (mirBASE v.20), miRNAs are ranked numerically

Table A4.16 HIV replication enhancing miRNA hits associated with regulation of the actin cytoskeleton pathway*

hsa-miR-1260a	hsa-miR-335-3p
hsa-miR-1260b	hsa-miR-34c-3p
hsa-miR-1271-5p	hsa-miR-378a-5p
hsa-miR-136-3p	hsa-miR-3938
hsa-miR-141-5p	hsa-miR-4318
hsa-miR-188-5p	hsa-miR-550a-3p
hsa-miR-200a-5p	hsa-miR-576-3p
hsa-miR-200b-5p	hsa-miR-587
hsa-miR-218-1-3p	hsa-miR-625-3p
hsa-miR-22-3p	hsa-miR-649
hsa-miR-2277-5p	hsa-miR-668-3p
hsa-miR-3171	hsa-miR-891b

*miRNA (mirBASE v.20), miRNAs are ranked numerically

Table A4.17 HIV-suppressive miRNA hits associated with the Hippo signalling pathway*

hsa-miR-1231	hsa-miR-3605-5p
hsa-miR-124-3p	hsa-miR-3616-5p
hsa-miR-1269a	hsa-miR-3622a-5p
hsa-miR-127-5p	hsa-miR-3691-5p
hsa-miR-1270	hsa-miR-383-5p
hsa-miR-1273e	hsa-miR-3918
hsa-miR-1295a	hsa-miR-3927-3p
hsa-miR-1306-3p	hsa-miR-4256
hsa-miR-135b-3p	hsa-miR-4270
hsa-miR-138-5p	hsa-miR-431-3p
hsa-miR-145-3p	hsa-miR-4314
hsa-miR-192-5p	hsa-miR-483-5p
hsa-miR-193b-5p	hsa-miR-491-5p
hsa-miR-2110	hsa-miR-497-5p
hsa-miR-3166	hsa-miR-518a-5p
hsa-miR-3173-3p	hsa-miR-520d-5p
hsa-miR-3179	hsa-miR-624-3p
hsa-miR-3189-3p	hsa-miR-650
hsa-miR-3190-5p	hsa-miR-654-5p
hsa-miR-3192-5p	hsa-miR-671-3p
hsa-miR-3200-3p	hsa-miR-889-3p
hsa-miR-342-5p	hsa-miR-892b
hsa-miR-34a-3p	hsa-miR-940

*miRNA (mirBASE v.20), miRNAs are ranked numerically

Table A4.18 HIV-replication enhancing miRNA hits associated with the Hippo signalling pathway*

hsa-miR-625-3p	hsa-miR-1271-5p
hsa-miR-218-1-3p	hsa-miR-378a-5p
hsa-miR-34c-3p	hsa-miR-587
hsa-miR-335-3p	hsa-miR-3938
hsa-miR-668-3p	hsa-miR-4318
hsa-miR-22-3p	hsa-miR-136-3p
hsa-miR-1260b	hsa-miR-891b
hsa-miR-576-3p	hsa-miR-550a-3p
hsa-miR-1260a	hsa-miR-200a-5p

hsa-miR-141-5p	hsa-miR-200b-5p
hsa-miR-188-5p	hsa-miR-2277-5p

*miRNA (mirBASE v.20)

Table A4.19 miRNA hits exclusively associated with Hippo signalling and enhanced HIV replication

Gene symbols (KEGG identifiers)		
FZD8	AXIN2	BMP7
SMAD4	PPP2R1A	WNT7B

Table A4.20 miRNA hits exclusively associated with Hippo signalling and suppressed HIV replication

Gene symbols (KEGG identifiers)			
WTIP	TCF7L2	ID2	CRB2
WNT9A	TCF7L1	ID1	CRB1
WNT8B	TCF7	GLI2	CCND3
WNT7A	STK3	GDF6	BMPR1B
WNT5B	SNAI2	FZD7	BMPR1A
WNT4	SAV1	FZD5	BMP6
WNT3	RASSF6	FZD1	BMP5
WNT2B	RASSF1	FGF1	BMP2
WNT16	PPP2CB	DVL3	BBC3
TP73	PPP1CA	DVL2	APC
TP53BP2	NF2	DVL1	
TGFBR2	LLGL2	DLG4	
TEAD4	LLGL1	DLG3	
TEAD3	LIMD1	DLG1	
TEAD2	LEF1	CTNNA3	

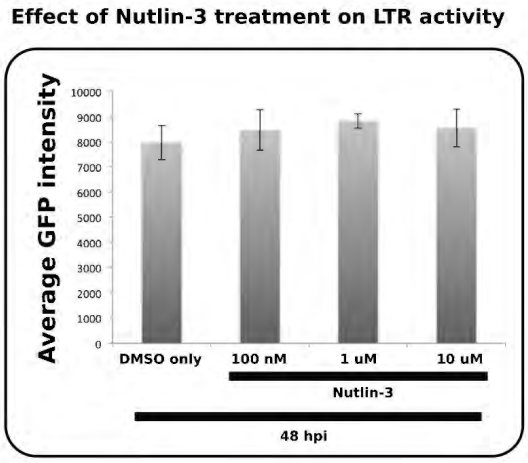

Figure A4.4 Effect of Nutlin-3 treatment on HIV replication

GHOST(3) cells, were treated with either variable concentrations of the MDM2-inhibitor Nutlin-3 or DMSO for 24hr prior to HIV exposure. Cells were fixed, processed and imaged at 48 hpi. Images were acquired on the IXU at 20x, n=2.

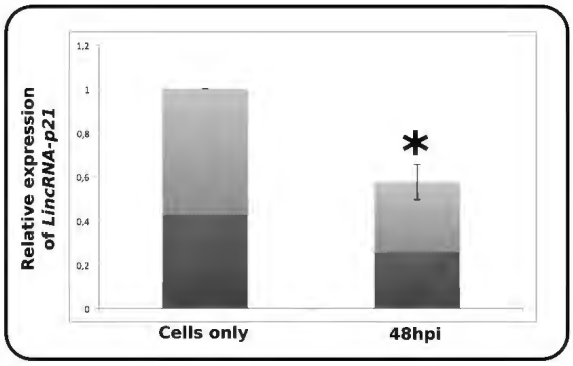

Figure A4.5 siRNA-mediated knockdown of lincRNA-p21

qPCR analysis of LincRNA-p21 transcript levels 24 hr post-transfection with si-LincRNA-p21 (25nM). Expression levels normalized against reference gene *HPRT*, * = $p<0.05$, n=3.

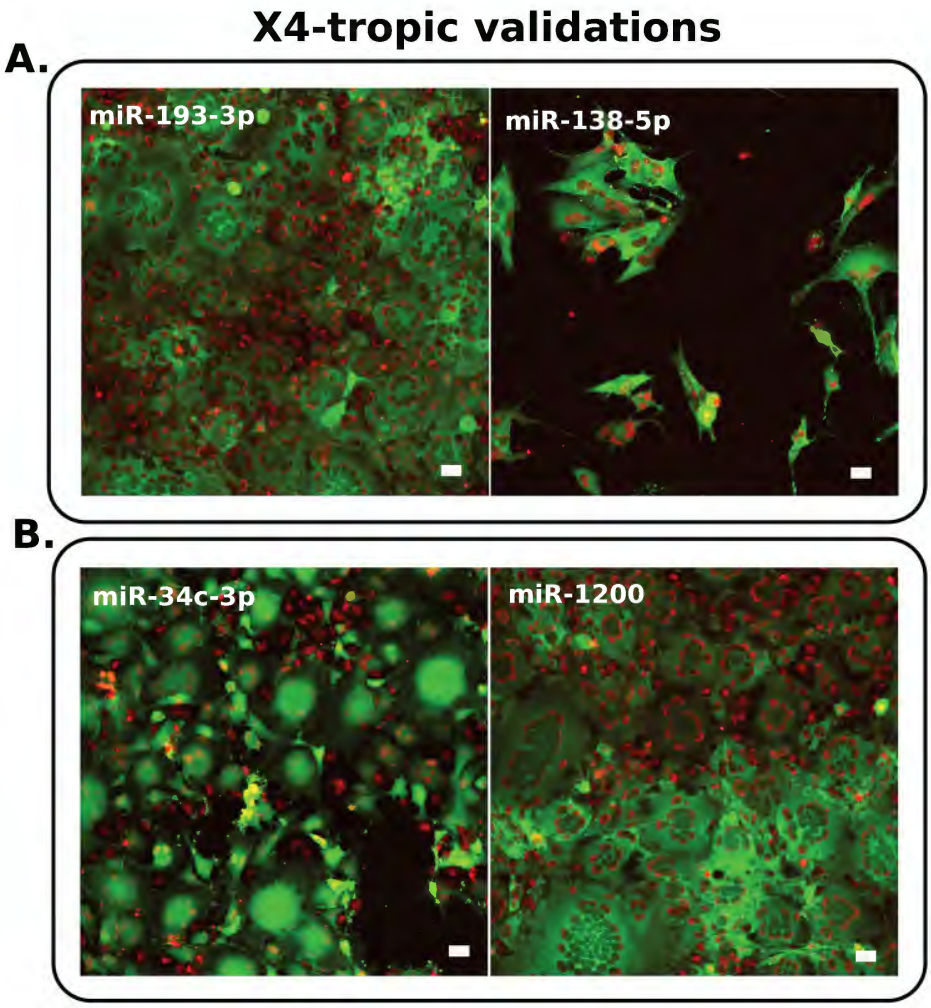

Figure A4.6 HCS HIV-suppressive miRNA hits that did not inhibit HIV Gag-iGFP replication

A) HIV-suppressive miRNA hits that were not effective against X4-tropic HIV variant, **B)** HIV replication enhancing hit, miR-34c-3p, exhibited elevated GFP signal output. miR-1200 (which was below the hit selection cut off) exhibited a heightened rate of syncytia formation (circularised polynucleated structures). Images represent overlays of single FOVs acquired at 20x in the 405 and 488 excitation channels. Nuclei counterstained with Hoechst (red), HIV iGag-GFP/ LTR reporter (green), scale bars = 20 μm.

Appendix 5

Oncology drug panel: 10 μM raw data plots

Specific well locations within the oncology screen datasets exhibited seemingly biased distributions as a direct result of the small number of experimental plates (n = 3), and the drug-associated cellular toxicities of many compounds in the oncology panel (Figure A5.1 & A5.3).. The biased distribution plots were confirmed by a comparison of the pre- and post-HIV exposure screen datasets. HIV replication attenuated many of the cytotoxic phenotypes obtained in the pre-

HIV and ‘drug only’ datasets, resulting in reformed distribution plots (Figure A5.2). Apart from this issue, the general data distribution trends were very similar to those of the Kinase panel drug screens.

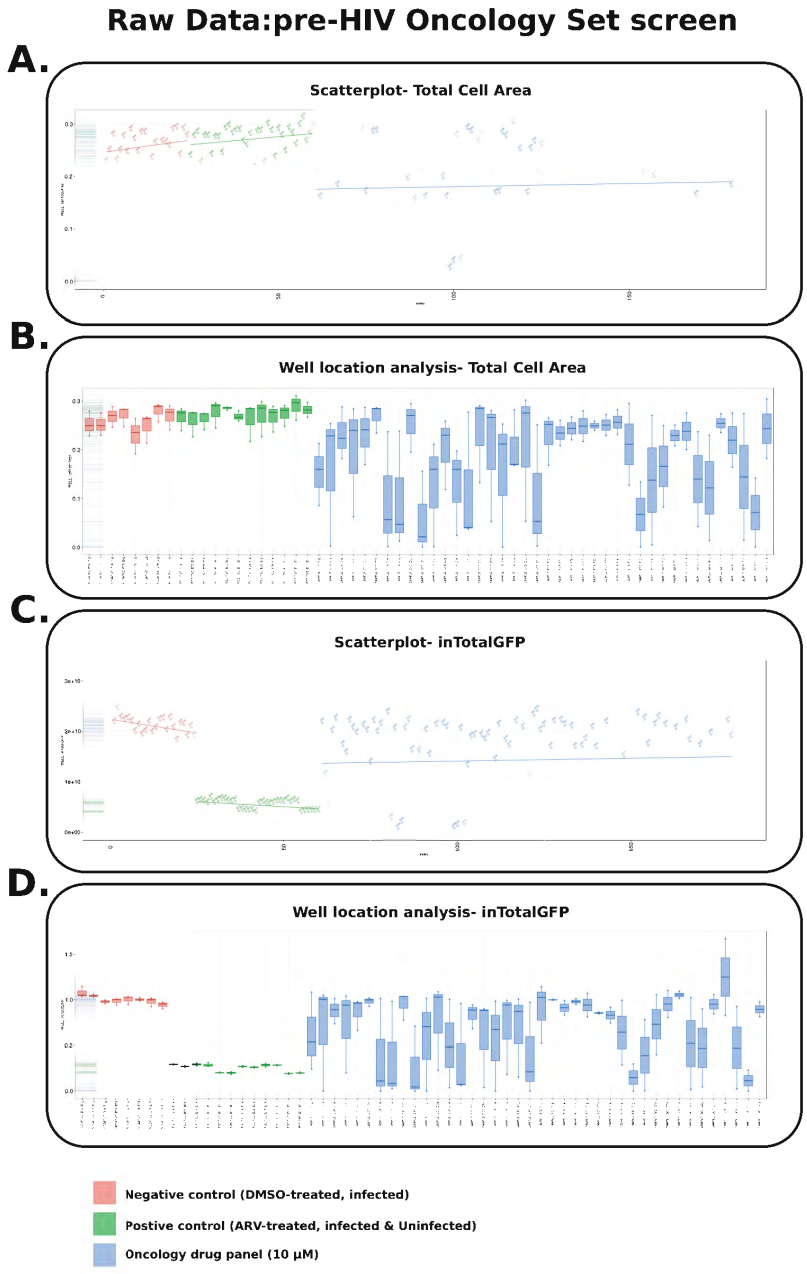

Figure A5.1 Unprocessed data distribution plots for all replicates of ‘pre-HIV exposure’ Oncology panel (10µM).

A) Scatterplot representing the distribution of individual experimental controls and treatments across three screen replicates in relation to the extracted Total Cell Area feature scores. No significant variability in Total cell area was noted between the positive (green) and negative (red) controls. Experimental treatments (blue) exhibited a broad distribution range, notably below the

lower limits of phenotypic controls. **B)** Box plot representing the average Total Cell Area scores obtained for specific well locations across all experimental plates and replicates. Negative (red) and positive (green) control well locations exhibited consistent distribution ranges that were not distinct from each other. Well locations corresponding to experimental treatments exhibited broader distribution ranges exceeding those of the phenotypic controls. **C)** Scatterplot representing the distribution of individual experimental control and treatment wells across three screen replicates in relation to the extracted inTotalGFP feature scores. Positive (green) and negative (red) controls exhibited distinct distribution ranges from each other. Experimental wells (blue) exhibited broader distribution ranges below the lower limits of negative controls. **D)** Box plot representing the average InTotalGFP scores obtained for specific well locations across all experimental plates and replicates. Negative (red) and positive (green) control well locations exhibited consistent and distinct distribution ranges. Well locations corresponding to experimental treatments exhibited broader distribution ranges, exceeding those of the negative controls.

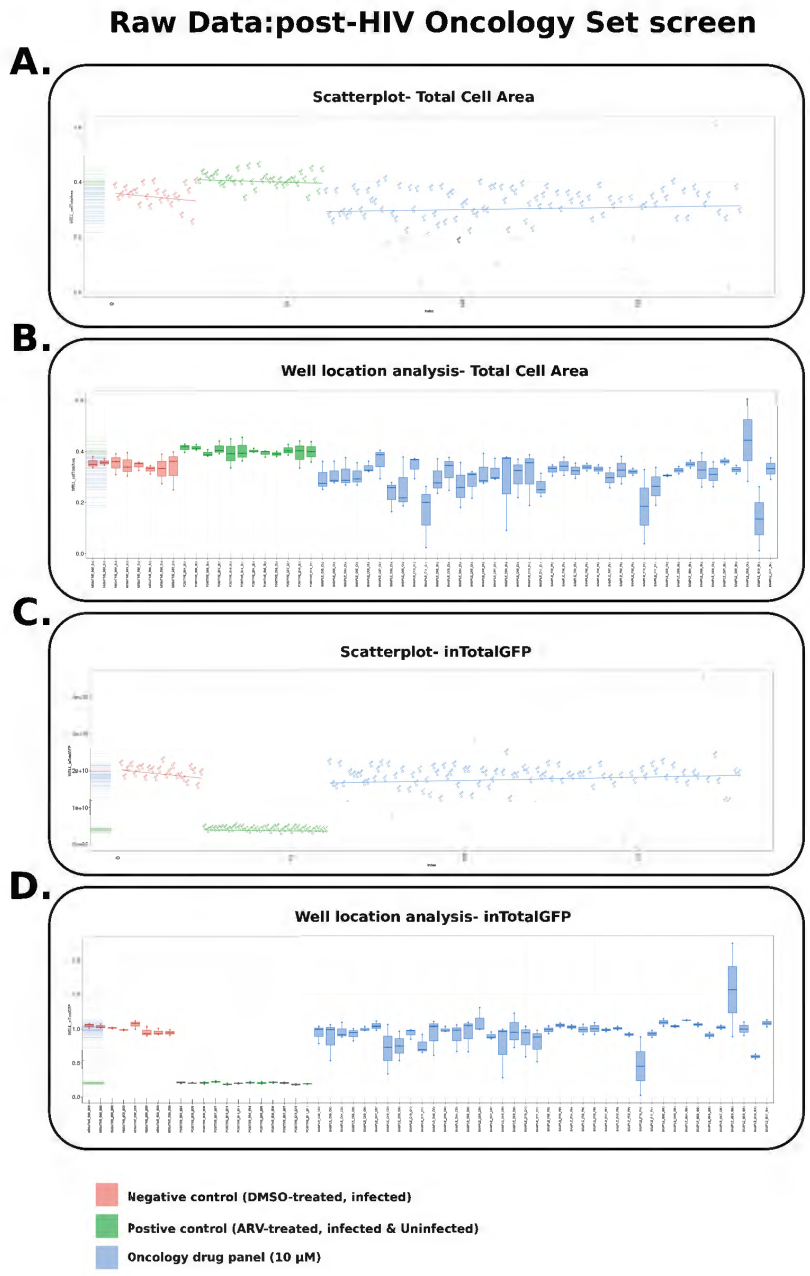

Figure A5.2 Unprocessed data distribution plots for all replicates of 'post-HIV exposure' Oncology panel (10µM).

A) Scatterplot representing the distribution of individual experimental controls and treatments across three screen replicates in relation to the extracted Total Cell Area feature scores. The positive (green) and negative (red) controls exhibited noticeable but nonsignificant variation in their respective distribution ranges. Experimental wells (blue) exhibited a broad distribution range beyond the upper and lower limits of phenotypic controls. **B)** Box plot representing the average Total Cell Area scores obtained for specific well locations across all experimental plates and replicates. Negative (red) and positive (green) control well locations exhibited consistent and tight distribution ranges. Well locations corresponding to experimental treatments exhibited broad distribution ranges exceeding those of phenotypic controls. **C)** Scatterplot representing the

distribution of individual experimental control and treatment wells across three screen replicates in relation to the extracted inTotalGFP feature scores. Positive (green) and negative (red) controls exhibited distinct distribution ranges. Experimental wells (blue) revealed broader distribution ranges, mostly below the lower limits of negative controls. **D)** Box plot representing the average InTotalGFP scores obtained for specific well locations across all experimental plates and replicates. Negative (red) and positive (green) control well locations exhibited consistent and distinct distribution ranges. Well locations corresponding to experimental treatments exhibited broader distribution ranges, exceeding those of negative controls.

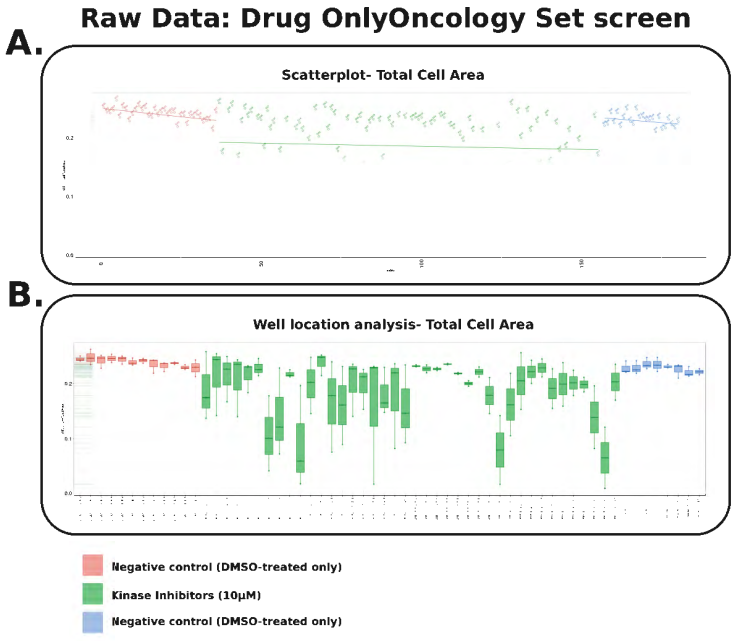

Figure A5.3 Unprocessed data distribution plots for all replicates of 'Drug Only' Oncology panel (10μM) based on Total Cell Area feature scores
A) Scatterplot representing the distribution of individual negative controls and treatments across three screen replicates in relation to the extracted Total Cell Area feature scores. Negative controls located on the left (red) and right (red) halves of experimental plates did not differ in their distribution ranges. Experimental treatments (green) exhibited a broad distribution range, predominantly below the lower limits of negative controls. **B)** Box plot representing the average Total Cell Area scores obtained for specific well locations across all experimental plates and replicates. Negative control well locations (red and blue) exhibited consistent and tight distribution ranges irrespective of their positions on experimental plates. Well locations corresponding to experimental treatments (green) exhibited broad distribution ranges exceeding those of phenotypic controls, with biased distributions for specific well locations.

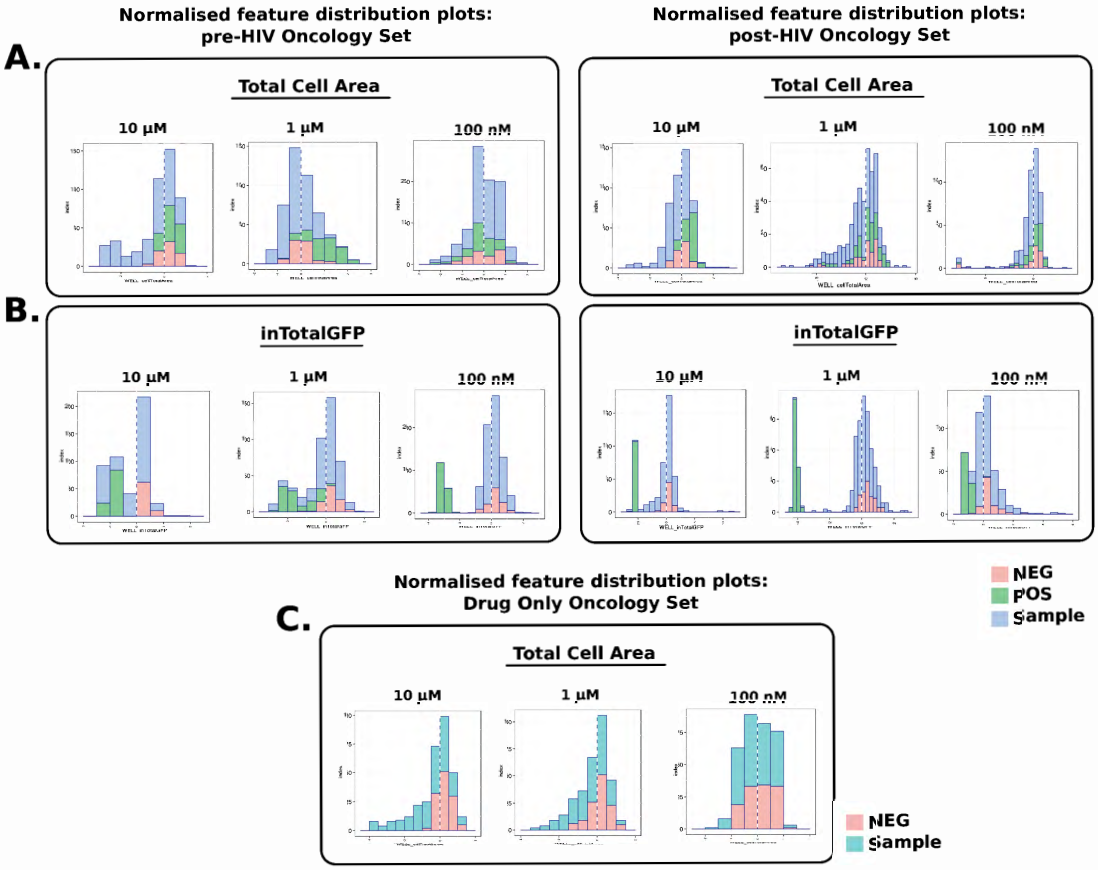

Figure A5.4 Normalised feature plots for Oncology drug panel screens
A) Normalised Total cell Area distribution plots for pre-HIV and post-HIV treatment screens at 10 µM, 1 µM and 100 nM treatment concentrations. **B)** Normalised inTotalGFP distribution plots for pre-HIV and post-HIV treatment screens at 10 µM, 1 µM and 100 nM treatment concentrations. **C)** Normalised Total cell Area distribution plots for Drug only screens at 10 µM, 1 µM and 100 nM treatment concentrations. DMSO only controls (NEG), ARV-treatments (POS), experimental treatments (sample).

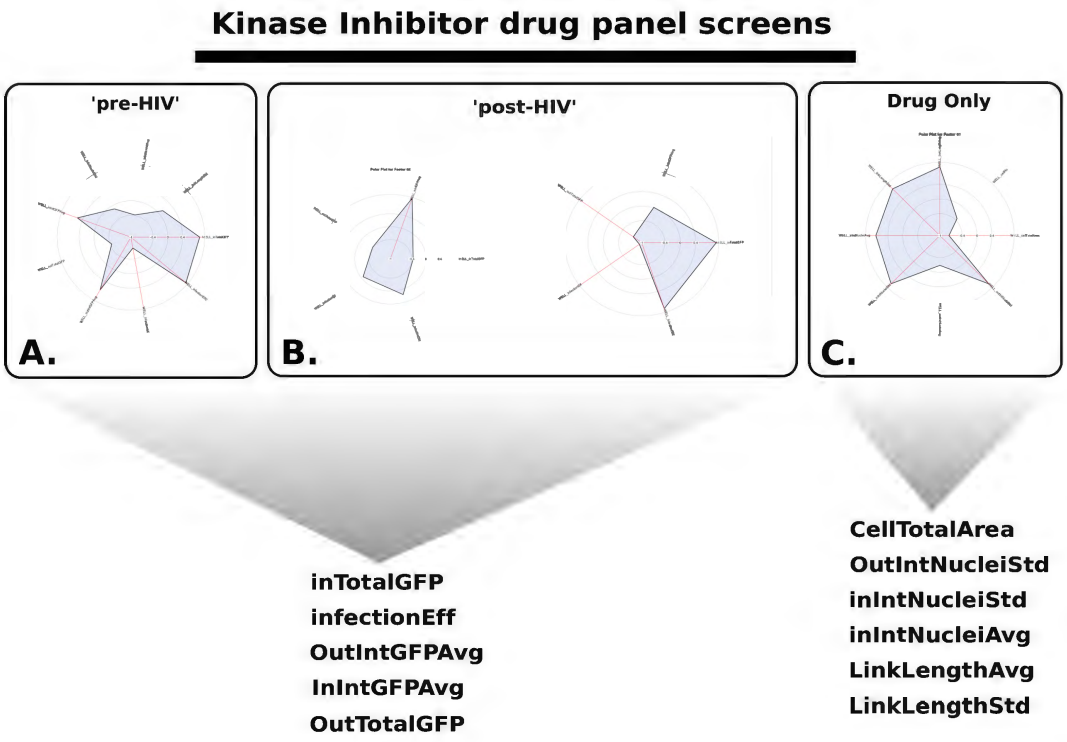

Figure A5.5 Example of factors utilised for hit selection in Kinase 10 μM drug panel screens.
Single factor indicators PCA-based data reduction (A,C) while two factors indicate an MDS-based approach (B).

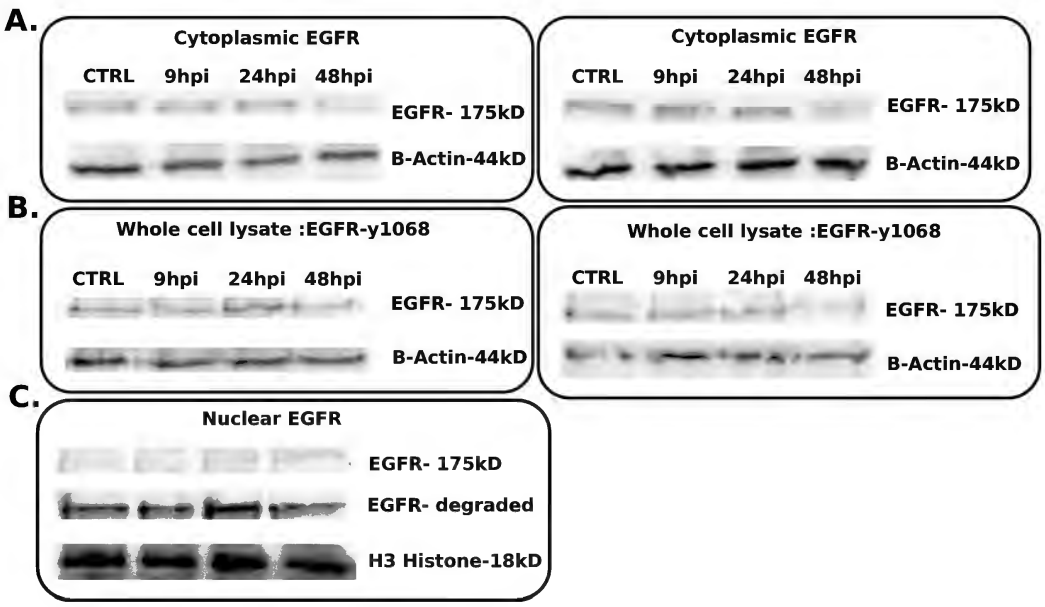

Figure A5.6 EGFR western blot analysis.
A) Replicate Western Blot gels stained for EGFR obtained from cytoplasmic and B) whole cell lysate fractions. C) Similar Western blot data obtained from nuclear fraction. Histone H3 was

utilized as a loading control for nuclear fractions and ß-Actin as a control for cytoplasmic fractions.

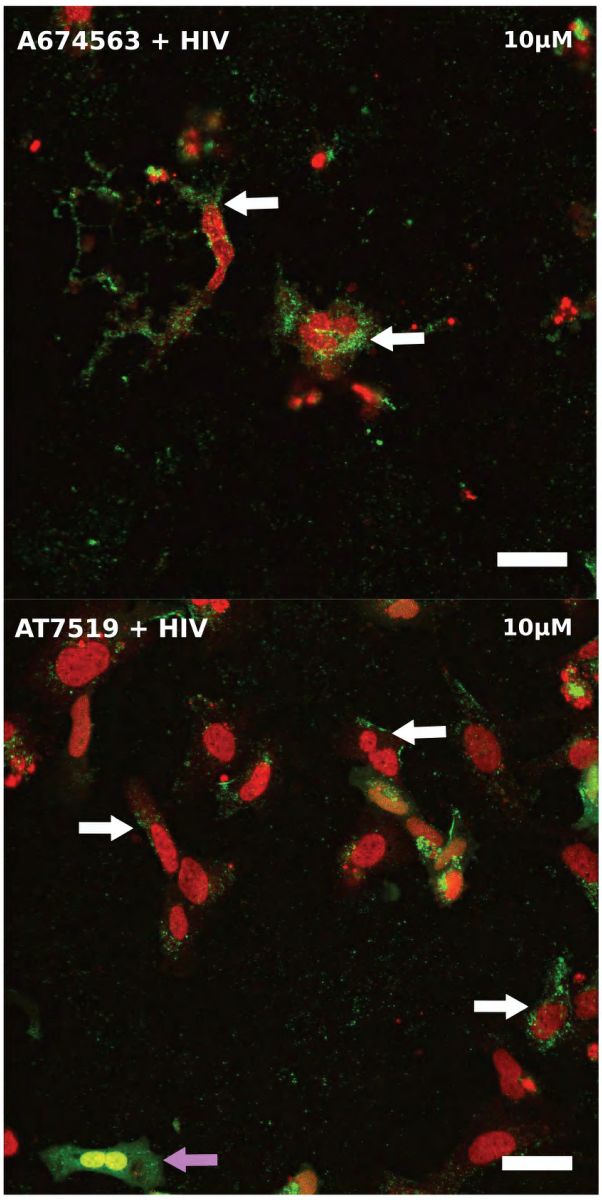

Figure A5.7 Additional enlarged images from HIV-tropism validation experiments

Upper) 10 µM A-674563 treatment phenotype. **Lower)** 10 µM AT7519 treatment. White arrows indicate examples of cells where HIV capsid/virions are present in either the cytoplasm, or at the cell surface. Pink arrows indicate examples of stably infected cells. Images represent overlays acquired from a single FOV at 40x, GFP-HIV capsid/ LTR-reporter (green), nuclei counterstained with Hoechst (red), scale bars = 20 µm.

References

Abraham, S., et al. (2003). "Regulation of MCP-1 gene transcription by Smads and HIV-1 Tat in human glial cells." Virology **309**(2): 196-202.

Abram, M. E., et al. (2010). "Nature, position, and frequency of mutations made in a single cycle of HIV-1 replication." Journal of Virology **84**(19): 9864-9878.

Agarwal, V., et al. (2015). "Predicting effective microRNA target sites in mammalian mRNAs." Elife **4**: e05005.

Ahluwalia, J. K., et al. (2008). "Human cellular microRNA hsa-miR-29a interferes with viral nef protein expression and HIV-1 replication." Retrovirology **5**(1): 117.

Ako-Adjei, D., et al. (2015). "HIV-1, human interaction database: current status and new features." Nucleic acids research **43**(D1): D566-D570.

Al-Amri, S. S. and N. V. Kalyankar (2010). "Image segmentation by using threshold techniques." arXiv preprint arXiv:1005.4020.

Al-Mawsawi, L. Q. and N. Neamati (2007). "Blocking interactions between HIV-1 integrase and cellular cofactors: an emerging anti-retroviral strategy." Trends in Pharmacological Sciences **28**: 526-535.

Alexaki, A., et al. (2008). "Cellular reservoirs of HIV-1 and their role in viral persistence." Current HIV research **6**(5): 388.

Alexiou, P., et al. (2009). "Lost in translation: an assessment and perspective for computational microRNA target identification." Bioinformatics **25**(23): 3049-3055.

Ali, A., et al. (2009). "Identification of Flavopiridol Analogues that Selectively Inhibit Positive Transcription Elongation Factor (P□TEFb) and Block HIV□1 Replication." Chembiochem **10**(12): 2072-2080.

Allan, C., et al. (2012). "OMERO: flexible, model-driven data management for experimental biology." Nature methods **9**(3): 245-253.

Allen, T. D., et al. (2000). "The nuclear pore complex: mediator of translocation between nucleus and cytoplasm." Journal of Cell Science **113**(10): 1651-1659.

Ambrose, Z. and C. Aiken (2014). "HIV-1 uncoating: connection to nuclear entry and regulation by host proteins." Virology **454-455**: 371-379.

Andersen, J. L., et al. (2006). "HIV-1 Vpr-induced apoptosis is cell cycle dependent and requires Bax but not ANT." PLoS Pathog **2**(12): e127.

Anderson, J. and R. Akkina (2008). "Human Immunodeficiency Virus Type 1 Restriction by Human–Rhesus Chimeric Tripartite Motif 5 α (TRIM 5 α) in CD34 + Cell-Derived Macrophages In Vitro and in T Cells In Vivo in Severe Combined Immunodeficient (SCID-hu) Mice Transplanted with Human Fetal Tissue " Human Gene Therapy **19**: 217-228.

Anderson, J., et al. (2003). "Bispecific short hairpin siRNA constructs targeted to CD4, CXCR4, and CCR5 confer HIV-1 resistance." Oligonucleotides **13**(5): 303-312.

Anokye-Danso, F., et al. (2011). "Highly efficient miRNA-mediated reprogramming of mouse and human somatic cells to pluripotency." Cell stem cell **8**(4): 376-388.

Aqil, M., et al. (2013). "The HIV-1 Nef protein binds argonaute-2 and functions as a viral suppressor of RNA interference." PLoS One **8**(9): e74472.

Arhel, N. (2010). "Revisiting HIV-1 uncoating." Retrovirology **7**: 96.

Arhel, N. and F. Kirchhoff (2010). "Host proteins involved in HIV infection: new therapeutic targets." Biochimica et Biophysica Acta (BBA)-Molecular Basis of Disease **1802**(3): 313-321.

Arhel, N. J., et al. (2007). "HIV-1 DNA Flap formation promotes uncoating of the pre-integration complex at the nuclear pore." The EMBO journal **26**: 3025-3037.

Arriola, E. L., et al. (1999). "Differential regulation of p21 waf-1/cip-1 and Mdm2 by etoposide: etoposide inhibits the p53-Mdm2 autoregulatory feedback loop." Oncogene **18**(4).

Arts, E. J. and D. J. Hazuda (2012). "HIV-1 Antiretroviral Drug Therapy." Cold Spring Harbor perspectives in medicine **2**: a007161-a007161.

Ashe, M. P., et al. (1995). "Poly (A) site selection in the HIV-1 provirus: inhibition of promoter-proximal polyadenylation by the downstream major splice donor site." Genes & development **9**(23): 3008-3025.

Autran, B., et al. (1997). "Positive effects of combined antiretroviral therapy on CD4+ T cell homeostasis and function in advanced HIV disease." Science **277**(5322): 112-116.

Aza-Blanc, P., et al. (2003). "Identification of modulators of TRAIL-induced apoptosis via RNAi-based phenotypic screening." Molecular cell **12**(3): 627-637.

Bachand, F., et al. (1999). "Incorporation of Vpr into human immunodeficiency virus type 1 requires a direct interaction with the p6 domain of the p55 gag precursor." Journal of Biological Chemistry **274**(13): 9083-9091.

Baigude, H., et al. (2012). "miR□TRAP: A Benchtop Chemical Biology Strategy to Identify microRNA Targets." Angewandte Chemie **124**(24): 5982-5985.

Bailey, J. R., et al. (2008). "Transmission of human immunodeficiency virus type 1 from a patient who developed AIDS to an elite suppressor." Journal of Virology **82**(15): 7395-7410.

Baker, B., et al. (2009). "Elite control of HIV infection: implications for vaccine design."

Bakre, A., et al. (2013). "Identification of host kinase genes required for influenza virus replication and the regulatory role of MicroRNAs." PLoS One **8**(6): e66796.

Balakrishnan, I., et al. (2014). "Genome□Wide Analysis of miRNA□mRNA Interactions in Marrow Stromal Cells." Stem Cells **32**(3): 662-673.

Bargaje, R., et al. (2012). "Identification of novel targets for miR-29a using miRNA proteomics."

Barichievy, S., et al. (2015). "Non-coding RNAs and HIV: viral manipulation of host dark matter to shape the cellular environment." Frontiers in genetics **6**.

Barre-Sinoussi, F., et al. (1983). "Isolation of a T-lymphotropic retrovirus from a patient at risk for acquired immune deficiency syndrome (AIDS)." Science **220**: 868-871.

Barretina, J., et al. (2012). "The Cancer Cell Line Encyclopedia enables predictive modelling of anticancer drug sensitivity." Nature **483**(7391): 603-607.

Bartel, D. P. (2009). "MicroRNAs: target recognition and regulatory functions." Cell **136**(2): 215-233.

Bell, N. M. and A. M. Lever (2013). "HIV Gag polyprotein: processing and early viral particle assembly." Trends in microbiology **21**(3): 136-144.

Belzile, J.-P., et al. (2007). "HIV-1 Vpr-mediated G2 arrest involves the DDB1-CUL4AVPRBP E3 ubiquitin ligase." PLoS Pathog **3**(7): e85.

Bennasser, Y., et al. (2005). "Evidence that HIV-1 encodes an siRNA and a suppressor of RNA silencing." Immunity **22**(5): 607-619.

Bennasser, Y., et al. (2006). "HIV-1 TAR RNA subverts RNA interference in transfected cells through sequestration of TAR RNA-binding protein, TRBP." Journal of Biological Chemistry **281**(38): 27674-27678.

Bennett, N. C., et al. (2010). "Molecular cell biology of androgen receptor signalling." The international journal of biochemistry & cell biology **42**(6): 813-827.

Bensaude, O. (2011). "Inhibiting eukaryotic transcription. Which compound to choose? How to evaluate its activity? Which compound to choose? How to evaluate its activity?" Transcription **2**(3): 103-108.

Bergamaschi, A. and G. Pancino (2010). "Review Host hindrance to HIV-1 replication in monocytes and macrophages."

Berkhout, B., et al. (1989). "Tat trans-activates the human immunodeficiency virus through a nascent RNA target." Cell **59**(2): 273-282.

Berro, R., et al. (2008). "CDK13, a new potential human immunodeficiency virus type 1 inhibitory factor regulating viral mRNA splicing." Journal of Virology **82**(14): 7155-7166.

Bhattacharyya, S. N., et al. (2006). "Relief of microRNA-mediated translational repression in human cells subjected to stress." Cell **125**(6): 1111-1124.

Bilodeau, P. S., et al. (2001). "RNA splicing at human immunodeficiency virus type 1 3′ splice site A2 is regulated by binding of hnRNP A/B proteins to an exonic splicing silencer element." Journal of Virology **75**(18): 8487-8497.

Bivalkar-Mehla, S., et al. (2011). "Viral RNA silencing suppressors (RSS): novel strategy of viruses to ablate the host RNA interference (RNAi) defense system." Virus research **155**(1): 1-9.

Blankson, J. N. (2010). "Effector mechanisms in HIV-1 infected elite controllers: highly active immune responses?" Antiviral research **85**(1): 295-302.

Bleul, C. C., et al. (1996). "The lymphocyte chemoattractant SDF-1 is a ligand for LESTR/fusin and blocks HIV-1 entry."

Bobardt, M. D., et al. (2004). "Contribution of proteoglycans to human immunodeficiency virus type 1 brain invasion." Journal of Virology **78**(12): 6567-6584.

Bosinger, S. E., et al. (2004). "Gene expression profiling of host response in models of acute HIV infection." The Journal of Immunology **173**(11): 6858-6863.

Bouchie, A. (2013). "First microRNA mimic enters clinic." Nature biotechnology **31**(7): 577-577.

Bour, S., et al. (1995). "The human immunodeficiency virus type 1 Vpu protein specifically binds to the cytoplasmic domain of CD4: implications for the mechanism of degradation." Journal of Virology **69**(3): 1510-1520.

Boutros, M. and J. Ahringer (2008). "The art and design of genetic screens: RNA interference." Nature Reviews Genetics **9**(7): 554-566.

Brasey, A., et al. (2003). "The leader of human immunodeficiency virus type 1 genomic RNA harbors an internal ribosome entry segment that is active during the G2/M phase of the cell cycle." Journal of Virology **77**(7): 3939-3949.

Brass, A. L., et al. (2008). "Identification of host proteins required for HIV infection through a functional genomic screen." Science **319**(5865): 921-926.

Bray, M.-A., et al. (2012). "Workflow and metrics for image quality control in large-scale high-content screens." Journal of biomolecular screening **17**(2): 266-274.

Brégnard, C., et al. (2014). "DNA damage repair machinery and HIV escape from innate immune sensing." Frontiers in microbiology **5**.

Briggs, J. A. G. (2003). "Structural organization of authentic, mature HIV-1 virions and cores." The EMBO journal **22**: 1707-1715.

Brik, A. and C.-H. Wong (2003). "HIV-1 protease: mechanism and drug discovery." Organic & biomolecular chemistry **1**(1): 5-14.

Brinkman, K., et al. (1998). "Adverse effects of reverse transcriptase inhibitors: mitochondrial toxicity as common pathway." Aids **12**(14): 1735-1744.

Brodin, P. and T. Christophe (2011). "High-content screening in infectious diseases." Current opinion in chemical biology **15**(4): 534-539.

Buchser, W., et al. (2004). "Assay development guidelines for image-based high content screening, high content analysis and high content imaging."

Burton, D. R., et al. (2012). "A blueprint for HIV vaccine discovery." Cell host & microbe **12**(4): 396-407.

Bushman, F. D., et al. (2009). "Host cell factors in HIV replication: meta-analysis of genome-wide studies." PLoS Pathog **5**(5): e1000437.

Butel, J. S. (2000). "Viral carcinogenesis: revelation of molecular mechanisms and etiology of human disease." Carcinogenesis **21**(3): 405-426.

Cai, X., et al. (2004). "Human microRNAs are processed from capped, polyadenylated transcripts that can also function as mRNAs." RNA **10**(12): 1957-1966.

Campbell, S., et al. (2001). "Lipid rafts and HIV-1: from viral entry to assembly of progeny virions." Journal of Clinical Virology **22**(3): 217-227.

Cannell, I. and M. Bushell (2010). "Regulation of Myc by miR-34c: A mechanism to prevent genomic instability?" Cell Cycle **9**(14): 2798-2802.

Carlson, L.-A., et al. (2010). "Cryo electron tomography of native HIV-1 budding sites." PLoS Pathog **6**(11): e1001173.

CDC (1981). Kaposi's sarcoma and pneumocystis pneumonia among homosexual men-New York City and California. Morbidity & Mortality Weekly Report. **30:** 305-308.

CDC (1982). Epidemiologic notes and reports: possible transfusion-associated acquired immune deficiency syndrome, AIDS - California. Morbidity & Mortality Weekly Report. **31:** 652-654.

CDC (1983). Epidemiologic notes and reports: immunodeficiency among female sexual partners of males with acquired immune deficiency syndrome (AIDS) - New York. New York. Morbidity & Mortality Weekly Report**:** 697-698.

Cecilia, D., et al. (1998). "Neutralization profiles of primary human immunodeficiency virus type 1 isolates in the context of coreceptor usage." Journal of Virology **72**(9): 6988-6996.

Cen, S., et al. (2004). "The interaction between HIV-1 Gag and APOBEC3G." Journal of Biological Chemistry **279**(32): 33177-33184.

Cha, S. B., et al. (2013). "Early transcriptional responses of internalization defective Brucella abortus mutants in professional phagocytes, RAW 264.7." BMC genomics **14**(1): 1.

Chan, D. C. and P. S. Kim (1998). "HIV Entry and Its Inhibition." Cell **93**: 681-684.

Chang, S. T., et al. (2013). "Next-generation sequencing of small RNAs from HIV-infected cells identifies phased microRNA expression patterns and candidate novel microRNAs differentially expressed upon infection." MBio **4**(1): e00549-00512.

Chang, T.-C., et al. (2007). "Transactivation of miR-34a by p53 broadly influences gene expression and promotes apoptosis." Molecular cell **26**(5): 745-752.

Chao, S.-H., et al. (2000). "Flavopiridol inhibits P-TEFb and blocks HIV-1 replication." Journal of Biological Chemistry **275**(37): 28345-28348.

Chen, A. K., et al. (2014). "MicroRNA binding to the HIV-1 Gag protein inhibits Gag assembly and virus production." Proceedings of the National Academy of Sciences **111**(26): E2676-E2683.- Referred to as “Chen, 2014a” in text.

Chen, J., et al. (2010). "MicroRNA-193b represses cell proliferation and regulates cyclin D1 in melanoma." The American journal of pathology **176**(5): 2520-2529.

Chen, J., et al. (2014). "Cytoplasmic HIV-1 RNA is mainly transported by diffusion in the presence or absence of Gag protein." Proceedings of the National Academy of Sciences **111**(48): E5205-E5213.

Chen, R., et al. (2004). "Vpr-mediated incorporation of UNG2 into HIV-1 particles is required to modulate the virus mutation rate and for replication in macrophages." Journal of Biological Chemistry **279**(27): 28419-28425.

Chen, R., et al. (2009). "Mechanism of action of SNS-032, a novel cyclin-dependent kinase inhibitor, in chronic lymphocytic leukemia." Blood **113**(19): 4637-4645.

Chen, Y., et al. (2014). "Viral carcinogenesis: Factors inducing DNA damage and virus integration." Cancers **6**(4): 2155-2186.

Cheng, K., et al. (2013). "MicroRNAs in HIV-associated nephropathy (HIVAN)." Experimental and molecular pathology **94**(1): 65-72.

Cherry, S. (2009). "What have RNAi screens taught us about viral–host interactions?" Current opinion in microbiology **12**(4): 446-452.

Chiang, K., et al. (2013). "miR-132 enhances HIV-1 replication." Virology **438**(1): 1-4.

Chiang, K., et al. (2012). "Regulation of cyclin T1 and HIV-1 Replication by microRNAs in resting CD4+ T lymphocytes." Journal of Virology **86**(6): 3244-3252.

Christopherson, R. I., et al. (2014). "Mechanisms of action of fludarabine nucleoside against human Raji lymphoma cells." Nucleosides, Nucleotides and Nucleic Acids **33**(4-6): 375-383.

Chun, T.-W., et al. (1998). "Early establishment of a pool of latently infected, resting CD4+ T cells during primary HIV-1 infection." Proceedings of the National Academy of Sciences **95**(15): 8869-8873.

Ciuffi, A., et al. (2005). "A role for LEDGF/p75 in targeting HIV DNA integration." Nature medicine **11**(12): 1287-1289.

Clavel, F., et al. (1986). "Isolation of a new human retrovirus from West African patients with AIDS." Science **233**: 343-346.

Clerzius, G., et al. (2011). "Multiple levels of PKR inhibition during HIV□1 replication." Reviews in medical virology **21**(1): 42-53.

Cloonan, N., et al. (2008). "The miR-17-5p microRNA is a key regulator of the G1/S phase cell cycle transition." Genome biology **9**(8): R127.

Coffin, J., et al. (1986). "Human immunodeficiency viruses." Science **232**: 697.

Coffin, J. and R. Swanstrom (2013). "HIV pathogenesis: dynamics and genetics of viral populations and infected cells." Cold Spring Harbor perspectives in medicine **3**(1): a012526.

Coffin, J. M. (1995). "HIV population dynamics in vivo: implications for genetic variation, pathogenesis, and therapy." Science **267**(5197): 483-489.

Col, E., et al. (2005). "HIV□1 Tat targets Tip60 to impair the apoptotic cell response to genotoxic stresses." The EMBO journal **24**(14): 2634-2645.

Coley, W., et al. (2010). "Absence of DICER in monocytes and its regulation by HIV-1." Journal of Biological Chemistry **285**(42): 31930-31943.

Colgan, D. F. and J. L. Manley (1997). "Mechanism and regulation of mRNA polyadenylation." Genes & development **11**(21): 2755-2766.

Connell, B. J. and H. Lortat-Jacob (2013). "Human immunodeficiency virus and heparan sulfate: from attachment to entry inhibition." Frontiers in immunology **4**.

Connor, R. I. (1997). "Change in Coreceptor Use Correlates with Disease Progression in HIV-1-Infected Individuals." Journal of Experimental Medicine **185**: 621-628.

Connor, R. I., et al. (1995). "Vpr is required for efficient replication of human immunodeficiency virus type-1 in mononuclear phagocytes." Virology **206**(2): 935-944.

Contreras, J. and D. Rao (2012). "MicroRNAs in inflammation and immune responses." Leukemia **26**(3): 404-413.

Cosnefroy, O., et al. (2012). "Stimulation of the human RAD51 nucleofilament restricts HIV-1 integration in vitro and in infected cells." Journal of Virology **86**(1): 513-526.

Cox, J. E., et al. (2015). "Pan-viral-microRNA screening identifies interferon inhibition as a common function of diverse viruses." Proceedings of the National Academy of Sciences **112**(6): 1856-1861.

Coyle-Rink, J., et al. (2002). "Interaction between TGFβ signaling proteins and C/EBP controls basal and Tat-mediated transcription of HIV-1 LTR in astrocytes." Virology **299**(2): 240-247.

Craigie, R. (2001). "HIV integrase, a brief overview from chemistry to therapeutics." Journal of Biological Chemistry **276**(26): 23213-23216.

Crum, N. F., et al. (2006). "Comparisons of causes of death and mortality rates among HIV-infected persons: analysis of the pre-, early, and late HAART (highly active antiretroviral therapy) eras." JAIDS Journal of Acquired Immune Deficiency Syndromes **41**(2): 194-200.

Cujec, T. P., et al. (1997). "The HIV transactivator TAT binds to the CDK-activating kinase and activates the phosphorylation of the carboxy-terminal domain of RNA polymerase II." Genes & development **11**(20): 2645-2657.

Cummins, N. W. and A. D. Badley (2013). "Anti-apoptotic mechanisms of HIV: lessons and novel approaches to curing HIV." Cellular and Molecular Life Sciences **70**(18): 3355-3363.

Cy, C. and T. Rana (2006). "Translation repression in human cells by microRNA-induced gene silencing requires RCK/p54." PLoS Biol **4**(7): e210.

D'arc, M., et al. (2015). "Origin of the HIV-1 group O epidemic in western lowland gorillas." Proc Natl Acad Sci USA **112**: E1343-E1352.

da Silva, S. R. and D. E. de Oliveira (2011). "HIV, EBV and KSHV: viral cooperation in the pathogenesis of human malignancies." Cancer letters **305**(2): 175-185.

Dahabieh, M. S., et al. (2013). "A doubly fluorescent HIV-1 reporter shows that the majority of integrated HIV-1 is latent shortly after infection." Journal of Virology **87**(8): 4716-4727.

Das, A. T., et al. (1999). "A hairpin structure in the R region of the human immunodeficiency virus type 1 RNA genome is instrumental in polyadenylation site selection." Journal of Virology **73**(1): 81-91.

Daugherty, M. D., et al. (2008). "A solution to limited genomic capacity: using adaptable binding surfaces to assemble the functional HIV Rev oligomer on RNA." Molecular cell **31**(6): 824-834.

Daugherty, M. D., et al. (2010). "Structural basis for cooperative RNA binding and export complex assembly by HIV Rev." Nature structural & molecular biology **17**(11): 1337-1342.

Davey, R. T., et al. (1999). "HIV-1 and T cell dynamics after interruption of highly active antiretroviral therapy (HAART) in patients with a history of sustained viral suppression." Proceedings of the National Academy of Sciences **96**(26): 15109-15114.

De Boer, R. J., et al. (2010). "Current estimates for HIV-1 production imply rapid viral clearance in lymphoid tissues."

De Iaco, A., et al. (2013). "TNPO3 protects HIV-1 replication from CPSF6-mediated capsid stabilization in the host cell cytoplasm." Retrovirology **10**(1): 20-20.

De Leys, R., et al. "Isolation and partial characterization of an unusual human immunodeficiency retrovirus from two persons of west-central African origin." Journal of Virology **64**(30): 1207-1216.

De Rijck, J., et al. (2010). "High-resolution profiling of the LEDGF/p75 chromatin interaction in the ENCODE region." Nucleic acids research: gkq410.

Decroly, E., et al. (1994). "The convertases furin and PC1 can both cleave the human immunodeficiency virus (HIV)-1 envelope glycoprotein gp160 into gp120 (HIV-1 SU) and gp41 (HIV-I TM)." Journal of Biological Chemistry **269**(16): 12240-12247.

Delaney, M. (2006). "History of HAART–the true story of how effective multi-drug therapy was developed for treatment of HIV disease." Retrovirology **3**(Suppl 1): S6.

Dempsey, L. A. (2014). "Killing bystander T cells." Nature immunology **15**(3): 222-222.

Deshmane, S. L., et al. (2011). "Regulation of the HIV-1 promoter by HIF-1a and Vpr proteins." Virology journal **8**: 477.

Di Nunzio, F., et al. (2012). "Human nucleoporins promote HIV-1 docking at the nuclear pore, nuclear import and integration." PLoS One **7**(9): e46037.

Dingwall, C., et al. (1990). "HIV-1 tat protein stimulates transcription by binding to a U-rich bulge in the stem of the TAR RNA structure." The EMBO journal **9**(12): 4145.

Doitsh, G., et al. (2014). "Cell death by pyroptosis drives CD4 T-cell depletion in HIV-1 infection." Nature **505**(7484): 509-514.

Dorr, P., et al. (2005). "Maraviroc (UK-427,857), a potent, orally bioavailable, and selective small-molecule inhibitor of chemokine receptor CCR5 with broad-spectrum anti-human immunodeficiency virus type 1 activity." Antimicrobial agents and chemotherapy **49**(11): 4721-4732.

Dubé, M., et al. (2011). "HIV□1 Vpu Antagonizes BST□2 by Interfering Mainly with the Trafficking of Newly Synthesized BST□2 to the Cell Surface." Traffic **12**(12): 1714-1729.

Dulude, D., et al. (2006). "Decreasing the frameshift efficiency translates into an equivalent reduction of the replication of the human immunodeficiency virus type 1." Virology **345**(1): 127-136.

Dürr, O., et al. (2007). "Robust hit identification by quality assurance and multivariate data analysis of a high-content, cell-based assay." Journal of biomolecular screening **12**(8): 1042-1049.

Eckstein, D. A., et al. (2001). "HIV-1 Vpr enhances viral burden by facilitating infection of tissue macrophages but not nondividing CD4+ T cells." The Journal of experimental medicine **194**(10): 1407-1419.

Ehrhardt, C. and S. Ludwig (2009). "A new player in a deadly game: influenza viruses and the PI3K/Akt signalling pathway." Cellular microbiology **11**(6): 863-871.

Elbashir, S. M., et al. (2001). "Duplexes of 21-nucleotide RNAs mediate RNA interference in cultured mammalian cells." Nature **411**(6836): 494-498.

Engels, E. A., et al. (2006). "Trends in cancer risk among people with AIDS in the United States 1980–2002." Aids **20**: 1645-1654.

Espeseth, A. S., et al. (2011). "siRNA screening of a targeted library of DNA repair factors in HIV infection reveals a role for base excision repair in HIV integration."

Esquela-Kerscher, A. and F. J. Slack (2006). "Oncomirs—microRNAs with a role in cancer." Nature Reviews Cancer **6**(4): 259-269.

Eulalio, A., et al. (2012). "The mammalian microRNA response to bacterial infections." RNA biology **9**(6): 742-750.

Evans, P., et al. (2009). "Prediction of HIV-1 virus-host protein interactions using virus and host sequence motifs." BMC medical genomics **2**(1): 1.

Fabian, M. R. and N. Sonenberg (2012). "The mechanics of miRNA-mediated gene silencing: a look under the hood of miRISC." Nature structural & molecular biology **19**(6): 586-593.

Faraoni, I., et al. (2009). "miR-155 gene: a typical multifunctional microRNA." Biochimica et Biophysica Acta (BBA)-Molecular Basis of Disease **1792**(6): 497-505.

Farberov, L., et al. (2015). "MicroRNA□mediated regulation of p21 and TASK1 cellular restriction factors enhances HIV□1 infection." Journal of Cell Science **128**(8): 1607-1616.

Feinberg, M. B., et al. (1991). "The role of Tat in the human immunodeficiency virus life cycle indicates a primary effect on transcriptional elongation." Proceedings of the National Academy of Sciences **88**(9): 4045-4049.

Felber, B. K., et al. (1990). "Feedback regulation of human immunodeficiency virus type 1 expression by the Rev protein." Journal of Virology **64**(8): 3734-3741.

Finkel, T., et al. (1995). "Apoptosis occurs predominantly in bystander cells and not in productively infected cells of HIV-and SIV-infected lymph nodes." Nature medicine **1**(2): 129-134.

Fire, A., et al. (1998). "Potent and specific genetic interference by double-stranded RNA in Caenorhabditis elegans." Nature **391**(6669): 806-811.

Fischer-Smith, T., et al. (2004). "Macrophage/microglial accumulation and proliferating cell nuclear antigen expression in the central nervous system in human immunodeficiency virus encephalopathy." The American journal of pathology **164**(6): 2089-2099.

Fletcher, C. V., et al. (2014). "Persistent HIV-1 replication is associated with lower antiretroviral drug concentrations in lymphatic tissues." Proceedings of the National Academy of Sciences **111**(6): 2307-2312.

Frankel, A. D. and J. A. Young (1998). "HIV-1: fifteen proteins and an RNA." Annual review of biochemistry **67**(1): 1-25.

Frankfurt, O. and J. D. Licht (2013). "Ponatinib—a step forward in overcoming resistance in chronic myeloid leukemia." Clinical Cancer Research **19**(21): 5828-5834.

Freed, E. O. (2001). "HIV-1 replication." Somatic cell and molecular genetics **26**(1-6): 13-33.

Freed, E. O. (2004). "HIV-1 and the host cell: an intimate association." Trends in microbiology **12**(4): 170-177.

Frentz, D., et al. (2012). "Temporal changes in the epidemiology of transmission of drug-resistant HIV-1 across the world." AIDs Rev **14**(1): 17-27.

Friedman, R. C., et al. (2009). "Most mammalian mRNAs are conserved targets of microRNAs." Genome research **19**(1): 92-105.

Friedrich, B. M., et al. (2011). "Host factors mediating HIV-1 replication." Virus research **161**(2): 101-114.

Fujinaga, K., et al. (1998). "The ability of positive transcription elongation factor B to transactivate human immunodeficiency virus transcription depends on a functional kinase domain, cyclin T1, and Tat." Journal of Virology **72**(9): 7154-7159.

Furfine, E. S. and J. E. Reardon (1991). "Human immunodeficiency virus reverse transcriptase ribonuclease H: specificity of tRNALys3-primer excision." Biochemistry **30**: 7041-7046.

Gainor, J. F. and B. A. Chabner (2015). "Ponatinib: Accelerated Disapproval." The oncologist **20**(8): 847-848.

Galkin, A. V., et al. (2007). "Identification of NVP-TAE684, a potent, selective, and efficacious inhibitor of NPM-ALK." Proceedings of the National Academy of Sciences **104**(1): 270-275.

Gallo, R., et al. (1984). "Frequent detection and isolation of cytopathic retroviruses (HTLV-III) from patients with AIDS and at risk for AIDS." Science **224**: 500-503.

Gangaraju, V. K. and H. Lin (2009). "MicroRNAs: key regulators of stem cells." Nature reviews Molecular cell biology **10**(2): 116-125.

Garcia, J. A., et al. (1989). "Human immunodeficiency virus type 1 LTR TATA and TAR region sequences required for transcriptional regulation." The EMBO journal **8**(3): 765.

Garg, H. and R. Blumenthal (2006). "HIV gp41-induced apoptosis is mediated by caspase-3-dependent mitochondrial depolarization, which is inhibited by HIV protease inhibitor nelfinavir." Journal of leukocyte biology **79**(2): 351-362.

Gasparri, F. (2009). "An overview of cell phenotypes in HCS: limitations and advantages."

Gaudin, R., et al. (2013). "HIV trafficking in host cells: motors wanted!" Trends in cell biology **23**(12): 652-662.

Gekonge, B., et al. (2012). "Retinoblastoma protein induction by HIV viremia or CCR5 in monocytes exposed to HIV-1 mediates protection from activation-induced apoptosis: ex vivo and in vitro study." Journal of leukocyte biology **92**(2): 397-405.

Gennarino, V. A., et al. (2012). "Identification of microRNA-regulated gene networks by expression analysis of target genes." Genome research **22**(6): 1163-1172.

Genovesio, A., et al. (2011). "Automated genome-wide visual profiling of cellular proteins involved in HIV infection." Journal of biomolecular screening **16**(9): 945-958.

Georges, S. A., et al. (2008). "Coordinated regulation of cell cycle transcripts by p53-Inducible microRNAs, miR-192 and miR-215." Cancer research **68**(24): 10105-10112.

Ghosh, A., et al. (2011). "Structural insights to how mammalian capping enzyme reads the CTD code." Molecular cell **43**(2): 299-310.

Gilbert, C., et al. (2007). "Involvement of Src and Syk tyrosine kinases in HIV-1 transfer from dendritic cells to CD4+ T lymphocytes." The Journal of Immunology **178**(5): 2862-2871.

Gilmartin, G. M., et al. (1995). "CPSF recognition of an HIV-1 mRNA 3'-processing enhancer: multiple sequence contacts involved in poly (A) site definition." Genes & development **9**(1): 72-83.

Gontarek, R. R. and D. Derse (1996). "Interactions among SR proteins, an exonic splicing enhancer, and a lentivirus Rev protein regulate alternative splicing." Molecular and cellular biology **16**(5): 2325-2331.

Goodrich, J. A., et al. (1996). "Contacts in context: promoter specificity and macromolecular interactions in transcription." Cell **84**(6): 825-830.

Gorry, P. R., et al. (2005). "Pathogenesis of macrophage tropic HIV-1." Current HIV research **3**(1): 53-60.

Gottlieb, M. S., et al. (1981). "Pneumocystis carinii Pneumonia and Mucosal Candidiasis in Previously Healthy Homosexual Men " New England Journal of Medicine **305**: 1425-1431.

Gottlinger, H. G., et al. (1989). "Role of capsid precursor processing and myristoylation in morphogenesis and infectivity of human immunodeficiency virus type 1." Proceedings of the National Academy of Sciences **86**: 5781-5785.

Greenway, A. L., et al. (2002). "Human immunodeficiency virus type 1 Nef binds to tumor suppressor p53 and protects cells against p53-mediated apoptosis." Journal of Virology **76**(6): 2692-2702.

Grimson, A., et al. (2007). "MicroRNA targeting specificity in mammals: determinants beyond seed pairing." Molecular cell **27**(1): 91-105.

Grobler, J. A., et al. (2002). "Diketo acid inhibitor mechanism and HIV-1 integrase: implications for metal binding in the active site of phosphotransferase enzymes." Proceedings of the National Academy of Sciences **99**(10): 6661-6666.

Grove, J. and M. Marsh (2011). "The cell biology of receptor-mediated virus entry." The Journal of cell biology **195**(7): 1071-1082.

Gu, M. and C. D. Lima (2005). "Processing the message: structural insights into capping and decapping mRNA." Current opinion in structural biology **15**(1): 99-106.

Guan, E., et al. (2002). "Natural truncation of the chemokine MIP-1β/CCL4 affects receptor specificity but not anti-HIV-1 activity." Journal of Biological Chemistry **277**(35): 32348-32352.

Guennewig, B., et al. (2014). "Synthetic pre-microRNAs reveal dual-strand activity of miR-34a on TNF-α." RNA **20**(1): 61-75.

Guenzel, C. A., et al. (2014). "HIV-1 Vpr—a still “enigmatic multitasker”." Frontiers in microbiology **5**.

Guo, Y. E. and J. A. Steitz (2014). "Virus meets host microRNA: the destroyer, the booster, the hijacker." Molecular and cellular biology **34**(20): 3780-3787.

Gupta, A., et al. (2011). "Comparative expression profile of miRNA and mRNA in primary peripheral blood mononuclear cells infected with human immunodeficiency virus (HIV-1)." PLoS One **6**(7): e22730.

Gurdasani, D., et al. (2014). "A systematic review of definitions of extreme phenotypes of HIV control and progression." AIDS (London, England) **28**(2): 149.

Gurunathan, S., et al. (2009). "Use of predictive markers of HIV disease progression in vaccine trials." Vaccine **27**(14): 1997-2015.

Ha, M. and V. N. Kim (2014). "Regulation of microRNA biogenesis." Nature reviews Molecular cell biology **15**(8): 509-524.

Hadzopoulou-Cladaras, M., et al. (1989). "The rev (trs/art) protein of human immunodeficiency virus type 1 affects viral mRNA and protein expression via a cis-acting sequence in the env region." Journal of Virology **63**(3): 1265-1274.

Hafner, M., et al. (2010). "Transcriptome-wide identification of RNA-binding protein and microRNA target sites by PAR-CLIP." Cell **141**(1): 129-141.

Hanahan, D. and R. A. Weinberg (2011). "Hallmarks of cancer: the next generation." Cell **144**(5): 646-674.

Hannon, G. J. and J. J. Rossi (2004). "Unlocking the potential of the human genome with RNA interference." Nature **431**(7006): 371-378.

Haralick, R. M., et al. (1973). "Textural features for image classification." Systems, Man and Cybernetics, IEEE Transactions on(6): 610-621.

Hariharan, M., et al. (2005). "Targets for human encoded microRNAs in HIV genes." Biochemical and biophysical research communications **337**(4): 1214-1218.

Harmon, B., et al. (2010). "Role of Abl kinase and the Wave2 signaling complex in HIV-1 entry at a post-hemifusion step." PLoS Pathog **6**(6): e1000956.

Hausser, J. and M. Zavolan (2014). "Identification and consequences of miRNA-target interactions [mdash] beyond repression of gene expression." Nature Reviews Genetics **15**(9): 599-612.

Hayes, A. M., et al. (2011). "Tat RNA silencing suppressor activity contributes to perturbation of lymphocyte miRNA by HIV-1." Retrovirology **8**(1): 36.

He, N., et al. (2010). "HIV-1 Tat and host AFF4 recruit two transcription elongation factors into a bifunctional complex for coordinated activation of HIV-1 transcription." Molecular cell **38**(3): 428-438.

He, X., et al. (2014). "MicroRNAs: new regulators of Toll-like receptor signalling pathways." BioMed research international **2014**.

He, Y., et al. (2013). "Structural visualization of key steps in human transcription initiation." Nature **495**(7442): 481-486.

Helwak, A., et al. (2013). "Mapping the human miRNA interactome by CLASH reveals frequent noncanonical binding." Cell **153**(3): 654-665.

Hemelaar, J., et al. (2006). "Global and regional distribution of HIV-1 genetic subtypes and recombinants in 2004." Aids **20**: W13-W23.

Henderson, B. R. and P. Percipalle (1997). "Interactions between HIV Rev and nuclear import and export factors: the Rev nuclear localisation signal mediates specific binding to human importin-β." Journal of molecular biology **274**(5): 693-707.

Henry, K., et al. (1998). "Severe premature coronary artery disease with protease inhibitors." The Lancet **351**(9112): 1328.

Herbein, G., et al. (2010). "Review Macrophage signaling in HIV-1 infection."

Hermeking, H. (2010). "The miR-34 family in cancer and apoptosis." Cell Death & Differentiation **17**(2): 193-199.

Herold, N., et al. (2014). "HIV-1 entry in SupT1-R5, CEM-ss, and primary CD4+ T cells occurs at the plasma membrane and does not require endocytosis." Journal of Virology **88**(24): 13956-13970.

Hietanen, S., et al. (2000). "Activation of p53 in cervical carcinoma cells by small molecules." Proceedings of the National Academy of Sciences **97**(15): 8501-8506.

Hilberg, F., et al. (2008). "BIBF 1120: triple angiokinase inhibitor with sustained receptor blockade and good antitumor efficacy." Cancer research **68**(12): 4774-4782.

Hill, M., et al. (2005). "The packaging and maturation of the HIV-1 Pol proteins." Current HIV research **3**(1): 73-85.

Hillebrand, F., et al. (2014). "The PI3K pathway acting on alternative HIV-1 pre-mRNA splicing." Journal of General Virology **95**(Pt 8): 1809-1815.

Hinnebusch, A. G. (2014). "The scanning mechanism of eukaryotic translation initiation." Annual review of biochemistry **83**: 779-812.

Ho, B.-C., et al. (2011). "Enterovirus-induced miR-141 contributes to shutoff of host protein translation by targeting the translation initiation factor eIF4E." Cell host & microbe **9**(1): 58-69.

Hodgson, C. P. and F. Solaiman (1996). "Virosomes: cationic liposomes enhance retroviral transduction." Nature biotechnology **14**(3): 339-342.

Houzet, L., et al. (2012). "The extent of sequence complementarity correlates with the potency of cellular miRNA-mediated restriction of HIV-1." Nucleic acids research **40**(22): 11684-11696.

Houzet, L., et al. (2008). "MicroRNA profile changes in human immunodeficiency virus type 1 (HIV-1) seropositive individuals." Retrovirology **5**(1): 118.

Hu, W.-S. and S. H. Hughes (2012). "HIV-1 Reverse Transcription." Cold Spring Harbor perspectives in medicine **2**: a006882-a006882.

Huang, J., et al. (2007). "Cellular microRNAs contribute to HIV-1 latency in resting primary CD4+ T lymphocytes." Nature medicine **13**(10): 1241-1247.

Huang, W.-C., et al. (2011). "Nuclear translocation of epidermal growth factor receptor by Akt-dependent phosphorylation enhances breast cancer-resistant protein expression in gefitinib-resistant cells." Journal of Biological Chemistry **286**(23): 20558-20568.

Huang, Y., et al. (2011). "Biological functions of microRNAs: a review." Journal of physiology and biochemistry **67**(1): 129-139.

Huarte, M., et al. (2010). "A large intergenic noncoding RNA induced by p53 mediates global gene repression in the p53 response." Cell **142**(3): 409-419.

Hubert, P., et al. (1995). "HIV□1 glycoprotein gp120 disrupts CD4□p56lck/CD3□T cell receptor interactions and inhibits CD3 signaling." European journal of immunology **25**(5): 1417-1425.

Hübner, W., et al. (2007). "Sequence of human immunodeficiency virus type 1 (HIV-1) Gag localization and oligomerization monitored with live confocal imaging of a replication-competent, fluorescently tagged HIV-1." Journal of Virology **81**(22): 12596-12607.

Hulme, A. E., et al. (2011). "Complementary assays reveal a relationship between HIV-1 uncoating and reverse transcription." Proceedings of the National Academy of Sciences **108**: 9975-9980.

Hurley, J. H. and P. I. Hanson (2010). "Membrane budding and scission by the ESCRT machinery: it's all in the neck." Nature reviews Molecular cell biology **11**(8): 556-566.

Hütter, G., et al. (2009). "Long-term control of HIV by CCR5 Delta32/Delta32 stem-cell transplantation." New England Journal of Medicine **360**(7): 692-698.

Hwang, H. and J. Mendell (2006). "MicroRNAs in cell proliferation, cell death, and tumorigenesis." British journal of cancer **94**(6): 776-780.

Ishida, H., et al. (2011). "Alterations in microRNA expression profile in HCV-infected hepatoma cells: involvement of miR-491 in regulation of HCV replication via the PI3 kinase/Akt pathway." Biochemical and biophysical research communications **412**(1): 92-97.

Ivey, K. N. and D. Srivastava (2010). "MicroRNAs as regulators of differentiation and cell fate decisions." Cell stem cell **7**(1): 36-41.

Ivey, K. N. and D. Srivastava (2015). "microRNAs as Developmental Regulators." Cold Spring Harbor perspectives in biology **7**(7): a008144.

Iwasaki, S., et al. (2010). "Hsc70/Hsp90 chaperone machinery mediates ATP-dependent RISC loading of small RNA duplexes." Molecular cell **39**(2): 292-299.

Jacks, T., et al. (1988). "Characterization of ribosomal frameshifting in HIV-1 gag-pol expression." Nature **331**: 280-283.

Jackson, D., et al. (2010). "HCS Road An Enterprise System for Integrated HCS Data Management and Analysis." Journal of biomolecular screening **15**(7): 882-891.

Jackson, R. J., et al. (2012). "Termination and post-termination events in eukaryotic translation." Adv Protein Chem Struct Biol **86**: 45-93.

Jackson, R. J., et al. (2010). "The mechanism of eukaryotic translation initiation and principles of its regulation." Nature reviews Molecular cell biology **11**(2): 113-127.

Jacqué, J. M., et al. (1998). "Modulation of HIV□1 infectivity by MAPK, a virion–associated kinase." The EMBO journal **17**(9): 2607-2618.

Jäger, S., et al. (2012). "Global landscape of HIV-human protein complexes." Nature **481**(7381): 365-370.

Jalali, S., et al. (2013). "Systematic transcriptome wide analysis of lncRNA-miRNA interactions." PLoS One **8**(2): e53823.

Janssen, H. L., et al. (2013). "Treatment of HCV infection by targeting microRNA." New England Journal of Medicine **368**(18): 1685-1694.

Jasin, M. and R. Rothstein (2013). "Repair of strand breaks by homologous recombination." Cold Spring Harbor perspectives in biology **5**(11): a012740.

Jin, Y.-J., et al. (2005). "HIV Nef-mediated CD4 down-regulation is adaptor protein complex 2 dependent." The Journal of Immunology **175**(5): 3157-3164.

Johnston, S. M., et al. (2014). Automation Considerations for RNAi Library Formatting and High Throughput Transfection. Frontiers in RNAi. R. A. Tripp and J. M. Karpilow, Bentham Science. **1:** 21-39.

Jopling, C. L., et al. (2005). "Modulation of hepatitis C virus RNA abundance by a liver-specific MicroRNA." Science **309**(5740): 1577-1581.

Jouvenet, N., et al. (2009). "Imaging the interaction of HIV-1 genomes and Gag during assembly of individual viral particles." Proceedings of the National Academy of Sciences **106**(45): 19114-19119.

Kaiser, H. F. (1958). "The varimax criterion for analytic rotation in factor analysis." Psychometrika **23**(3): 187-200.

Kanki, Phyllis J., et al. (1999). "Human Immunodeficiency Virus Type 1 Subtypes Differ in Disease Progression." The Journal of Infectious Diseases **179**: 68-73.

Kanki, P. J., et al. (1994). "Slower heterosexual spread of HIV-2 than HIV-1." The Lancet **343**: 943-946.

Kappes, J. C. and X. Wu (2005). Cell-based method and assay for measuring the infectivity and drug sensitivity of immunodeficiency virus, US Patent 20,050,032,046.

Karginov, F. V. and G. J. Hannon (2013). "Remodeling of Ago2–mRNA interactions upon cellular stress reflects miRNA complementarity and correlates with altered translation rates." Genes & development **27**(14): 1624-1632.

Karn, J. (2011). "The molecular biology of HIV latency: breaking and restoring the Tat-dependent transcriptional circuit." Current opinion in HIV and AIDS **6**(1): 4.

Katahira, J. (2012). "mRNA export and the TREX complex." Biochimica et Biophysica Acta (BBA)-Gene Regulatory Mechanisms **1819**(6): 507-513.

Keele, B. F. (2006). "Chimpanzee Reservoirs of Pandemic and Nonpandemic HIV-1." Science **313**: 523-526.

Keele, B. F., et al. (2008). "Identification and characterization of transmitted and early founder virus envelopes in primary HIV-1 infection." Proceedings of the National Academy of Sciences **105**: 7552-7557.

Khvorova, A., et al. (2003). "Functional siRNAs and miRNAs exhibit strand bias." Cell **115**(2): 209-216.

Kim, J., et al. (2007). "A MicroRNA feedback circuit in midbrain dopamine neurons." Science **317**(5842): 1220-1224.

Kim, T., et al. (2011). "p53 regulates epithelial–mesenchymal transition through microRNAs targeting ZEB1 and ZEB2." The Journal of experimental medicine **208**(5): 875-883.

Kim, Y. K., et al. (2002). "Phosphorylation of the RNA polymerase II carboxyl-terminal domain by CDK9 is directly responsible for human immunodeficiency virus type 1 Tat-activated transcriptional elongation." Molecular and cellular biology **22**(13): 4622-4637.

Kincaid, R. P. and C. S. Sullivan (2012). "Virus-encoded microRNAs: an overview and a look to the future." PLoS Pathog **8**(12): e1003018.

Kino, T., et al. (2005). "HIV-1 Accessory Protein Vpr Inhibits the Effect of Insulin on the Foxo Subfamily of Forkhead Transcription Factors by Interfering With Their Binding to 14-3-3 Proteins Potential Clinical Implications Regarding the Insulin Resistance of HIV-1–Infected Patients." Diabetes **54**(1): 23-31.

Klarmann, G. J., et al. (2000). "Site-specific Incorporation of Nucleoside Analogs by HIV-1 Reverse Transcriptase and the Template Grip Mutant P157S: TEMPLATE INTERACTIONS INFLUENCE SUBSTRATE RECOGNITION AT THE POLYMERASE ACTIVE SITE." Journal of Biological Chemistry **275**: 359-366.

Klase, Z., et al. (2012). "MicroRNAs and HIV-1: complex interactions." Journal of Biological Chemistry **287**(49): 40884-40890.

Kleiman, L. (2002). "tRNALys3: The Primer tRNA for Reverse Transcription in HIV-1." IUBMB Life (International Union of Biochemistry and Molecular Biology: Life) **53**: 107-114.

Kohavi, R. (1994). Feature subset selection as search with probabilistic estimates. AAAI fall symposium on relevance.

Komanduri, K. V., et al. (1998). "Restoration of cytomegalovirus-specific CD4+ T-lymphocyte responses after ganciclovir and highly active antiretroviral therapy in individuals infected with HIV-1." Nature medicine **4**(8): 953-956.

König, R. and S. Stertz (2015). "Recent strategies and progress in identifying host factors involved in virus replication." Current opinion in microbiology **26**: 79-88.

König, R., et al. (2008). "Global analysis of host-pathogen interactions that regulate early-stage HIV-1 replication." Cell **135**(1): 49-60.

Konopka, K., et al. (1991). "Enhancement of human immunodeficiency virus type 1 infection by cationic liposomes: the role of CD4, serum and liposome-cell interactions." J. Gen. Virol **72**(Pt 11): 2685.

Korgaonkar, S. N., et al. (2008). "HIV-1 upregulates VEGF in podocytes." Journal of the American Society of Nephrology **19**(5): 877-883.

Koyama, T., et al. (2013). "DNA damage enhances integration of HIV-1 into macrophages by overcoming integrase inhibition." Retrovirology **10**(1): 1-18.

Kozomara, A. and S. Griffiths-Jones (2014). "miRBase: annotating high confidence microRNAs using deep sequencing data." Nucleic acids research **42**(D1): D68-D73.

Krebs, F. C., et al. (2001). "Lentiviral LTR-directed expression, sequence variation, and disease pathogenesis." HIV sequence compendium: 29-70.

Krek, A., et al. (2005). "Combinatorial microRNA target predictions." Nature genetics **37**(5): 495-500.

Krol, J., et al. (2010). "The widespread regulation of microRNA biogenesis, function and decay." Nature Reviews Genetics **11**(9): 597.

Krummheuer, J., et al. (2007). "A minimal uORF within the HIV-1 vpu leader allows efficient translation initiation at the downstream env AUG." Virology **363**(2): 261-271.

Kuhn, M., et al. (2008). "STITCH: interaction networks of chemicals and proteins." Nucleic acids research **36**(suppl 1): D684-D688.

Kulkarni, S., et al. (2011). "Differential microRNA regulation of HLA-C expression and its association with HIV control." Nature **472**(7344): 495-498.

Kumamoto, K., et al. (2008). "Nutlin-3a activates p53 to both down-regulate inhibitor of growth 2 and up-regulate mir-34a, mir-34b, and mir-34c expression, and induce senescence." Cancer research **68**(9): 3193-3203.

Kuo, L. J. and L.-X. Yang (2008). "γ-H2AX-a novel biomarker for DNA double-strand breaks." In Vivo **22**(3): 305-309.

Kwak, P. B. and Y. Tomari (2012). "The N domain of Argonaute drives duplex unwinding during RISC assembly." Nature structural & molecular biology **19**(2): 145-151.

Kwong, P. D., et al. (1998). HIV-1 GP120 CORE COMPLEXED WITH CD4 AND A NEUTRALIZING HUMAN ANTIBODY, Protein Data Bank, Rutgers University.

Lagos, D., et al. (2010). "miR-132 regulates antiviral innate immunity through suppression of the p300 transcriptional co-activator." Nature cell biology **12**(5): 513-519.

Laguette, N. and M. Benkirane (2015). "Shaping of the host cell by viral accessory proteins." Frontiers in microbiology **6**.

Laguette, N., et al. (2014). "Premature activation of the SLX4 complex by Vpr promotes G2/M arrest and escape from innate immune sensing." Cell **156**(1): 134-145.

Lahaye, X., et al. (2013). "The capsids of HIV-1 and HIV-2 determine immune detection of the viral cDNA by the innate sensor cGAS in dendritic cells." Immunity **39**(6): 1132-1142.

Lai, M., et al. (2005). "Activation of the ATR pathway by human immunodeficiency virus type 1 Vpr involves its direct binding to chromatin in vivo." Journal of Virology **79**(24): 15443-15451.

Lam, W.-Y., et al. (2013). "Effect of avian influenza A H5N1 infection on the expression of microRNA-141 in human respiratory epithelial cells." BMC microbiology **13**(1): 1.

Landi, A., et al. (2011). "One protein to rule them all: modulation of cell surface receptors and molecules by HIV Nef." Current HIV research **9**(7): 496.

Larder, B. A. and S. D. Kemp (1989). "Multiple mutations in HIV-1 reverse transcriptase confer high-level resistance to zidovudine (AZT)." Science **246**(4934): 1155-1158.

Larsson, M., et al. (2013). "Molecular signatures of T-cell inhibition in HIV-1 infection." Retrovirology **10**(1): 31.

Le Douce, V., et al. (2010). "Review Molecular mechanisms of HIV-1 persistence in the monocyte-macrophage lineage."

Lecellier, C.-H., et al. (2005). "A cellular microRNA mediates antiviral defense in human cells." Science **308**(5721): 557-560.

Lederman, M. M., et al. (1998). "Immunologic responses associated with 12 weeks of combination antiretroviral therapy consisting of zidovudine, lamivudine, and ritonavir: results of AIDS Clinical Trials Group Protocol 315." Journal of Infectious Diseases **178**(1): 70-79.

Lee, K., et al. (2010). "Flexible use of nuclear import pathways by HIV-1." Cell host & microbe **7**(3): 221-233.

Lee, M., et al. (2013). "Stabilization of p21 (Cip1/WAF1) following Tip60-dependent acetylation is required for p21-mediated DNA damage response." Cell Death & Differentiation **20**(4): 620-629.

Lee, R. C., et al. (1993). "The C. elegans heterochronic gene lin-4 encodes small RNAs with antisense complementarity to lin-14." Cell **75**(5): 843-854.

Lee, Y., et al. (2004). "MicroRNA genes are transcribed by RNA polymerase II." The EMBO journal **23**(20): 4051-4060.

Lemons, D., et al. (2013). "Developing microRNA screening as a functional genomics tool for disease research." Frontiers in physiology **4**.

Levine, A. J. and M. Oren (2009). "The first 30 years of p53: growing ever more complex." Nature Reviews Cancer **9**(10): 749-758.

Lewis, B. P., et al. (2003). "Prediction of mammalian microRNA targets." Cell **115**(7): 787-798.

Liccardi, G., et al. (2011). "EGFR nuclear translocation modulates DNA repair following cisplatin and ionizing radiation treatment." Cancer research **71**(3): 1103-1114.

Lin, M.-T., et al. (2001). "IL-6 inhibits apoptosis and retains oxidative DNA lesions in human gastric cancer AGS cells through up-regulation of anti-apoptotic gene mcl-1." Carcinogenesis **22**(12): 1947-1953.

Ling, S. H. M., et al. (2011). "Structural and functional insights into eukaryotic mRNA decapping." Wiley Interdisciplinary Reviews-Rna **2**(2): 193-208. (C) 2010 John Wiley & Sons, Ltd. WIREs RNA 2011 2 193-208 DOI: 10.1002/wrna.44

Linsley, P. S., et al. (2007). "Transcripts targeted by the microRNA-16 family cooperatively regulate cell cycle progression." Molecular and cellular biology **27**(6): 2240-2252.

Little, S. J., et al. (1999). "Viral dynamics of acute HIV-1 infection." The Journal of experimental medicine **190**(6): 841-850.

Liu, F., et al. (2015). "miR□34c□3p functions as a tumour suppressor by inhibiting eIF4E expression in non□small cell lung cancer." Cell Proliferation **48**(5): 582-592.

Liu, G., et al. (2015). "Kaposi sarcoma-associated herpesvirus promotes tumorigenesis by modulating the Hippo pathway." Oncogene **34**(27): 3536-3546.

Liu, H., et al. (2010). "[MiR26a and miR939 regulate the replication of H1N1 influenza virus in MDCK cell]." Wei sheng wu xue bao= Acta microbiologica Sinica **50**(10): 1399-1405.

Liu, J., et al. (2004). "Argonaute2 is the catalytic engine of mammalian RNAi." Science **305**(5689): 1437-1441.

Liu, L., et al. (2011). "A whole genome screen for HIV restriction factors." Retrovirology **8**(1): 1-15.

Liu, R., et al. (1996). "Homozygous defect in HIV-1 coreceptor accounts for resistance of some multiply-exposed individuals to HIV-1 infection." Cell **86**(3): 367-377.

Liu, S., et al. (2012). "Effect of CCR5-Delta32 heterozygosity on HIV-1 susceptibility: a meta-analysis." PLoS One **7**(4): e35020.

Liu, X., et al. (2012). "Precursor microRNA-programmed silencing complex assembly pathways in mammals." Molecular cell **46**(4): 507-517.

Livak, K. J. and T. D. Schmittgen (2001). "Analysis of relative gene expression data using real-time quantitative PCR and the 2− ΔΔCT method." Methods **25**(4): 402-408.

López, J. A. and L. M. Alvarez-Salas (2011). "Differential effects of miR-34c-3p and miR-34c-5p on SiHa cells proliferation apoptosis, migration and invasion." Biochemical and biophysical research communications **409**(3): 513-519.

Lu, K., et al. (2011). "Structural determinants and mechanism of HIV-1 genome packaging." Journal of molecular biology **410**(4): 609-633.

Lundholt, B. K., et al. (2003). "A simple technique for reducing edge effect in cell-based assays." Journal of biomolecular screening **8**(5): 566-570.

Lundquist, C. A., et al. (2004). "Nef stimulates human immunodeficiency virus type 1 replication in primary T cells by enhancing virion-associated gp120 levels: coreceptor-dependent requirement for Nef in viral replication." Journal of Virology **78**(12): 6287-6296.

Ma, L., et al. (2014). "miRNA-1236 inhibits HIV-1 infection of monocytes by repressing translation of cellular factor VprBP." PLoS One **9**(6): e99535.

MacRae, I. J., et al. (2008). "In vitro reconstitution of the human RISC-loading complex." Proceedings of the National Academy of Sciences **105**(2): 512-517.

MacRae, I. J., et al. (2006). "Structural basis for double-stranded RNA processing by Dicer." Science **311**(5758): 195-198.

Maddukuri, A., et al. (2003). "Pharmacological cyclin-dependent kinase inhibitors as HIV-1 antiviral therapeutics." Current HIV research **1**(2): 131-152.

Maertens, G., et al. (2003). "LEDGF/p75 is essential for nuclear and chromosomal targeting of HIV-1 integrase in human cells." Journal of Biological Chemistry **278**(35): 33528-33539.

Malim, M. H. (2009). "APOBEC proteins and intrinsic resistance to HIV-1 infection." Philosophical Transactions of the Royal Society B: Biological Sciences **364**(1517): 675-687.

Mangeat, B., et al. (2003). "Broad antiretroviral defence by human APOBEC3G through lethal editing of nascent reverse transcripts." Nature **424**(6944): 99-103.

Manna, S. K. and B. B. Aggarwal (2000). "Differential requirement for p56lck in HIV-tat versus TNF-induced cellular responses: effects on NF-κB, activator protein-1, c-Jun N-terminal kinase, and apoptosis." The Journal of Immunology **164**(10): 5156-5166.

Marchant, D. (2006). "Human immunodeficiency virus types 1 and 2 have different replication kinetics in human primary macrophage culture." Journal of General Virology **87**: 411-418.

Marini, B., et al. (2015). "Nuclear architecture dictates HIV-1 integration site selection." Nature.

Marlink, R., et al. (1994). "Reduced rate of disease development after HIV-2 infection as compared to HIV-1." Science **265**: 1587-1590.

Marshall, N. F., et al. (1996). "Control of RNA polymerase II elongation potential by a novel carboxyl-terminal domain kinase." Journal of Biological Chemistry **271**(43): 27176-27183.

Martin, M. P., et al. (1998). "Genetic acceleration of AIDS progression by a promoter variant of CCR5." Science **282**(5395): 1907-1911.

Mathonnet, G., et al. (2007). "MicroRNA inhibition of translation initiation in vitro by targeting the cap-binding complex eIF4F." Science **317**(5845): 1764-1767.

Matreyek, K. A. and A. Engelman (2013). "Viral and cellular requirements for the nuclear entry of retroviral preintegration nucleoprotein complexes." Viruses **5**(10): 2483-2511.

Matsui, T., et al. (1980). "Multiple factors required for accurate initiation of transcription by purified RNA polymerase II." Journal of Biological Chemistry **255**(24): 11992-11996.

Mauclère, P., et al. (1997). "Serological and virological characterization of HIV-1 group O infection in Cameroon." Aids **11**: 445-453.

McDonald, D. (2002). "Visualization of the intracellular behavior of HIV in living cells." The Journal of cell biology **159**: 441-452.

McKeating, J. A. and R. L. Willey (1989). "Structure and function of the HIV envelope." Aids **3**: S35-42.

Meek, D. W. and C. W. Anderson (2009). "Posttranslational modification of p53: cooperative integrators of function." Cold Spring Harbor perspectives in biology **1**(6): a000950.

Meliopoulos, V. A., et al. (2012). "Host gene targets for novel influenza therapies elucidated by high-throughput RNA interference screens." The FASEB Journal **26**(4): 1372-1386.

Meliopoulos, V. A., et al. (2012). "MicroRNA regulation of human protease genes essential for influenza virus replication." PLoS One **7**(5): e37169.

Michel, N., et al. (2005). "The Nef protein of human immunodeficiency virus establishes superinfection immunity by a dual strategy to downregulate cell-surface CCR5 and CD4." Current Biology **15**(8): 714-723.

Mikhail, M., et al. (2003). "Mechanisms involved in non-progressive HIV disease." AIDs Rev **5**(4): 230-244.

Miki, K., et al. (2015). "Efficient Detection and Purification of Cell Populations Using Synthetic MicroRNA Switches." Cell stem cell.

Milano, V., et al. (2009). "Dasatinib-induced autophagy is enhanced in combination with temozolomide in glioma." Molecular cancer therapeutics **8**(2): 394-406.

Millevoi, S. and S. Vagner (2009). "Molecular mechanisms of eukaryotic pre-mRNA 3′ end processing regulation." Nucleic acids research: gkp1176.

Mocquet, V., et al. (2015). "How Retroviruses Escape the Nonsense-Mediated mRNA Decay." AIDS research and human retroviruses **31**(10): 948-958.

Mohr, S. E., et al. (2014). "RNAi screening comes of age: improved techniques and complementary approaches." Nature reviews Molecular cell biology **15**(9): 591-600.

Mongroo, P. S. and A. K. Rustgi (2010). "The role of the miR-200 family in epithelial-mesenchymal transition." Cancer biology & therapy **10**(3): 219-222.

Monroe, K. M., et al. (2014). "IFI16 DNA sensor is required for death of lymphoid CD4 T cells abortively infected with HIV." Science **343**(6169): 428-432.

Morgan, D., et al. (2000). "Survival by AIDS defining condition in rural Uganda." Sexually Transmitted Infections **76**(3): 193-197.

Motomura, K., et al. (2007). "Genetic Recombination between Human Immunodeficiency Virus Type 1 (HIV-1) and HIV-2, Two Distinct Human Lentiviruses." Journal of Virology **82**: 1923-1933.

Moulard, M., et al. (1999). "Processing and routage of HIV glycoproteins by furin to the cell surface." Virus research **60**(1): 55-65.

Mukherji, S., et al. (2011). "MicroRNAs can generate thresholds in target gene expression." Nature genetics **43**(9): 854-859.

Münk, C., et al. (2012). "An ancient history of gene duplications, fusions and losses in the evolution of APOBEC3 mutators in mammals." BMC evolutionary biology **12**(1): 71.

Nabell, L. M., et al. (1994). "Human Immunodeficiency Virus 1 Tat Stimulates Transcription of the Transforming Growth Factor Gene in an Epidermal Growth Factor-dependent Manner." Cell growth and differentiation **5**: 87-87.

Nakagawa, F., et al. (2013). "Life expectancy living with HIV: recent estimates and future implications." Current opinion in infectious diseases **26**(1): 17-25.

Nakagawa, F., et al. (2015). "Projected lifetime healthcare costs associated with HIV infection." PLoS One **10**(4): e0125018.

Nakai-Murakami, C., et al. (2007). "HIV-1 Vpr induces ATM-dependent cellular signal with enhanced homologous recombination." Oncogene **26**(4): 477-486.

Nakamachi, Y., et al. (2009). "MicroRNA□124a is a key regulator of proliferation and monocyte chemoattractant protein 1 secretion in fibroblast□like synoviocytes from patients with rheumatoid arthritis." Arthritis & Rheumatism **60**(5): 1294-1304.

Namy, O., et al. (2006). "A mechanical explanation of RNA pseudoknot function in programmed ribosomal frameshifting." Nature **441**(7090): 244-247.

Neagu, M. R., et al. (2009). "Potent inhibition of HIV-1 by TRIM5-cyclophilin fusion proteins engineered from human components." Journal of Clinical Investigation **119**: 3035-3047.

Neil, S. J., et al. (2008). "Tetherin inhibits retrovirus release and is antagonized by HIV-1 Vpu." Nature **451**(7177): 425-430.

Ng, W., et al. (2014). "OCT4 as a target of miR-34a stimulates p63 but inhibits p53 to promote human cell transformation." Cell death & disease **5**(1): e1024.

Nicoletti, F., et al. (2011). "mTOR as a multifunctional therapeutic target in HIV infection." Drug discovery today **16**(15): 715-721.

Nishihara, T., et al. (2013). "miRISC recruits decapping factors to miRNA targets to enhance their degradation." Nucleic acids research: gkt619.

Normanno, N., et al. (2006). "Epidermal growth factor receptor (EGFR) signaling in cancer." Gene **366**(1): 2-16.

Nottrott, S., et al. (2006). "Human let-7a miRNA blocks protein production on actively translating polyribosomes." Nature structural & molecular biology **13**(12): 1108-1114.

Novina, C. D., et al. (2002). "siRNA-directed inhibition of HIV-1 infection." Nature medicine **8**(7): 681-686.

Nowsheen, S. and E. Yang (2012). "The intersection between DNA damage response and cell death pathways." Experimental oncology **34**(3): 243.

Nunes, M., et al. (2004). "Phosphorylation of extracellular signal-regulated kinase 1 and 2, protein kinase B, and signal transducer and activator of transcription 3 are differently inhibited by an epidermal growth factor receptor inhibitor, EKB-569, in tumor cells and normal human keratinocytes." Molecular cancer therapeutics **3**(1): 21-27.

O'Connell, R. M., et al. (2012). "microRNA regulation of inflammatory responses." Annual review of immunology **30**: 295-312.

O'Neil, P. K., et al. (2002). "Mutational analysis of HIV-1 long terminal repeats to explore the relative contribution of reverse transcriptase and RNA polymerase II to viral mutagenesis." Journal of Biological Chemistry **277**(41): 38053-38061.

Obaya, A. and J. Sedivy (2002). "Regulation of cyclin-Cdk activity in mammalian cells." Cellular and Molecular Life Sciences CMLS **59**(1): 126-142.

Obbard, D. J., et al. (2009). "The evolution of RNAi as a defence against viruses and transposable elements." Philosophical Transactions of the Royal Society B: Biological Sciences **364**(1513): 99-115.

Ocwieja, K. E., et al. (2011). "HIV integration targeting: a pathway involving Transportin-3 and the nuclear pore protein RanBP2." PLoS Pathog **7**(3): e1001313-e1001313.

Ocwieja, K. E., et al. (2012). "Dynamic regulation of HIV-1 mRNA populations analyzed by single-molecule enrichment and long-read sequencing." Nucleic acids research **40**(20): 10345-10355.

Okulicz, J. F., et al. (2009). "Clinical outcomes of elite controllers, viremic controllers, and long-term nonprogressors in the US Department of Defense HIV natural history study." Journal of Infectious Diseases **200**(11): 1714-1723.

Okuzumi, T., et al. (2010). "Synthesis and evaluation of indazole based analog sensitive Akt inhibitors." Molecular Biosystems **6**(8): 1389-1402.

Olson, A. D., et al. (2014). "Evaluation of Rapid Progressors in HIV Infection as an Extreme Phenotype." Journal of acquired immune deficiency syndromes (1999) **67**(1): 15.

Ono, A., et al. (2004). "Phosphatidylinositol (4, 5) bisphosphate regulates HIV-1 Gag targeting to the plasma membrane." Proceedings of the National Academy of Sciences of the United States of America **101**(41): 14889-14894.

Osmond, D., et al. (1994). "Changes in AIDS survival time in two San Francisco cohorts of homosexual men, 1983 to 1993." Jama **271**(14): 1083-1087.

Ozsolak, F., et al. (2008). "Chromatin structure analyses identify miRNA promoters." Genes & development **22**(22): 3172-3183.

Pache, L., et al. (2011). "Identifying HIV-1 host cell factors by genome-scale RNAi screening." Methods **53**(1): 3-12.

Palella Jr, F. J., et al. (1998). "Declining morbidity and mortality among patients with advanced human immunodeficiency virus infection." New England Journal of Medicine **338**(13): 853-860.

Palmer, S., et al. (2003). "New real-time reverse transcriptase-initiated PCR assay with single-copy sensitivity for human immunodeficiency virus type 1 RNA in plasma." Journal of clinical microbiology **41**(10): 4531-4536.

Pan, D. (2010). "The hippo signaling pathway in development and cancer." Developmental cell **19**(4): 491-505.

Pantaleo, G., et al. (1993). "HIV infection is active and progressive in lymphoid tissue during the clinically latent stage of disease." Nature **362**(6418): 355-358.

Panté, N. and M. Kann (2002). "Nuclear pore complex is able to transport macromolecules with diameters of≈ 39 nm." Molecular biology of the cell **13**(2): 425-434.

Parkin, N. T., et al. (1992). "Human immunodeficiency virus type 1 gag-pol frameshifting is dependent on downstream mRNA secondary structure: demonstration by expression in vivo." Journal of Virology **66**(8): 5147-5151.

Pasquinelli, A. E. (2012). "MicroRNAs and their targets: recognition, regulation and an emerging reciprocal relationship." Nature Reviews Genetics **13**(4): 271-282.

Pauls, E., et al. (2014). "Cell cycle control and HIV-1 susceptibility are linked by CDK6-dependent CDK2 phosphorylation of SAMHD1 in myeloid and lymphoid cells." The Journal of Immunology **193**(4): 1988-1997.

Peel, S., et al. (2011). "Divergent pathways lead to ESCRT-III-catalyzed membrane fission." Trends in biochemical sciences **36**(4): 199-210.

Pepin, J., et al. (1991). "HIV-2-induced immunosuppression among asymptomatic West African prostitutes." Aids **5**: 1165-1172.

Pereira, L. A., et al. (2000). "SURVEY AND SUMMARY A compilation of cellular transcription factor interactions with the HIV-1 LTR promoter." Nucleic acids research **28**(3): 663-668.

Perelson, A. S., et al. (1996). "HIV-1 dynamics in vivo: virion clearance rate, infected cell life-span, and viral generation time." Science **271**(5255): 1582-1586.

Pericle, F., et al. (1998). "Cutting Edge: HIV-1 infection induces a selective reduction in STAT5 protein expression." The Journal of Immunology **160**(1): 28-31.

Petersen, C. P., et al. (2006). "Short RNAs repress translation after initiation in mammalian cells." Molecular cell **21**(4): 533-542.

Picard-Jean, F., et al. (2013). "The immunosuppressive agent mizoribine monophosphate is an inhibitor of the human RNA capping enzyme." PLoS One **8**(1).

Pierangeli, A., et al. (2015). "Immunodeficiency-associated viral oncogenesis." Clinical Microbiology and Infection **21**(11): 975-983.

Pillai, R. S. (2005). "MicroRNA function: multiple mechanisms for a tiny RNA?" RNA **11**(12): 1753-1761.

Pincus, S. H. and K. Wehrly (1990). "AZT Demonstrates Anti-HIV-l Activity in Persistently Infected Cell Lines: Implications for Combination Chemotherapy and Immunotherapy." Journal of Infectious Diseases **162**: 1233-1238.

Pitisuttithum, P., et al. (2006). "Randomized, double□blind, placebo□controlled efficacy trial of a bivalent recombinant glycoprotein 120 HIV□1 vaccine among injection drug users in Bangkok, Thailand." Journal of Infectious Diseases **194**(12): 1661-1671.

Plank, T.-D. M., et al. (2014). "Internal translation initiation from HIV-1 transcripts is conferred by a common RNA structure." Translation **2**(1): e27694.

Plantier, J.-C., et al. (2009). "A new human immunodeficiency virus derived from gorillas." Nat Med **15**: 871-872.

Poiesi, C., et al. (2008). "HIV-1 p17 binds heparan sulfate proteoglycans to activated CD4+ T cells." Virus research **132**(1): 25-32.

Poropatich, K. and D. J. Sullivan (2011). "Human immunodeficiency virus type 1 long-term non-progressors: the viral, genetic and immunological basis for disease non-progression." Journal of General Virology **92**(2): 247-268.

Purcell, D. and M. A. Martin (1993). "Alternative splicing of human immunodeficiency virus type 1 mRNA modulates viral protein expression, replication, and infectivity." Journal of Virology **67**(11): 6365-6378.

Qian, S., et al. (2009). "HIV-1 Tat RNA silencing suppressor activity is conserved across kingdoms and counteracts translational repression of HIV-1." Proceedings of the National Academy of Sciences **106**(2): 605-610.

Quiros, S., et al. (2011). "Rad51 and BRCA2-New molecular targets for sensitizing glioma cells to alkylating anticancer drugs." PLoS One **6**(11): e27183.

Rasaiyaah, J., et al. (2013). "HIV-1 evades innate immune recognition through specific cofactor recruitment." Nature **503**(7476): 402-405.

Ratner, L., et al. (1985). "Complete nucleotide sequence of the AIDS virus, HTLV-III." Nature **313**: 277-284.

Rato, S., et al. (2010). "Novel HIV-1 knockdown targets identified by an enriched kinases/phosphatases shRNA library using a long-term iterative screen in Jurkat T-cells." PLoS One **5**(2): e9276.

Rawat, S. S., et al. (2005). "Sphingolipids: modulators of HIV-1 infection and pathogenesis." Bioscience reports **25**(5-6): 329-343.

Reynoso, R., et al. (2014). "MicroRNAs differentially present in the plasma of HIV elite controllers reduce HIV infection in vitro." Scientific reports **4**.

Richards, K. H. and P. R. Clapham (2006). "Human immunodeficiency viruses: propagation, quantification, and storage." Current protocols in microbiology: 15J. 11.11-15J. 11.22.

Richman, D. D. (2001). "HIV chemotherapy." Nature **410**: 995-1001.

Rittner, K., et al. (1995). "The human immunodeficiency virus long terminal repeat includes a specialised initiator element which is required for Tat-responsive transcription." Journal of molecular biology **248**(3): 562-580.

Rodriguez, A., et al. (2004). "Identification of mammalian microRNA host genes and transcription units." Genome research **14**(10a): 1902-1910.

Roeder, R. G. (1996). "The role of general initiation factors in transcription by RNA polymerase II." Trends in biochemical sciences **21**(9): 327-335.

Roeth, J. F., et al. (2004). "HIV-1 Nef disrupts MHC-I trafficking by recruiting AP-1 to the MHC-I cytoplasmic tail." The Journal of cell biology **167**(5): 903-913.

Romani, B., et al. (2015). "HIV-1 Vpr Protein Enhances Proteasomal Degradation of MCM10 DNA Replication Factor through the Cul4-DDB1 [VprBP] E3 Ubiquitin Ligase to Induce G2/M Cell Cycle Arrest." Journal of Biological Chemistry **290**(28): 17380-17389.

Ruelas, D. S., et al. (2015). "MicroRNA-155 Reinforces HIV Latency." Journal of Biological Chemistry **290**(22): 13736-13748.

Ruiz, A., et al. (2015). "Cyclin D3-dependent control of the dNTP pool and HIV-1 replication in human macrophages." Cell Cycle(just-accepted): 00-00.

Saad, J. S., et al. (2006). "Structural basis for targeting HIV-1 Gag proteins to the plasma membrane for virus assembly." Proceedings of the National Academy of Sciences **103**(30): 11364-11369.

Sáez-Cirión, A., et al. (2011). "Restriction of HIV-1 replication in macrophages and CD4+ T cells from HIV controllers." Blood **118**(4): 955-964.

Salmena, L., et al. (2011). "A ceRNA hypothesis: the Rosetta Stone of a hidden RNA language?" Cell **146**(3): 353-358.

Sanghvi, V. R. and L. F. Steel (2011). "The cellular TAR RNA binding protein, TRBP, promotes HIV-1 replication primarily by inhibiting the activation of double-stranded RNA-dependent kinase PKR." Journal of Virology **85**(23): 12614-12621.

Santhakumar, D., et al. (2010). "Combined agonist–antagonist genome-wide functional screening identifies broadly active antiviral microRNAs." Proceedings of the National Academy of Sciences **107**(31): 13830-13835.

Santiago, M. L., et al. (2005). "Simian Immunodeficiency Virus Infection in Free-Ranging Sooty Mangabeys (Cercocebus atys atys) from the Tai Forest, Cote d'Ivoire: Implications for the Origin of Epidemic Human Immunodeficiency Virus Type 2." Journal of Virology **79**: 12515-12527.

Sarafianos, S. G., et al. (2009). "Structure and Function of HIV-1 Reverse Transcriptase: Molecular Mechanisms of Polymerization and Inhibition." Journal of molecular biology **385**: 693-713.

Saunders, M., et al. (2005). "p73 modulates HIV-1 Tat transcriptional and apoptotic activities in human astrocytes." Apoptosis **10**(6): 1419-1431.

Sawaya, B. E., et al. (1998). "Cooperative actions of HIV-1 Vpr and p53 modulate viral gene transcription." Journal of Biological Chemistry **273**(32): 20052-20057.

Schaller, T., et al. (2011). "HIV-1 capsid-cyclophilin interactions determine nuclear import pathway, integration targeting and replication efficiency." PLoS pathogens **7**(12): e1002439.

Schindelin, J., et al. (2012). "Fiji: an open-source platform for biological-image analysis." Nature methods **9**(7): 676-682.

Schindler, M., et al. (2005). "Human immunodeficiency virus type 1 inhibits DNA damage-triggered apoptosis by a Nef-independent mechanism." Journal of Virology **79**(9): 5489-5498.

Schnell, G., et al. (2009). "Compartmentalized human immunodeficiency virus type 1 originates from long-lived cells in some subjects with HIV-1-associated dementia." PLoS Pathog **5**(4): e1000395.

Schnell, U., et al. (2012). "Immunolabeling artifacts and the need for live-cell imaging." Nature methods **9**(2): 152-158.

Schoolmeesters, A., et al. (2009). "Functional profiling reveals critical role for miRNA in differentiation of human mesenchymal stem cells."

Schröder, A. R., et al. (2002). "HIV-1 integration in the human genome favors active genes and local hotspots." Cell **110**(4): 521-529.

Schwartz, S., et al. (1990). "Cloning and functional analysis of multiply spliced mRNA species of human immunodeficiency virus type 1." Journal of Virology **64**(6): 2519-2529.

Schwartz, S., et al. (1990). "Env and Vpu proteins of human immunodeficiency virus type 1 are produced from multiple bicistronic mRNAs." Journal of Virology **64**(11): 5448-5456.

Schwegmann, A. and F. Brombacher (2008). "Host-directed drug targeting of factors hijacked by pathogens." Science signaling **1**(29): re8-re8.

Schweizer, M. T. and E. S. Antonarakis (2012). "Abiraterone and other novel androgen-directed strategies for the treatment of prostate cancer: a new era of hormonal therapies is born." Therapeutic advances in urology: 1756287212452196.

Seddiki, N., et al. (2014). "Role of miR□155 in the regulation of lymphocyte immune function and disease." Immunology **142**(1): 32-38.

Selby, M. J., et al. (1989). "Structure, sequence, and position of the stem-loop in tar determine transcriptional elongation by tat through the HIV-1 long terminal repeat." Genes & development **3**(4): 547-558.

Selcuklu, S. D., et al. (2009). "miR-21 as a key regulator of oncogenic processes." Biochemical Society Transactions **37**(4): 918.

Semenza, G. L. (2007). "Hypoxia-inducible factor 1 (HIF-1) pathway." Sci. Stke **2007**(407): cm8-cm8.

Shah, V. B., et al. (2013). "The host proteins transportin SR2/TNPO3 and cyclophilin A exert opposing effects on HIV-1 uncoating." Journal of Virology **87**(1): 422-432.

Shamir, L., et al. (2010). "Pattern recognition software and techniques for biological image analysis." PLoS Comput Biol **6**(11): e1000974-e1000974.

Shariff, A., et al. (2010). "Automated image analysis for high-content screening and analysis." Journal of biomolecular screening **15**(7): 726-734.

Sharkey, M. E. and M. Stevenson (2001). "Two long terminal repeat circles and persistent HIV-1 replication." Current opinion in infectious diseases **14**(1): 5-11.

Sharp, P. M. and B. H. Hahn (2011). "Origins of HIV and the AIDS Pandemic." Cold Spring Harbor perspectives in medicine **1**: a006841-a006841.

Sheehy, A. M., et al. (2002). "Isolation of a human gene that inhibits HIV-1 infection and is suppressed by the viral Vif protein." Nature **418**(6898): 646-650.

Shen, C.-J., et al. (2012). "Translation of Pur-α is targeted by cellular miRNAs to modulate the differentiation-dependent susceptibility of monocytes to HIV-1 infection." The FASEB Journal **26**(11): 4755-4764.

Sherrill-Mix, S., et al. (2013). "HIV latency and integration site placement in five cell-based models." Retrovirology **10**(1): 90.

Shirakawa, K., et al. (2013). "Reactivation of latent HIV by histone deacetylase inhibitors." Trends in microbiology **21**(6): 277-285.

Shishido, T., et al. (2012). "Selected drugs with reported secondarycell-differentiating capacity prime latent HIV-1 infection for reactivation." Journal of Virology: JVI. 00793-00712.

Shun, M.-C., et al. (2007). "LEDGF/p75 functions downstream from preintegration complex formation to effect gene-specific HIV-1 integration." Genes & development **21**(14): 1767-1778.

Shun, T. Y., et al. (2011). "Identifying Actives from HTS Data Sets Practical Approaches for the Selection of an Appropriate HTS Data-Processing Method and Quality Control Review." Journal of biomolecular screening **16**(1): 1-14.

Sibley, C. R., et al. (2011). "The biogenesis and characterization of mammalian microRNAs of mirtron origin." Nucleic acids research: gkr722.

Siddiquee, K. A. Z. and J. Turkson (2008). "STAT3 as a target for inducing apoptosis in solid and hematological tumors." Cell research **18**(2): 254-267.

Siliciano, J. D., et al. (2003). "Long-term follow-up studies confirm the stability of the latent reservoir for HIV-1 in resting CD4+ T cells." Nature medicine **9**(6): 727-728.

Siliciano, R. F. and W. C. Greene (2011). "HIV latency." Cold Spring Harbor perspectives in medicine **1**(1): a007096.

Simon, F., et al. (1998). "Identification of a new human immunodeficiency virus type 1 distinct from group M and group O." Nat Med **4**: 1032-1037.

Singhal, P. C., et al. (2000). "HIV□1 gp120 envelope protein modulates proliferation of human glomerular epithelial cells." Journal of cellular biochemistry **76**(1): 61-70.

Skalsky, R. L., et al. (2012). "The viral and cellular microRNA targetome in lymphoblastoid cell lines." PLoS Pathog **8**(1): e1002484.

Smith, W. W., et al. (2005). "Leucine-rich repeat kinase 2 (LRRK2) interacts with parkin, and mutant LRRK2 induces neuronal degeneration." Proceedings of the National Academy of Sciences of the United States of America **102**(51): 18676-18681.

Sodroski, J., et al. (1985). "Trans-acting transcriptional regulation of human T-cell leukemia virus type III long terminal repeat." Science **227**(4683): 171-173.

Song, B., et al. (2008). "miR-192 Regulates dihydrofolate reductase and cellular proliferation through the p53-microRNA circuit." Clinical Cancer Research **14**(24): 8080-8086.

St Clair, M., et al. (1991). "Resistance to ddI and sensitivity to AZT induced by a mutation in HIV-1 reverse transcriptase." Science **253**(5027): 1557-1559.

Stewart, M. (2010). "Nuclear export of mRNA." Trends in biochemical sciences **35**(11): 609-617.

Stolp, B. and O. T. Fackler (2011). "How HIV takes advantage of the cytoskeleton in entry and replication." Viruses **3**(4): 293-311.

Stoltzfus, C. M. and J. M. Madsen (2006). "Role of viral splicing elements and cellular RNA binding proteins in regulation of HIV-1 alternative RNA splicing." Current HIV research **4**(1): 43-55.

Stopak, K., et al. (2003). "HIV-1 Vif blocks the antiviral activity of APOBEC3G by impairing both its translation and intracellular stability." Molecular cell **12**(3): 591-601.

Strain, M., et al. (2003). "Heterogeneous clearance rates of long-lived lymphocytes infected with HIV: intrinsic stability predicts lifelong persistence." Proceedings of the National Academy of Sciences **100**(8): 4819-4824.

Strambio-De-Castillia, C., et al. (2010). "The nuclear pore complex: bridging nuclear transport and gene regulation." Nature reviews Molecular cell biology **11**(7): 490-501.

Strebel, K. (2013). "HIV accessory proteins versus host restriction factors." Current opinion in Virology **3**(6): 692-699.

Strebel, K., et al. (1987). "The HIV A (sor) gene product is essential for virus infectivity."

Stremlau, M., et al. (2004). "The cytoplasmic body component TRIM5α restricts HIV-1 infection in Old World monkeys." Nature **427**: 848-853.

Stremlau, M., et al. (2006). "Specific recognition and accelerated uncoating of retroviral capsids by the TRIM5 restriction factor." Proceedings of the National Academy of Sciences **103**: 5514-5519.

Sun, G., et al. (2011). "Interplay between HIV-1 infection and host microRNAs." Nucleic acids research: gkr961.

Sung, T.-L. and A. P. Rice (2009). "miR-198 inhibits HIV-1 gene expression and replication in monocytes and its mechanism of action appears to involve repression of cyclin T1." PLoS Pathog **5**(1): e1000263.

Swaminathan, G., et al. (2014). "MicroRNAs and HIV-1 infection: antiviral activities and beyond." Journal of molecular biology **426**(6): 1178-1197.

Swaminathan, G., et al. (2012). "A role for microRNA-155 modulation in the anti-HIV-1 effects of Toll-like receptor 3 stimulation in macrophages."

Swinney, D. C. and J. Anthony (2011). "How were new medicines discovered?" Nature reviews Drug discovery **10**(7): 507-519.

Szakacs, G., et al. (2008). "The role of ABC transporters in drug absorption, distribution, metabolism, excretion and toxicity (ADME–Tox)." Drug discovery today **13**(9): 379-393.

Tahirov, T. H., et al. (2010). "Crystal structure of HIV-1 Tat complexed with human P-TEFb." Nature **465**(7299): 747-751.

Takimoto, K., et al. (2009). "Mammalian GW182 contains multiple Argonaute-binding sites and functions in microRNA-mediated translational repression." RNA **15**(6): 1078-1089.

Tan, J. Y., et al. (2015). "Extensive microRNA-mediated crosstalk between lncRNAs and mRNAs in mouse embryonic stem cells." Genome research: gr. 181974.181114.

Tang, J., et al. (2015). "Inhibition of TLR8 Mediated Signaling Promotes BCG Induced Apoptosis in THP-1 Cells." Microbial pathogenesis.

Tebas, P., et al. (2000). "Accelerated bone mineral loss in HIV-infected patients receiving potent antiretroviral therapy." AIDS (London, England) **14**(4): F63.

Terwilliger, E. F., et al. (1989). "Functional role of human immunodeficiency virus type 1 vpu." Proceedings of the National Academy of Sciences **86**(13): 5163-5167.

Thomsen, H., et al. (1981). "KAPOSI SARCOMA AMONG HOMOSEXUAL MEN IN EUROPE." The Lancet **318**: 688.

Tomkowicz, B., et al. (2006). "The Src kinase Lyn is required for CCR5 signaling in response to MIP-1β and R5 HIV-1 gp120 in human macrophages." Blood **108**(4): 1145-1150.

Topisirovic, I., et al. (2011). "Cap and cap-binding proteins in the control of gene expression." Wiley Interdisciplinary Reviews-Rna **2**(2): 277-298. John Wiley & Sons, Ltd. WIREs RNA 2011 2 277-298 DOI: 10.1002/wrna.52

Triboulet, R., et al. (2007). "Suppression of microRNA-silencing pathway by HIV-1 during virus replication." Science **315**(5818): 1579-1582.

Tsang, J., et al. (2007). "MicroRNA-mediated feedback and feedforward loops are recurrent network motifs in mammals." Molecular cell **26**(5): 753-767.

Tyagi, M., et al. (2010). "Establishment of HIV latency in primary CD4+ cells is due to epigenetic transcriptional silencing and P-TEFb restriction." Journal of Virology **84**(13): 6425-6437.

Uhlmann, S., et al. (2012). "Global microRNA level regulation of EGFR□driven cell□cycle protein network in breast cancer." Molecular systems biology **8**(1): 570.

UNAIDS (1996). End 1996 Global estimates, http://www.fao.org/docrep/x0259e/x0259e07.htm#P367_58896 accesed on 27th May 2015.

UNAIDS (2006). AIDS Epidemic Update December 2006., http://www.unaids.org acessed on 27th May 2015
.

UNAIDS (2014). World Aids Day 2014 report, http://www.unaids.org acessed on 27th May 2015.

Usami, Y., et al. (2009). "The ESCRT pathway and HIV-1 budding." Biochemical Society Transactions **37**(1): 181.

Valente, S. T., et al. (2009). "HIV-1 mRNA 3′ end processing is distinctively regulated by eIF3f, CDK11, and splice factor 9G8." Molecular cell **36**(2): 279-289.

Valiathan, R. R. and M. D. Resh (2004). "Expression of human immunodeficiency virus type 1 gag modulates ligand-induced downregulation of EGF receptor." Journal of Virology **78**(22): 12386-12394.

Vallari, A., et al. (2010). "Confirmation of Putative HIV-1 Group P in Cameroon." Journal of Virology **85**: 1403-1407.

Vandegraaff, N., et al. (2006). "Biochemical and genetic analyses of integrase-interacting proteins lens epithelium-derived growth factor (LEDGF)/p75 and hepatoma-derived growth factor related protein 2 (HRP2) in preintegration complex function and HIV-1 replication." Virology **346**: 415-426.

Vassilev, L. T., et al. (2004). "In vivo activation of the p53 pathway by small-molecule antagonists of MDM2." Science **303**(5659): 844-848.

Vigneron, A. M., et al. (2010). "Cytoplasmic ASPP1 inhibits apoptosis through the control of YAP." Genes & development **24**(21): 2430-2439.

Visnegarwala, F., et al. (1997). "Severe diabetes associated with protease inhibitor therapy." Annals of internal medicine **127**(10): 947-948.

Vlachos, I. S., et al. (2015). "DIANA-miRPath v3. 0: deciphering microRNA function with experimental support." Nucleic acids research: gkv403.

Vyas, T. K., et al. (2006). "Nanoparticulate drug carriers for delivery of HIV/AIDS therapy to viral reservoir sites."

Wain-Hobson, S., et al. (1985). "Nucleotide sequence of the AIDS virus, LAV." Cell **40**: 9-17.

Walker, B. D. and G. Y. Xu (2013). "Unravelling the mechanisms of durable control of HIV-1." Nature Reviews Immunology **13**(7): 487-498.

Walther, T. C., et al. (2002). "The cytoplasmic filaments of the nuclear pore complex are dispensable for selective nuclear protein import." The Journal of cell biology **158**(1): 63-77.

Wang, G. P., et al. (2007). "HIV integration site selection: analysis by massively parallel pyrosequencing reveals association with epigenetic modifications." Genome research **17**(8): 1186-1194.

Wang, H., et al. (2008). "Role of Purα in the modulation of homologous recombination-directed DNA repair by HIV-1 Tat." Anticancer research **28**(3A): 1441-1447.

Wang, L., et al. (2015). "MicroRNA regulation of viral immunity, latency, and carcinogenesis of selected tumor viruses and HIV." Reviews in medical virology **25**(5): 320-341.

Wang, X., et al. (2003). "Breast cancer resistance protein (BCRP/ABCG2) induces cellular resistance to HIV-1 nucleoside reverse transcriptase inhibitors." Molecular pharmacology **63**(1): 65-72.

Wang, X., et al. (2009). "Cellular microRNA expression correlates with susceptibility of monocytes/macrophages to HIV-1 infection." Blood **113**(3): 671-674.

Wang, Y., et al. (2014). "HIV-1 Vif inhibits G to A hypermutations catalyzed by virus-encapsidated APOBEC3G to maintain HIV-1 infectivity." Retrovirology **11**(1): 89-89.

Wang, Y., et al. (2013). "Endogenous miRNA sponge lincRNA-RoR regulates Oct4, Nanog, and Sox2 in human embryonic stem cell self-renewal." Developmental cell **25**(1): 69-80.

Watkins, B. A., et al. (1997). "Syncytium formation induced by human immunodeficiency virus type 1 isolates correlates with affinity for CD4." Journal of General Virology **78**(10): 2513-2522.

Wei, P., et al. (1998). "A novel CDK9-associated C-type cyclin interacts directly with HIV-1 Tat and mediates its high-affinity, loop-specific binding to TAR RNA." Cell **92**(4): 451-462.

Westendorp, M., et al. (1995). "HIV-1 Tat potentiates TNF-induced NF-kappa B activation and cytotoxicity by altering the cellular redox state." The EMBO journal **14**(3): 546.

Westerhout, E. M., et al. (2005). "HIV-1 can escape from RNA interference by evolving an alternative structure in its RNA genome." Nucleic acids research **33**(2): 796-804.

Westrop, S. J., et al. (2009). "Transient nature of long-term nonprogression and broad virus-specific proliferative T-cell responses with sustained thymic output in HIV-1 controllers." PLoS One **4**(5): e5474.

Whisnant, A. W., et al. (2013). "In-depth analysis of the interaction of HIV-1 with cellular microRNA biogenesis and effector mechanisms." MBio **4**(2): e00193-00113.

Whitney, J. B., et al. (2011). "Serpin induced antiviral activity of prostaglandin synthetase-2 against HIV-1 replication." PLoS One **6**(4): e18589.

WHO (2014). "HIV/AIDS Fact Sheet." Retrieved 27 May, 2015, from http://www.who.int/mediacentre/factsheets/fs360/en/

Willey, R., et al. (1992). "Human immunodeficiency virus type 1 Vpu protein induces rapid degradation of CD4." Journal of Virology **66**(12): 7193-7200.

Williams, S. A., et al. (2006). "NF□κB p50 promotes HIV latency through HDAC recruitment and repression of transcriptional initiation." The EMBO journal **25**(1): 139-149.

Wittkop, L., et al. (2011). "Effect of transmitted drug resistance on virological and immunological response to initial combination antiretroviral therapy for HIV (EuroCoord-CHAIN joint project): a European multicohort study." The Lancet infectious diseases **11**(5): 363-371.

Witwer, K. W., et al. (2012). "Relationships of PBMC microRNA expression, plasma viral load, and CD4+ T-cell count in HIV-1-infected elite suppressors and viremic patients." Retrovirology **9**(5): 1-15.

Wolf, D., et al. (2001). "HIV-1 Nef associated PAK and PI3-kinases stimulate Akt-independent Bad-phosphorylation to induce anti-apoptotic signals." Nature medicine **7**(11): 1217-1224.

Wolff, B., et al. (1997). "Leptomycin B is an inhibitor of nuclear export: inhibition of nucleo-cytoplasmic translocation of the human immunodeficiency virus type 1 (HIV-1) Rev protein and Rev-dependent mRNA." Chemistry & biology **4**(2): 139-147.

Wu, Y. and A. Yoder (2009). "Chemokine coreceptor signaling in HIV-1 infection and pathogenesis." PLoS Pathog **5**(12): e1000520.

Xia, X. and S. T. Wong (2012). "Concise Review: A High□Content Screening Approach to Stem Cell Research and Drug Discovery." Stem Cells **30**(9): 1800-1807.

Xiang, J., et al. (2004). "Inhibition of HIV-1 replication by GB virus C infection through increases in RANTES, MIP-lα, MIP-1β, and SDF-1." The Lancet **363**(9426): 2040-2046.

Xie, Q.-H., et al. (2011). "MiR-192 inhibits nucleotide excision repair by targeting ERCC3 and ERCC4 in HepG2. 2.15 cells." Biochemical and biophysical research communications **410**(3): 440-445.

Xu, L., et al. (2016). "Concurrent targeting Akt and sphingosine kinase 1 by A-674563 in acute myeloid leukemia cells." Biochemical and biophysical research communications.

Yamashita, M. and M. Emerman (2009). "Cellular restriction targeting viral capsids perturbs human immunodeficiency virus type 1 infection of nondividing cells." Journal of Virology **83**(19): 9835-9843.

Yamashita-Kashima, Y., et al. (2014). "Importance of formalin fixing conditions for HER2 testing in gastric cancer: immunohistochemical staining and fluorescence in situ hybridization." Gastric Cancer **17**(4): 638-647.

Yedavalli, V. S. and K.-T. Jeang (2010). "Trimethylguanosine capping selectively promotes expression of Rev-dependent HIV-1 RNAs." Proceedings of the National Academy of Sciences **107**(33): 14787-14792.

Yeung, M. L., et al. (2005). "Changes in microRNA expression profiles in HIV-1-transfected human cells." Retrovirology **2**(1): 81.

Yeung, M. L., et al. (2009). "A genome-wide short hairpin RNA screening of jurkat T-cells for human proteins contributing to productive HIV-1 replication." Journal of Biological Chemistry **284**(29): 19463-19473.

Yi, R., et al. (2003). "Exportin-5 mediates the nuclear export of pre-microRNAs and short hairpin RNAs." Genes & development **17**(24): 3011-3016.

Yoon, C.-H., et al. (2015). "p53-Derived Host Restriction of HIV-1 Replication by Protein Kinase R-Mediated Tat Phosphorylation and Inactivation." Journal of Virology **89**(8): 4262-4280.

Yoon, J.-H., et al. (2014). Functional interactions among microRNAs and long noncoding RNAs. Seminars in cell & developmental biology, Elsevier.

Yu, X., et al. (2003). "Induction of APOBEC3G ubiquitination and degradation by an HIV-1 Vif-Cul5-SCF complex." Science **302**(5647): 1056-1060.

Yu, X. G. and M. Lichterfeld (2012). "Elite control of HIV: p21 (waf-1/cip-1) at its best." Cell Cycle **11**(22): 4097-4098.

Zanella, F., et al. (2010). "High content screening: seeing is believing." Trends in biotechnology **28**(5): 237-245.

Zapp, M. L., et al. (1991). "Oligomerization and RNA binding domains of the type 1 human immunodeficiency virus Rev protein: a dual function for an arginine-rich binding motif." Proceedings of the National Academy of Sciences **88**(17): 7734-7738.

Zeng, B., et al. (2012). "Epigenetic regulation of miR-124 by hepatitis C virus core protein promotes migration and invasion of intrahepatic cholangiocarcinoma cells by targeting SMYD3." FEBS letters **586**(19): 3271-3278.

Zeng, L., et al. (2005). "Selective small molecules blocking HIV-1 Tat and coactivator PCAF association." Journal of the American Chemical Society **127**(8): 2376-2377.

Zhang, H., et al. (2003). "The cytidine deaminase CEM15 induces hypermutation in newly synthesized HIV-1 DNA." Nature **424**(6944): 94-98.

Zhang, H.-S., et al. (2012). "MiR-217 is involved in Tat-induced HIV-1 long terminal repeat (LTR) transactivation by down-regulation of SIRT1." Biochimica et Biophysica Acta (BBA)-Molecular Cell Research **1823**(5): 1017-1023.

Zhang, J., et al. (2012). "Temozolomide: mechanisms of action, repair and resistance." Current molecular pharmacology **5**(1): 102-114.

Zhang, J. C., et al. (2014). "Expression of breast cancer resistance protein in peripheral T cell subsets from HIV□1□infected patients with antiretroviral therapy." Molecular medicine reports **10**(2): 939-946.

Zhang, Q., et al. (2013). "NEAT1 long noncoding RNA and paraspeckle bodies modulate HIV-1 posttranscriptional expression." MBio **4**(1): e00596-00512.

Zhang, S.-M., et al. (2012). "HIV-1 Tat impairs cell cycle control by targeting the Tip60, Plk1 and cyclin B1 ternary complex." Cell Cycle **11**(6): 1217-1234.

Zhang, X. D. (2008). "Novel analytic criteria and effective plate designs for quality control in genome-scale RNAi screens." Journal of biomolecular screening **13**(5): 363-377.

Zhang, Z., et al. (2012). "Quality control of cell-based high-throughput drug screening." Acta Pharmaceutica Sinica B **2**(5): 429-438.

Zhang, Z., et al. (2007). "Negative elongation factor NELF represses human immunodeficiency virus transcription by pausing the RNA polymerase II complex." Journal of Biological Chemistry **282**(23): 16981-16988.

Zhao, E., et al. (2012). "Bone marrow and the control of immunity." Cellular & molecular immunology **9**(1): 11-19.

Zhao, L., et al. (2015). "Identification of cellular microRNA-136 as a dual regulator of RIG-I-mediated innate immunity that antagonizes H5N1 IAV replication in A549 cells." Scientific reports **5**.

Zhou, H., et al. (2008). "Genome-scale RNAi screen for host factors required for HIV replication." Cell host & microbe **4**(5): 495-504.

Zhou, M., et al. (2000). "Tat modifies the activity of CDK9 to phosphorylate serine 5 of the RNA polymerase II carboxyl-terminal domain during human immunodeficiency virus type 1 transcription." Molecular and cellular biology **20**(14): 5077-5086.

Zhou, W. and R. König (2003). "T cell receptor-independent CD4 signalling: CD4–MHC class II interactions regulate intracellular calcium and cyclic AMP." Cellular signalling **15**(8): 751-762.

Zimmerman, P. A., et al. (1997). "Inherited resistance to HIV-1 conferred by an inactivating mutation in CC chemokine receptor 5: studies in populations with contrasting clinical phenotypes, defined racial background, and quantified risk." Molecular Medicine **3**(1): 23.

Zuva, T., et al. (2011). "Image segmentation, available techniques, developments and open issues." Canadian Journal on Image Processing and Computer Vision **2**(3): 20-29.